Heterobimetallic Ruthenium Complexes Containing Ferrocene as Anti-Cancer Agents

Matthew Steven Allison

Submitted in accordance with the requirements for the degree of
Doctor of Philosophy

The University of Leeds
School of Chemistry

April, 2018

The candidate confirms that the work submitted is his own and that appropriate credit has been given where reference has been made to the work of others.

Acknowledgements

I would like to give a huge thank you to Paddy for taking a chance on a bumbling MChem and giving me the opportunity to undertake this project. The advice, guidance and support you have shown me throughout the past few years has given me the confidence and skills to make this project my own.

My gratitude is also extended to all of my collaborators, Prof. Roger Phillips at the University of Huddersfield for the cytotoxicity studies, especially Pablo for the time and effort he has put into the cell work. Further thanks go to Dr. Rianne Lord at the University of Bradford for the comet assay work and her help with upcoming papers. I am also grateful to Prof. Andrew Nelson, Shezi and Danielle for the artificial biomembrane studies, and to the Community for Open Antimicrobial Drug Discovery (COADD) at the University of Queensland for the antimicrobial investigations. Thank you to Ms. Tanya Marinko-Covell and Mr. Stephen Boyer (London Metropolitan University) for the microanalyses.

I would especially like to thank Dr. Chris Pask, not only for his assistance with crystallography, but also as a friend. I really appreciate all the help you have given me during my PhD: answering my X-ray problems, chemical conundrums and stacks of proof reading, while always being friendly and approachable (even if you havn't had a cup of tea yet). It is no lie that this project would have been much more arduous in your absence; you're a great person Chris, Thank you.

I have loved every moment of my time as part of the McGowan group, a feeling that stems from the joy of working alongside such great people. Carlo, thank you for welcoming me to the group and passing down to me your column wisdom, your stereotypically Italian gestures are now part of my psyche. Laura, I am so glad to have found someone in the group who has a sense of humour just as childish and inappropriate as mine. You really made me feel welcome to the group and made coming in to the office everyday a hilarious experience. Cecilia, the yin to my yang, even though we are very different people the friendship we have formed is one I truly cherish. It has been a blessing to have you as a group member, not only for the wine you give to me at conferences, but for your sanity in a sometimes strange place.

Pablo, you're crazy, but I love you. You are like the brother that I never had and I hope our bromance never dies! I'm going to miss our coffee mornings with Cecilia (even though you always eat all the biscuits) and intermittent elastic band fights which always go too far.

Thank you to the rest of team inorganic, The Halcrows: Raf, Amedeo, Tom, Laurence, Sam, Kay, Izar, Iurii and Namrah; The Willans: Heba, Mike, Jordan, Bank and Frances; and the Hardies: Flo, Vikki, Sam, Jonny, Hayder and Ed. The viva celebrations, Christmas parties and otherwise any other drunken occasion have been brilliant (the sober times were ok too, I guess).

Arran, Ben, Chad, Coxy, Deaks, Gilly, Niko and Wedge, we have known each other for a very long time and I would like to thank you all. Together we are a rag-tag bunch of misfits - a dysfunctional family, you could say - but I couldn't ask for a more loyal, hilarious and down-to-earth group of people to call my friends. You have been a light for me in dark places, when all other lights went out.

Most importantly I would like to thank my family: Mum, Amanda, Auntie Carol, Arlie, Emma, Lewis and, of course, Danni. Even though we are only a small family, you mean everything to me and I love you all. Mum, it is not possible for me to thank you enough for everything you have done for me; you have always believed in me and have been there for me, especially when things got tough. Without your love and support I would not have made it this far. I love you and I don't know where I would be without you. Danni, I thank you for all the times you have put a smile on my face and for being there to pick me up when I've been down, especially throughout my PhD. You have always had faith in me and I couldn't ask for a better girlfriend; you're my best friend and I love you.

My final Thank you is reserved for my grandparents - Cora, Eric and Ken - who are my inspiration and to whom I dedicate this thesis; without their love, support, care and guidance I would not be half the man I am today. Their battles with cancer are the reason I sought to undertake this project and I only wish that they could be here so see me finish it. I miss you dearly and hope I have made you proud, I love you.

Abstract

This thesis details the synthesis and characterisation of ruthenium metal complexes containing functionalised ferrocene β-diketonate ligands. The anticancer and antimicrobial potential of these complexes has been explored and structural activity relationships investigated through further mechanistic investigations.

A library of functionalised ferrocene β-diketonate ligands were synthesised and used in the formation of two libraries of ruthenium complexes. The first series of complexes consist of organometallic ruthenium(II) arene complexes and the second series comprising of ruthenium(II) *bis*-bipyridyl coordination complexes. Detailed synthetic routes are outlined and all complexes are fully characterised by ^{1}H NMR spectroscopy, ^{13}C [^{1}H] NMR spectroscopy, mass spectrometry and elemental analysis. X-ray crystallographic data was obtained when possible.

The complexes were screened for their activity against one healthy and two cancerous cell lines; the ruthenium arene complexes were found to be highly selective towards the cancerous cell lines while the ruthenium *bis*-bipyridyl complexes were found to possess potent toxicity towards all cell lines. Selected complexes from each series were then studied in a low oxygen environment which caused a reduction in the cytotoxicity of the complexes. The antibacterial and antifungal properties of the two series of ruthenium complexes have also been assessed. Mechanistic studies have been conducted on selected complexes in the form of hydrolysis, hydrophobicity, biomembrane CV and comet assay in order to deduce a possible mechanism of action and mode of transport of these complexes.

Table of Contents

List of Abbreviations

°	degrees
δ	chemical shift
η	hapticity
λ	wavelength
µg	microgram
µL	microliter
µM	micromolar
µm	micrometre
Å	Angstrom
A	adenine
acac	acetylacetonate
ARPE-19	human retinal pigment epithelial cell line
ATP	adenosine triphosphate
BC	Before Christ
bpy	2,2'-bipyridine
[C]	concentration
°C	degrees Celsius
CAMHB	cation adjusted Mueller Hinton broth
CC_{50}	concentration for 50 % cell death
CLSM	confocal laser scanning microscopy
cm	centimetre
CO-ADD	Community for Open Antimicrobial Drug Discovery
Cp	cyclopentadiene
Cp*	pentamethylcyclopentadiene
CRT1	copper transporter 1

d	deuterated
d	doublet
Da	Dalton
dm	decimetre
DFT	density functional theory
Dmd	4,4’-dimethyl-2,2’-bipyridine
DMSO	dimethyl sulphoxide
DNA	deoxyridonucleic acid
DOPC	dioleoyl phosphatidylcholine
dppz	dipyridophenazine
DSB	double strand breakage
EDTA	ethylenediaminetetraacetic acid
e.g.	*exempli gratia,* for example
en	ethylenediamine
ES	electrospray
et al.	and others
g	gram
G	Gauss
G	guanine
h	hours
HBSS	HBSS Hank’s balanced salt solution
HC_{10}	concentration for 10 % haemolysis
HCT116++	human colon cancer cell line
HEK293	human embryonic kidney cell line
HIF-1	hypoxia inducible factor-1
HMG	high mobility group

hsA	human serum albumin protein
IC_{50}	concentration for 50 % growth inhibition
ICP-MS	inductively coupled plasma mass spectrometry
i.e.	*id est*, that is
IFI	invasive fungal infection
IGF	insulin-like growth factor
IR	infrared
in vacuo	under vacuum
in vitro	in glass
in vivo	in a living organism
J	coupling constant
K	degrees Kelvin
log*P*	partition coefficient
m	multiplet
MHz	mega Hertz
MIA PaCa-2	human pancreatic carcinoma cell line
MIC	minimum inhibitory concentration
min	minute
mL	millilitre
mM	millimolar
mm	millimetre
mmol	millimole
MRSA	methicillin-resistant staphylococcus aureus
MS	mass spectrometry
MTT	3-(4,5-dimethylthiazol-2-yl)-2,5-diphenyltetrazolium bromide
mV	millivolt*

NAD(H)	nicotinamide adenine dinucleotide
NADP(H)	nicotinamide adenine dinucleotide phosphate
NBS	non-binding surface
NHS	National Health Service
NIR	near infrared
nm	nanometre
NMR	nuclear magnetic resonance
PACT	photodynamic antimicrobial chemotherapy
PACT	photoactivated chemotherapy
PBS	phosphate buffered saline
PDT	photodynamic therapy
pH	potential of hydrogen
phen	phenanthroline
ppm	parts per million
PTA	1,3,5-triaza-7-phosphaadamantane
RCV	rapid cyclic voltagram
ROS	reactive oxygen species
s	second
s	singlet
SAR	structure activity relationship
SD	standard deviation
SFI	superficial fungal infection
sh	shoulder
SSB	single strand breakage
t	triplet
tpa	*tris*(2-methylpyridyl)amine

TrxR	thioredoxin reductase
UK	United Kingdom
UV	ultraviolet
UV/vis	ultraviolet-visible
V	volt
VEGF	vascular endothelial growth factor
via	by way of

Chapter 1: Introduction

1.1 Cancer

Cancer is a disease which affects almost everybody's lives in one way or another, whether it be through a personal diagnosis, or a family member or friend who is fighting the disease. In Great Britain the incident rates related to cancer have steadily increased since the mid-1970s by 23% in males and 43% in females to the point where every two minutes someone is now diagnosed. The UK had more than 440 deaths related to cancer every day in 2012, which is more than one person every four minutes, and accounted for a quarter of all deaths, with those figures increasing to more than half in people aged over 75.[1] The most common forms of cancers are breast, lung, prostate and bowel cancer which together account for 54% of all cancer cases.[1] In males, the most common case is prostate cancer accounting for 27% of all cases and, in females, breast cancer is the most common totalling 29% of all cases.[2] Cancer services cost the NHS £5 billion annually, but including costs due to loss of productivity, society as a whole is losing £18.3 billion.[3] Although these statistics look bleak, recent findings have now shown that 50% of cancer patients are surviving for ten years or more after treatment.[4] This is almost certainly due to the increase in research effort into combating the disease, however the UK survival rates are still lacking in comparison to other less wealthy countries.[3]

Cancer is a disease which involves the alteration of the cellular genome causing the growth of a tumour.[5] The expression or function of genes controlling cell differentiation and growth are affected by these alterations and form cancer genes called oncogenes, with dominant gain of function (rapid growth), and tumour suppressor genes, with recessive loss of function. These cancer genes control cell mitosis which is a process of cellular growth through cell division. If one or more of these genes has a mutation then the cell will divide uncontrollably and allow cells which would usually undergo cell death to proliferate.[6] This can lead to the formation of either a benign tumour which is easily treated and not life threatening, or a malignant tumour which can be difficult to treat as they can undergo the process of metastasis, allowing the flow of cancerous cells into the bloodstream. These metastasising cells can be carried to various other parts of the body where they may attach to tissue and proliferate.[7] There are many different forms of cancer

depending on what type of cell is affected. To correctly combat the cancer an appropriate form of cancer therapy must be used, sometimes in tandem with another. These include surgery, radiotherapy, chemotherapy, immunotherapy and hormonal therapy.[8]

1.2 Metal Based Drugs

The use of metal based medicine has been found to date back thousands of years to the early days of civilisation. To sterilise water, the famous Greek physician Hippocrates used mercury and the ancient Egyptians used copper for the same application. China has records of gold being used in medical applications dating back to 2500 BC but it was not until the discovery of Salvarsan in the 1900s that metal-based drugs started to make an impact on modern medicine.[9]

Salvarsan was first produced in 1910 by Ehrlich as a remedy for syphilis and is regarded as the introduction of targeted chemotherapy to the medicinal community. The arsenic based compound is formed from the reaction of 3-nitro-4-hydrophenylarsonic acid with dithionite which simultaneously reduces both the NO_2 group to NH_2 and As^V to As^I. Ehrlich originally thought the structure was a dimer bound together *via* a double bond but it has since been found to actually form trimers and pentamers (**Figure 1.1**).[10]

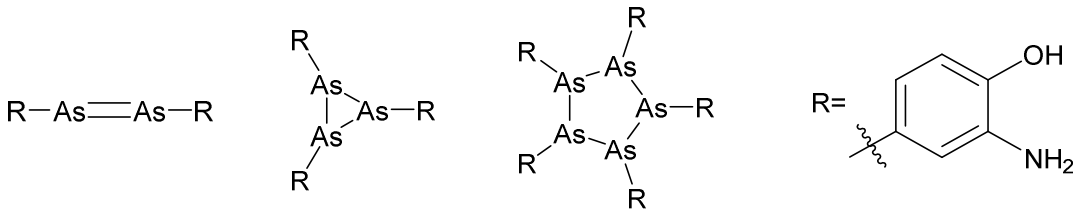

Figure 1.1 Structures of Salvarsan[10]

The early 20th century paved the way for the modern use of gold in medicine, termed chrysotherapy, when Professors Ander-Jean Chrestien and Pierre Figuier described the chemical formulation of many gold compounds and determined them valuable in the treatment of tuberculosis.[11] Robert Koch's observation that gold cyanide exhibited antibacterial effects *in vitro* against *tubercle bacilli* started a 40 year long

search for gold derivatives which could be used in the treatment for both human and bovine strains of the bacteria.[12] The assumption that rheumatoid disease was similar to tuberculosis created the chance discovery that gold compounds were effective at treating rheumatoid arthritis.[13] The most frequently used drugs were aurothioglucose and sodium aurothiomalate which are polymeric and must be administered by intramuscular injection. An oral drug became available in the 1970s with the discovery of a monomeric gold(I) phosphine drug called Auranofin™ (**Figure 1.2**).[14]

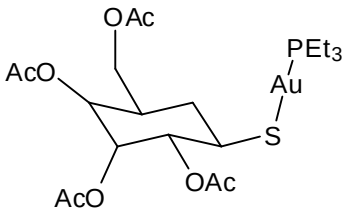

Figure 1.2 Auranofin[14]

There is now a diversity of metal based compounds which have successfully been used to combat a range of illnesses and diseases such as malaria, blood diseases and trypanosomiasis to name a few.[15] Undoubtedly the biggest breakthrough in the field of metal based drugs came with the discovery of the platinum based anti-cancer drug, cisplatin.

1.3 Cisplatin

In 1965, Barnett Rosenberg was investigating the effects of electromagnetic radiation on mammalian and bacterial cells to see if either the magnetic or electric fields altered the cell division process. His work consisted of using platinum electrodes on *Escherichia coli* grown in an ammonium chloride buffer, but the applied field caused the bacteria to appear as abnormally long filaments rather than the expected short rods. It was found that this phenomenon was due to the electrolysis products formed from the use of the platinum electrodes, one of which was cisplatin [*cis*-diamminedichloroplatinum(II)] (**Figure 1.3**).[16] Analysis of cisplatin showed that it had been synthesised before by Peyrone in 1845 under the name

Peyrone's salt.[17] However, Rosenberg was the first to test cisplatin's anti-cancer properties and it has since had widespread use in combating many forms of cancer including head and neck, cervical, ovarian, lung and especially testicular cancer.[18] The overall cure rate for patients with testicular cancer who are treated with cisplatin is greater than 95% and even 80% for the metastatic form.[19]

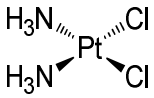

Figure 1.3 Cisplatin[16]

When in the bloodstream, cisplatin takes advantage of the change in chloride concentration between the inside and outside of its target cells. The high chloride concentration (100 mM) outside of the cell prevents aquation of the chloride leaving groups. Intact cisplatin molecules can then enter the cell primarily through the copper transporter CRT1 transmembrane channels.[20,21] Inside the cell, the chloride concentration is much lower (4-20 mM) and therefore cisplatin can become activated by a series of spontaneous aquation reactions. The chloride ligands are substituted with water ligands to form a charged complex which cannot readily leave the cell. The monoaquated species is highly reactive and susceptible to cytoplasmic inactivation by intercellular components but its formation is rate limiting in the interaction with nucleophiles inside the cell.[22] *In vitro* experiments on the monoaquated species have shown that it is involved in no less than 98% of the DNA binding in the cell nucleus.[23]

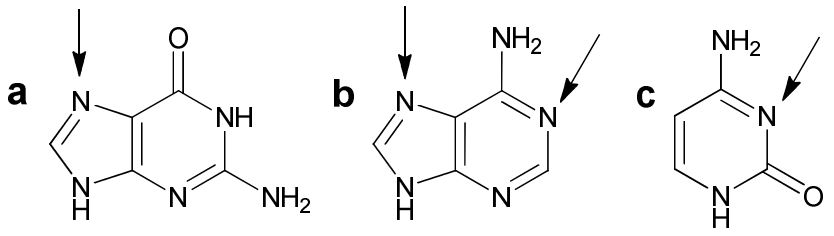

Figure 1.4 Molecular structures of **a** guanine, **b** adenine and **c** cytosine. Arrows indicate potential binding sites.[23]

The platinum binds to one of the available bases on DNA, the N7 of guanine is the preferred initial binding site as it is the most nucleophilic but it is also possible to bind to the nitrogen lone pairs on cytosine and adenine (**Figure 1.4**).[23] In order for cisplatin to be effective against cancer cells it must bind to two sites on DNA, forming a bifunctional adduct. This can occur in one of two ways, either directly from the monofunctional adduct or the aquation of the second chloride ligand and consequently binding to a second DNA base.[24] Guanine-guanine intrastrand adducts are formed approximately 65% of the time and adenine-guanine intrastrand 25%.[25] When cisplatin forms these intrastrand crosslinked DNA structures it distorts the DNA duplex causing it to bend towards the major groove, exposing the minor groove surface. Proteins such as high mobility group (HMG) box proteins can bind to this exposed surface, leading to cell death/initiation of DNA damage repair (**Scheme 1.1**).[26] Although cisplatin is a very popular and effective anti-cancer agent, it is highly toxic towards healthy organs, particularly the kidneys and gastrointestinal tract.[27] Hence, work has since been done in an attempt to develop cisplatin analogues which retain their cytotoxicity but are less harmful towards healthy cells.

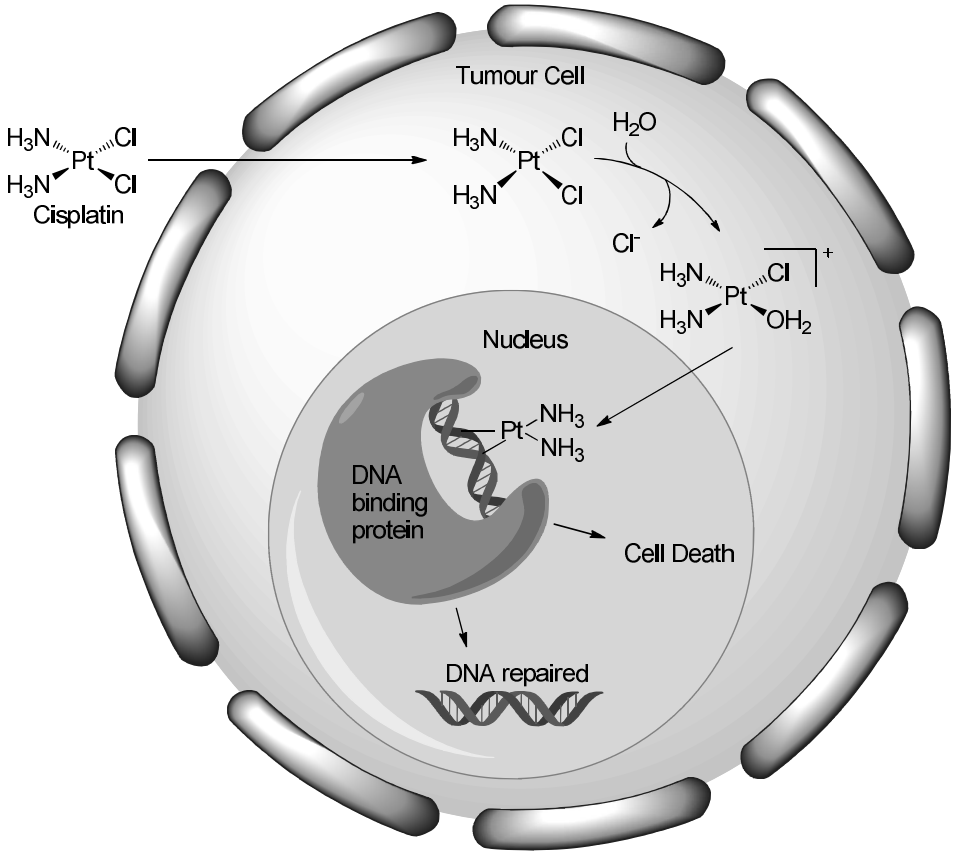

Scheme 1.1 Cytotoxic pathway for cisplatin

1.4 Further Generations of Platinum Based Anti-cancer Drugs

Carboplatin (**Figure 1.5 a**), also invented by Rosenberg, is another platinum based compound which has gained widespread approval for use on a range of different cancers.[28,29] It was designed to minimise the toxicity related to the rapid aquation of cisplatin's chloride leaving groups, causing unintended and harmful biological interactions.[30] The bis-carboxylate bidentate ligand undergoes substitution much slower than the chloride ligands as it is much more stable and therefore shows reduced toxicity as the drug has more time to reach the target cells. This is advantageous in cancer therapy as although its cytotoxicity is an order of magnitude lower than that of cisplatin, carboplatin can be administered in much higher doses due to its less toxic side effects, resulting in an increased cancer cell death rate.[31] As carboplatin and cisplatin have very similar activities and modes of action, the cancer cell lines resistant to cisplatin will also not be affected by carboplatin.

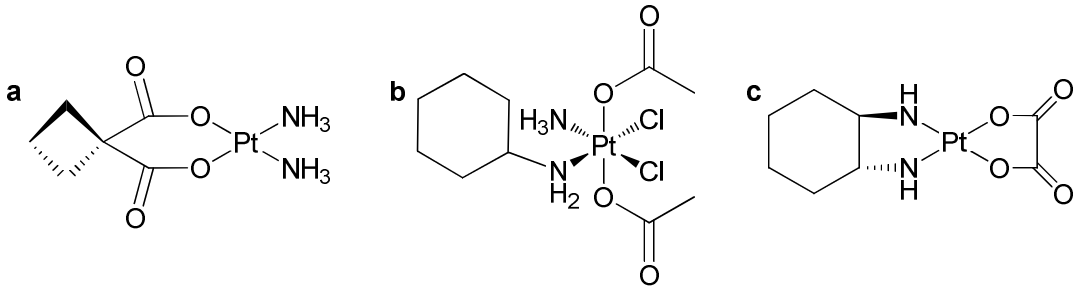

Figure 1.5 Molecular structures of **a** carboplatin,[28] **b** satraplatin[32] and **c** oxaliplatin[35]

Satraplatin (**Figure 1.5 b**) is a platinum (IV) based anti-cancer drug rationally designed to accommodate two axial acetate groups, increasing the lipophilicity of the compound, which in turn makes it the first orally bioavailable platinum analogue.[32] With comparable efficiency to many well established platinum drugs, activity against cisplatin resistant cell lines *in vitro* and low toxicity levels similar to that of carboplatin,[33] satraplatin could possibly be a highly successful drug if it is passed through its current phase III trials.[34]

Oxaliplatin (**Figure 1.5 c**) was the first approved drug that was able to combat cisplatin resistant cancer strains, particularly colorectal cancer where it is active

against six of the eight cancer cell lines.[35] This activity is attributed to the bulky diaminocyclohexane moiety which is present after aquation.[36]

The success of cisplatin and its analogues caused much of the early work on metal based cancer therapy to be developed based on their interactions with DNA. It has since become apparent that many other metal complexes, such as ruthenium, can show similar activity to cisplatin without necessarily behaving in the same manner.

1.5 Ruthenium Based Anti-Cancer Compounds

Ruthenium is a popular candidate in the search for new metal based anticancer drugs. The flexible and easily tuneable properties of ruthenium complexes has facilitated the formation of potent cytotoxic complexes active against a wide range of cancer cell lines, while also being relatively benign towards healthy cells. There are several important properties that ruthenium complexes possess which make them particularly attractive candidates for cancer therapeutic applications;

1) Geometry

Ruthenium complexes, like many other metal scaffolds, can cover more biologically relevant chemical space in comparison to organic compounds. Their octahedral coordination geometry facilitates the organisation of substituents around the metal centre, increasing the number of spatial positions which it is possible to occupy. For example an octahedral centre with six different ligands is able to adopt 30 stereoisomers.[37]

2) Ligand Exchange

The rate of ligand exchange can play a large role in determining a complex's biological activity as very few metal complexes reach their intended biological target site without being modified to some degree.[38] Ruthenium(II) and ruthenium(III) complexes have similar ligand exchange rates to that of platinum(II) complexes which is typically in the range of minutes to days when a small molecule such as water is considered.[39, 40] This kinetic stability and resistance to rapid equilibrium reactions allows their ligand exchange time scale to mimic that of many cell division

processes, and is therefore thought to be a key factor which contributes to their antineoplastic properties.[41]

3) Oxidation States

Variations in the oxidation state of ruthenium between (II), (III) and (IV) can be achieved under physiological conditions and play a very important role in allowing the complexes to exist in biological fluids. By the appropriate choice of ligands, it is possible to control and stabilise the different oxidation states of the metal centre and tune the redox potential of the complexes.[42, 43] Compared to ruthenium(II)/(IV), ruthenium(III) complexes tend to be more biologically inert and can be administered as "pro-drugs" which undergo a reduction or oxidation process inside the body. Such a reduction can be achieved inside tumours where the oxygen concentration is low due to their high metabolism. This creates an internal reducing environment that activates the pro-drug and subsequently increases the tumour selectivity of the compound.[44]

4) Iron Mimicking

It has been suggested that ruthenium has the ability to mimic iron in binding to proteins such as albumin and transferrin (**Figure 1.6**), which are iron-carriers present in blood plasma, in order to mediate the uptake of ruthenium into cancerous cells.[45] Ruthenium (and some other metal complexes) can strongly bind to transferrin *via* the two iron(III) binding sites, and as transferrin in human serum is only 30% saturated with iron, this leaves the remaining 70% of the sites vacant and free to bind to other metal ions.[46,47] Tumours require increased amounts of iron for growth, metabolism and development, hence there are higher levels of transferrin receptors on their surface compared to healthy cells.[48] The iron mimicking potential of ruthenium complexes therefore allows an increase in their selectivity, with *in vivo* studies showing a 2- to 12-fold increase in ruthenium concentration present in cancerous cell over healthy cells, increasing their cytotoxic potency while simultaneously decreasing general toxicity.[49] However, it should be noted that this area is still under debate due in part to the rather sterically hindered binding sites on the transport proteins.

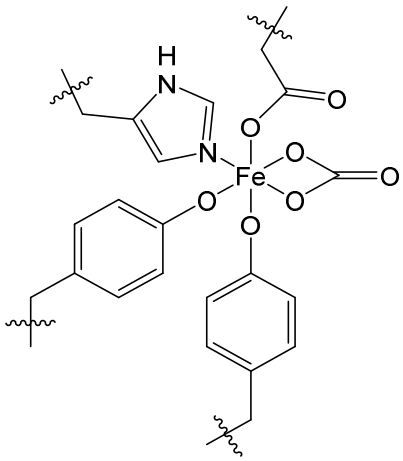

Figure 1.6 Molecular structures of Fe(III) binding site on transferrin[45]

1.5.1 NAMI-A

NAMI-A (imidazolium *trans*-imidazoledimethylsulfoxidetetrachlororuthenate, **Figure 1.7**), was the first ruthenium complex to enter clinical trials and has shown a metastasis reduction of up to 100% in preclinical models including Lewis lung carcinoma, TS/A mammary adeno carcinoma, MCa mammary carcinoma, b16 melanoma and H460M2 lung cancer.[50-51]

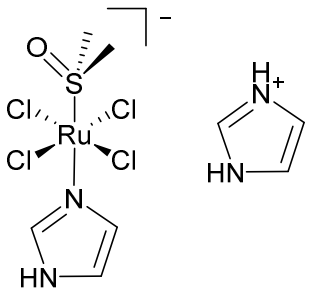

Figure 1.7 NAMI-A[50]

In vitro testing showed low levels of cytotoxicity from cisplatin-like interactions with DNA and has suggested that its activity is related to disruptions with the G_2/M phase of the cell cycles leading to cell cycle arrest, inhibiting proliferation.[52] Furthermore, NAMI-A has been shown to prevent tumour cells from spreading to surrounding healthy tissue by increasing the extracellular matrix around tumour blood vessels and also increasing the capsule thickness surrounding the primary tumour. Toxicology studies on dogs and mice have also yielded promisingly low results.[53]

1.5.2 KP1019

KP1019 (indazolium bisindazoletetrachlororuthenate, **Figure 1.8**) is another promising ruthenium based anti-cancer drug which has shown good results from phase I clinical trials, being particularly effective against colorectal tumours, most excitingly the chemoresistant MAC15A colon carcinoma.[54]

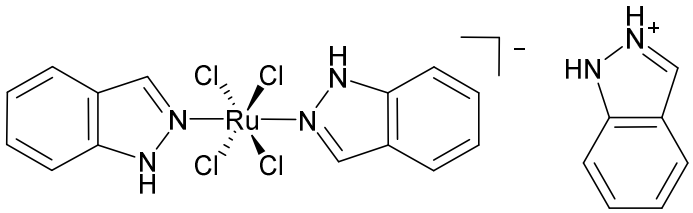

Figure 1.8 KP1019[54]

After incubation with KP1019, the nucleus of cells were found to harbour 55% of the total intracellular ruthenium,[55] which is considerably greater than that of many other metal based drugs such as cisplatin (less than 10%).[56] This efficient uptake into cells increases the amount of damage and oxidative stress towards DNA, causing apoptosis towards cells also at the primary tumour site, exhibiting more than just the anti-metastatic properties from NAMI-A.[57] With respect to its mechanism of action it is typical of many metal based anti-cancer drugs, becoming more cytotoxic after reduction, and undergoes similar interactions with DNA to that of cisplatin but with lower intensity.[58] However, due to transport issues in the bloodstream arising from the low water solubility of KP1019 it has been superseded by KP1339, which is the sodium salt of KP1019, and therefore has increased solubility.[59]

1.5.3 Ruthenium Arene Complexes

Organometallic ruthenium complexes have been extensively studied for their use in cancer therapeutics since Sheldrick *et al.* first reported the biological applications of half-sandwich ruthenium complexes with piano stool geometry, demonstrating that η^6-arene ruthenium(II) complexes containing L-alanine and L-alanine methyl ester are able to coordinate to the N7 nitrogen atom of guanine derivatives (**Figure 1.9**).[60]

In the decades following this discovery, η^6-arene ruthenium complexes have formed some of the most promising anticancer candidates. Their structural activity relationships have been scrutinised and their structures honed in attempts to understand their mechanism of action and improve their cytotoxicity.

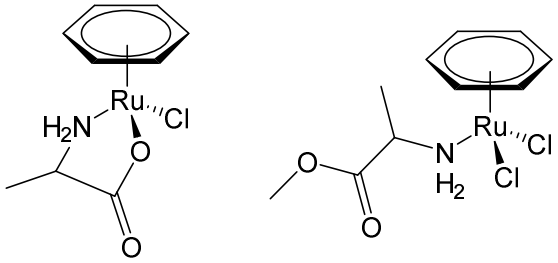

Figure 1.9 η^6-arene-ruthenium(II) L-alanine and L-alanine methyl ester complexes[60]

RM175 ($[(\eta^6\text{-}C_6H_5C_6H_5)RuCl(H_2NCH_2CH_2NH_2\text{-}N,N')]^+$ $[PF_6]^-$, **Figure 1.10**) is a ruthenium-arene complex specifically designed to combat cancer through its DNA interactions and is one of many "piano stool" structures which have been produced and studied by Sadler *et al.* Existing as ruthenium(II), this does not follow the mechanism which is seen from the ruthenium(III) complexes in which the reduction of the metal causes its activation.[61, 62]

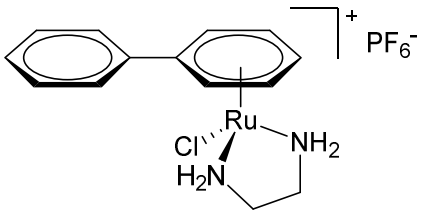

Figure 1.10 RM175[61]

These types of ruthenium complexes are thought to aquate much faster than cisplatin, resulting in a product that will react rapidly with guanine.[63] DNA interactions with complexes with non-single ring arene ligands can involve a combination of different forms of binding to DNA (**Figure 1.11**). Besides the typical binding to DNA *via* the guanine N7 position, the arene ligands give the drug scope for non-covalent, hydrophobic interactions with DNA and the possibility of arene intercalation and minor groove binding. Sadler *et al.* studied the interaction of these

complexes with guanine derivatives *in vitro* and a crystal structure was determined which demonstrates the intermolecular π-π stacking between the pendant phenyl ring and the guanine base, along with hydrogen bond interactions between the NH of the ethylendiamine and guanine O6.[61]

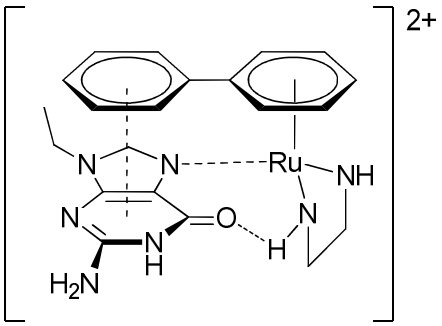

Figure 1.11 Interactions between RM175 and ethyl guanine[61]

In vitro testing has shown RM175 to exhibit comparable, and in most cases greater, cytotoxic effects in comparison to those of carboplatin with minimal cross-resistance from platinum based drugs.[64] RM175 also acts in a similar way to NAMI-A as there is a significant delay of tumour growth observed *in vivo*.[65]

RAPTA-T ([Ru(η_6-toluene)Cl_2(PTA)], **Scheme 1.2**), developed by Dyson *et al.,* is another ruthenium organometallic complex that adopts the "piano stool" conformation. It belongs to the RAPTA series of complexes where a characteristic PTA (1,3,5-triaza-7-phosphoadamantane) ligand is present in place of the ethylendiamine used by Sadler *et al*.,[66] and it is this PTA moiety which is responsible for the drug's biologically active properties in the low oxygen environment of solid tumours. *In vitro* testing showed almost no damage was caused to DNA at pH > 7, which is the pH region in which healthy cells grow, whereas at pH < 7 there was prevalent damage observed towards DNA.[67] Therefore, at the low pH levels inside the tumour, the PTA ligand can become protonated (**Scheme 1.2**), and therefore activated, selectively causing damage towards the DNA of cancerous cells.[68]

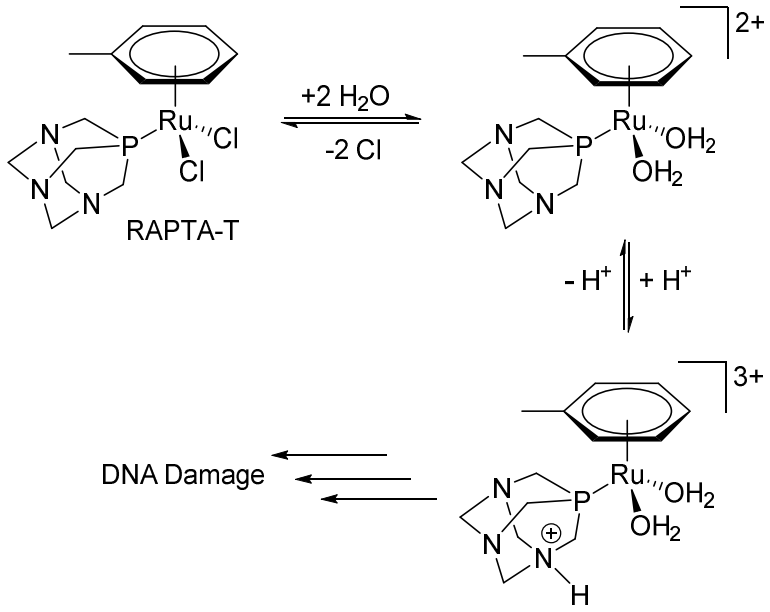

Scheme 1.2 Hydrolysis and protonation of RAPTA-T leading to DNA damage[68]

Even though this is a ruthenium(II) organometallic complex, it exhibits similar anti-cancer behaviour to that of NAMI-A, which is a ruthenium(III) complex. They are both active towards secondary metastasis tumours, such as MCa mammary carcinoma, but are not active with regard to the primary tumour site.[69] They also show very low levels of toxicity and pharmacokinetic studies show that, in the case of RAPTA-C, ruthenium is rapidly removed from the organs and bloodstream.[67]

1.5.4 Ruthenium Polypyridyl Complexes

Ruthenium complexes with pyridyl-based ligands are of great interest in the field of inorganic medicinal drug applications. The combination of the potential therapeutic properties and useful photophysical diagnostic capabilities combine into what is known as a theragnostic agent. As well as imparting the fluorescent capabilities to the complexes, which facilitate the possibility of monitoring cellular accumulation, trafficking, biodistribution and even the characterisation of cancer cells, the multidentate polypyridyl ligands confer shape and chirality which can be customised to achieve increased DNA/biomolecule binding.[70-72] The structure and chemical

composition of DNA provides many potential binding modes for molecular substrates with binding interactions being either reversible or irreversible.[73]

Irreversible binding

"Classical chemotherapy", such as that observed from cisplatin and its derivatives, is based on the induction of DNA damage through a molecule forming a covalent bond to the phosphodiester backbone, sugar residue or nucleic bases which make up DNA. Cancer cells are not able to correctly deal with the molecular irregularity caused by this binding event and consequently undergo cell cycle arrest.[74]

Reversible binding

Interest is increasing in coordination complexes that reversibly bind to DNA. These systems achieve successful binding through the three-dimensional arrangements of ligands around the metal centre and, as ligands are easily changed or modified, allow control over the binding affinity, selectivity, hydrophobicity and cellular uptake. However, ligand choice does not only play a part in molecular binding, the astute pairing of ligands and metal centres can tune the overall photophysical properties of the complex, a property which is prevalent in many octahedral d^6 metal complexes containing polypyridyl ligands.[75] There are several reversible binding motifs that these systems can exploit:

I. **Electrostatic interaction**. A vast number of coordination complexes are charged, the cationic portion of these complexes have the ability to associate with the negative charge of DNA biopolymer. Simple metal complexes (such as $[Ru(bpy)_3]^{2+}$) rely solely on this weak electrostatic binding interaction to interact with DNA, but this offers very low binding affinity. For larger and more complex compounds, the electrostatic interaction only contributes slightly to the overall binding affinity as they predominantly recognise DNA through other, stronger, binding modes.

II. **Intercalation.** One such binding mode is intercalation, which involves the overlap of the π system of planar aromatic compounds and DNA bases upon insertion of the compound between the DNA base pairs. Enforced by van der Waals, hydrophobic and electrostatic interactions,

intercalation can massively distort the DNA double helix, causing it to unwind and increase in length.[76-78]

III. **Groove binding**. It is also possible for compounds to reversibly bind to DNA *via* association within the major and minor grooves around the double helix. Molecules which are able to associate to DNA through this binding mode often span many base pairs and have high sequence-selective recognition, dictated by a combination of specific hydrogen bonding motifs, van der Waals, hydrophobic and electrostatic interactions.[79-81]

Besides the more "classical" methods of inducing cancer cell death through DNA binding, there are multiple different approaches to the development of ruthenium polypyridyl complexes which exploit their photophysical and photochemical attributes for use in the light-mediated treatment of cancer, some of which are shown in **Figure 1.12**.[82-84]

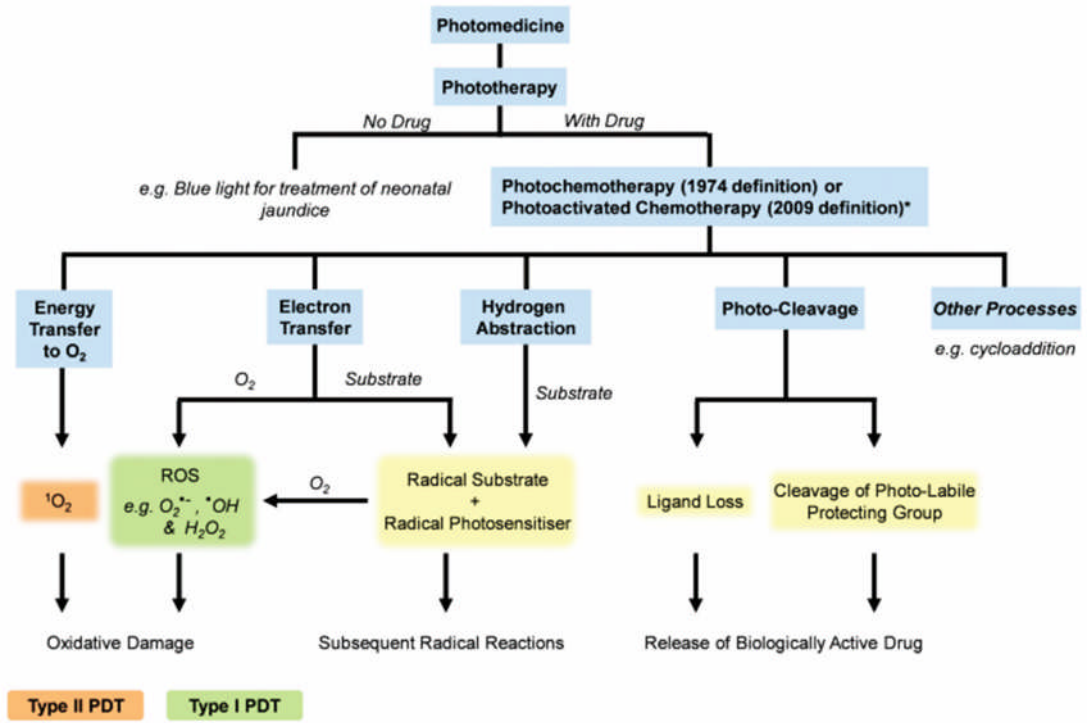

Figure 1.12 Flow chart demonstrating many of the potential photochemical and photophysical mechanisms which lead to a therapeutic response from ruthenium polypyridyl complexes[82]

One such photosensitiser (PS) designed to be used in photodynamic therapy (PDT) is TLD-1433 ($[Ru(dmb)_2(IP\text{-}TT)]^{2+}$ dmb = 4,4'-dimethyl-2,2'-bipyridine, IP-TT = 2-(2',2'':5'',2''-terthiophene)-imidazo[4,5-*f*][1,10]phenanthroline) reported by McFarland *et al.*,[85] a ruthenium(II) polypyridyl complex containing an α-oligothiophene moiety (**Figure 1.13**) which is entering phase Ib clinical trials against non-muscle invasive bladder cancer.[86-88] This complex, and many of its analogues, have been shown to be excellent DNA binders with light-sensitive cytotoxic activity, exhibiting no DNA interference in the dark but with IC_{50} values in the low micromolar range against HL-60 cells when exposed to visible/red light. A major part of this activity is due to the α-oligothiophene ligand as these small organic molecules are good $^1O_2$ generators and biophotosensitisers. This combination of α-oligothiophene and ruthenium polypyridyl complex form a system capable of acting as dual type I/II photosensitiser, meaning that after light absorption the reactive excited state complex can transfer an electron (type I) or energy (type II) to ground state oxygen, forming ROS of either superoxide radical anions or singlet oxygen, respectively, depending on the local oxygen environment.[89]

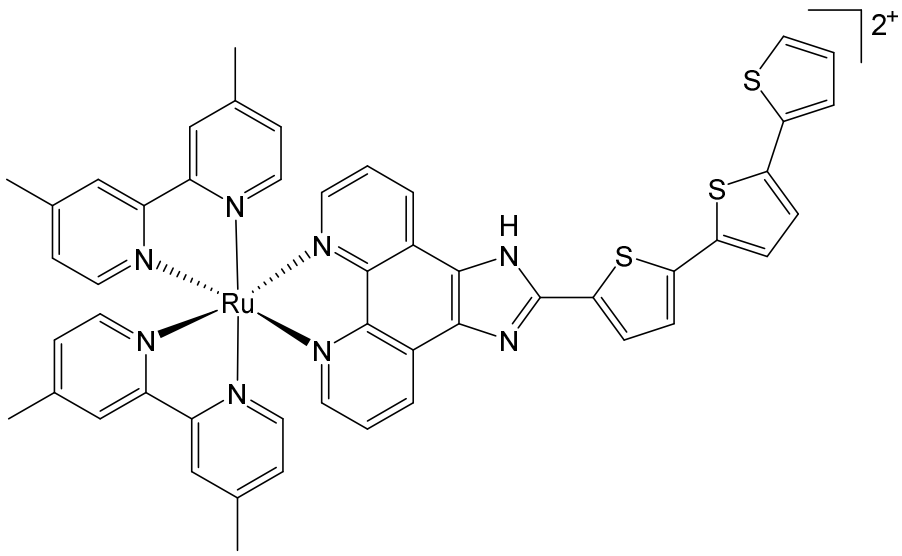

Figure 1.13 Molecualr structure of TLD-1433[85]

A particularly exciting development into TLD-1433 was uncovered when the compound was incubated with the iron-binding protein transferrin, forming a new TLD-1433-transferrin complex with greatly improved biomedical properties. These enhancements increased the efficiency of TLD-1433, more than doubling the

maximum tolerated dose. The PDT efficiency of the drug was also increased through greater photostabilty and longer photoactivation (increased ROS generation), extension of its absorbance window into the red/near infrared region of light for deeper tissue penetration, and reduced cell toxicity in the dark.[86, 87]

Vidimar *et al.* has had some excellent results in the fight against cancer using ruthenium(II) bis-phenanthroline complexes, work which has built upon the demonstrated structural-activity relationship between ruthenium(II) compounds showing a general increase in the IC_{50} value when bound to a phenanthroline ligand.[90] It was for this reason that a second phenanthroline ligand was used along with electron-withdrawing and -donating substituents bound to the ligand (**Figure 1.14**). Complexes were tested against HCT116 (human colon cancer cell line) and it was shown that the complex containing the electron-withdrawing NO_2 group (IC_{50} < 2 µM) is not only more active than the electron-donating NH_2 equivalent (IC_{50} 2-4 µM) but also more active than cisplatin (IC_{50} 8 µM). Studies into their mode of action have shown that they trigger cell death by the production of ROS and the activation of caspase-8 (a protein that plays a central role in the execution-phase of cell apoptosis) as blocking these pathways gave a significant reduction in the activity of each compound.[91, 92]

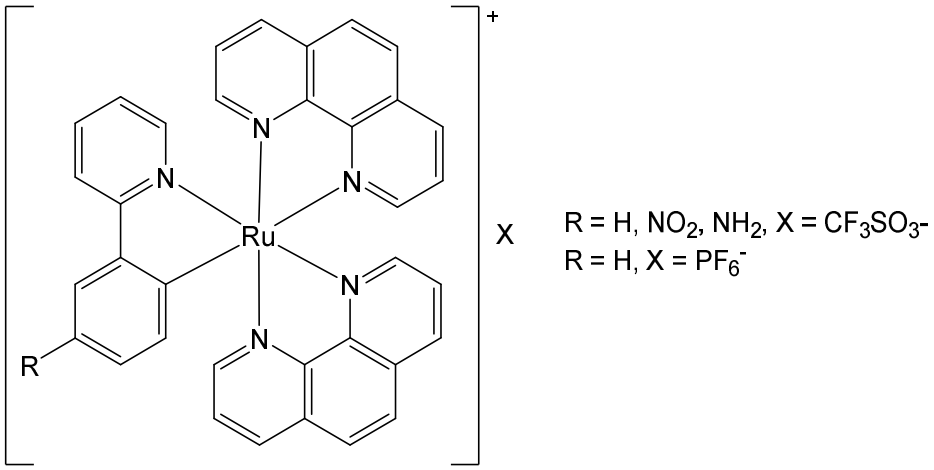

Figure 1.14 Ruthenium(II) phenanthroline complexes[90]

Ruthenium complexes with distorted octahedral geometry have been shown to undergo a photo-irradiation initiated ligand dissociation pathway to form aqua species which can bind to DNA in a similar fashion to that of cisplatin.[93, 94] This is one type of light-mediated treatment known as photoactivated chemotherapy (PACT). Unlike PDT, PACT has no reliance on the presence of oxygen in its mechanism of action, which is one of the main drawbacks of PDT due to the low oxygen conditions inside hypoxic tumours. Glazer *et al.* have used this concept in the formation of ruthenium bis-bipy complexes along with a third ligand causing a distorted strain by the use of methyl substituents (**Figure 1.15**).[95]

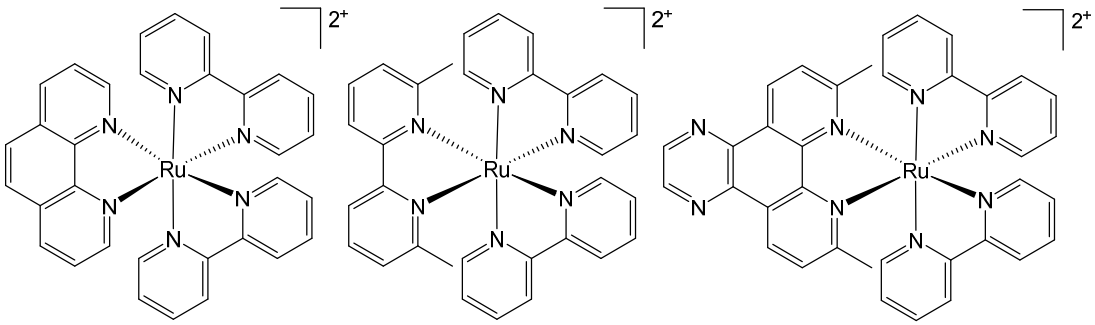

Figure 1.15 Strained ruthenium(II) bis-bipy complexes[95]

When exposed to >450nm light irradiation they were able to observe the photoejection of the methylated ligands from both of the strained complexes (**Scheme 1.3**) and decided to study the activity of the newly formed aqua species on biomolecules. It was found that DNA damage was observed strictly from the complexes irradiated with the aforementioned light irradiation (including the unstrained complex). The complexes were then tested *in vitro* against cancer cell lines HL60 (leukemia) and A549 (lung cancer) to see if the DNA damage would correlate to an increased anti-cancer activity. The complexes were incubated with the cells in dark conditions before irradiation with >450 nm light for 3 minutes, followed by further incubation. All three complexes showed little-to-no toxicity (IC_{50} >100 μM) in the dark over the same period of incubation but the compounds exposed to the light irradiation gave a huge increase in activity, with IC_{50} values

recorded between 1-2 μM for the strained complexes against both cell lines (more active than cisplatin and the unstrained complex).[96]

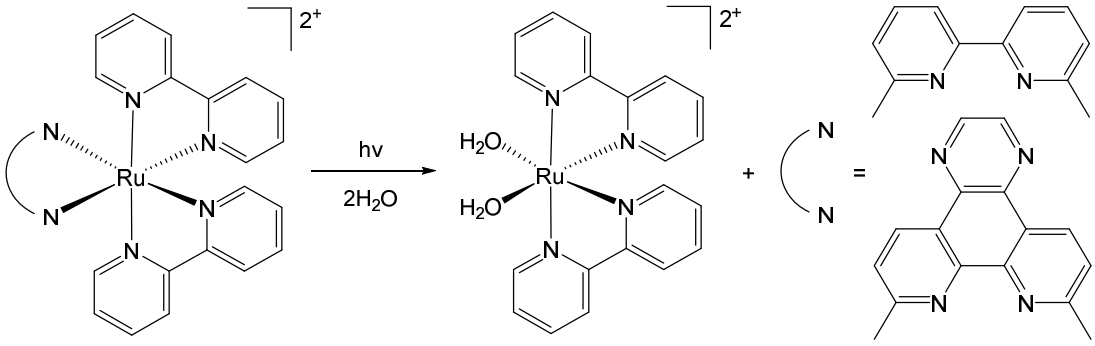

Scheme 1.3 Photoejection process of the methylated ruthenium(II) bis-bipy complexes[96]

Structural-activity relationships of polypyridyl ligands have been explored by Schatzschneider *et al.* Varying the N^N ligand in a series of $[Ru(bpy)_2(N^N)]^{2+}$ complexes (N^N = bpy, phen, dppz, dppn) and studying their cytotoxicity towards HT-29 and MCF-7 cancer cell lines the authors found there to be a positive correlation between the ligand size and anticancer activity, with the $[Ru(bpy)_2(dppn)]^{2+}$ complex (**Figure 1.16**) displaying cytotoxicity of a similar order of magnitude to cisplatin.[97] Further work on these complexes by Li *et al.* has shown that they posses the capability to efficiently photoinactivate the bacteria *E. coli*. The combination of these two key observations may be due to the complexes' ability to produce reactive oxygen species capable of cleaving DNA after photoexcitation, demonstrating the potential for these types of complexes to be used as photosensitisers in photodynamic antimicrobial chemotherapy (also known as PACT).[98-100] Yet this is one of a plethora of cases of antibacterial activity observed for ruthenium polypyridyl complexes. Aldrich-Wright and Bolhuis have shown three ruthenium(II) intercalators all exhibit antibacterial ability, with the Ru(dppz) complex emitting the greatest activity against *B. subtilis, S. aureus* and, more notably, MRSA strains of bacteria.[101]

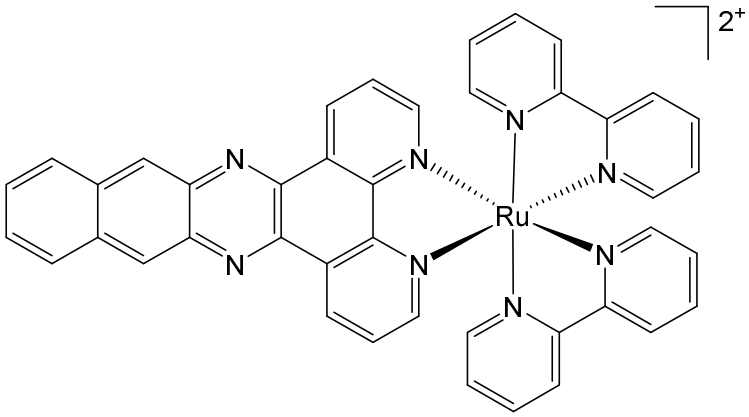

Figure 1.16 Cytotoxic and antibacterial agent Ru dppn[97]

A study into the mechanism by which a series of ruthenium(II) complexes that contain β-carboline alkaloid ligands (**Figure 1.17**) generate their anti-proliferative effects has been carried out by Xu *et al.* revealing that these complexes are able to provoke ROS generation and autophagy followed by apoptosis in human cancer cell lines. Additionally, they found that the cell membrane penetration abilities and *in vitro* DNA binding affinities of these complexes correlated with the cytotoxicity, and with CLMS studies indicating that these complexes accumulate mainly in the nucleus of the cell. This reinforces the theory that the activity is due to DNA binding interactions. However, the most active complex actually showed limited nuclear accumulation but rather was found to be distributed throughout the cytosol, suggesting that DNA binding may not be the sole cytotoxic mechanism.[102] Their more recent work involving a coordinated naturally occurring β-carboline alkaloid Norharman (9H-pyrido[3,4-b]indole) showed potent anticancer activity towards a range of cell lines. Apoptosis, in this case, was shown to be induced by mitochondrial dysfunction and ROS generation, with *in vitro* studies again showing DNA is a potential cellular target.[103]

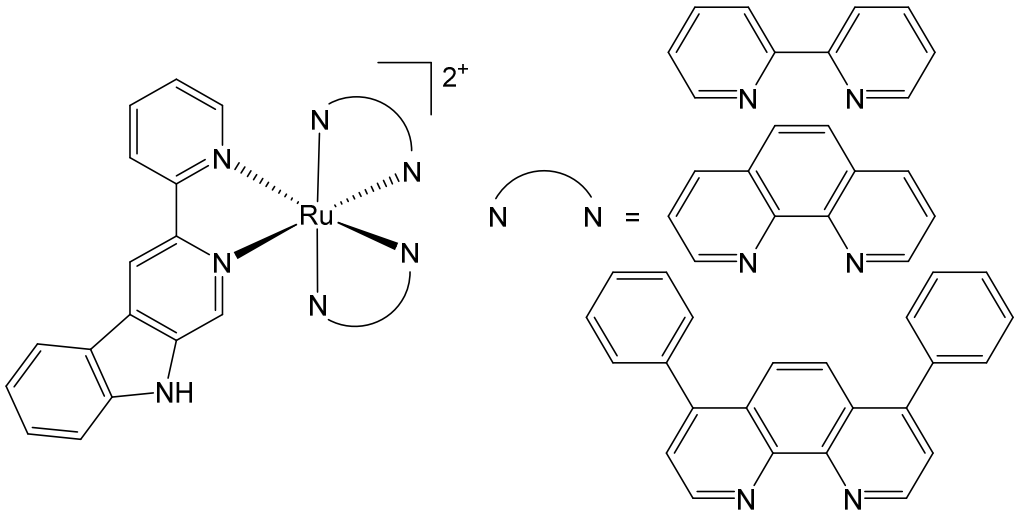

Figure 1.17 Ruthenium(II) β-carboline alkaloid complexes[103]

1.6 Ferrocene in Cancer Therapy

Ferrocene (**Figure 1.18**) is a sandwich compound consisting of an iron atom bound between two cyclopentadienyl ligands. Its discovery in 1951 is regarded by some as the starting point for modern organometallic chemistry, with its stability in aqueous, aerobic media, the availability of many derivatives, and its electrochemical properties having made it an extremely popular choice for many biological applications.[104, 105] The anti-tumour activity of ferrocene takes advantage of its ease of oxidation as it involves the radical induced electron transfer between itself and another molecule, typically water, which will produce hydroxyl radicals to cleave DNA strands.[106]

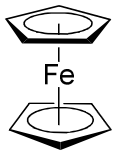

Figure 1.18 Ferrocene[104]

1.6.1 Functionalised Ferrocene

The incorporation of organometallic functionality on to a hormone was first explored by Jaouen *et al.* in the 1980s by incorporating a variety of different metal complexes

onto a protected estradiol steroid.[107] The aim of labelling hormones with organometallic moieties was to develop biochemical markers to detect an increased amount of estrogen receptors which is associated with breast cancer.[108] Among the different species formed, the ferrocene-containing 17α-ferrocenyl-17β-estradiol (**Figure 1.19**) was found to be a strong receptor inhibitor and the cytotoxic activity of ferrocenium showed the potential of functionalising drugs with organometallic groups.[109]

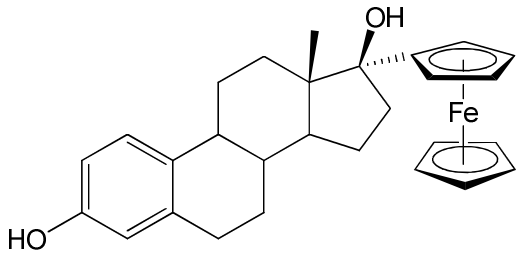

Figure 1.19 Structure of 17α-ferrocenyl 17β-estradiol[109]

In 1996, building upon their previous discovery, Jaouen *et al.* synthesised the first compound of ferrocene coupled with hydroxytamoxifen (**Figure 1.20**), the active metabolite of tamoxifen, a popular breast cancer targeting drug.[110,111] Incorporation of a biologically active metal with a biologically active molecule resulted in a collaborative effect which enhanced the anti-cancer properties of both species. The hydroxytamoxifen moiety showed activity against hormone dependant and independent tumours, whereas tamoxifen is only active towards the hormone dependant strains,[112] and the ferrocene imparts increased lipophilicity to increase cellular uptake, leading to the oxidation of the iron atom core, facilitating the formation of quinine methides which are highly cytotoxic.[113]

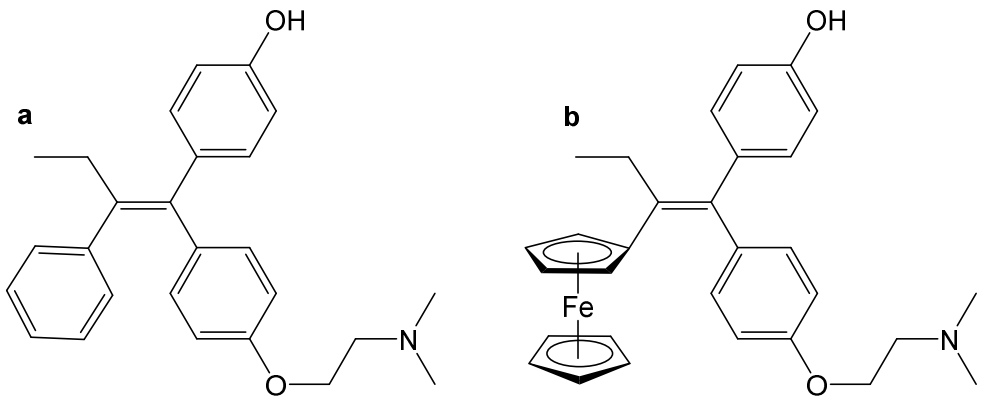

Figure 1.20 Molecular structures of **a** hydroxytamoxifen and **b** ferrocifen[110]

The success of the work done by Jaouen *et al.* has spurred the search for more ferrocene-based drugs/drug collaborations. Swarts *et al.* have produced a series containing β-diketones (**Figure 1.21**) and investigated their antineoplastic activity against human cancer cell lines. Their investigation showed that not only does the redox potential of the ferrocenyl group determine the antineoplastic activity, but also other features such as substituent chain length and relative acidity of these complexes all contributed to its cytotoxicity. The most successful compound ($R = CF_3$) was found to be up to three times more selective than cisplatin in decreasing cell growth and also showed considerable activity towards some cisplatin resistant cell lines.[114]

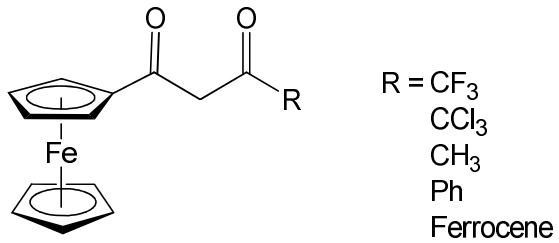

Figure 1.21 Structure of ferrocene-containing β-diketones[114]

One of the most important classes of anti-cancer agents are thioureas, aroylthioureas, *N*-nitrosoureas, diarylsulfonylureas and benzoylureas as they have a wide range of activity against solid tumours.[115] However, the low lipophilicity of these compounds causes the need for high doses of the drug to be administered to patients which is associated with adverse side effects such as the initiation of

leukaemia and other diseases.[116] Ferrocene-based *N,N'*-distributed thioureas (**Figure 1.22**) have been synthesised in an attempt to increase lipophilicity and decrease the aforementioned side effects while at the same time reducing healthy cell toxicity.[117]

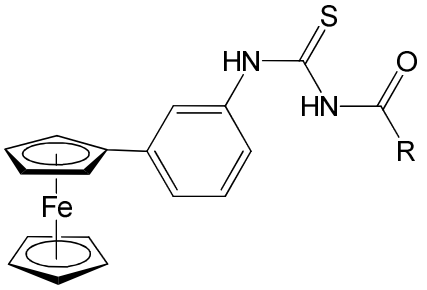

Figure 1.22 Ferrocenyl thioureas where R = phenyl groups[117]

While these compounds were not as active towards some ovarian cancer strains as cisplatin they have in fact shown activity against some cisplatin resistant tumour models. This is thought to be due to their different binding mode with DNA as voltammetric measurements have suggested that they interact electrostatically with the anionic phosphate backbone.[117]

Similarly, Huang *et al.* have recently built upon their own previous research into ferrocene derivatives as anti-cancer drugs and developed some novel ferrocene containing pyrazolyl complexes (**Figure 1.23**).[118] They found that the drugs were not quite as potent *in vitro* as cisplatin on the cell lines tested but still showed promising results.[119]

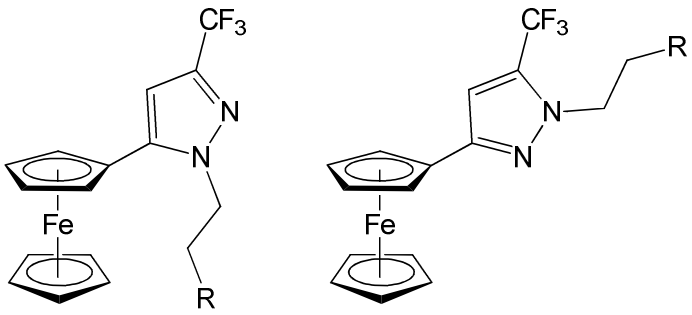

Figure 1.23 Ferrocene containing pyrazolyl where R = N-alkyl[118]

1.6.2 Ferrocene/Metal Drug Infusions

Some interesting work by Goswami *et al.* has focused on the photocytotoxic properties of ternary copper(II) complexes containing ferrocene-conjugated L-tyrosine reduced Schiff base and phenanthroline bases (**Figure 1.24**). These complexes, designed to have a dual action of DNA binding and photosensitising, showed much lower IC_{50} values in dark conditions (2.31-13.84 μM) against human cervical cancer cells in comparison to cisplatin (71.3 μM) and the phototoxic drug photofrin (41 μM) with a further reduction in those values of approximately 50% when exposed to visible light. Significant cytotoxicity was also observed towards breast cancer cells with photo-induced DNA cleavage activity occurring in blue, green and red light. Furthermore, complexes lacking the ferrocene moiety showed much lower cytotoxicity and decreased activity to DNA photocleavage, demonstrating the importance of the ferrocene in the medicinal application of these drugs.[120]

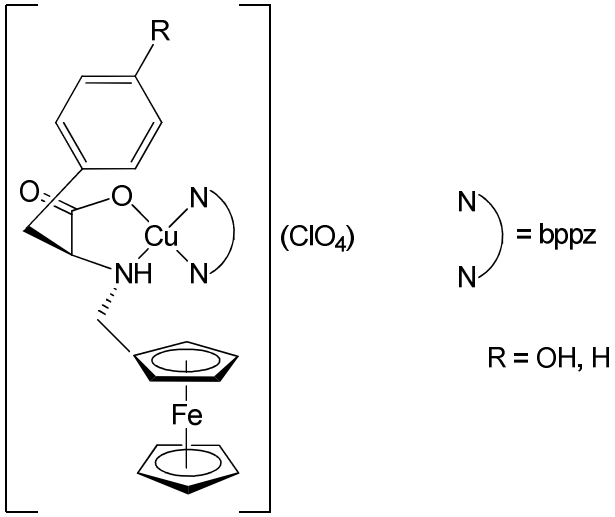

Figure 1.24 Phototoxic copper(II) complexes containing ferrocene[120]

The potential of ruthenium(II) arene complexes as anti-cancer drugs has been previously discussed within this chapter. Auzias *et al.* have combined these ruthenium complexes with ferrocene based ligands to produce novel anti-cancer agents (**Figure 1.25**). *In vitro* tests on human ovarian cancer cell lines showed that the diruthenium complexes were twice as active when compared to their monorutheium counterparts, leading to the deduction that the ruthenium-arene

motifs are responsible for the complexes activity. However, ruthenium complexes linked by an alkyl chain did not show an increase in cytotoxicity over the mononuclear analogues,[121] This suggests that the different redox potential of ferrocene is in part responsible for the increase anti-cancer effects. The IC_{50} values obtained (14.8-49.5 μM) were greater than that of cisplatin (1.6 μM) towards the same cancer cell lines although these are generally low values for ruthenium anti-cancer complexes, which are usually less active *in vitro*.[122]

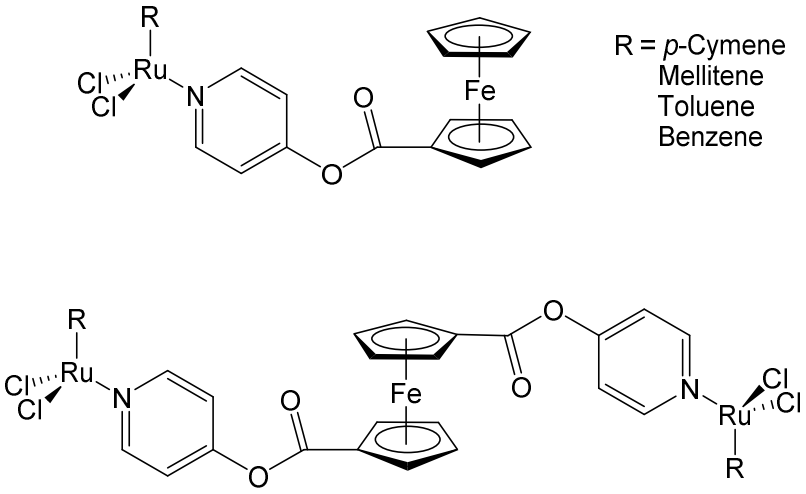

Figure 1.25 Ferrocenoyl pyridine arene ruthenium complexes[121]

Building on the success of the antimetastatic ruthenium drug NAMI-A, a series of ferrocene functionalised NAMI-A analogues (**Figure 1.26**) have been produced by Walsby *et al*.[123] Both metal components of the complexes were found to be crucial to the overall biological activity, exhibiting a synergistic effect, with the water solubility of the ferrocenylpyridine ligands vastly improving upon coordination to the NAMI salt, which in turn activated the complexes in aqueous media. The ferrocene-absent NAMI-Pyr was shown to be at least an order of magnitude less active against SW480 colorectal adenocarcinoma cells (IC_{50} > 400 μM) than the NAMI-Fc complexes (IC_{50} 35-69 μM) which have comparable cytotoxicity to that of the successful antineoplastic ruthenium(III) complexes KP1019 and NKP1339. [124-128] Further studies revealed that the presence of the ferrocene in these complexes enhanced the noncoordinate interactions with human serum albumin (hsA) protein and reduce the formation of protein-coordinated species, increasing the bioavailability of the

complexes through enhanced transmembrane transport. One of the most important properties of NAMI-A is its anti-invasive effects. Migration assays carried out on the NAMI-Fc complexes revealed that the ability to inhibit cell motility does not change in the presence of the ferrocenylpyridine ligands. The antimetastatic behaviour of these complexes, coupled with the cytotoxic properties, demonstrates the potential of these drugs in future studies and also highlights the beneficial pharmaceutical effects of the incorporated ferrocene.[123]

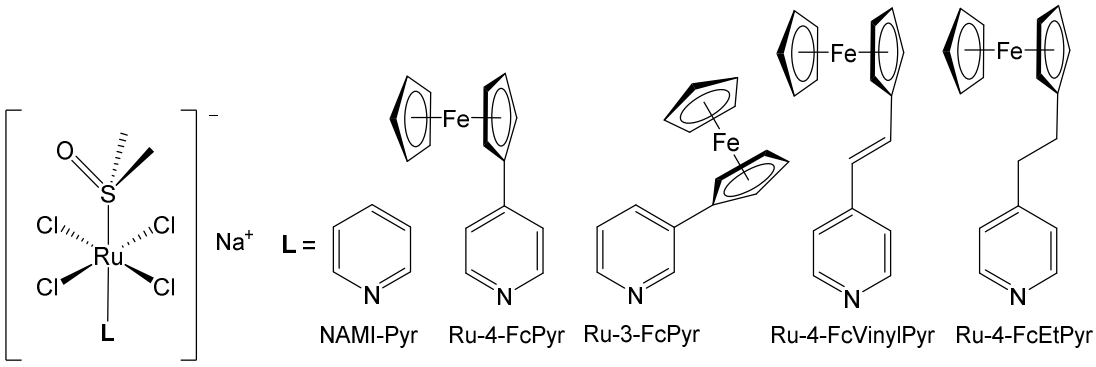

Figure 1.26 Ferrocene functionalised NAMI-A analogues[123]

Due to the huge success of platinum based complexes in cancer therapy, there has been much interest into forming a successful platinum-ferrocene collaborative drug. Dichlorido(ethane-1,2-diamine)platinum(IV) complexes and oxaliplatin derivatives (**Figure 1.27**) have been synthesised by Keppler *et al.* and their activity tested in cisplatin resistant/sensitive colon and ovarian carcinomas as well as non-small cell lung carcinomas. The anti-proliferative effects of these compounds were found to be greatest in the ovarian cancer cell lines with IC_{50} values in the low micromolar range (0.84-2.3 μM) but in contrast the IC_{50} values found for the colon (2.7-46 μM) and lung carcinomas (24-84 μM) were in the intermediate range with the oxaliplatin derivatives possessing more cytotoxicity in all cases.[129] It is worth noting that the complexes reported by Keppler *et al*. are platinum(IV) metals whereas cisplatin and oxaliplatin are in the +2 oxidation state, therefore the platinum(IV) complexes have to be activated inside the organism by reduction so they cannot be assessed based solely on their *in vitro* investigations.

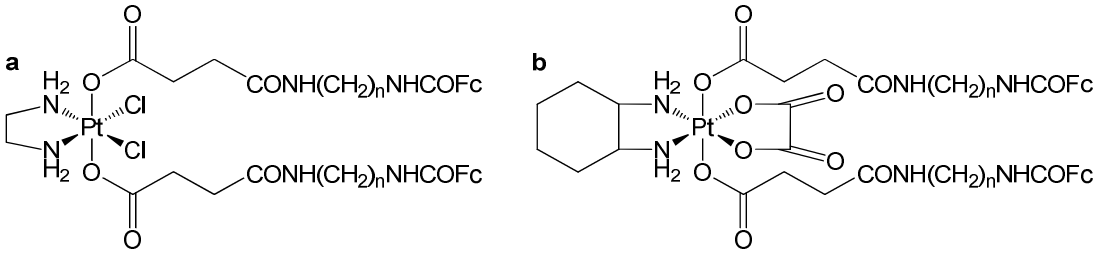

Figure 1.27 Example of **a** a dichlorido(ethane-1,2-diamine)platinum(IV) complex and **b** an oxaliplatin derivative[129]

Recent work by Nieto *et al.* who were studying the anti-cancer activity of heterometallic platinum(II) compounds with β-aminoethylferrocenes has yielded very promising results.[130] They have demonstrated the synthesis and first cell culture tests of ferrocene-platinum derivatives with one particularly exciting result (**Figure 1.28**). This *cis*-configured complex showed *in vitro* activity against multiple cancer cell lines including human breast, lung, colon and cervical cancers with IC_{50} values in the low micromolar range (1.7-2.3 µM) for all lines tested. What makes this complex exceptional is that its anti-proliferative activity is superior to that of cisplatin (1.9-26 µM), especially in the more drug resistant colon cell lines (2.3 µM compared to cisplatin's 26 µM).[130] Cell cycle studies have shown that these compounds undergo a different mechanism of action than cisplatin but further investigations are required to identify the specific mechanism and the exact biological target.

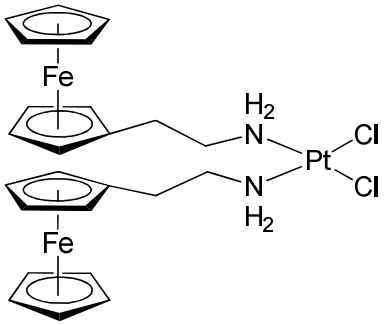

Figure 1.28 Heterometallic platinum(II) compound with β-aminoethylferrocenes[130]

1.7 Aims and Objectives

This project aims to build upon the recent success of ferrocene-based ligands used in conjunction with other metal complexes to enhance their anti-cancer activity. The overall objective of this project is to synthesise novel metal complexes by binding ruthenium metal centres to ferrocene through different bidendate β-diketonate ligands containing O- donor atoms (**Scheme 1.4**). The anti-cancer potential of the synthesised complexes will be evaluated through cell line testing and further studies will be undertaken to deduce any structural activity relationships.

The overall objectives are as follows:

- Synthesise a range of β-diketonate ferrocene ligands (**Scheme 1.4, Route A**), varying their electronic and steric properties to maximise their anti-cancer potential when incorporated into the complex. These will be fully characterised using ^{1}H NMR spectroscopy, ^{13}C NMR spectroscopy, mass spectrometry, micro-analysis and X-ray crystallographic studies.
- Synthesise a range of bimetallic metal complexes containing β-diketonate ferrocene ligands (**Scheme 1.4, Route B/C**), and fully characterise them using ^{1}H NMR spectroscopy, ^{13}C NMR spectroscopy, mass spectrometry, micro-analysis and X-ray crystallographic studies.
- Investigate the anti-cancer potential of these complexes and ligands by the use of several biological assays to determine their cytotoxicity and effect on healthy cells.
- Structural activity relationships (SAR) of the metal complexes will be probed further through studies to determine their hydrolysis and hydrophobic properties, for example.

The β-diketonate ferrocene ligands will be formed from adapted versions of the synthetic routes used by Swarts *et al.* and Shi *et al.* (**Scheme 1.4, Route A**).[114,131]

The production of the ruthenium complexes will follow the synthetic routes previously used by members of the McGowan group (**Scheme 1.4, Route B**)[132] and adapted methods from literature procedure (**Scheme 1.4, Route C**).[133]

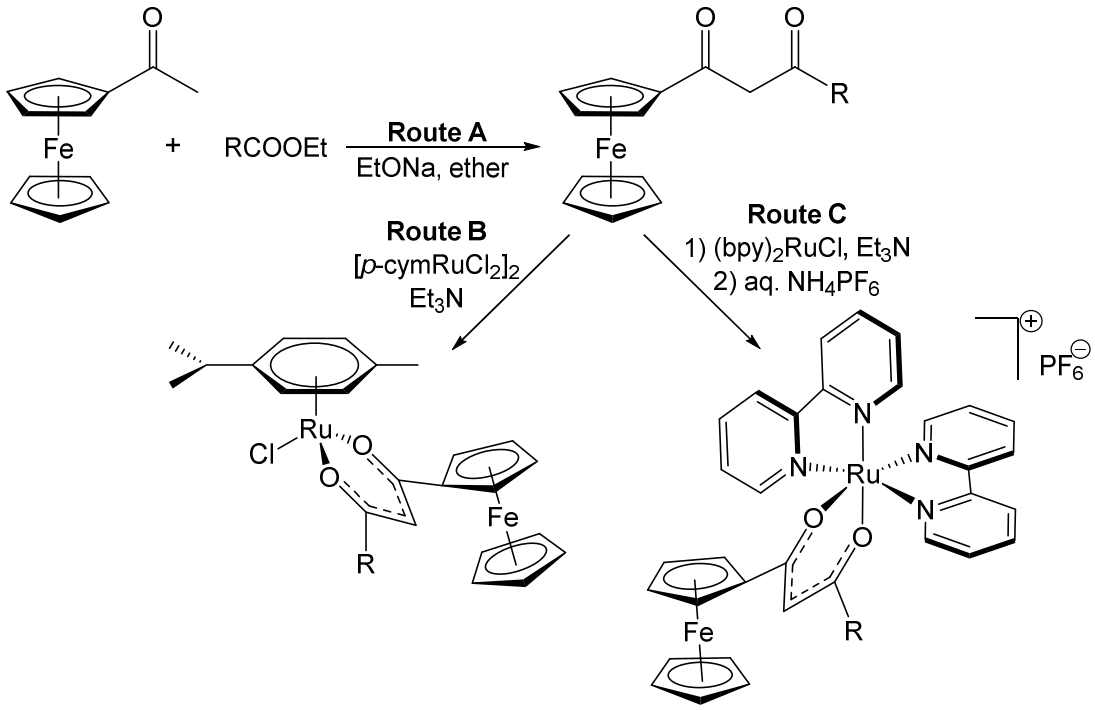

Scheme 1.4 Proposed starting synthetic routes for the formation of ferrocene β-diketonate ruthenium metal complexes

1.8 References

1. Cancer Research UK, *Cancer Incidence and Mortality in the UK*, http://publications.cancerresearchuk.org/downloads/Product/CS_REPORT_TOP10INCMORT.pdf, Accessed 03/10/2014, 2014.
2. R. Siegel, J. Ma, Z. Zou and A. Jemal, *CA: A Cancer Journal for Clinicians*, 2014, **64**, 9-29.
3. Department of Health, *Helping More People Survive Cancer*, https://www.gov.uk/government/policies/helping-more-people-survive-cancer, Accessed 03/10/2014, 2014.
4. Cancer Research UK, *Cancer Stats: Cancer Statistics for the UK*, https://www.gov.uk/government/policies/helping-more-people-survive-cancer, Accessed 03/10/2014, 2014.
5. J. L. Bos, *Cancer Research*, 1989, **49**, 4682-4689.
6. D. Hanahan and R. A. Weinberg, *Cell*, 2000, **100**, 57-70.
7. S. Jain, *Cancer Cell International*, 2002, **2**, 13.
8. A. B. Miller, B. Hoogstraten, M. Staquet and A. Winkler, *Cancer*, 1981, **47**, 207-214.
9. S. P. Fricker, *Dalton Transactions*, 2007, 4903-4917.
10. N. C. Lloyd, H. W. Morgan, B. K. Nicholson and R. S. Ronimus, *Angewandte Chemie International Edition*, 2005, **44**, 941-944.
11. W. Kean, C. Lock and H. Howard-Lock, *Inflammopharmacology*, 1991, **1**, 103-114.
12. E. A. Pacheco, E. R. Tiekink and M. W. Whitehouse, *Gold: Science and Applications*, 2010, 217.
13. W. Kean, L. Hart and W. Buchanan, *Rheumatology*, 1997, **36**, 560-572.
14. C. F. Shaw, *Chemical Reviews*, 1999, **99**, 2589-2600.
15. G. Jaouen and N. Metzler-Nolte, *Medicinal Organometallic Chemistry*, Springer, 2010.
16. L. Kelland, *Nature Reviews Cancer*, 2007, **7**, 573-584.
17. J. Schacht, A. E. Talaska and L. P. Rybak, *The Anatomical Record: Advances in Integrative Anatomy and Evolutionary Biology*, 2012, **295**, 1837-1850.
18. E. R. Jamieson and S. J. Lippard, *Chemical Reviews*, 1999, **99**, 2467-2498.

19. D. R. Feldman, G. J. Bosl, J. Sheinfeld and R. J. Motzer, *JAMA*, 2008, **299**, 672-684.
20. V. M. Gonzalez, M. A. Fuertes, C. Alonso and J. M. Perez, *Molecular Pharmacology*, 2001, **59**, 657-663.
21. A. K. Holzer, G. Samimi, K. Katano, W. Naerdemann, X. Lin, R. Safaei and S. B. Howell, *Molecular Pharmacology*, 2004, **66**, 817-823.
22. Z. H. Siddik, *Oncogene*, 0000, **22**, 7265-7279.
23. M. S. Davies, S. J. Berners-Price and T. W. Hambley, *Inorganic Chemistry*, 2000, **39**, 5603-5613.
24. T. W. Hambley, *Journal of the Chemical Society, Dalton Transactions*, 2001, 2711-2718.
25. R. A. Alderden, M. D. Hall and T. W. Hambley, *Journal of Chemical Education*, 2006, **83**, 728.
26. D. Wang and S. J. Lippard, *Nature Reviews Drug Discovery*, 2005, **4**, 307-320.
27. E. Cvitkovic, *Cancer Treatment Reviews*, 1998, **24**, 265-281.
28. R. B. Weiss and M. C. Christian, *Drugs*, 1993, **46**, 360-377.
29. D. Lebwohl and R. Canetta, *European Journal of Cancer*, 1998, **34**, 1522-1534.
30. U. Frey, J. D. Ranford and P. J. Sadler, *Inorganic Chemistry*, 1993, **32**, 1333-1340.
31. N. J. Wheate, S. Walker, G. E. Craig and R. Oun, *Dalton Transactions*, 2010, **39**, 8113-8127.
32. L. R. Kelland, *Expert Opinion on Investigational Drugs*, 2000, **9**, 1373-1382.
33. H. Choy, C. Park and M. Yao, *Clinical Cancer Research*, 2008, **14**, 1633-1638.
34. C. Ceresa, A. Bravin, G. Cavaletti, M. Pellei and C. Santini, *Current Medicinal Chemistry*, 2014, **21**, 2237-2265.
35. M. L. Rothenberg, A. M. Oza, R. H. Bigelow, J. D. Berlin, J. L. Marshall, R. K. Ramanathan, L. L. Hart, S. Gupta, C. A. Garay, B. G. Burger, N. Le Bail and D. G. Haller, *Journal of Clinical Oncology*, 2003, **21**, 2059-2069.
36. I. Judson and L. R. Kelland, *Drugs*, 2000, **59**, 29-36.
37. E. Meggers, *Current Opinion in Chemical Biology*, 2007, **11**, 287-292.
38. C. S. Allardyce and P. J. Dyson, *Platinum Metals Review*, 2001, **45**, 62-69.
39. M. Bloemink and J. Reedijk, *Metal Ions in Biological Systems*, 1996, **32**, 641.

40. H. Yamada, T. Koike and J. K. Hurst, *Journal of the American Chemical Society*, 2001, **123**, 12775-12780.

41. E. S. Antonarakis and A. Emadi, *Cancer Chemotherapy and Pharmacology*, 2010, **66**, 1-9.

42. J. Chakravarty and S. Bhattacharya, *Polyhedron*, 1996, **15**, 1047-1055.

43. S. Baitalik and B. Adhikary, *Polyhedron*, 1997, **16**, 4073-4080.

44. E. Musgrove, C. Rugg, I. Taylor and D. Hedley, *Journal of Cellular Physiology*, 1984, **118**, 6-12.

45. F. Kratz and L. Messori, *Journal of Inorganic Biochemistry*, 1993, **49**, 79-82.

46. H. Sun, H. Li and P. J. Sadler, *Chemical Reviews*, 1999, **99**, 2817-2842.

47. J. Weaver, H. Zhan and S. Pollack, *British Journal of Haematology*, 1993, **83**, 138-144.

48. S. S. Yun, I.-H. Suh, S.-S. Choi, T.-H. Kim and S. Lee, *Journal of Coordination Chemistry*, 1999, **47**, 315-318.

49. G. Sava and A. Bergamo, *International Journal of Oncology*, 2000, **17**, 353-418.

50. A. Bergamo, R. Gagliardi, V. Scarcia, A. Furlani, E. Alessio, G. Mestroni and G. Sava, *Journal of Pharmacology and Experimental Therapeutics*, 1999, **289**, 559-564.

51. B. Gava, S. Zorzet, P. Spessotto, M. Cocchietto and G. Sava, *Journal of Pharmacology and Experimental Therapeutics*, 2006, **317**, 284-291.

52. M. Bacac, A. C. G. Hotze, K. v. d. Schilden, J. G. Haasnoot, S. Pacor, E. Alessio, G. Sava and J. Reedijk, *Journal of Inorganic Biochemistry*, 2004, **98**, 402-412.

53. M. Bouma, B. Nuijen, M. T. Jansen, G. Sava, A. Flaibani, A. Bult and J. H. Beijnen, *International Journal of Pharmaceutics*, 2002, **248**, 239-246.

54. C. G. Hartinger, M. A. Jakupec, S. Zorbas-Seifried, M. Groessl, A. Egger, W. Berger, H. Zorbas, P. J. Dyson and B. K. Keppler, *Chemistry & Biodiversity*, 2008, **5**, 2140-2155.

55. M. Pongratz, P. Schluga, M. A. Jakupec, V. B. Arion, C. G. Hartinger, G. Allmaier and B. K. Keppler, *Journal of Analytical Atomic Spectrometry*, 2004, **19**, 46-51.

56. E. Lindauer and E. Holler, *Biochemical Pharmacology*, 1996, **52**, 7-14.

57. I. Ott and R. Gust, *Archiv der Pharmazie*, 2007, **340**, 117-126.

58. C. G. Hartinger, S. Zorbas-Seifried, M. A. Jakupec, B. Kynast, H. Zorbas and B. K. Keppler, *Journal of Inorganic Biochemistry*, 2006, **100**, 891-904.

59. C. G. Hartinger, S. Zorbas-Seifried, M. A. Jakupec, B. Kynast, H. Zorbas and B. K. Keppler, *Journal of Inorganic Biochemistry*, 2006, **100**, 891-904.

60. W. Sheldrick and S. Heeb, *Inorganica Chimica Acta*, 1990, **168**, 93-100.

61. H. Chen, J. A. Parkinson, S. Parsons, R. A. Coxall, R. O. Gould and P. J. Sadler, *Journal of the American Chemical Society*, 2002, **124**, 3064-3082.

62. H. Chen, J. A. Parkinson, R. E. Morris and P. J. Sadler, *Journal of the American Chemical Society*, 2003, **125**, 173-186.

63. O. Novakova, H. Chen, O. Vrana, A. Rodger, P. J. Sadler and V. Brabec, *Biochemistry*, 2003, **42**, 11544-11554.

64. R. Aird, J. Cummings, A. Ritchie, M. Muir, R. Morris, H. Chen, P. Sadler and D. Jodrell, *British Journal of Cancer*, 2002, **86**, 1652-1657.

65. A. Bergamo, A. Masi, A. F. A. Peacock, A. Habtemariam, P. J. Sadler and G. Sava, *Journal of Inorganic Biochemistry*, 2010, **104**, 79-86.

66. C. S. Allardyce, P. J. Dyson, D. J. Ellis and S. L. Heath, *Chemical Communications*, 2001, 1396-1397.

67. C. Scolaro, A. Bergamo, L. Brescacin, R. Delfino, M. Cocchietto, G. Laurenczy, T. J. Geldbach, G. Sava and P. J. Dyson, *Journal of Medicinal Chemistry*, 2005, **48**, 4161-4171.

68. B. Lippert, *Verlag Helvetica Chimica Acta, Zürich*, 1999.

69. P. J. Dyson and G. Sava, *Dalton Transactions*, 2006, 1929-1933.

70. C.-W. Jiang, H. Chao, X.-L. Hong, H. Li, W.-J. Mei and L.-N. Ji, *Inorganic Chemistry Communications*, 2003, **6**, 773-775.

71. J.-G. Liu, B.-H. Ye, Q.-L. Zhang, X.-H. Zou, Q.-X. Zhen, X. Tian and L.-N. Ji, *JBIC Journal of Biological Inorganic Chemistry*, 2000, **5**, 119-128.

72. H.-L. Huang, Z.-Z. Li, Z.-H. Liang and Y.-J. Liu, *European Journal of Inorganic Chemistry*, 2011, **2011**, 5538-5547.

73. M. R. Gill and J. A. Thomas, *Chemical Society Reviews*, 2012, **41**, 3179-3192.

74. M. B. Kastan and J. Bartek, *Nature*, 2004, **432**, 316-323.

75. C. Metcalfe and J. A. Thomas, *Chemical Society Reviews*, 2003, **32**, 215-224.

76. A. E. Friedman, J. C. Chambron, J. P. Sauvage, N. J. Turro and J. K. Barton, *Journal of the American Chemical Society*, 1990, **112**, 4960-4962.

77. R. M. Hartshorn and J. K. Barton, *Journal of the American Chemical Society*, 1992, **114**, 5919-5925.

78. C. Hiort, P. Lincoln and B. Norden, *Journal of the American Chemical Society*, 1993, **115**, 3448-3454.

79. J. K. Barton, A. Danishefsky and J. Goldberg, *Journal of the American Chemical Society*, 1984, **106**, 2172-2176.

80. S. Satyanarayana, J. C. Dabrowiak and J. B. Chaires, *Biochemistry*, 1993, **32**, 2573-2584.

81. G. I. Pascu, A. C. G. Hotze, C. Sanchez-Cano, B. M. Kariuki and M. J. Hannon, *Angewandte Chemie*, 2007, **119**, 4452-4456.

82. F. E. Poynton, S. A. Bright, S. Blasco, D. C. Williams, J. M. Kelly and T. Gunnlaugsson, *Chemical Society Reviews*, 2017, **46**, 7706-7756.

83. F. Heinemann, J. Karges and G. Gasser, *Accounts of Chemical Research*, 2017, **50**, 2727-2736.

84. C. Mari and G. Gasser, *CHIMIA International Journal for Chemistry*, 2015, **69**, 176-181.

85. G. Shi, S. Monro, R. Hennigar, J. Colpitts, J. Fong, K. Kasimova, H. Yin, R. DeCoste, C. Spencer, L. Chamberlain, A. Mandel, L. Lilge and S. A. McFarland, *Coordination Chemistry Reviews*, 2015, **282-283**, 127-138.

86. TheraLase, *Theralase Files US Patent Application for Increased Targeting of Photo Dynamic Therapy*, http://theralase.com/pressrelease/theralase-files-us-patent-application-increased-targeting-photo-dynamic-therapy/.

87. P. Kaspler, S. Lazic, S. Forward, Y. Arenas, A. Mandel and L. Lilge, *Photochemical & Photobiological Sciences*, 2016, **15**, 481-495.

88. J. Fong, K. Kasimova, Y. Arenas, P. Kaspler, S. Lazic, A. Mandel and L. Lilge, *Photochemical & Photobiological Sciences*, 2015, **14**, 2014-2023.

89. G. Shi, S. Monro, R. Hennigar, J. Colpitts, J. Fong, K. Kasimova, H. Yin, R. DeCoste, C. Spencer and L. Chamberlain, *Coordination Chemistry Reviews*, 2015, **282**, 127-138.

90. C. Gaiddon, P. Jeannequin, P. Bischoff, M. Pfeffer, C. Sirlin and J. P. Loeffler, *Journal of Pharmacology and Experimental Therapeutics*, 2005, **315**, 1403-1411.

91. V. Vidimar, X. Meng, M. Klajner, C. Licona, L. Fetzer, S. Harlepp, P. Hébraud, M. Sidhoum, C. Sirlin, J.-P. Loeffler, G. Mellitzer, G. Sava, M. Pfeffer and C. Gaiddon, *Biochemical Pharmacology*, 2012, **84**, 1428-1436.

92. L. Fetzer, B. Boff, M. Ali, M. Xiangjun, J.-P. Collin, C. Sirlin, C. Gaiddon and M. Pfeffer, *Dalton Transactions*, 2011, **40**, 8869-8878.

93. B. Durham, J. V. Caspar, J. K. Nagle and T. J. Meyer, *Journal of the American Chemical Society*, 1982, **104**, 4803-4810.

94. P. C. Ford, *Coordination Chemistry Reviews*, 1982, **44**, 61-82.

95. B. S. Howerton, D. K. Heidary and E. C. Glazer, *Journal of the American Chemical Society*, 2012, **134**, 8324-8327.

96. C. Mari, V. Pierroz, S. Ferrari and G. Gasser, *Chemical Science*, 2015, **6**, 2660-2686.

97. U. Schatzschneider, J. Niesel, I. Ott, R. Gust, H. Alborzinia and S. Wölfl, *ChemMedChem*, 2008, **3**, 1104-1109.

98. W. Lei, Q. Zhou, G. Jiang, B. Zhang and X. Wang, *Photochemical & Photobiological Sciences*, 2011, **10**, 887-890.

99. S. P. Foxon, M. A. Alamiry, M. G. Walker, A. J. Meijer, I. V. Sazanovich, J. A. Weinstein and J. A. Thomas, *The Journal of Physical Chemistry A*, 2009, **113**, 12754-12762.

100. Y. Sun, L. E. Joyce, N. M. Dickson and C. Turro, *Chemical Communications*, 2010, **46**, 2426-2428.

101. A. Bolhuis, L. Hand, J. E. Marshall, A. D. Richards, A. Rodger and J. Aldrich-Wright, *European Journal of Pharmaceutical Sciences*, 2011, **42**, 313-317.

102. C. Tan, S. Lai, S. Wu, S. Hu, L. Zhou, Y. Chen, M. Wang, Y. Zhu, W. Lian and W. Peng, *Journal of Medicinal Chemistry*, 2010, **53**, 7613-7624.

103. C. Tan, S. Wu, S. Lai, M. Wang, Y. Chen, L. Zhou, Y. Zhu, W. Lian, W. Peng and L. Ji, *Dalton Transactions*, 2011, **40**, 8611-8621.

104. D. R. van Staveren and N. Metzler-Nolte, *Chemical Reviews*, 2004, **104**, 5931-5986.

105. M. Patra and G. Gasser, *Nature Reviews Chemistry*, 2017, **1**, 0066.

106. D. Osella, M. Ferrali, P. Zanello, F. Laschi, M. Fontani, C. Nervi and G. Cavigiolio, *Inorganica Chimica Acta*, 2000, **306**, 42-48.

107. G. Jaouen, S. Top, A. Laconi, D. Couturier and J. Brocard, *Journal of the American Chemical Society*, 1984, **106**, 2207-2208.

108. A. Vessieres, S. Top, A. A. Ismail, I. S. Butler, M. Louer and G. Jaouen, *Biochemistry*, 1988, **27**, 6659-6666.

109. E. Meléndez, *Inorganica Chimica Acta*, 2012, **393**, 36-52.

110. S. Top, B. Dauer, J. Vaissermann and G. Jaouen, *Journal of Organometallic Chemistry*, 1997, **541**, 355-361.

111. S. Top, J. Tang, A. Vessières, D. Carrez, C. Provot and G. Jaouen, *Chemical Communications*, 1996, 955-956.

112. A. Nguyen, A. Vessières, E. A. Hillard, S. Top, P. Pigeon and G. Jaouen, *CHIMIA International Journal for Chemistry*, 2007, **61**, 716-724.

113. G. Sava, A. Bergamo and P. J. Dyson, *Dalton Transactions*, 2011, **40**, 9069-9075.

114. J. C. Swarts, T. G. Vosloo, S. J. Cronje, W. C. Du Plessis, C. E. J. Van Rensburg, E. Kreft and J. E. Van Lier, *Anticancer Research*, 2008, **28**, 2781-2784.

115. Y.-M. Zhang, T.-B. Wei, L. Xian and L.-M. Gao, *Phosphorus, Sulfur, and Silicon and the Related Elements*, 2004, **179**, 2007-2013.

116. S. Nishizawa, P. Bühlmann, K. P. Xiao and Y. Umezawa, *Analytica Chimica Acta*, 1998, **358**, 35-44.

117. B. Lal, A. Badshah, A. A. Altaf, M. N. Tahir, S. Ullah and F. Huq, *Australian Journal of Chemistry*, 2013, **66**, 1352-1360.

118. X.-F. Huang, J.-F. Tang, J.-L. Ji, X.-L. Wang and B.-F. Ruan, *Journal of Organometallic Chemistry*, 2012, **706–707**, 113-123.

119. X.-F. Huang, L.-Z. Wang, L. Tang, Y.-X. Lu, F. Wang, G.-Q. Song and B.-F. Ruan, *Journal of Organometallic Chemistry*, 2014, **749**, 157-162.

120. T. K. Goswami, S. Gadadhar, A. A. Karande and A. R. Chakravarty, *Polyhedron*, 2013, **52**, 1287-1298.

121. H. Chen, J. A. Parkinson, O. Nováková, J. Bella, F. Wang, A. Dawson, R. Gould, S. Parsons, V. Brabec and P. J. Sadler, *Proceedings of the National Academy of Sciences*, 2003, **100**, 14623-14628.

122. M. Auzias, B. Therrien, G. Süss-Fink, P. Štěpnička, W. H. Ang and P. J. Dyson, *Inorganic Chemistry*, 2007, **47**, 578-583.

123. C. Mu, S. W. Chang, K. E. Prosser, A. W. Y. Leung, S. Santacruz, T. Jang, J. R. Thompson, D. T. T. Yapp, J. J. Warren, M. B. Bally, T. V. Beischlag and C. J. Walsby, *Inorganic Chemistry*, 2016, **55**, 177-190.

124. S. Kapitza, M. Pongratz, M. Jakupec, P. Heffeter, W. Berger, L. Lackinger, B. Keppler and B. Marian, *Journal of Cancer Research and Clinical Oncology*, 2005, **131**, 101-110.

125. C. Bartel, A. E. Egger, M. A. Jakupec, P. Heffeter, M. Galanski, W. Berger and B. K. Keppler, *JBIC Journal of Biological Inorganic Chemistry*, 2011, **16**, 1205-1215.

126. P. Heffeter, K. Böck, B. Atil, M. A. R. Hoda, W. Körner, C. Bartel, U. Jungwirth, B. K. Keppler, M. Micksche and W. Berger, *JBIC Journal of Biological Inorganic Chemistry*, 2010, **15**, 737-748.

127. M. A. Jakupec, E. Reisner, A. Eichinger, M. Pongratz, V. B. Arion, M. Galanski, C. G. Hartinger and B. K. Keppler, *Journal of Medicinal Chemistry*, 2005, **48**, 2831-2837.

128. S. Kapitza, M. A. Jakupec, M. Uhl, B. K. Keppler and B. Marian, *Cancer Letters*, 2005, **226**, 115-121.

129. J. Banfić, A. A. Legin, M. A. Jakupec, M. Galanski and B. K. Keppler, *European Journal of Inorganic Chemistry*, 2014, **2014**, 484-492.

130. D. Nieto, A. M. Gonzalez-Vadillo, S. Bruna, C. J. Pastor, C. Rios-Luci, L. G. Leon, J. M. Padron, C. Navarro-Ranninger and I. Cuadrado, *Dalton Transactions*, 2012, **41**, 432-441.

131. Y.-C. Shi, H.-M. Yang, W.-B. Shen, C.-G. Yan and X.-Y. Hu, *Polyhedron*, 2004, **23**, 15-21.

132. R. M. Lord, University of Leeds, PhD thesis, 2014.

133. Y. Y. Lee, D. B. Walker, J. J. Gooding and B. A. Messerle, *Dalton Transactions*, 2014, **43**, 12734-12742.

Chapter 2: Synthesis of Ferrocene β-diketonate Ligands

2.0 Ligand Synthesis

The ligands synthesised in this report have been prepared from adapted methods used by Swarts *et al.*[1] and have built upon the library of β-diketonate ligands which have previously been synthesised in the McGowan group.[2,3] All ligands have been fully characterised by ^{1}H NMR spectroscopy, ^{13}C [^{1}H] NMR spectroscopy, mass spectrometry and micro-analysis (**Figure 2.1**). X-ray crystallographic data has also been obtained for all ligands where possible.

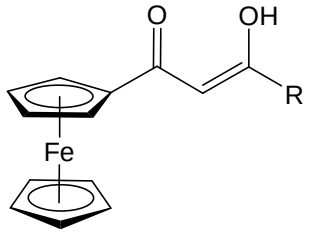

R = Me	**L1**	3'-MePh	**L9**	3',5'-ClPh	**L17**	4-Py	**L25**
CF_3	**L2**	3',5'-MePh	**L10**	4'-BrPh	**L18**	2-Py	**L26**
CHF_2	**L3**	4'-FPh	**L11**	3'-BrPh	**L19**		
3-Furan	**L4**	3'-FPh	**L12**	4'-IPh	**L20**		
2-Furan	**L5**	2'-FPh	**L13**	3'-IPh	**L21**		
Ph	**L6**	3',5'-FPh	**L14**	4'-OMePh	**L22**		
1-Naph	**L7**	4'-ClPh	**L15**	3'-OMePh	**L23**		
4'-MePh	**L8**	3'-ClPh	**L16**	4'-OEtPh	**L24**		

Figure 2.1 Synthesised β-diketonate ligands reported in this chapter

2.1 β-Diketonate Ferrocene Ligands

2.1.1 Synthesis of β-Diketonate Ferrocene Ligands

β-Diketonate ferrocene ligands have been produced *via* a Claisen condensation type reaction from acetyl ferrocene with a range of benzoates and acetates in the presence of sodium ethoxide (**Scheme 2.1**).[4] All of the ligands were purified by column chromatography to give pure solids with yields ranging from 20-96 %.

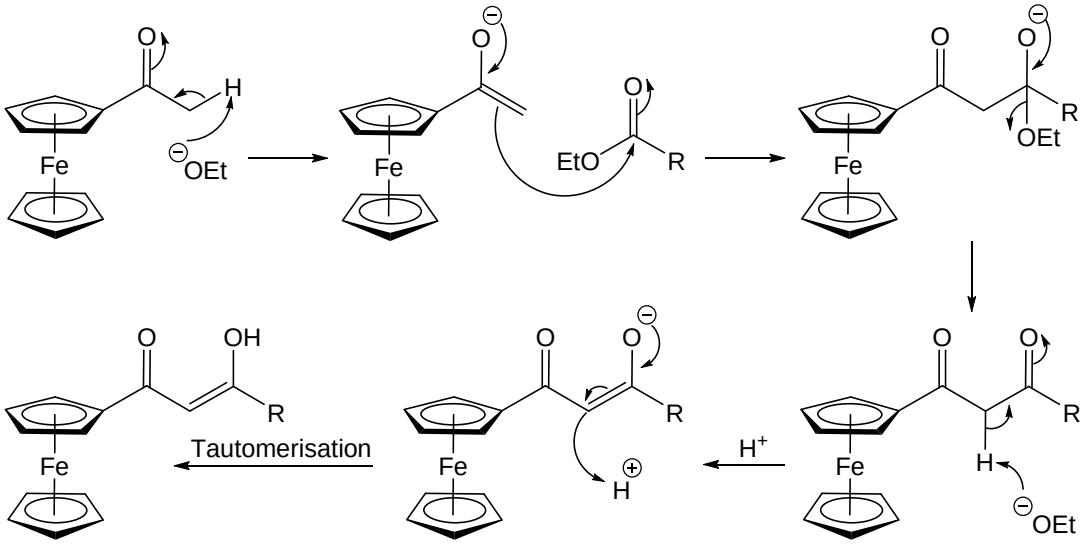

Scheme 2.1 Claisen condensation mechanism for the formation of β-diketonate ferrocene ligands

2.1.2 NMR Characterisation of β-Diketonate Ferrocene Ligands

The ^{1}H NMR data of all the β-diketonate ligands (**Figure 2.2**) show a characteristic methine singlet peak from the hydrogen in the centre of the enol which occurs around 5.6-6.9 ppm. This was used to deduce whether or not the reaction was successful. NMR samples were first prepared in chloroform-d but the obtained spectra showed broad peaks (**Figure 2.2**). This was attributed partly to the fluctuating nature of the ligands as they can undergo tautomerisation between the cyclic enol and diketo forms. The use of more polar deuterated solvents were able to stabilise the enol system through hydrogen bonding interactions, producing sharp peaks in the NMR spectra (**Figure 2.2**).[5]

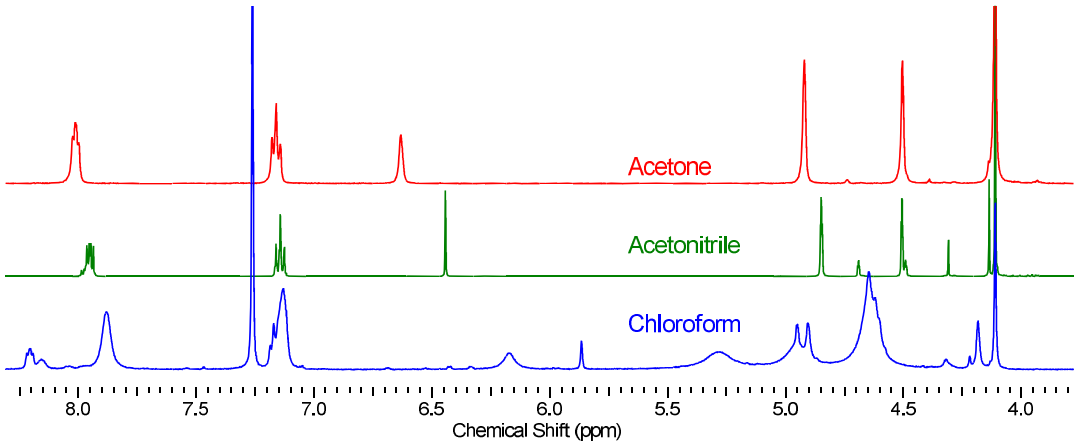

Figure 2.2 ^{1}H NMR spectra (500MHz) for β-diketonate ferrocene ligand **L11** in varying deuterated solvents

The ^{1}H NMR spectra of the ligands all follow the general trend (an example is shown in **Figure 2.3**) with the highest chemical shifts in the region of 7.0-8.0 ppm which are assigned to any aromatic hydrogens (**i** and **J**). The characteristic methine proton (**f**) singlet peak is found in the region of 5.5-7.0 ppm. The hydrogens bound to the Cp rings of ferrocene produce three peaks; two from the different proton environments of the top Cp ring (**b** and **c**), typically found in the region of 4.5-5.0 ppm, and one from the bottom Cp ring (**a**) where all protons are in the same environment and therefore produce a large singlet peak in the NMR spectra in the region of 4.0-4.5 ppm. In the cases where alkyl moieties are present, the proton signals are found in the region of 2.0-4.0 ppm.

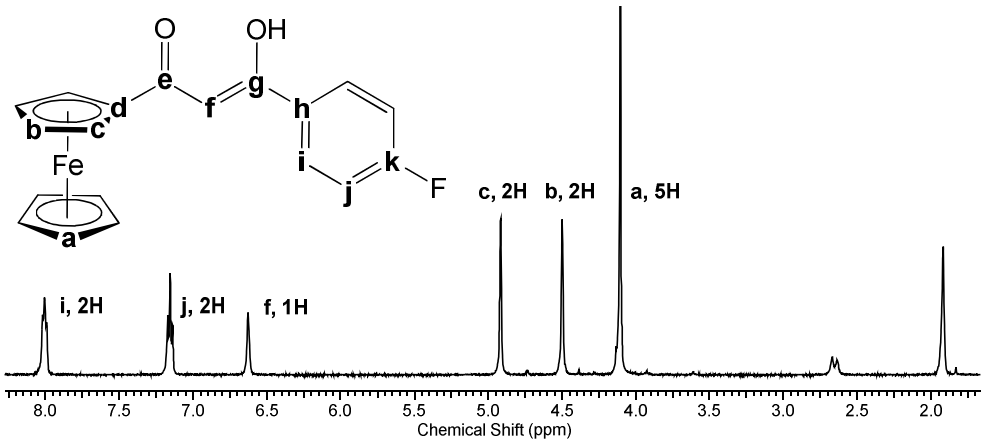

Figure 2.3 ^{1}H NMR spectra (500 MHz, Acetone-d_6) for β-diketonate ferrocene ligand **L11**

The ^{13}C [^{1}H] NMR spectra of the pure ligands also follow a general trend. The greatest chemical shift arises from the carbonyl carbons (**e** and **g**) due to the deshielding from the adjacent oxygen atoms; these peaks arise in the region of 175-195 ppm. Quaternary aromatic carbon (**h** and **k**) peaks are in the region of 130-160 ppm and protonated aromatic carbon (**i** and **j**) peaks arise in the region of 100-130 ppm. The peak from the methine carbon (**f**) is in the region of 90-95 ppm which is slightly higher than that of the carbons in the ferrocene Cp rings (**a**-**d**), found in the region of 65-80 ppm. Any alkyl moieties present in the ligands show peaks in the NMR between 20-30 ppm. Full assignments given in Chapter 7.

2.1.3 X-ray Characterisation of β-Diketonate Ferrocene Ligands

X-ray crystallographic data was obtained for all ligands except **L17** and **L25.** Ligands **L1**,[1] **L2**,[1] **L5**,[6] **L6**[7] and **L26**[8] had previously been synthesised but no crystal structure was obtained. Crystals suitable for X-ray crystallographic analysis were obtained by the slow evaporation of acetonitrile for all ligands apart from **L2** and **L3**, which were grown from the vapour diffusion of pentane into dichloromethane solutions; red/orange crystals were obtained in all cases. A typical labelling scheme is shown in **Figure 2.4** and molecular structures of the ligands are shown in **Figure 2.5**. The ligands crystallised into monoclinic cells in all cases except for **L1**, **L5** and **L23** (orthorhombic), **L14** (triclinic) and **L4** and **L21** (tetragonal). Structural solutions were performed in $P2_1/c$ (**L6**, **L10**, **L11**, **L13**, **L10**, **L22**, **L24** and **L26**), $P2_1/n$ (**L2**, **L3**, **L7**-**L9**, **L12**, **L15** and **L18**), $P2_12_12_1$ (**L1** and **L5**), $P4_2/n$ (**L21**), *Pbca* (**L23**), *P*-1 (**L14**), C_2/c (**L16** and **L19**) and *I*-4 (**L4**) with one molecule per asymmetric unit in all cases except **L7** which possesses four molecules per asymmetric unit.

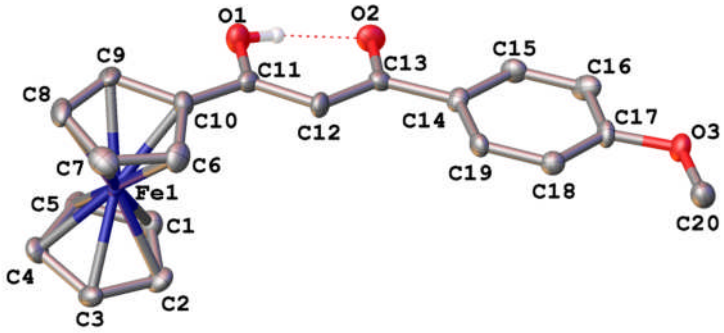

Figure 2.4 Typical labelling scheme for all ligands. Hydrogen atoms are omitted for clarity and thermal ellipsoids at the 50% probability level.

The ferrocene moiety adopts an eclipsed geometry in all cases (except **L24** which adopts a staggered geometry), which has been postulated to be the energetically preferred conformer.[9-11] All ligand molecules display a planar structure with angles of 119-122˚ and bond lengths of 1.3-1.4 Å around the β-diketonate centre which is typical of the enol tautomeric form.[12, 13] The O2-C13-C12 bond angle of **L2** (125.5˚), **L3** (126.2˚) and **L7** (117.5˚) deviates from this general observation. In the case of **L7**, the increased steric bulk and electronic repulsion of the naphthyl moiety may repel O2, decreasing the O2-C13-C12 bond angle. The larger O2-C13-C12 bond angle of **L2** and **L3** may arise from potential hydrogen bonding interactions between the CF_3/CHF_2 substituents and O2-H. Short intramolecular hydrogen bonding interactions are observed between O-H…O at a distance of 2.4-2.5 Å (D…A) in all cases which is characteristic for acetylacetone molecules in their enol formation.[12, 13] Notable bond lengths and angles are shown in **Table 2.1** and **Table 2.2**, respectively.

Table 2.1 Notable bond lengths for ligands. ESDs given in parentheses.

Ligand	Bond Distance (Å)			
	O1-C11	O2-C13	C11-C12	C12-C13
L1	1.286(4)	1.304(4)	1.413(4)	1.393(4)
L2	1.291(7)	1.268(8)	1.420(9)	1.379(9)
L3	1.255(9)	1.313(12)	1.445(11)	1.342(11)
L4	1.311(4)	1.279(4)	1.384(4)	1.410(4)
L5	1.313(4)	1.296(5)	1.398(5)	1.397(5)
L6	1.292(3)	1.304(3)	1.397(4)	1.388(4)
L7	1.290(5)	1.306(5)	1.405(6)	1.383(5)
L8	1.265(6)	1.325(6)	1.428(7)	1.365(7)
L9	1.278(3)	1.316(3)	1.423(3)	1.372(3)
L10	1.270(2)	1.330(2)	1.433(3)	1.374(3)
L11	1.305(2)	1.293(2)	1.398(2)	1.400(3)
L12	1.264(3)	1.329(3)	1.439(3)	1.364(3)
L13	1.270(2)	1.325(2)	1.429(2)	1.376(2)
L14	1.280(3)	1.312(3)	1.417(3)	1.381(3)
L15	1.274(7)	1.332(7)	1.436(8)	1.355(8)
L16	1.263(2)	1.329(2)	1.441(3)	1.355(3)
L18	1.274(9)	1.319(10)	1.426(10)	1.360(11)
L19	1.265(2)	1.334(2)	1.439(3)	1.364(3)
L20	1.280(3)	1.323(3)	1.420(4)	1.372(4)
L21	1.295(5)	1.315(5)	1.410(6)	1.368(6)
L22	1.286(4)	1.304(4)	1.413(4)	1.393(4)
L23	1.264(3)	1.321(3)	1.436(4)	1.369(4)
L24	1.274(3)	1.316(3)	1.426(3)	1.375(3)
L26	1.286(3)	1.298(3)	1.414(4)	1.380(4)

Table 2.2 Notable bond angles for ligands. ESDs given in parenthesis.

Ligand	Bond Angle (˚)		
	O1-C11-C12	O2-C13-C12	C11-C12-C13
L1	120.1(6)	121.2(5)	120.7(5)
L2	119.9(6)	125.5(6)	120.3(5)
L3	121.9(7)	126.2(10)	117.9(9)
L4	121.2(3)	121.4(3)	119.7(3)
L5	120.1(3)	122.5(3)	120.0(3)
L6	120.5(3)	120.1(3)	121.2(3)
L7	120.2(4)	117.5(3)	120.6(4)
L8	120.5(4)	120.6(3)	120.8(4)
L9	120.7(2)	120.3(2)	120.0(2)
L10	120.9(2)	121.3(2)	120.2(2)
L11	120.7(2)	120.7(2)	120.3(2)
L12	120.8(2)	121.1(2)	120.8(2)
L13	120.3(1)	121.1(2)	119.4(1)
L14	120.6(2)	120.8(2)	120.2(2)
L15	120.2(5)	121.4(6)	120.5(5)
L16	120.6(2)	122.2(2)	120.2(2)
L18	120.5(7)	121.6(7)	120.2(7)
L19	120.8(2)	122.0(2)	120.7(2)
L20	120.6(3)	120.4(3)	120.6(3)
L21	120.0(4)	120.8(4)	120.6(4)
L22	120.8(3)	119.3(3)	119.2(3)
L23	120.8(2)	121.0(2)	120.4(2)
L24	121.1(2)	120.2(2)	120.0(2)
L26	120.5(3)	121.8(2)	120.1(3)

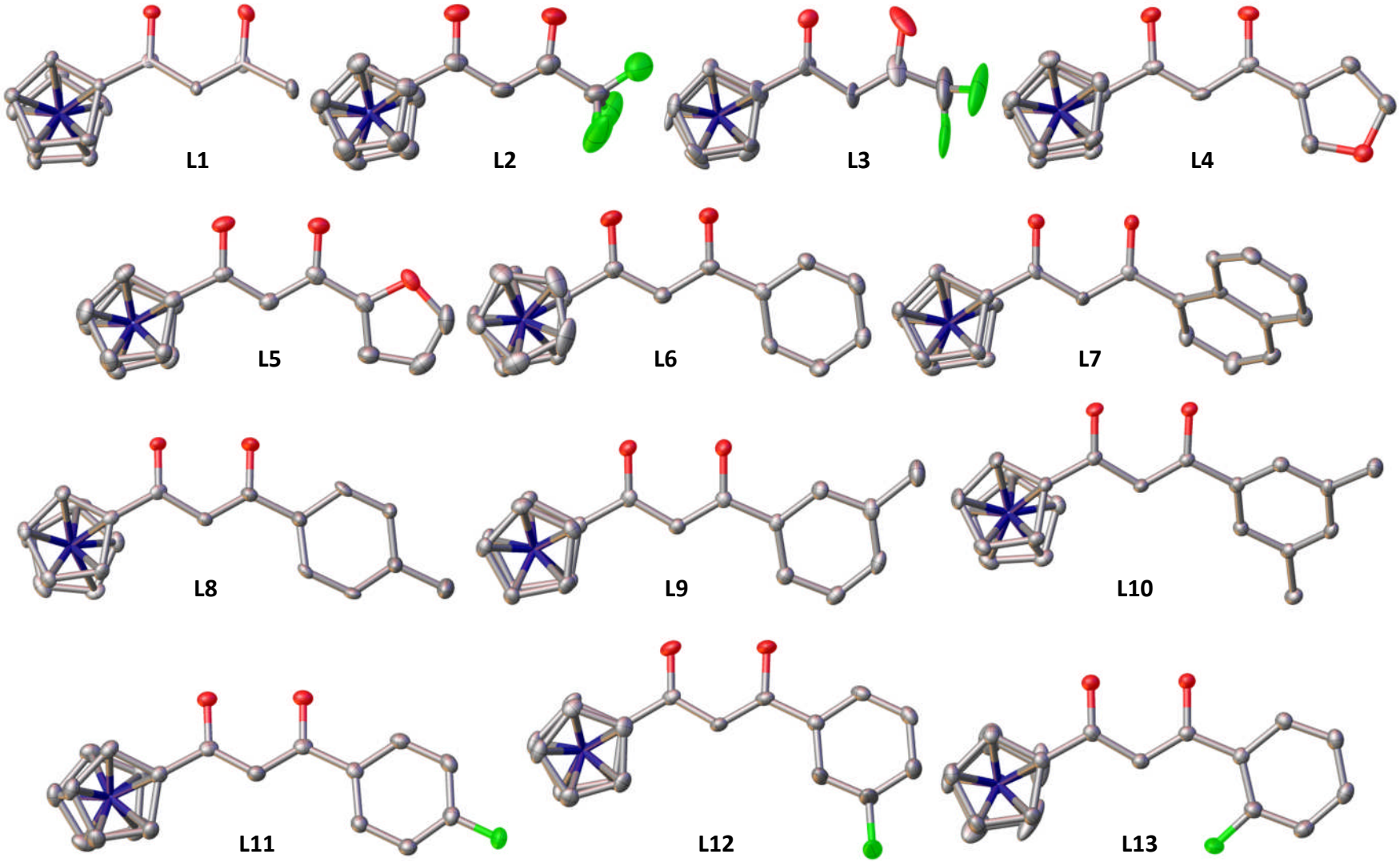
L1
L2
L3
L4
L5
L6
L7
L8
L9
L10
L11
L12
L13

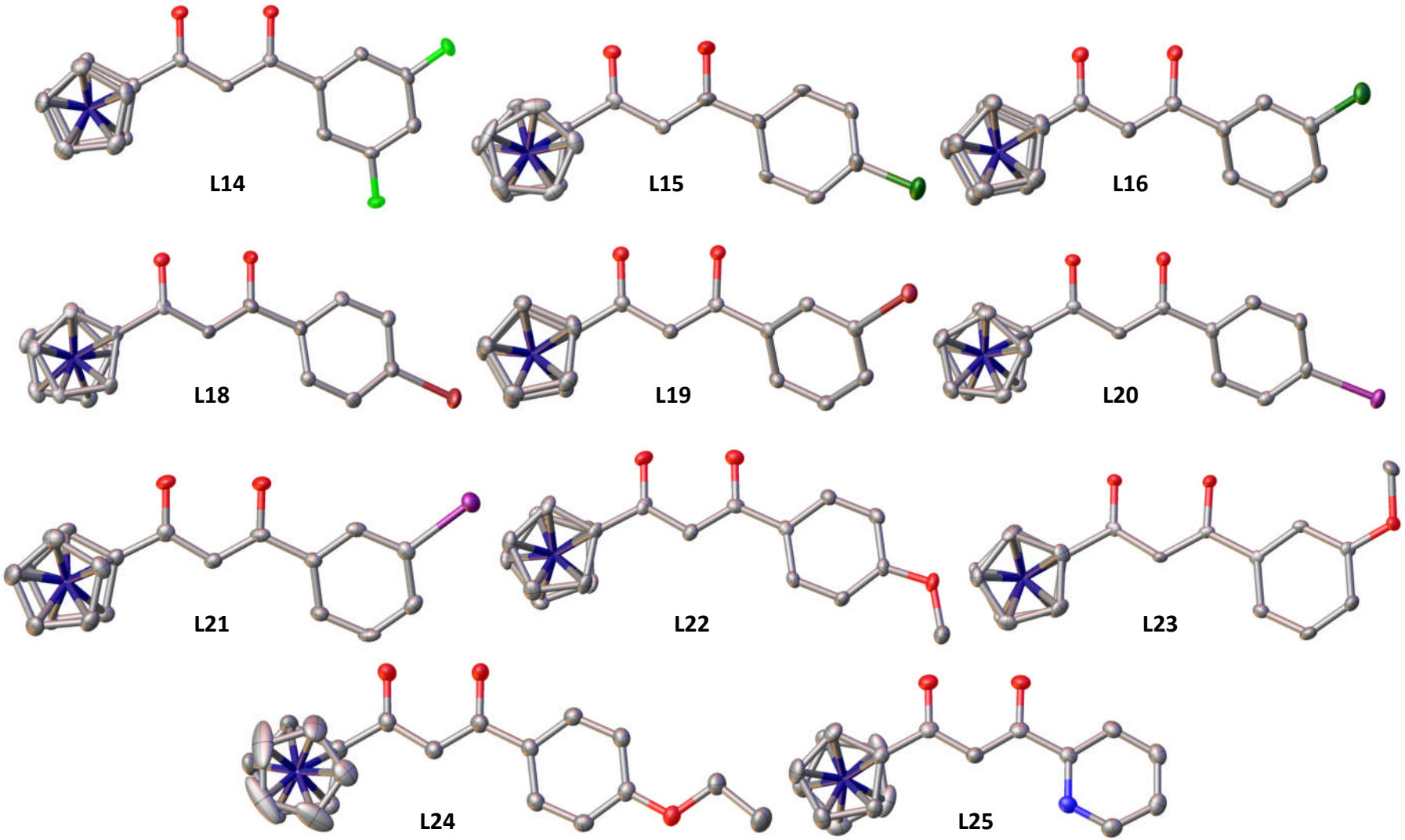

Figure 2.5 Molecular structures of ligands. Hydrogen atoms are omitted for clarity and thermal ellipsoids at the 50% probability level.

2.2 Conclusion

A library of ferrocene β-diketonate ligands with differing electronic and steric properties has been produced. These ligands have been fully characterised by ^{1}H and ^{13}C [^{1}H] NMR, mass spectrometry and micro-analysis with X-ray crystallography data being obtained for the ligands when possible. X-ray crystallographic structural solutions were performed in monoclinic space groups for all ligand complexes except for the **L1**, **L5** and **L23** (orthorhombic), **L14** (triclinic) and **L4** and **L21** (tetragonal). Ferrocene β-diketonate ligands show intramolecular hydrogen bonding between O-H…O at a distance of 2.4-2.5 Å (D…A) in all cases which restrains them into a planar orientation and the ferrocene adopts an eclipsed geometry (except **L24**). Angles of 118-126˚ and bond lengths of 1.3-1.4 Å are observed around the enol centres which is expected from a planar system and similar to previously reported acetylacetone molecules.[12, 13] Ligands were used in the formation of ruthenium-based complexes in the following chapters.

2.3 References

1. J. C. Swarts, T. G. Vosloo, S. J. Cronje, W. C. Du Plessis, C. E. J. Van Rensburg, E. Kreft and J. E. Van Lier, *Anticancer Research*, 2008, **28**, 2781-2784.
2. R. M. Lord, University of Leeds, PhD thesis, 2014.
3. A. M. B. H. Basri, University of Leeds, PhD thesis, 2014.
4. R. J. Heath and C. O. Rock, *Natural Product Reports*, 2002, **19**, 581-596.
5. T. J. Zielinski and A. Grushow, *Journal of Chemical Education*, 2002, **79**, 707.
6. L. Wolf, *Zeitschrift für Anorganische und Allgemeine Chemie*, 1963, **3**, 469-470.
7. C. E. Cain, T. A. Mashburn and C. R. Hauser, *The Journal of Organic Chemistry*, 1961, **26**, 1030-1034.
8. L. Wolf and H. Hennig, *Zeitschrift für Anorganische und Allgemeine Chemie*, 1965, **341**, 1-10.
9. F. Wang, S. Islam and V. Vasilyev, *Materials*, 2015, **8**, 7723-7737.
10. S. Carter and J. N. Murrell, *Journal of Organometallic Chemistry*, 1980, **192**, 399-408.
11. J. D. Bourke, M. T. Islam, S. P. Best, C. Q. Tran, F. Wang and C. T. Chantler, *The Journal of Physical Chemistry Letters*, 2016, **7**, 2792-2796.
12. M. S. Gordon and R. D. Koob, *Journal of the American Chemical Society*, 1973, **95**, 5863-5867.
13. A. Lowrey, C. George, P. d'Antonio and J. Karle, *Journal of the American Chemical Society*, 1971, **93**, 6399-6403.

Chapter 3: Synthesis and Characterisation of Ruthenium(II) Arene Complexes

3.0 Ruthenium(II) Arene Metal Complexes

Ruthenium compounds have been investigated in a range of medical applications such as antimicrobial agents, nitric oxide scavengers, immunosuppressants and antimalarials.[1] Work in this chapter aims to build upon the "piano stool" like ruthenium complexes with (N,N), (N,O) and (O,O) chelating ligands which have been previously studied in the McGowan and Sadler groups, among others.[2-4]

Sadler *et al.* have worked widely in this area, producing ruthenium compounds as potential anti-cancer agents.[5, 6] The bulk of these compounds follow the same recipe of a stable bidentate ligand, hydrophobic arene ligand and a single ligand exchange centre which is commonly a halogen (**Figure 3.1**). The IC_{50} values for many of these compounds were shown to be comparable, and in many cases superior, to that of cisplatin and carboplatin against A2780*cis* (cisplatin resistant human ovarian carcinoma) and A2780 (human ovarian carcinoma) cell lines.

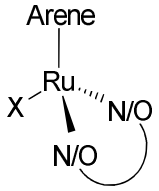

Figure 3.1 Ruthenium complex backbone used by Sadler *et al.*[2]

Recent work from McGowan *et al.* has produced a series of Cp* diphosphine ruthenium complexes with their activities biologically tested against A2780 (human ovarian carcinoma) and HT-29 (human colon carcinoma).[7] Hypoxic and normoxic studies demonstrated activity in the nanomolar range with the most active compound (**Figure 3.2 a**) producing IC_{50} values much lower than cisplatin in both environments. Further work on ruthenium β-ketoiminato complexes (**Figure 3.2 b**) from the McGowan group has yielded promising biological results by demonstrating significant cancer cell death by apoptosis and single strand DNA breakage.[8] The compounds were found to be active against MCF-7 (human breast carcinoma), HT-29 (human colon carcinoma) and A2780 with some shown to be three times more active than cisplatin towards A2780*cis*. Moreover, under hypoxic conditions the complexes

showed high activity with some showing a direct correlation between a decrease in oxygen concentration and activity.

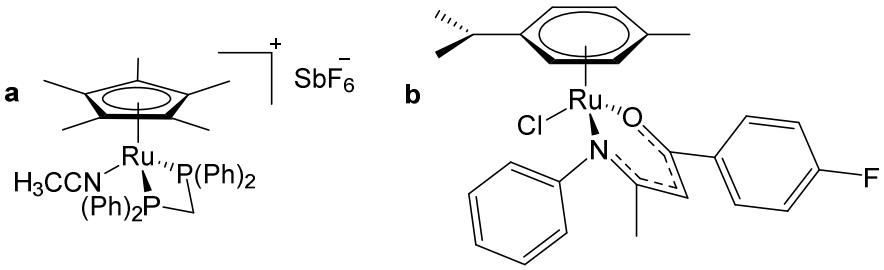

Figure 3.2 Compounds previously synthesised by McGowan *et al.*[7, 8]

3.1 Synthesis of Ruthenium(II) *p*-Cymene Complexes

All β-diketonate ruthenium complexes were prepared by methods adapted from those which have been previously used in the McGowan group.[9] Two equivalents of ferrocene β-diketonate ligand were stirred at room temperature overnight with triethylamine and $[p\text{-cymRuCl}_2]_2$ in dichloromethane (**Scheme 3.1**). Complexes were purified by column chromatography and obtained as orange micro-crystalline solids in yields of 68-91 %.

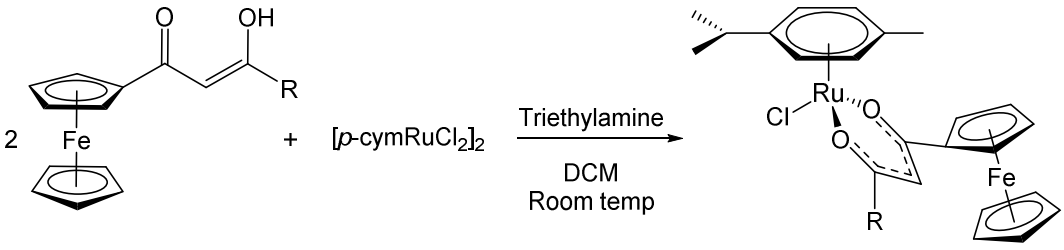

R = Me	**C1**	3'-MePh	**C9**	3',5'-ClPh	**C17**
CF_3	**C2**	3',5'-MePh	**C10**	4'-BrPh	**C18**
CHF_2	**C3**	4'-FPh	**C11**	3'-BrPh	**C19**
3-Furan	**C4**	3'-FPh	**C12**	4'-IPh	**C20**
2-Furan	**C5**	2'-FPh	**C13**	3'-IPh	**C21**
Ph	**C6**	3',5'-FPh	**C14**	4'-OMePh	**C22**
1-Naph	**C7**	4'-ClPh	**C15**	3'-OMePh	**C23**
4'-MePh	**C8**	3'-ClPh	**C16**	4'-OEtPh	**C24**

Scheme 3.1 General synthetic pathway for ruthenium(II) compounds

All complexes produced are novel (**C1**-**C24, Scheme 3.1**) and were fully characterised by ^{1}H NMR spectroscopy, ^{13}C [^{1}H] NMR spectroscopy, mass spectrometry and micro analysis. X-ray crystallographic data was obtained for all complexes except **C2**, **C7** and **C9.**

3.1.1 NMR Characterisation of Ruthenium(II) *p*-Cymene Complexes

The ^{1}H NMR spectra of all [(β-diketonate)(*p*-cym)Ru(II)Cl] complexes (**Figure 3.3**) show the upfield shift from the ferrocene top face Cp protons as two broad triplets (**k**) and two broad quartets (**j**), one proton per peak, at 4.2-5.0 ppm. Prior to the complexation the ferrocene top face Cp ring gave only two signals in the NMR spectra, two protons per peak, at 4.5-5.0 ppm, but due to intramolecular interactions and loss of symmetry of the ligand upon complexation the protons exist in different environments. Another characteristic shift from the complexation is the shift of the methine proton (**n**) much further upfield (in the case of **Figure 3.3**, 0.6 ppm from 6.6 ppm to 6.0 ppm) in comparison to the free β-diketonate ligands.

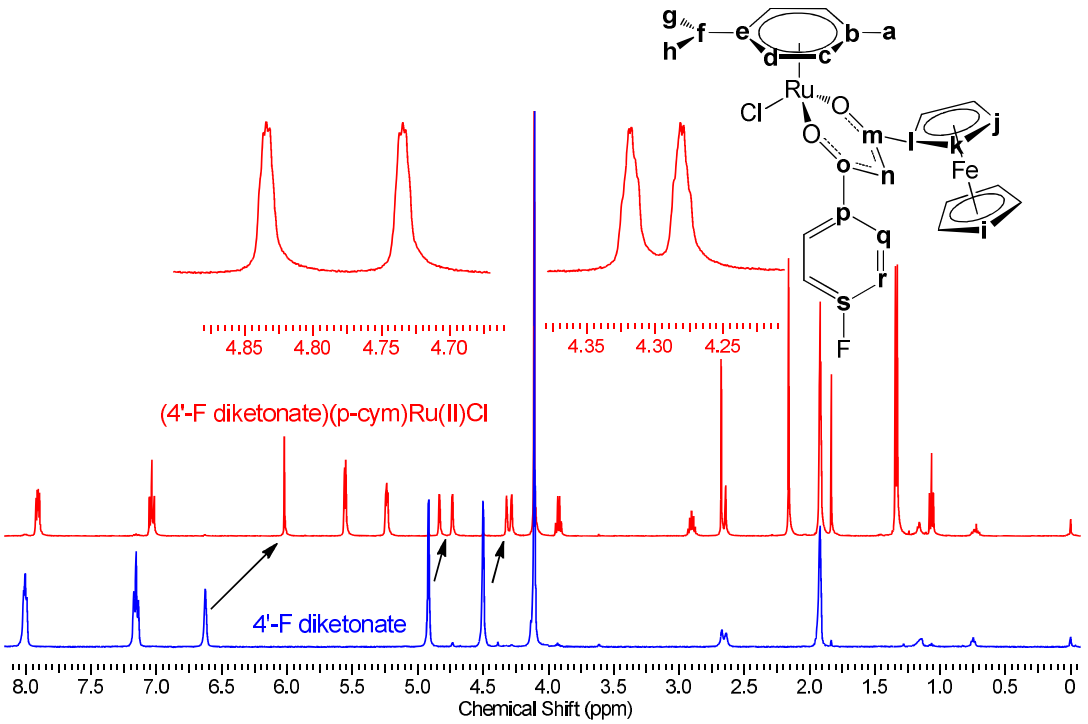

Figure 3.3 ^{1}H NMR (500 MHz, Acetone-d_6) for ruthenium complex (red) and free β-diketonate ligand (blue)

The ^{13}C [^{1}H] NMR spectra of all (β-diketonate)(*p*-cym)Ru(II)Cl complexes also follow a general trend. The furthest downfield peaks, which correspond to the carbonyl carbons (**o** and **m**), appear in the 170-190 ppm range. Although this is a similar range to the carbonyl carbons of the free ligands, there is an observed upfield shift of the corresponding peaks in the ^{13}C [^{1}H] NMR spectra of the complexes. The methine carbon (**n**) peak is also shifted slightly upfield during complexation reaction and is located in the same region the aromatic *p*-cymene carbon (**b**-**e**) signals in the region of 80-100 ppm. Furthermore, the complexation reaction splits the peaks seen between 65-85 ppm from the top Cp ring of ferrocene (**j-l**) in a similar manner to that previously mentioned in the ^{1}H NMR data, which is displayed as five separate peaks instead of the three seen in the case of the β-diketonate ligand only. Full characterisation given in Chapter 7.

3.1.2 X-Ray Characterisation of Ruthenium(II) *p*-Cymene Complexes

Single crystals of all complexes except **C2**, **C7** and **C9** were obtained from the slow evaporation or vapour diffusion methods which afforded red/orange irregular crystals in all cases. X-ray crystallographic data solutions were performed in monoclinic cells in all cases except complex **C14** which was triclinic and complex **C3** which was orthorhombic. All bound ferrocene ligands display a planar structure with the ferrocene adopting an eclipsed geometry, as seen in the case of the free ligands, for all complexes except **C13** and **C24**. Upon complexation, the bond lengths of the β-diketonate ligand centres become more symmetrical and similar in length compared to the free ligands; this is attributed to the delocalisation of electrons around the β-diketonate centre. Furthermore, there is a significant change in the bond angles around the β-diketonate ligand centres, increasing from 118-126˚ to 124-129˚, presumably due to the steric and electronic effects of binding to ruthenium. A typical labelling scheme is shown in **Figure 3.4.**

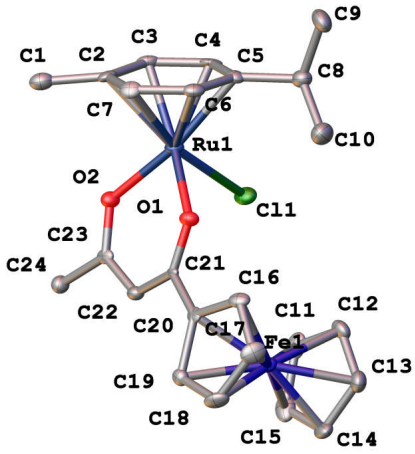

Figure 3.4 Typical labelling scheme for all complexes. Hydrogen atoms are omitted for clarity and thermal ellipsoids at the 50% probability level.

All complexes adopt the expected "piano stool" structures with the angles around the ruthenium metal centre showing geometry which is common for the *pseudo* octahedral structures. Bonding interactions observed in the solid state have been noted due to the potential for these interactions to play a crucial role in the anticancer activity through processes such as DNA or enzyme binding. Intramolecular hydrogen bonding interactions (D…A 3.3-4.0 Å) are seen between the bottom Cp ring of ferrocene (C11-C15) and Cl1 in all cases except complex **C3**; these interactions could be a contributing factor to the upfield shift and splitting of the Cp signals observed in the ^{1}H NMR spectra. Further intramolecular hydrogen bonding interactions are observed between the *p*-cymene C8-C10 and Cl1 in many cases, while interactions between the *p*-cymene C8-C10 and O1/O2 are observed in all complexes except **C3** and **C21**. Intermolecular hydrogen bonding interactions (D…A 3.1-4.1 Å) occur in all complexes, typically between the *p*-cymene moiety (C1-C10) and Cl1/O1/O2 of adjacent molecules, although multiple other intermolecular hydrogen bonding interactions occur depending on the electronic and steric properties of the R substituent. Complex **C23** was the only molecule which displayed π-π stacking interactions.

3.1.2.1 X-Ray Characterisation of Complex C1

Orange single crystals of complex **C1** were obtained by the vapour diffusion of dichloromethane and pentane at 4 ˚C. The molecular structure is shown in **Figure 3.5** with notable bond lengths and angles stated in **Table 3.1**. Intramolecular and intermolecular interactions are shown in **Figure 3.6** with bond lengths and angles stated in **Table 3.2**. Complex **C1** crystallised in a monoclinic cell and structural solution performed in the $P2_1/c$ space group with two molecules per asymmetric unit. Atoms corresponding to the second molecule in the asymmetric unit are marked by an asterisk.

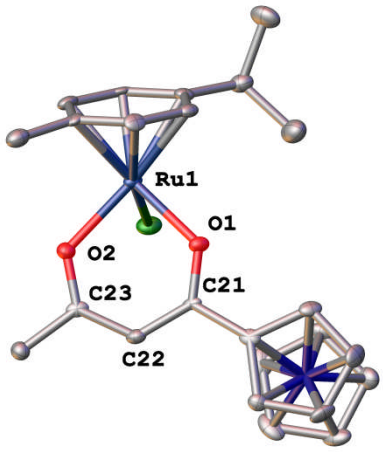

Figure 3.5 Molecular structure of complex **C1.** Hydrogen atoms are omitted for clarity and thermal ellipsoids at the 50% probability level.

Bond	Distance (Å)	Bond	Angle (˚)
Ru1-O1	**2.057(3)**	**O1-Ru1-O2**	**87.78(12)**
Ru1-O2	**2.079(3)**	**Ru1-O1-C21**	**126.2(3)**
O1-C21	**1.279(5)**	**Ru1-O2-C23**	**125.7(3)**
O2-C23	**1.275(5)**	**O1-C21-C22**	**126.1(4)**
C21-C22	**1.400(6)**	**O2-C23-C22**	**126.2(4)**
C22-C23	**1.392(6)**	**C21-C22-C23**	**125.0(4)**

Table 3.1 Bond lengths and angles for complex **C1**. ESDs given in parentheses.

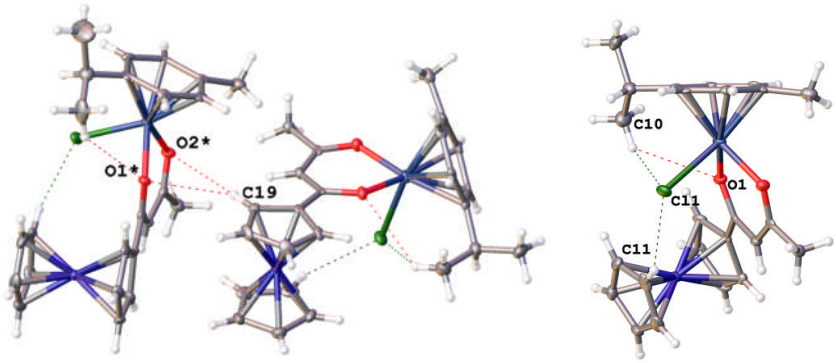

Figure 3.6 Intermolecular and intramolecular interactions for complex **C1**. Only selected intermolecular interactions shown for charity.

Interaction	Bond D…A	Distance (Å)	Bond D…A	Distance (Å)
Intramolecular	**C11-H…Cl1**	**3.790(5)**	**C10-H…Cl1**	**3.880(6)**
	C10-H…O1	**3.548(7)**		
Intermolecular	**C7*-H…O2**	**3.257(5)**	**C3-H…Cl1***	**3.775(5)**
	C7*-H…Cl1	**3.900(4)**	**C19-H…O1***	**3.601(6)**
	C3-H…O2*	**3.300(3)**	**C19-H…O2***	**3.925(5)**

Table 3.2 Intermolecular and intramolecular bond lengths and angles for complex **C1.** ESDs given in parentheses.

3.1.2.2 X-Ray Characterisation of Complex C3

Orange single crystals of complex **C3** were obtained by the slow evaporation of acetonitrile. The molecular structure is shown in **Figure 3.7** with notable bond lengths and angles stated in **Table 3.3**. Intramolecular and intermolecular interactions are shown in **Figure 3.8** with bond lengths and angles stated in **Table 3.4**. Complex **C3** crystallised in an orthorhombic cell and structural solution performed in the *Pbca* space group with one molecule per asymmetric unit. The structure showed disorder around the CHF_2 group, with the F atoms being split across three partitions in a 0.3:0.84:0.86 ratio.

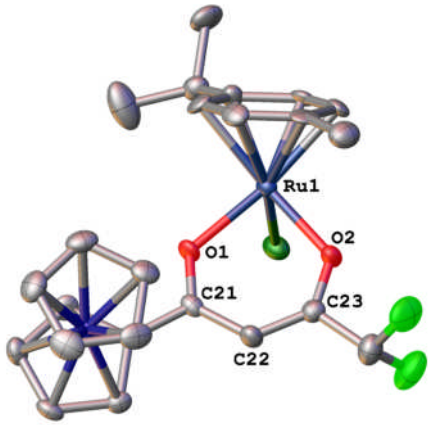

Figure 3.7 Molecular structure of complex **C3**. Hydrogen atoms are omitted for clarity and thermal ellipsoids at the 50% probability level.

Bond	Distance (Å)	Bond	Angle (˚)
Ru1-O1	2.082(4)	O1-Ru1-O2	88.65(17)
Ru1-O2	2.076(4)	Ru1-O1-C21	127.4(4)
O1-C21	1.260(7)	Ru1-O2-C23	124.1(4)
O2-C23	1.282(8)	O1-C21-C22	125.0(6)
C21-C22	1.418(9)	O2-C23-C22	129.3(6)
C22-C23	1.362(9)	C21-C22-C33	125.4(6)

Table 3.3 Bond lengths and angles for complex **C3**. ESDs given in parentheses.

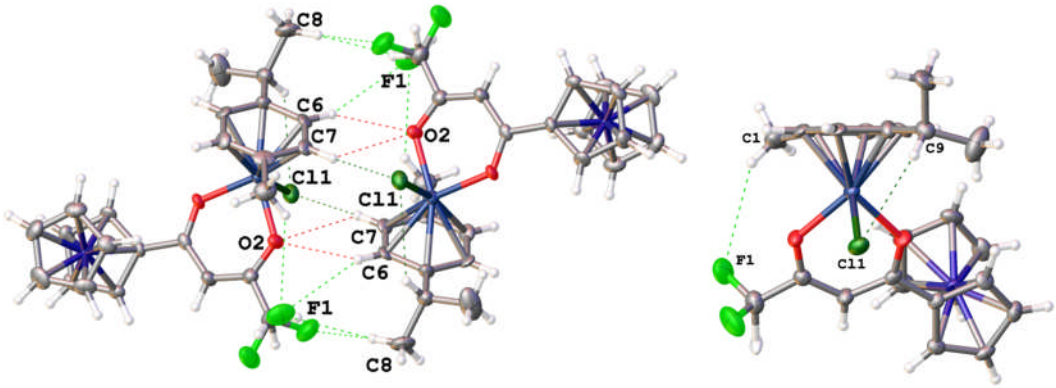

Figure 3.8 Intermolecular and intramolecular interactions for complex **C3**. Only selected intermolecular interactions shown for charity.

Interaction	Bond D…A	Distance (Å)	Bond D…A	Distance (Å)
Intramolecular	C1-H…F1	3.843(10)	C9-H…Cl1	3.620(7)
Intermolecular	C1-H…F1	3.742(10)	C7-H…O2	3.307(8)
	C1-H…F2	3.280(10)	C8-H…F1	3.771(10)
	C3-H…F2	3.568(10)	C8-H…F2	3.841(10)
	C6-H…F1	3.740(9)	C18-H…Cl1	3.600(7)
	C6-H…O2	3.359(7)	C18-H…O1	3.674(8)
	C7-H…Cl1	3.700(16)		

Table 3.4 Intermolecular and intramolecular bond lengths and angles for complex **C3.** ESDs given in parentheses.

3.1.2.3 X-Ray Characterisation of Complex C4

Orange single crystals of complex **C4** were obtained by the slow evaporation of acetonitrile. The molecular structure is shown in **Figure 3.9** with notable bond lengths and angles stated in **Table 3.5**. Intramolecular and intermolecular interactions are shown in **Figure 3.10** with bond lengths and angles stated in **Table 3.6**. Complex **C4** crystallised in a monoclinic cell and structural solution performed in the $P2_1/c$ space group with one molecule and one molecule of acetonitrile.

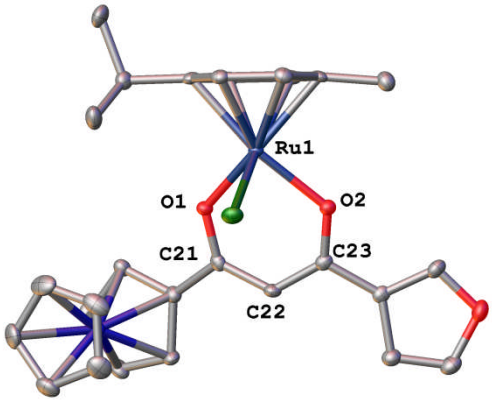

Figure 3.9 Molecular structure of complex **C4.** Hydrogen atoms and solvent molecule are omitted for clarity and thermal ellipsoids at the 50% probability level.

Bond	Distance (Å)	Bond	Angle (˚)
Ru1-O1	**2.080(2)**	**O1-Ru1-O2**	**87.23(7)**
Ru1-O2	**2.079(2)**	**Ru1-O1-C21**	**126.1(2)**
O1-C21	**1.282(3)**	**Ru1-O2-C23**	**125.6(2)**
O2-C23	**1.291(3)**	**O1-C21-C22**	**125.6(2)**
C21-C22	**1.398(4)**	**O2-C23-C22**	**125.9(2)**
C22-C23	**1.385(4)**	**C21-C22-C33**	**125.1(2)**

Table 3.5 Bond lengths and angles for complex **C4**. ESDs given in parentheses.

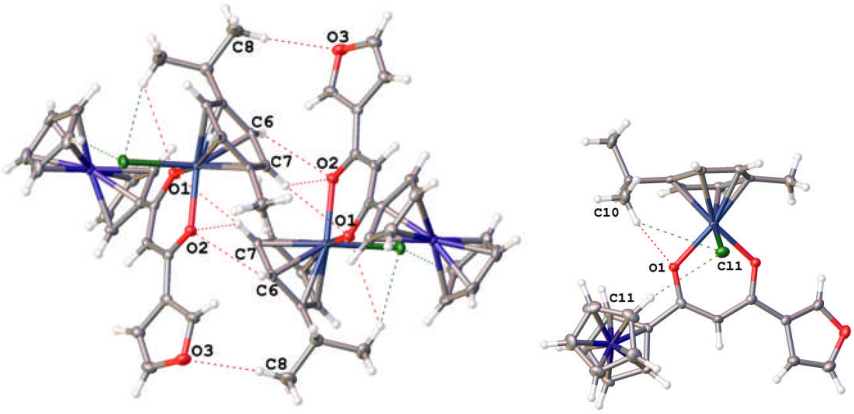

Figure 3.10 Intermolecular and intramolecular interactions for complex **C4.** Only selected intermolecular interactions shown for charity.

Interaction	Bond D…A	Distance (Å)	Bond D…A	Distance (Å)
Intramolecular	**C10-H…O1**	**3.750(4)**	**C11-H…Cl1**	**3.914(3)**
	C10-H…Cl1	**3.941(3)**		
Intermolecular	**C6-H…O2**	**3.423(3)**	**C10-H…O3**	**3.900(3)**
	C7-H…O1	**3.479(3)**	**C12-H…O2**	**3.504(4)**
	C7-H…O2	**3.414(3)**	**C27-H…Cl1**	**3.943(3)**
	C8-H…O3	**3.974(4)**		

Table 3.6 Intermolecular and intramolecular bond lengths and angles for complex **C4**. ESDs given in parentheses.

3.1.2.4 X-Ray Characterisation of Complex C5

Orange single crystals of complex **C5** were obtained by the slow evaporation of acetonitrile. The molecular structure is shown in **Figure 3.11** with notable bond lengths and angles stated in **Table 3.7**. Intramolecular and intermolecular interactions are shown in **Figure 3.12** with bond lengths and angles stated in **Table 3.8**. Complex **C5** crystallised in a monoclinic cell and structural solution performed in the $P2_1/n$ space group with one molecule per asymmetric unit.

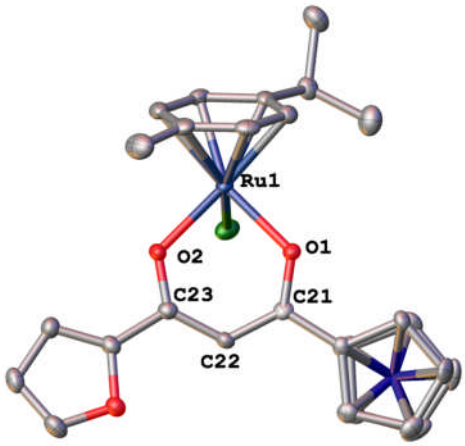

Figure 3.11 Molecular structure of complex **C5.** Hydrogen atoms are omitted for clarity and thermal ellipsoids at the 50% probability level.

Bond	Distance (Å)	Bond	Angle (˚)
Ru1-O1	**2.067(3)**	**O1-Ru1-O2**	**88.38(10)**
Ru1-O2	**2.066(3)**	**Ru1-O1-C21**	**125.5(3)**
O1-C21	**1.278(4)**	**Ru1-O2-C23**	**126.3(2)**
O2-C23	**1.279(5)**	**O1-C21-C22**	**127.1(4)**
C21-C22	**1.391(6)**	**O2-C23-C22**	**125.4(4)**
C22-C23	**1.401(5)**	**C21-C22-C23**	**125.1(3)**

Table 3.7 Bond lengths and angles for complex **C5**. ESDs given in parentheses.

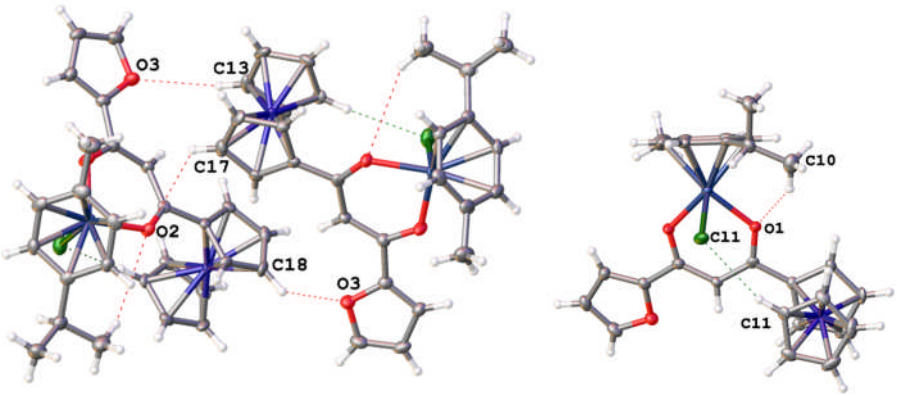

Figure 3.12 Intermolecular and intramolecular interactions for complex **C5.** Only selected intermolecular interactions shown for charity.

Interaction	Bond D…A	Distance (Å)	Bond D…A	Distance (Å)
Intramolecular	**C10-H…O1**	**3.913(6)**	**C11-H…Cl1**	**3.667(4)**
Intermolecular	**C17-H…O2**	**3.765(5)**	**C13-H…O3**	**3.769(5)**
	C18-H…O3	**3.362(5)**	**C7-H…Cl1**	**3.550(4)**
	C10-H…O3	**3.743(5)**	**C11-H…Cl1**	**3.667(4)**

Table 3.8 Intermolecular and intramolecular bond lengths and angles for complex **C5**. ESDs given in parentheses.

3.1.2.5 X-Ray Characterisation of Complex C6

Orange single crystals of complex **C6** were obtained by the slow evaporation of acetonitrile. The molecular structure is shown in **Figure 3.13** with notable bond lengths and angles stated in **Table 3.9**. Intramolecular and intermolecular interactions are shown in **Figure 3.14** with bond lengths and angles stated in **Table 3.10.** Complex **C6** crystallised in a monoclinic cell and structural solution performed in the $P2_1/n$ space group with one molecule per asymmetric unit.

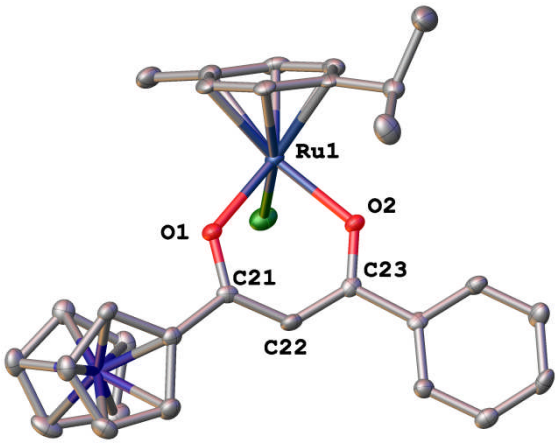

Figure 3.13 Molecular structure of complex **C6**. Hydrogen atoms are omitted for clarity and thermal ellipsoids at the 50% probability level.

Bond	Distance (Å)	Bond	Angle (˚)
Ru1-O1	2.065(2)	O1-Ru1-O2	88.07(9)
Ru1-O2	2.072(2)	Ru1-O1-C21	126.2(2)
O1-C21	1.280(4)	Ru1-O2-C23	126.3(2)
O2-C23	1.281(4)	O1-C21-C22	125.7(3)
C21-C22	1.398(5)	O2-C23-C22	125.3(3)
C22-C23	1.396(4)	C21-C22-C23	125.9(3)

Table 3.9 Bond lengths and angles for complex **C6**. ESDs given in parentheses.

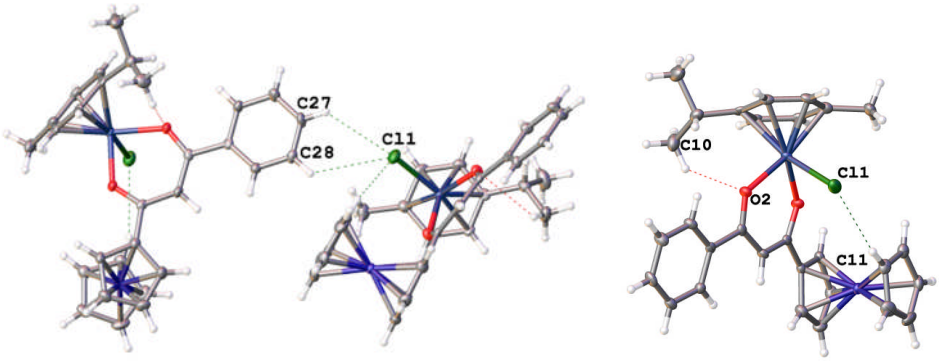

Figure 3.14 Intermolecular and intramolecular interactions for complex **C6.** Only selected intermolecular interactions shown for charity.

Interaction	Bond D…A	Distance (Å)	Bond D…A	Distance (Å)
Intramolecular	C10-H…O2	3.429(4)	C11-H…Cl1	3.741(4)
Intermolecular	C28-H…Cl1	3.691(4)	C9-H…Cl1	3.829(4)
	C27-H…Cl1	3.630(4)		

Table 3.10 Intermolecular and intramolecular bond lengths and angles for complex **C6**. ESDs given in parentheses.

3.1.2.6 X-Ray Characterisation of Complex C8

Orange single crystals of complex **C8** were obtained by the slow evaporation of acetonitrile. The molecular structure is shown in **Figure 3.15** with notable bond lengths and angles stated in **Table 3.11**. Intramolecular and intermolecular interactions are shown in **Figure 3.16** with bond lengths and angles stated in **Table 3.12**. Complex **C8** crystallised in a monoclinic cell and structural solution performed in the $P2_1/n$ space group with one molecule per asymmetric unit.

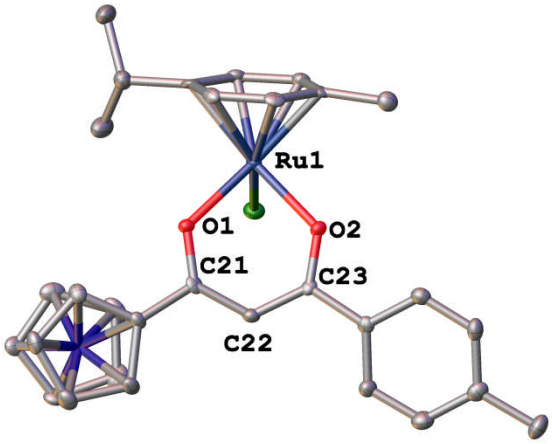

Figure 3.15 Molecular structure of complex **C8.** Hydrogen atoms are omitted for clarity and thermal ellipsoids at the 50% probability level.

Bond	Distance (Å)	Bond	Angle (˚)
Ru1-O1	2.079(2)	O1-Ru1-O2	86.79(9)
Ru1-O2	2.079(2)	Ru1-O1-C21	126.0(2)
O1-C21	1.287(4)	Ru1-O2-C23	126.6(2)
O2-C23	1.287(4)	O1-C21-C22	126.6(3)
C21-C22	1.400(5)	O2-C23-C22	125.2(3)
C22-C23	1.393(5)	C21-C22-C23	125.1(3)

Table 3.11 Bond lengths and angles for complex **C8**. ESDs given in parentheses.

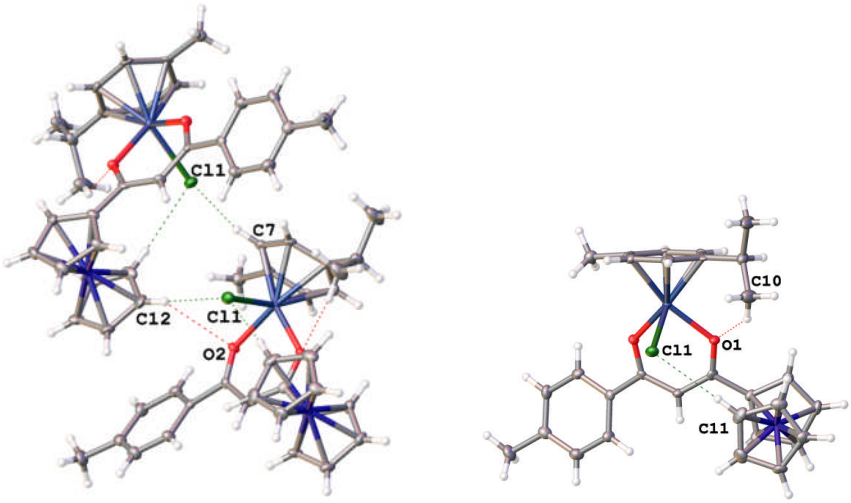

Figure 3.16 Intermolecular and intramolecular interactions for complex **C8.** Only selected intermolecular interactions shown for charity.

Interaction	Bond D…A	Distance (Å)	Bond D…A	Distance (Å)
Intramolecular	**C11-H…Cl1**	**3.706(4)**	**C10-H…O1**	**3.401(5)**
Intermolecular	**C3-H…O1**	**3.367(4)**	**C7-H…Cl1**	**3.583(4)**
	C3-H…O2	**3.453(4)**	**C12-H…Cl1**	**3.843(4)**
	C4-H…O2	**3.424(4)**	**C12-H…O2**	**3.415(4)**

Table 3.12 Intermolecular and intramolecular bond lengths and angles for complex **C8.** ESDs given in parentheses.

3.1.2.7 X-Ray Characterisation of Complex C10

Orange single crystals of complex **C10** were obtained by the slow evaporation of acetonitrile. The molecular structure is shown in **Figure 3.17** with notable bond lengths and angles stated in **Table 3.13**. Intramolecular and intermolecular interactions are shown in **Figure 3.18** with bond lengths and angles stated in **Table 3.14**. Complex **C10** was solved in a monoclinic cell and structural solution performed in the $P2_1/c$ space group with two molecule per asymmetric unit. Atoms corresponding to the second molecule in the asymmetric unit are marked by an asterisk.

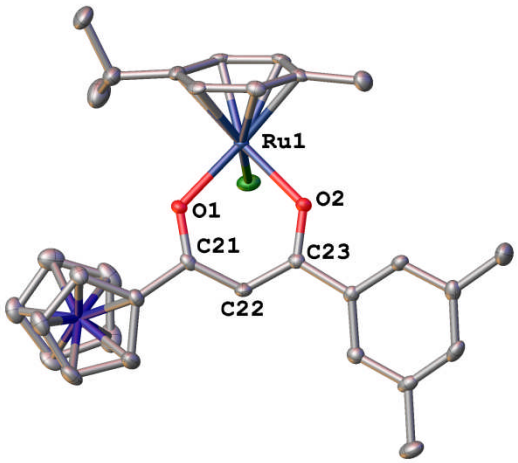

Figure 3.17 Molecular structure of complex **C10.** Hydrogen atoms are omitted for clarity and thermal ellipsoids at the 50% probability level.

Bond	Distance (Å)	Bond	Angle (˚)
Ru1-O1	**2.071(2)**	**O1-Ru1-O2**	**86.83(7)**
Ru1-O2	**2.070(2)**	**Ru1-O1-C21**	**126.4(2)**
O1-C21	**1.277(3)**	**Ru1-O2-C23**	**126.9(2)**
O2-C23	**1.288(3)**	**O1-C21-C22**	**126.4(3)**
C21-C22	**1.404(4)**	**O2-C23-C22**	**125.6(3)**
C22-C23	**1.386(4)**	**C21-C22-C23**	**124.3(3)**

Table 3.13 Bond lengths and angles for complex **C10**. ESDs given in parentheses.

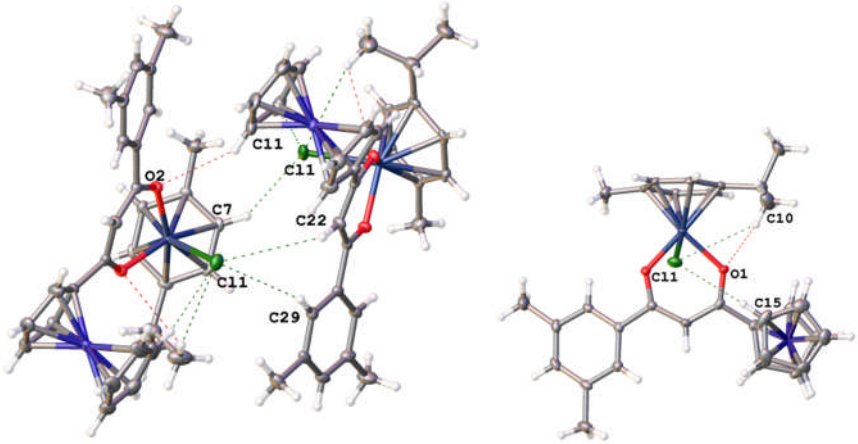

Figure 3.18 Intermolecular and intramolecular interactions for complex **C10.** Only selected intermolecular interactions shown for charity.

Interaction	Bond D…A	Distance (Å)	Bond D…A	Distance (Å)
Intramolecular	C10-H…O1	3.746(4)	C15-H…Cl1	3.843(4)
	C10-H…Cl1	4.031(4)		
Intermolecular	C3-H…O1	3.473(3)	C1*-H…Cl1*	3.579(3)
	C3-H…O2	3.515(4)	C3*-H…Cl1*	3.512(3)
	C4-H…O2	3.455(3)	C15*-H…O2*	3.531(4)
	C7-H…Cl1	3.590(3)	C19*-H…Cl1*	4.095(3)
	C11-H…O2	3.648(4)	C22*-H…Cl1*	3.992(3)
	C29-H…Cl1	3.839(3)	C25*-H…Cl1*	3.815(3)

Table 3.14 Intermolecular and intramolecular bond lengths and angles for complex **C10**. ESDs given in parentheses.

3.1.2.8 X-Ray Characterisation of Complex C11

Orange single crystals of complex **C11** were obtained by the slow evaporation of acetonitrile. The molecular structure is shown in **Figure 3.19** with notable bond lengths and angles stated in **Table 3.15**. Intramolecular and intermolecular interactions are shown in **Figure 3.20** with bond lengths and angles stated in **Table 3.16**. Complex **C11** crystallised in a monoclinic cell and structural solution performed in the *I*2/*a* space group with one molecule per asymmetric unit. Residual electron density could not be adequately modelled as solvent; hence the SQUEEZE routine of Platon was used.[10]

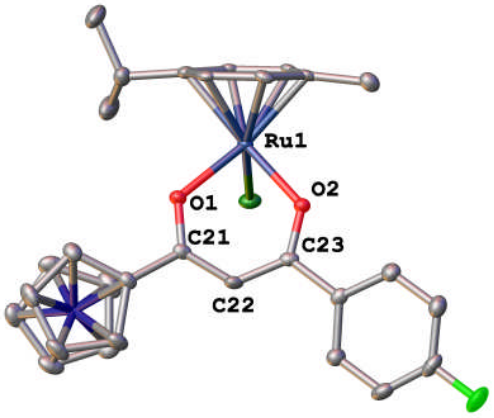

Figure 3.19 Molecular structure of complex **C11.** Hydrogen atoms are omitted for clarity and thermal ellipsoids at the 50% probability level.

Bond	Distance (Å)	Bond	Angle (˚)
Ru1-O1	2.081(2)	O1-Ru1-O2	87.72(6)
Ru1-O2	2.083(2)	Ru1-O1-C21	126.0(2)
O1-C21	1.282(3)	Ru1-O2-C23	124.8(2)
O2-C23	1.291(3)	O1-C21-C22	125.7(2)
C21-C22	1.398(3)	O2-C23-C22	126.2(2)
C22-C23	1.394(3)	C21-C22-C23	125.6(2)

Table 3.15 Bond lengths and angles for complex **C11**. ESDs given in parentheses.

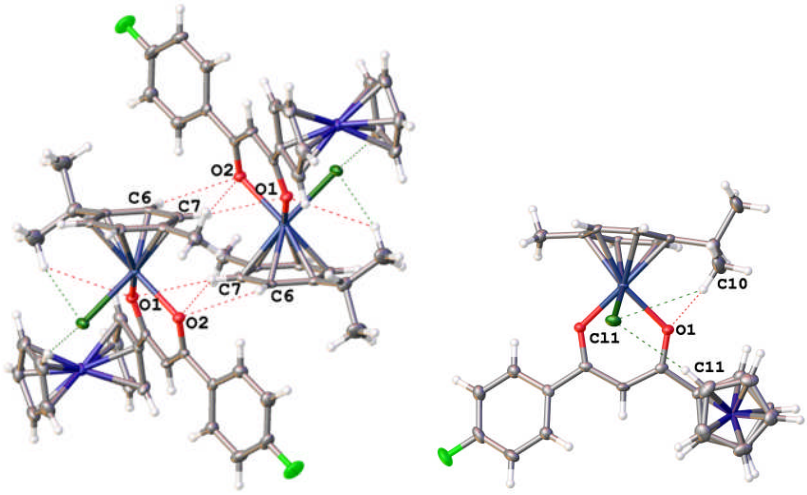

Figure 3.20 Intermolecular and intramolecular interactions for complex **C11.** Only selected intermolecular interactions shown for charity.

Interaction	Bond D…A	Distance (Å)	Bond D…A	Distance (Å)
Intramolecular	C10-H…Cl1	3.914(3)	C10-H…O1	3.576(4)
	C11-H…Cl1	3.800(3)		
Intermolecular	C3-H…Cl1	3.505(2)	C7-H…O2	3.415(3)
	C25-H…Cl1	3.793(3)	C7-H…O1	3.370(3)
	C15-H…O2	3.652(3)	C17-H…F1	3.511(3)
	C6-H…O2	3.382(3)		

Table 3.16 Intermolecular and intramolecular bond lengths and angles for complex **C11**. ESDs given in parentheses.

3.1.2.9 X-Ray Characterisation of Complex C12

Orange single crystals of complex **C12** were obtained by the slow evaporation of acetonitrile. The molecular structure is shown in **Figure 3.21** with notable bond lengths and angles stated in **Table 3.17**. Intramolecular and intermolecular interactions are shown in **Figure 3.22** with bond lengths and angles stated in **Table 3.18**. Complex **C12** crystallised in a monoclinic cell and structural solution performed

in the $P2_1/c$ space group with one molecule and one molecule of water per asymmetric unit. The structure shared disorder of the fluorine atom across two partitions, which was modelled in a 0.45:0.55 ratio.

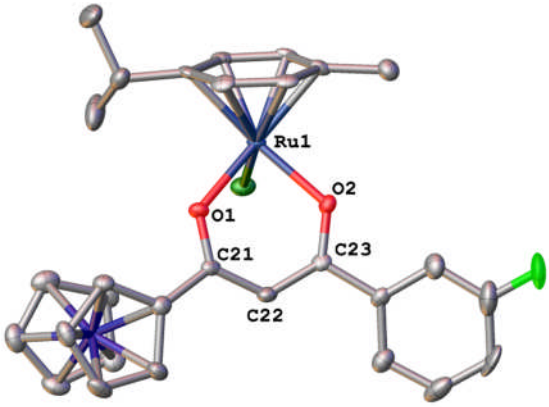

Figure 3.21 Molecular structure of complex **C12**. Hydrogen atoms and solvent are omitted for clarity and thermal ellipsoids at the 50% probability level.

Bond	Distance (Å)	Bond	Angle (˚)
Ru1-O1	**2.079(4)**	**O1-Ru1-O2**	**87.22(14)**
Ru1-O2	**2.081(4)**	**Ru1-O1-C21**	**126.1(3)**
O1-C21	**1.280(6)**	**Ru1-O2-C23**	**125.3(3)**
O2-C23	**1.280(6)**	**O1-C21-C22**	**126.3(5)**
C21-C22	**1.395(8)**	**O2-C23-C22**	**127.0(5)**
C22-C23	**1.396(8)**	**C21-C22-C23**	**124.2(5)**

Table 3.17 Bond lengths and angles for complex **C12**. ESDs given in parentheses.

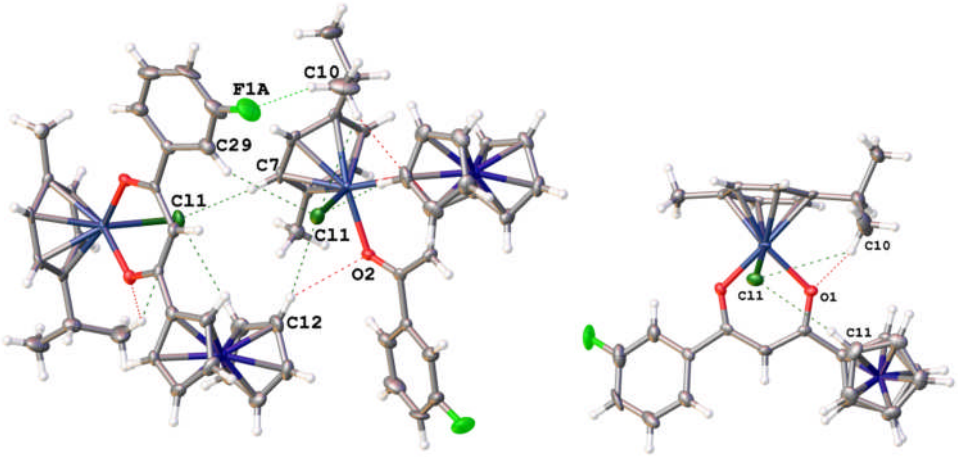

Figure 3.22 Intermolecular and intramolecular interactions for complex **C12.** Only selected intermolecular interactions shown for charity.

Interaction	Bond D…A	Distance (Å)	Bond D…A	Distance (Å)
Intramolecular	C10-H…O1	3.459(9)	C11-H…Cl1	3.860(7)
	C10-H…Cl1	3.892(7)		
Intermolecular	C10-H…F1a	3.389(14)	C29-H…Cl1	3.906(7)
	C14-H…F1a	3.467(11)	C3-H…O1	3.404(7)
	C10-H…F1b	3.411(11)	C3-H…O2	3.481(6)
	C9-H…F1b	3.358(11)	C4-H…O2	3.387(7)
	C7-H…Cl1	3.474(6)	C12-H…O2	3.424(7)
	C12-H…Cl1	3.945(7)		

Table 3.18 Intermolecular and intramolecular bond lengths and angles for complex **C12**. ESDs given in parentheses.

3.1.2.10 X-Ray Characterisation of Complex C13

Orange single crystals of complex **C13** were obtained by the vapour diffusion of diethyl ether into dichloromethane. The molecular structure is shown in **Figure 3.23** with notable bond lengths and angles stated in **Table 3.19**. Intramolecular and intermolecular interactions are shown in **Figure 3.24** with bond lengths and angles stated in **Table 3.20**. Complex **C13** crystallised in a monoclinic cell and structural solution performed in the $P2_1/c$ space group with one molecule per asymmetric unit.

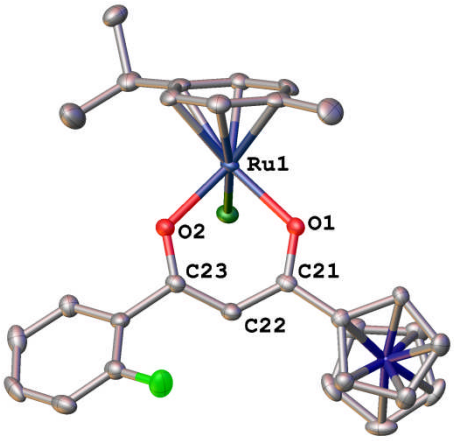

Figure 3.23 Molecular structure of complex **C13**. Hydrogen atoms are omitted for clarity and thermal ellipsoids at the 50% probability level.

Bond	Distance (Å)	Bond	Angle (˚)
Ru1-O1	2.080(3)	O1-Ru1-O2	89.06(12)
Ru1-O2	2.075(3)	Ru1-O1-C21	124.9(3)
O1-C21	1.283(5)	Ru1-O2-C23	124.4(3)
O2-C23	1.276(5)	O1-C21-C22	126.2(4)
C21-C22	1.397(6)	O2-C23-C22	127.3(4)
C22-C23	1.393(6)	C21-C22-C33	125.6(4)

Table 3.19 Bond lengths and angles for complex **C13**. ESDs given in parentheses.

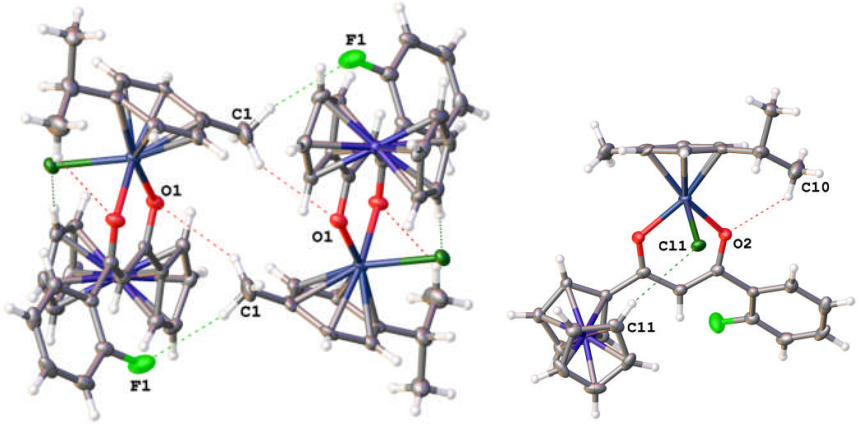

Figure 3.24 Intermolecular and intramolecular interactions for complex **C13.** Only selected intermolecular interactions shown for charity.

Interaction	Bond D…A	Distance (Å)	Bond D…A	Distance (Å)
Intramolecular	C10-H…O2	3.673(8)	C11-H…Cl1	3.807(8)
Intermolecular	C11-H…Cl1	3.807(8)	C10-H…O2	3.920(10)
	C14-H…Cl1	3.728(7)	C1-H…F1	3.587(6)
	C1-H…O1	3.994(10)	C27-H…F1	3.105(6)

Table 3.20 Intermolecular and intramolecular bond lengths and angles for complex **C13**. ESDs given in parentheses.

3.1.2.11 X-Ray Characterisation of Complex C14

Orange single crystals of complex **C14** were obtained by the slow evaporation of acetonitrile. The molecular structure is shown in **Figure 3.25** with notable bond lengths and angles stated in **Table 3.21**. Intramolecular and intermolecular interactions are shown in **Figure 3.26** with bond lengths and angles stated in **Table 3.22**. Complex **C14** crystallised in a triclinic cell and structural solution performed in the *P*-1 space group with one molecule per asymmetric unit.

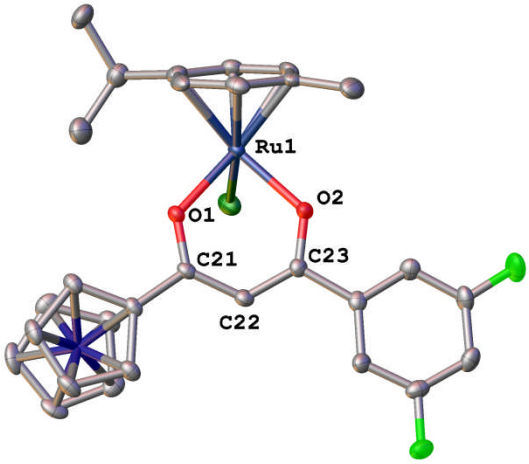

Figure 3.25 Molecular structure of complex **C14**. Hydrogen atoms are omitted for clarity and thermal ellipsoids at the 50% probability level.

Bond	Distance (Å)	Bond	Angle (˚)
Ru1-O1	**2.072(2)**	**O1-Ru1-O2**	**87.01(8)**
Ru1-O2	**2.065(2)**	**Ru1-O1-C21**	**126.5(2)**
O1-C21	**1.273(3)**	**Ru1-O2-C23**	**126.1(2)**
O2-C23	**1.282(4)**	**O1-C21-C22**	**125.3(3)**
C21-C22	**1.406(4)**	**O2-C23-C22**	**126.1(3)**
C22-C23	**1.377(4)**	**C21-C22-C33**	**125.3(3)**

Table 3.21 Bond lengths and angles for complex **C14**. ESDs given in parentheses.

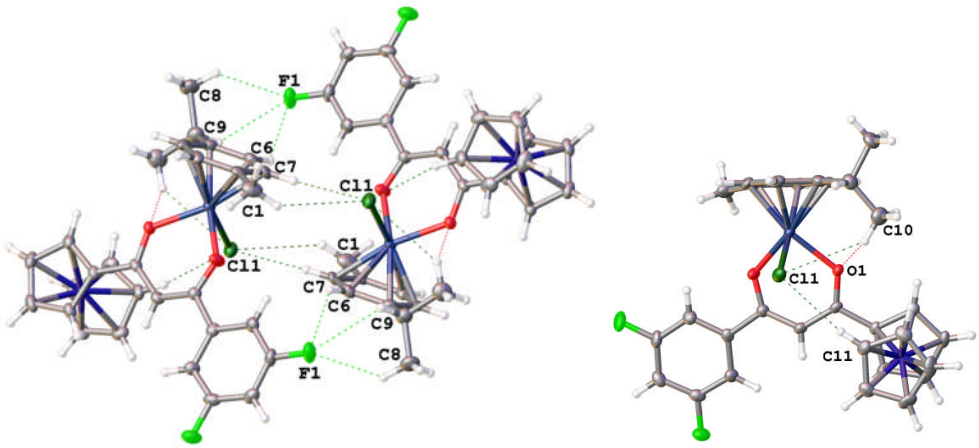

Figure 3.26 Intermolecular and intramolecular interactions for complex **C14.** Only selected intermolecular interactions shown for charity.

Interaction	Bond D…A	Distance (Å)	Bond D…A	Distance (Å)
Intramolecular	C10-H…O1	3.260(4)	C11-H…Cl1	3.722(4)
	C10-H…Cl1	3.840(4)		
Intermolecular	C1-H…Cl1	3.916(4)	C9-H…F1	3.483(4)
	C7-H…Cl1	3.641(3)	C13-H…F1	3.450(4)
	C8-H…Cl1	3.997(4)	C3-H…F2	3.361(4)
	C6-H…F1	3.731(4)	C12-H…F2	3.369(4)
	C8-H…F1	3.429(4)	C22-H…F2	3.232(3)

Table 3.22 Intermolecular and intramolecular bond lengths and angles for complex **C14**. ESDs given in parentheses.

3.1.2.12 X-Ray Characterisation of Complex C15

Orange single crystals of complex **C15** were obtained by the slow evaporation of acetonitrile. The molecular structure is shown in **Figure 3.27** with notable bond lengths and angles stated in **Table 3.23**. Intramolecular and intermolecular interactions are shown in **Figure 3.28** with bond lengths and angles stated in **Table 3.24**. Complex **C15** crystallised in a monoclinic cell and structural solution performed in the $P2_1/n$ space group with one molecule per asymmetric unit.

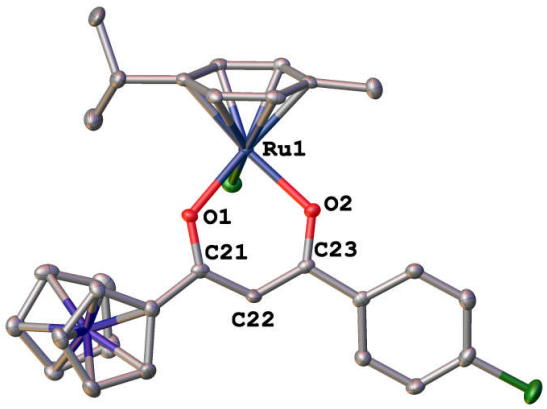

Figure 3.27 Molecular structure of complex **C15**. Hydrogen atoms are omitted for clarity and thermal ellipsoids at the 50% probability level.

Bond	Distance (Å)	Bond	Angle (˚)
Ru1-O1	2.085(2)	O1-Ru1-O2	86.92(6)
Ru1-O2	2.074(2)	Ru1-O1-C21	125.8(2)
O1-C21	1.286(4)	Ru1-O2-C23	126.2(2)
O2-C23	1.284(4)	O1-C21-C22	125.8(3)
C21-C22	1.399(4)	O2-C23-C22	125.6(3)
C22-C23	1.391(4)	C21-C22-C23	125.2(3)

Table 3.23 Bond lengths and angles for complex **C15**. ESDs given in parentheses.

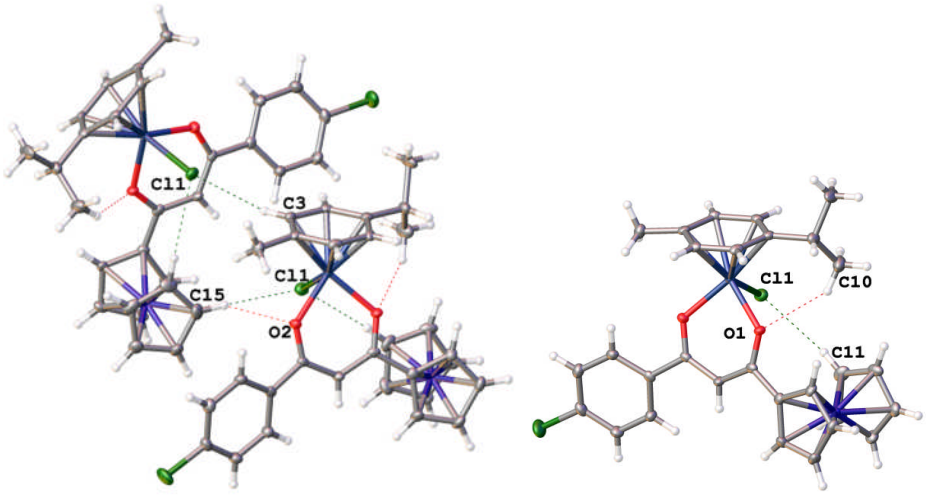

Figure 3.28 Intermolecular and intramolecular interactions for complex **C15.** Only selected intermolecular interactions shown for charity.

Interaction	Bond D…A	Distance (Å)	Bond D…A	Distance (Å)
Intramolecular	**C11-H…Cl1**	**3.751(4)**	**C10-H…O1**	**3.373(4)**
Intermolecular	**C6-H…O2**	**3.410(4)**	**C15-H…Cl1**	**3.847(4)**
	C7-H…O2	**3.434(4)**	**C3-H…Cl1**	**3.549(3)**
	C7-H…O1	**3.361(4)**	**C26-H…Cl2**	**3.846(4)**
	C15-H…O2	**3.424(4)**		

Table 3.24 Intermolecular and intramolecular bond lengths and angles for complex **C15**. ESDs given in parentheses.

3.1.2.13 X-Ray Characterisation of Complex C16

Orange single crystals of complex **C16** were obtained by the slow evaporation of ethyl acetate and hexane. The molecular structure is shown in **Figure 3.29** with notable bond lengths and angles stated in **Table 3.25**. Intramolecular and intermolecular interactions are shown in **Figure 3.30** with bond lengths and angles stated in **Table 3.26**. Complex **C16** crystallised in a monoclinic cell and structural solution performed in the *C*2/*c* space group with one molecule and one molecule of ethyl acetate per asymmetric unit.

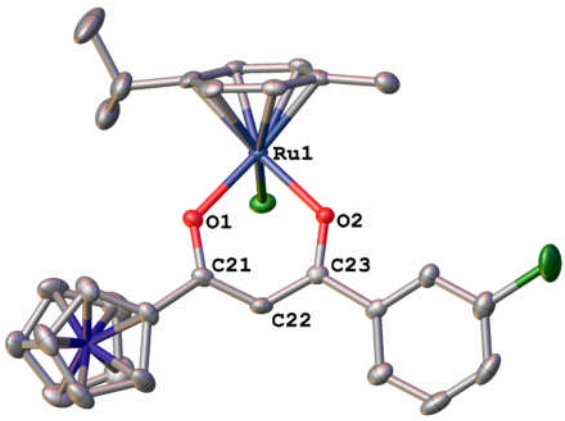

Figure 3.29 Molecular structure of complex **C16**. Hydrogen atoms and solvent are omitted for clarity and thermal ellipsoids at the 50% probability level.

Bond	Distance (Å)	Bond	Angle (˚)
Ru1-O1	**2.083(2)**	**O1-Ru1-O2**	**86.80(9)**
Ru1-O2	**2.068(2)**	**Ru1-O1-C21**	**126.8(2)**
O1-C21	**1.281(4)**	**Ru1-O2-C23**	**126.1(2)**
O2-C23	**1.286(4)**	**O1-C21-C22**	**125.1(3)**
C21-C22	**1.409(5)**	**O2-C23-C22**	**126.4(3)**
C22-C23	**1.385(5)**	**C21-C22-C23**	**124.7(3)**

Table 3.25 Bond lengths and angles for complex **C16**. ESDs given in parentheses.

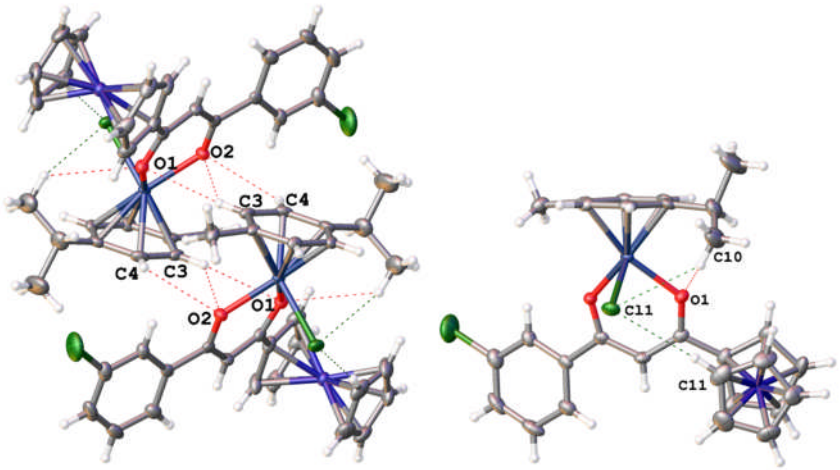

Figure 3.30 Intermolecular and intramolecular interactions for complex **C16.** Only selected intermolecular interactions shown for charity.

Interaction	Bond D…A	Distance (Å)	Bond D…A	Distance (Å)
Intramolecular	C10-H…Cl1	3.890(9)	C10-H…O1	3.668(10)
	C11-H…Cl1	3.878(9)		
Intermolecular	C3-H…O1	3.488(6)	C7-H…Cl1	3.593(7)
	C3-H…O2	3.436(7)	C12-H…Cl1	4.096(10)
	C4-H…O2	3.458(8)	C26-H…Cl1	4.140(8)
	C12-H…O2	3.518(9)	C12-H…F1	4.045(9)

Table 3.26 Intermolecular and intramolecular bond lengths and angles for complex **C16**. ESDs given in parentheses.

3.1.2.14 X-Ray Characterisation of Complex C17

Orange single crystals of complex **C17** were obtained by the slow evaporation of acetonitrile. The molecular structure is shown in **Figure 3.31** with notable bond lengths and angles stated in **Table 3.27**. Intramolecular and intermolecular interactions are shown in **Figure 3.32** with bond lengths and angles stated in **Table 3.28**. Complex **C17** crystallised in a monoclinic cell and structural solution performed in the $P2_1/c$ space group with two molecules per asymmetric unit. Atoms corresponding to the second molecule in the asymmetric unit are marked by an asterisk.

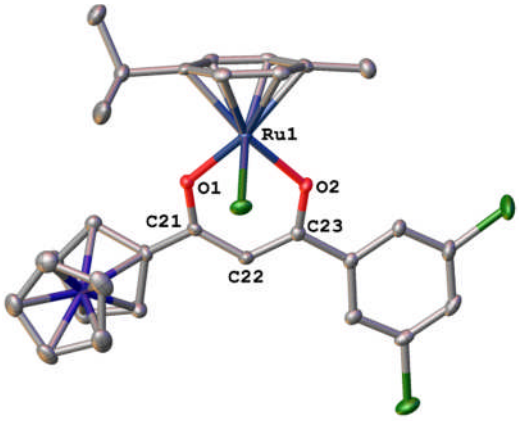

Figure 3.31 Molecular structure of complex **C17**. Hydrogen atoms are omitted for clarity and thermal ellipsoids at the 50% probability level.

Bond	Distance (Å)	Bond	Angle (˚)
Ru1-O1	2.076(18)	O1-Ru1-O2	86.33(7)
Ru1-O2	2.078(18)	Ru1-O1-C21	127.3(2)
O1-C21	1.274(3)	Ru1-O2-C23	126.6(2)
O2-C23	1.284(3)	O1-C21-C22	125.6(2)
C21-C22	1.413(4)	O2-C23-C22	126.1(2)
C22-C23	1.390(4)	C21-C22-C23	123.9(3)

Table 3.27 Bond lengths and angles for complex **C17**. ESDs given in parentheses.

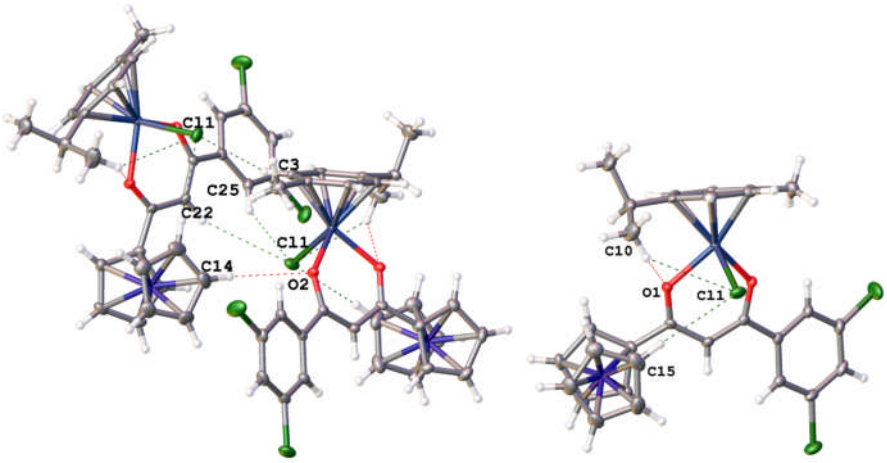

Figure 3.32 Intermolecular and intramolecular interactions for complex **C17.** Only selected intermolecular interactions shown for charity.

Interaction	Bond D…A	Distance (Å)	Bond D…A	Distance (Å)
Intramolecular	C10-H…Cl1	4.016(6)	C10-H…O1	3.711(6)
	C11-H…Cl1	3.928(5)		
Intermolecular	C13*-H…O2*	3.512(6)	C3-H…Cl1	3.529(4)
	C14-H…O2	3.593(6)	C25-H…Cl1	3.826(6)
	C6-H…O2	3.451(6)	C15*-H…Cl2	3.910(6)
	C1*-H…Cl1*	3.561(4)	C18*-H…Cl2	3.642(5)
	C7*-H…Cl1*	3.489(5)	C9*-H…Cl3	4.06(5)
	C16*-H…Cl1*	4.023(7)	C17-H…Cl2*	3.784(5)
	C22*-H…Cl1*	3.908(5)	C12-H…Cl2*	4.011(7)
	C29*-H…Cl1*	3.792(6)		

Table 3.28 Intermolecular and intramolecular bond lengths and angles for complex **C17**. ESDs given in parentheses.

3.1.2.15 X-Ray Characterisation of Complex C18

Orange single crystals of complex **C18** were obtained by the slow evaporation of acetonitrile. The molecular structure is shown in **Figure 3.33** with notable bond

lengths and angles stated in **Table 3.29**. Intramolecular and intermolecular interactions are shown in **Figure 3.34** with bond lengths and angles stated in **Table 3.30**. Complex **C18** crystallised in a monoclinic cell and structural solution performed in the $P2_1/n$ space group with one molecule per asymmetric unit.

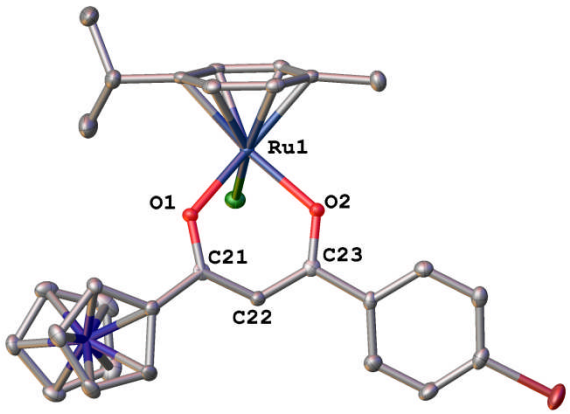

Figure 3.33 Molecular structure of complex **C18**. Hydrogen atoms are omitted for clarity and thermal ellipsoids at the 50% probability level.

Bond	Distance (Å)	Bond	Angle (˚)
Ru1-O1	**2.079(2)**	**O1-Ru1-O2**	**86.78(8)**
Ru1-O2	**2.071(2)**	**Ru1-O1-C21**	**126.6(2)**
O1-C21	**1.280(4)**	**Ru1-O2-C23**	**125.9(2)**
O2-C23	**1.286(4)**	**O1-C21-C22**	**125.3(3)**
C21-C22	**1.401(4)**	**O2-C23-C22**	**126.0(3)**
C22-C23	**1.390(4)**	**C21-C22-C23**	**125.0(3)**

Table 3.29 Bond lengths and angles for complex **C18**. ESDs given in parentheses.

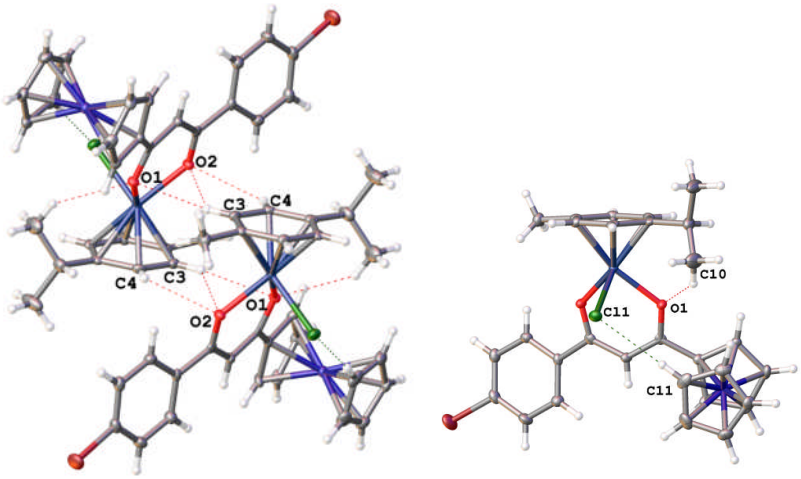

Figure 3.34 Intermolecular and intramolecular interactions for complex **C18.** Only selected intermolecular interactions shown for charity.

Interaction	Bond D…A	Distance (Å)	Bond D…A	Distance (Å)
Intramolecular	C10-H…O1	3.412(5)	C11-H…Cl1	3.737(4)
Intermolecular	C28-H…Br1	3.921(4)	C12-H…O2	3.454(4)
	C3-H…O1	3.391(4)	C7-H…Cl1	3.584(3)
	C3-H…O2	3.406(4)	C12-H…Cl1	3.872(4)
	C4-H…O2	3.401(4)		

Table 3.30 Intermolecular and intramolecular bond lengths and angles for complex **C18**. ESDs given in parentheses.

3.1.2.16 X-Ray Characterisation of Complex C19

Orange single crystals of complex **C19** were obtained by the slow evaporation of ethyl acetate and hexane. The molecular structure is shown in **Figure 3.35** with notable bond lengths and angles stated in **Table 3.31**. Intramolecular and intermolecular interactions are shown in **Figure 3.36** with bond lengths and angles stated in **Table 3.32**. Complex **C19** crystallised in a monoclinic cell and structural solution performed in the *C*2/*c* space group with one molecule and one ethyl acetate molecule per asymmetric unit.

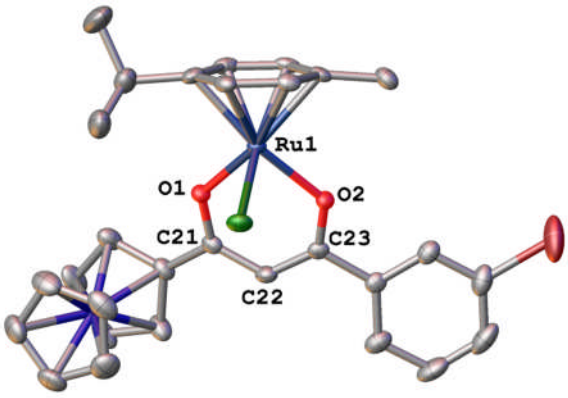

Figure 3.35 Molecular structure of complex **C19.** Hydrogen atoms and solvent are omitted for clarity and thermal ellipsoids at the 50% probability level.

Bond	Distance (Å)	Bond	Angle (˚)
Ru1-O1	2.084(3)	O1-Ru1-O2	87.04(13)
Ru1-O2	2.077(3)	Ru1-O1-C21	126.1(3)
O1-C21	1.286(6)	Ru1-O2-C23	125.4(3)
O2-C23	1.278(6)	O1-C21-C22	125.5(5)
C21-C22	1.398(7)	O2-C23-C22	127.0(5)
C22-C23	1.381(7)	C21-C22-C23	124.9(5)

Table 3.31 Bond lengths and angles for complex **C19**. ESDs given in parentheses.

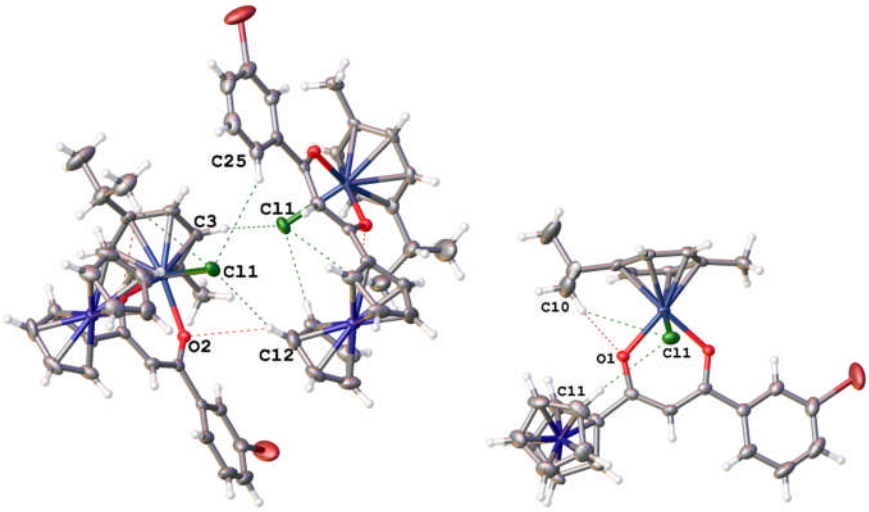

Figure 3.36 Intermolecular and intramolecular interactions for complex **C19.** Only selected intermolecular interactions shown for charity.

Interaction	Bond D…A	Distance (Å)	Bond D…A	Distance (Å)
Intramolecular	**C10-H…O1**	**3.663(10)**	**C11-H…Cl1**	**3.884(8)**
	C10-H…Cl1	**3.901(8)**		
Intermolecular	**C7-H…O1**	**3.488(7)**	**C3-H…Cl1**	**3.615(2)**
	C6-H…O2	**3.455(7)**	**C25-H…Cl1**	**4.069(7)**
	C7-H…O2	**3.439(7)**	**C17-H…Br1**	**4.035(7)**
	C12-H…O2	**3.539(8)**		

Table 3.32 Intermolecular and intramolecular bond lengths and angles for complex **C19**. ESDs given in parentheses.

3.1.2.17 X-Ray Characterisation of Complex C20

Orange single crystals of complex **C20** were obtained by the slow evaporation of acetonitrile. The molecular structure is shown in **Figure 3.37** with notable bond lengths and angles stated in **Table 3.33**. Intramolecular and intermolecular interactions are shown in **Figure 3.38** with bond lengths and angles stated in **Table 3.34**. Complex **C20** crystallised in a monoclinic cell and structural solution performed in the $P2_1/n$ space group with one molecule per asymmetric unit.

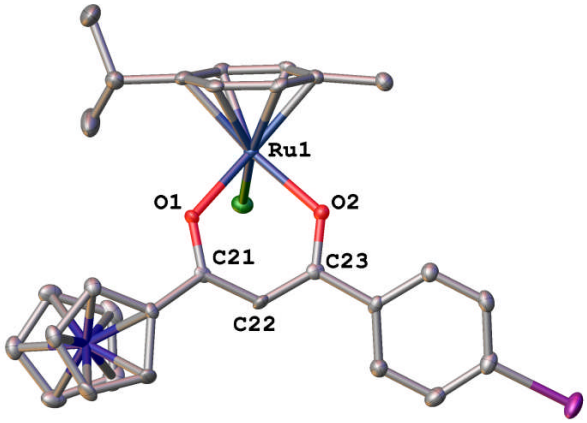

Figure 3.37 Molecular structure of complex **C20**. Hydrogen atoms are omitted for clarity and thermal ellipsoids at the 50% probability level.

Bond	Distance (Å)	Bond	Angle (˚)
Ru1-O1	**2.087(3)**	**O1-Ru1-O2**	**86.98(11)**
Ru1-O2	**2.067(3)**	**Ru1-O1-C21**	**126.9(3)**
O1-C21	**1.278(5)**	**Ru1-O2-C23**	**125.6(3)**
O2-C23	**1.291(5)**	**O1-C21-C22**	**124.9(4)**
C21-C22	**1.414(6)**	**O2-C23-C22**	**126.4(4)**
C22-C23	**1.380(6)**	**C21-C22-C23**	**125.0(4)**

Table 3.33 Bond lengths and angles for complex **C20**. ESDs given in parentheses.

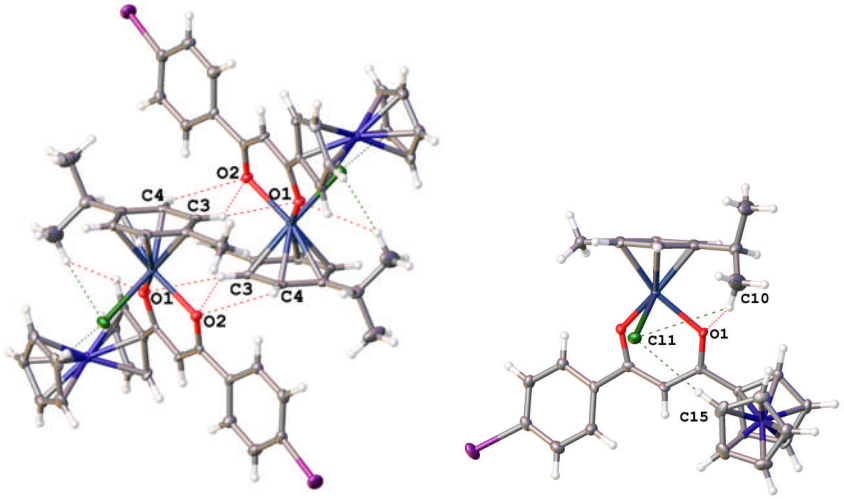

Figure 3.38 Intermolecular and intramolecular interactions for complex **C20.** Only selected intermolecular interactions shown for charity.

Interaction	Bond D…A	Distance (Å)	Bond D…A	Distance (Å)
Intramolecular	**C10-H…O1**	**3.501(6)**	**C15-H…Cl1**	**3.743(5)**
	C10-H…Cl1	**3.925(6)**		
Intermolecular	**C3-H…O1**	**3.445(5)**	**C11-H…O2**	**3.505(5)**
	C3-H…O2	**3.381(5)**	**C7-H…Cl1**	**3.667(4)**
	C4-H…O2	**3.374(5)**	**C11-H…Cl1**	**3.898(5)**

Table 3.34 Intermolecular and intramolecular bond lengths and angles for complex **C20**. ESDs given in parentheses.

3.1.2.18 X-Ray Characterisation of Complex C21

Orange single crystals of complex **C21** were obtained by the slow evaporation of acetonitrile. The molecular structure is shown in **Figure 3.39** with notable bond lengths and angles stated in **Table 3.35**. Intramolecular and intermolecular interactions are shown in **Figure 3.40** with bond lengths and angles stated in **Table 3.36**. Complex **C21** crystallised in a monoclinic cell and structural solution performed in the *I*2/*a* space group with one molecule per asymmetric unit.

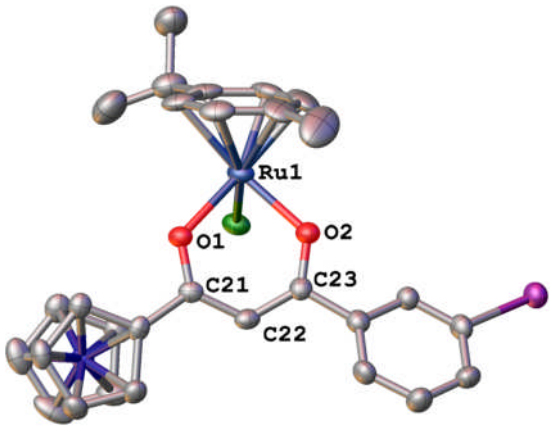

Figure 3.39 Molecular structure of complex **C21.** Hydrogen atoms are omitted for clarity and thermal ellipsoids at the 50% probability level.

Bond	Distance (Å)	Bond	Angle (˚)
Ru1-O1	**2.083(4)**	**O1-Ru1-O2**	**88.15(16)**
Ru1-O2	**2.064(4)**	**Ru1-O1-C21**	**125.4(4)**
O1-C21	**1.271(6)**	**Ru1-O2-C23**	**125.4(4)**
O2-C23	**1.278(7)**	**O1-C21-C22**	**126.0(6)**
C21-C22	**1.413(8)**	**O2-C23-C22**	**127.1(5)**
C22-C23	**1.392(8)**	**C21-C22-C23**	**124.6(5)**

Table 3.35 Bond lengths and angles for complex **C21**. ESDs given in parentheses.

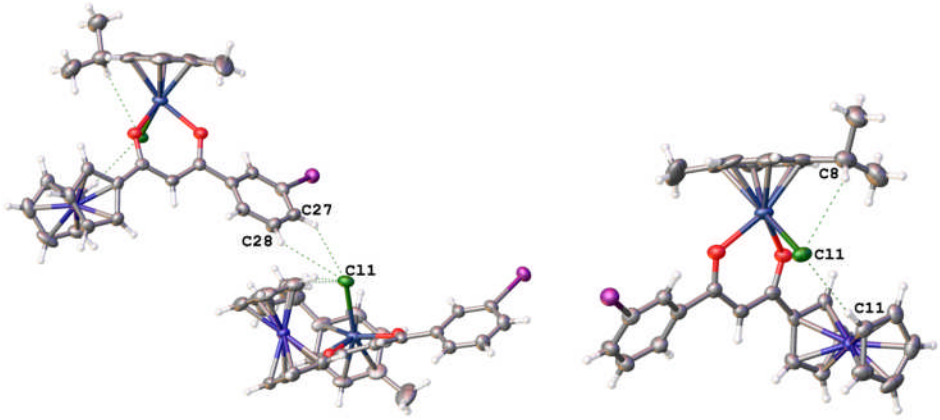

Figure 3.40 Intermolecular and intramolecular interactions for complex **C21.** Only selected intermolecular interactions shown for charity.

Interaction	Bond D…A	Distance (Å)	Bond D…A	Distance (Å)
Intramolecular	**C8-H…Cl1**	**3.470(5)**	**C11-H…Cl1**	**3.610(10)**
Intermolecular	**C27-H…Cl1**	**3.586(8)**	**C7-H…Cl1**	**3.594(3)**
	C28-H…Cl1	**3.618(7)**	**C12-H…O2**	**3.607(4)**

Table 3.36 Intermolecular and intramolecular bond lengths and angles for complex **C21.** ESDs given in parentheses.

3.1.2.19 X-Ray Characterisation of Complex C22

Orange single crystals of complex **C22** were obtained by the slow evaporation of acetonitrile. The molecular structure is shown in **Figure 3.41** with notable bond lengths and angles stated in **Table 3.37**. Intramolecular and intermolecular interactions are shown in **Figure 3.42** with bond lengths and angles stated in **Table 3.38**. Complex **C22** crystallised in a monoclinic cell and structural solution performed in the $P2_1/n$ space group with one molecule per asymmetric unit.

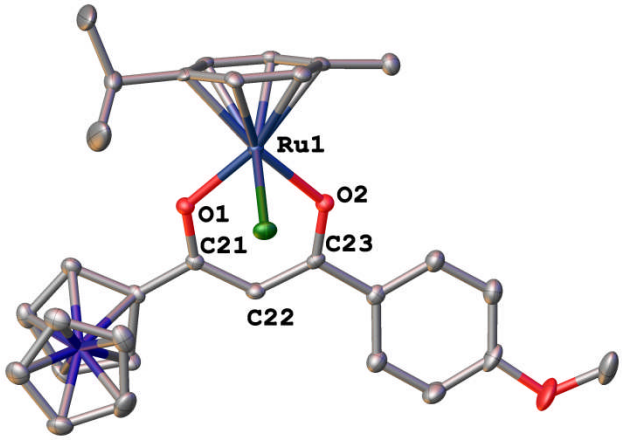

Figure 3.41 Molecular structure of complex **C22**. Hydrogen atoms are omitted for clarity and thermal ellipsoids at the 50% probability level.

Bond	Distance (Å)	Bond	Angle (˚)
Ru1-O1	2.075(2)	O1-Ru1-O2	87.25(8)
Ru1-O2	2.082(2)	Ru1-O1-C21	126.1(2)
O1-C21	1.282(4)	Ru1-O2-C23	125.4(2)
O2-C23	1.291(3)	O1-C21-C22	125.8(3)
C21-C22	1.398(4)	O2-C23-C22	125.6(3)
C22-C23	1.388(4)	C21-C22-C23	125.6(3)

Table 3.37 Bond lengths and angles for complex **C22**. ESDs given in parentheses.

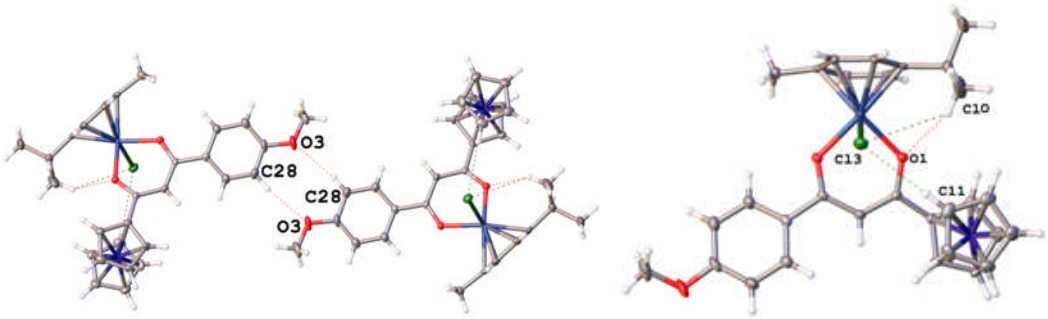

Figure 3.42 Intermolecular and intramolecular interactions for complex **C22.** Only selected intermolecular interactions shown for charity.

Interaction	Bond D…A	Distance (Å)	Bond D…A	Distance (Å)
Intramolecular	C10-H…Cl1	3.925(5)	C11-H…Cl1	3.708(4)
	C10-H…O1	3.585(6)		
Intermolecular	C28-H…O3	3.514(4)	C12-H…Cl1	3.964(4)
	C3-H…O2	3.388(4)	C7-H…Cl1	3.594(3)
	C4-H…O2	3.400(4)	C12-H…O2	3.607(4)
	C3-H…O1	3.447(4)		

Table 3.38 Intermolecular and intramolecular bond lengths and angles for complex **C22**. ESDs given in parentheses.

3.1.2.20 X-Ray Characterisation of Complex C23

Orange single crystals of complex **23** were obtained by the slow evaporation of acetonitrile. The molecular structure is shown in **Figure 3.43** with notable bond lengths and angles stated in **Table 3.39**. Intramolecular and intermolecular interactions are shown in **Figure 3.44** with bond lengths and angles stated in **Table 3.40**. Complex **23** crystallised in a monoclinic cell and structural solution performed in the $P2_1/c$ space group with one molecule per asymmetric unit.

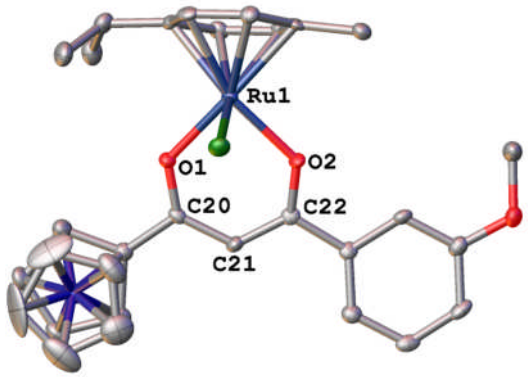

Figure 3.43 Molecular structure of complex **C23**. Hydrogen atoms are omitted for clarity and thermal ellipsoids at the 50% probability level.

Bond	Distance (Å)	Bond	Angle (˚)
Ru1-O1	**2.087(2)**	**O1-Ru1-O2**	**87.00(10)**
Ru1-O2	**2.073(3)**	**Ru1-O1-C21**	**127.1(2)**
O1-C21	**1.265(4)**	**Ru1-O2-C23**	**128.2(2)**
O2-C23	**1.280(4)**	**O1-C21-C22**	**125.9(3)**
C21-C22	**1.407(5)**	**O2-C23-C22**	**125.0(4)**
C22-C23	**1.391(5)**	**C21-C22-C23**	**125.9(4)**

Table 3.39 Bond lengths and angles for complex **C23**. ESDs given in parentheses.

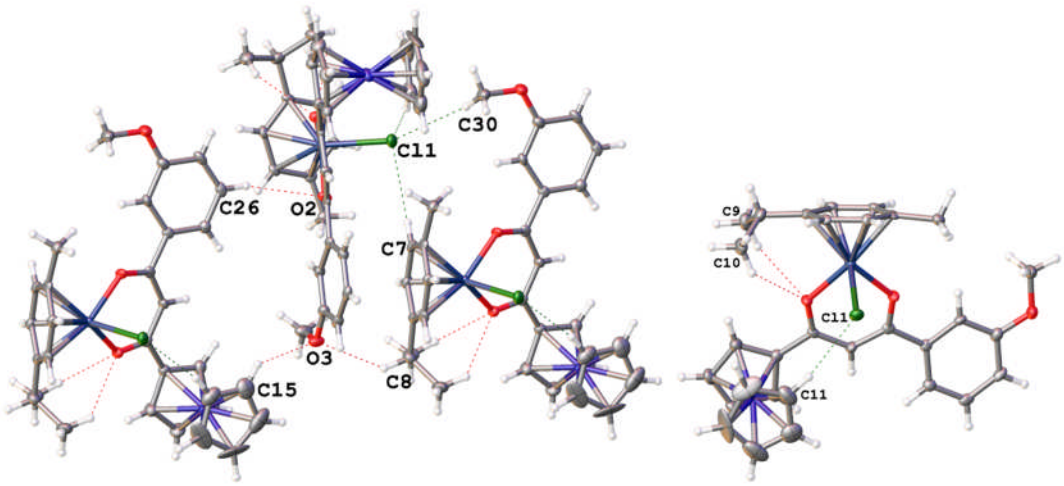

Figure 3.44 Intermolecular and intramolecular interactions for complex **C23.** Only selected intermolecular interactions shown for charity.

Interaction	Bond D…A	Distance (Å)	Bond D…A	Distance (Å)
Intramolecular	**C9-H…O1**	**3.331(5)**	**C11-H…Cl1**	**3.567(5)**
	C10-H…O1	**3.351(5)**		
Intermolecular	**C8-H…O3**	**3.498(5)**	**C19-H…Cl1**	**3.948(5)**
	C15-H…O3	**3.313(7)**	**C25-H…Cl1**	**3.881(4)**
	C26-H…O2	**3.636(4)**	**C30-H…Cl1**	**3.581(4)**
	C7-H…Cl1	**3.693(4)**	**π π**	**3.363(5)**

Table 3.40 Intermolecular and intramolecular bond lengths and angles for complex **C23**. ESDs given in parentheses.

3.1.2.21 X-Ray Characterisation of Complex C24

Orange single crystals of complex **C24** were obtained by the slow evaporation of acetonitrile. The molecular structure is shown in **Figure 3.45** with notable bond lengths and angles stated in **Table 3.41**. Intramolecular and intermolecular interactions are shown in **Figure 3.46** with bond lengths and angles stated in **Table 3.42**. Complex **C24** crystallised in a monoclinic cell and structural solution performed in the $P2_1/n$ space group with one molecule per asymmetric unit.

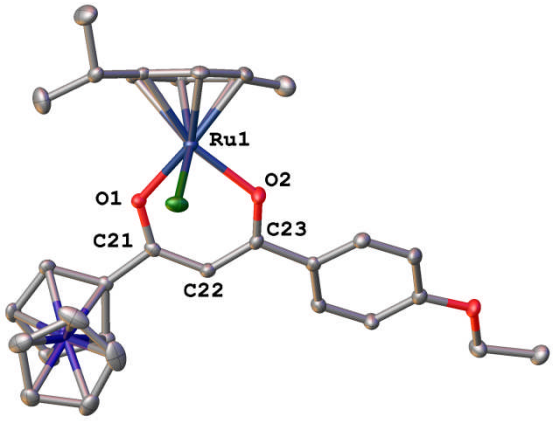

Figure 3.45 Molecular structure of complex **C24**. Hydrogen atoms are omitted for clarity and thermal ellipsoids at the 50% probability level.

Bond	Distance (Å)	Bond	Angle (˚)
Ru1-O1	**2.055(2)**	**O1-Ru1-O2**	**88.81(7)**
Ru1-O2	**2.070(2)**	**Ru1-O1-C21**	**126.4(2)**
O1-C21	**1.272(3)**	**Ru1-O2-C23**	**126.1(2)**
O2-C23	**1.273(3)**	**O1-C21-C22**	**125.9(2)**
C21-C22	**1.407(4)**	**O2-C23-C22**	**126.1(2)**
C22-C23	**1.391(4)**	**C21-C22-C23**	**125.4(3)**

Table 3.41 Bond lengths and angles for complex **C24**. ESDs given in parentheses.

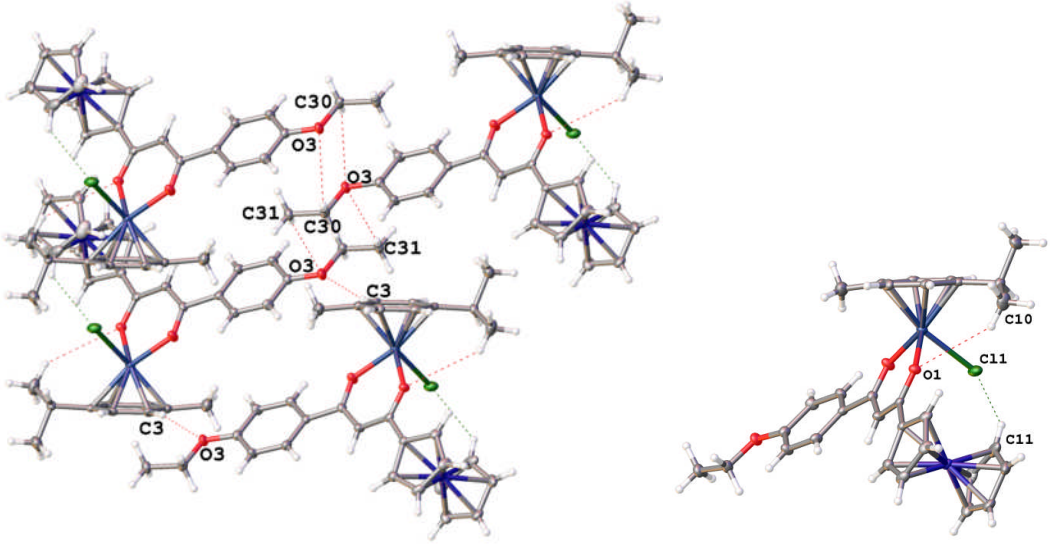

Figure 3.46 Intermolecular and intramolecular interactions for complex **C24.** Only selected intermolecular interactions shown for charity.

Interaction	Bond D…A	Distance (Å)	Bond D…A	Distance (Å)
Intramolecular	**C10-H…O1**	**4.002(4)**	**C11-H…Cl1**	**3.690(4)**
Intermolecular	**C3-H…O3**	**3.601(3)**	**C8-H…O1**	**3.554(3)**
	C30-H…O3	**3.736(4)**	**C25-H…Cl1**	**3.554(3)**
	C31-H…O3	**3.539(4)**		

Table 3.42 Intermolecular and intramolecular bond lengths and angles for complex **C24**. ESDs given in parentheses.

3.2 Conclusion

A library of novel ferrocene β-diketonate ruthenium(II) chloride "piano stool" complexes with varying electronic and steric properties have been synthesised. All complexes have been fully characterised by ^{1}H NMR, ^{13}C [^{1}H] NMR, micro-analysis and mass spectrometry. X-ray crystallographic data has been obtained when possible. ^{1}H NMR and ^{13}C [^{1}H] NMR spectra of the complexes show distinct shifts of the ligand peaks, especially the methine proton. Single crystals of these complexes were grown from the slow evaporation or vapour diffusion methods to give red/orange single crystals and structural solutions were performed in monoclinic, triclinic (**C14**) and orthorhombic (**C3**) cells. Observed angles around the ruthenium metal centre are close to 90˚ which is common for the *pseudo* octahedral geometry. Solid state bonding interactions in the form of hydrogen bonds and π-π stacking have been noted due to their potential involvement in the biological mode of action of the complexes. The *p*-cymene and the ferrocene Cp ring have been shown to be involved in both intramolecular and intermolecular interactions in the X-ray crystallographic data. Complex **C23** was the sole molecule which displayed π-π stacking interactions.

The various steric and electronic properties of the functionalised ferrocene β-diketonate ligands used in these complexes will allow for the determination of any structural activity relationships with regards to their biological activity. The ability of these complexes to act as anticancer and antimicrobial agents will be discussed in Chapter 5.

3.3 References

1. Y. K. Yan, M. Melchart, A. Habtemariam and P. J. Sadler, *Chemical Communications*, 2005, 4764-4776.
2. P. Zhang and P. J. Sadler, *Journal of Organometallic Chemistry*, 2017, **839**, 5-14.
3. L. Zeng, P. Gupta, Y. Chen, E. Wang, L. Ji, H. Chao and Z.-S. Chen, *Chemical Society Reviews*, 2017, **46**, 5771-5804.
4. C. S. Allardyce and P. J. Dyson, *Platinum Metals Review*, 2001, **45**, 62-69.
5. R. Aird, J. Cummings, A. Ritchie, M. Muir, R. Morris, H. Chen, P. Sadler and D. Jodrell, *British Journal of Cancer*, 2002, **86**, 1652-1657.
6. R. E. Morris, R. E. Aird, P. del Socorro Murdoch, H. Chen, J. Cummings, N. D. Hughes, S. Parsons, A. Parkin, G. Boyd and D. I. Jodrell, *Journal of Medicinal Chemistry*, 2001, **44**, 3616-3621.
7. A. Rodriguez-Barzano, R. M. Lord, A. M. Basri, R. M. Phillips, A. J. Blacker and P. C. McGowan, *Dalton Transactions*, 2015, **44**, 3265-3270.
8. R. M. Lord, A. J. Hebden, C. M. Pask, I. R. Henderson, S. J. Allison, S. L. Shepherd, R. M. Phillips and P. C. McGowan, *Journal of Medicinal Chemistry*, 2015, **58**, 4940-4953.
9. R. M. Lord, University of Leeds, PhD thesis, 2014.
10. A. Spek, *Journal of Applied Crystallography*, 2003, **36**, 7-13.

Chapter 4: Synthesis of Ruthenium(II) Bipyridyl Complexes

4.0 Bipyridyl Complexes

Ruthenium complexes with pyridyl-based ligands have been explored for a large scope for various medicinal applications such as cellular imaging, diagnostics and therapeutics.[1-4] Work in this chapter aims to extend the libraries of ruthenium complexes containing bipyridine chelating ligands, something which has not previously been attempted in the McGowan group.

The biological potential of ruthenium(II) polypyridyl complexes was first observed by Dwyer *et al.* in the 1950s when they illustrated the diverse biological activities of these types of complexes through enzyme inhibition, anticancer and antibacterial studies. Ignited by the findings of Dwyer, numerous research groups have worked in this area, with the number of ruthenium(II) pyridyl complexes being explored for their anticancer activity steadily increasing over the past several decades.[5-7]

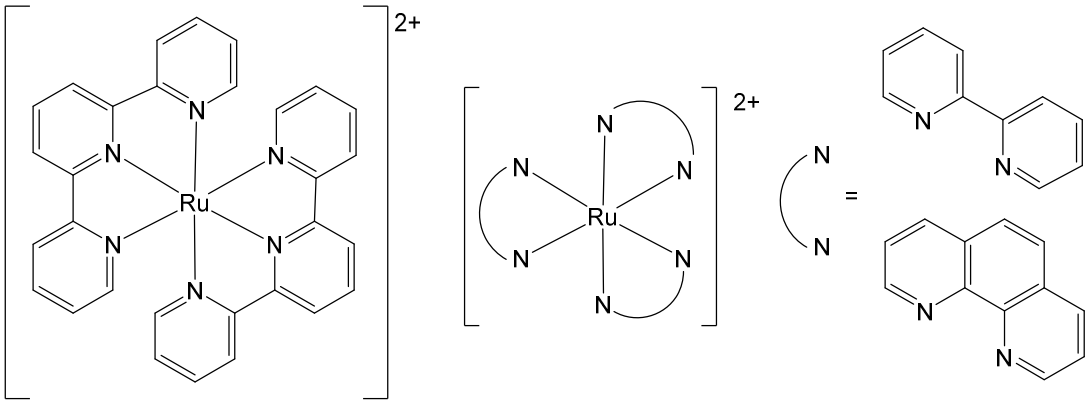

Figure 4.1 Ruthenium polypyridyl complexes tested by Dwyer *et al.* in 1952[5]

Their kinetically inert octahedral d^6 metal centre and rigid aromatic architectures, spanning all three spatial dimensions, impart excellent steric and electronic properties onto the complexes, allowing them to non-covalently bind to DNA with a high affinity.[8] It is these properties that allow them to function as DNA imaging agents but, given longer exposure times, also allow the complexes to exhibit antiproliferative effects. The central ruthenium metal atom can be considered as a central scaffold in many cases, to which active ligands may be conjugated. Control over the properties of the ancillary ligands influences the cytotoxicity of the complexes through the modulation of their cellular uptake and binding specificity.[9]

4.1 Synthesis of Ruthenium(II) Bipyridyl Complexes

Ruthenium complexes were prepared from an adapted literature procedure.[10] The complexation reactions took place in ethanol solutions of $Ru(bpy)_2Cl_2$, the appropriate ferrocene β-diketonate ligand and triethylamine at reflux for 48 hours (**Scheme 4.1**). A dark red solid was precipitated with aq. NH_4PF_6 before being dried overnight. The complexes were purified by column chromatography eluting with 20% acetonitrile/80% dichloromethane to obtain purple/black solid powder in yields of 19-39 %.

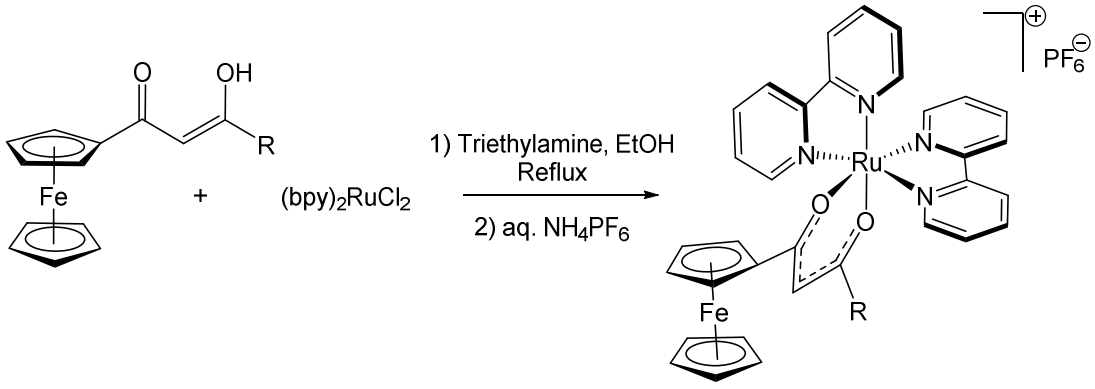

R = Me	**C'1**	4'-MePh	**C'6**	4'-ClPh	**C'11**
CF_3	**C'2**	3',5'-MePh	**C'7**	3',5'-ClPh	**C'12**
2-Furan	**C'3**	4'-FPh	**C'8**	4'-BrPh	**C'13**
Ph	**C'4**	3'-FPh	**C'9**	4'-IPh	**C'14**
1-Naph	**C'5**	3',5'-FPh	**C'10**	4'-OMePh	**C'15**

Scheme 4.1 General synthetic pathway for ruthenium(II) bipyridyl compounds

All complexes were fully characterised by ^{1}H NMR spectroscopy, ^{13}C [^{1}H] NMR spectroscopy, mass spectrometry and micro-analysis. Additionally, X-ray crystallographic data was obtained for all complexes except **C'3**, **C'5**, **C'6**, **C'9** and **C'15**

4.1.1 NMR Characterisation of Ruthenium(II) Bipyridyl Complexes

The ^{1}H NMR spectra of all [(β-diketonate)Ru(II)$(bpy)_2$]PF_6 complexes (example shown in **Figure 4.2**) show the clear upfield shift of all proton peaks corresponding to the β-diketonate ligand upon complexation, with an upfield shift of around 0.5 ppm

corresponding to the ferrocene bottom face Cp protons (**a**) at 3.5-4 ppm. Unlike the top face Cp protons observed for the complexes discussed in Chapter 3, which exist as four individual signals, for these types of complexes only one of the proton signals (**c**) splits upon complexation, arising from the loss of symmetry down the plane of the β-diketonate ligand. These changes in the NMR spectra are indicative of whether or not the reaction was successful.

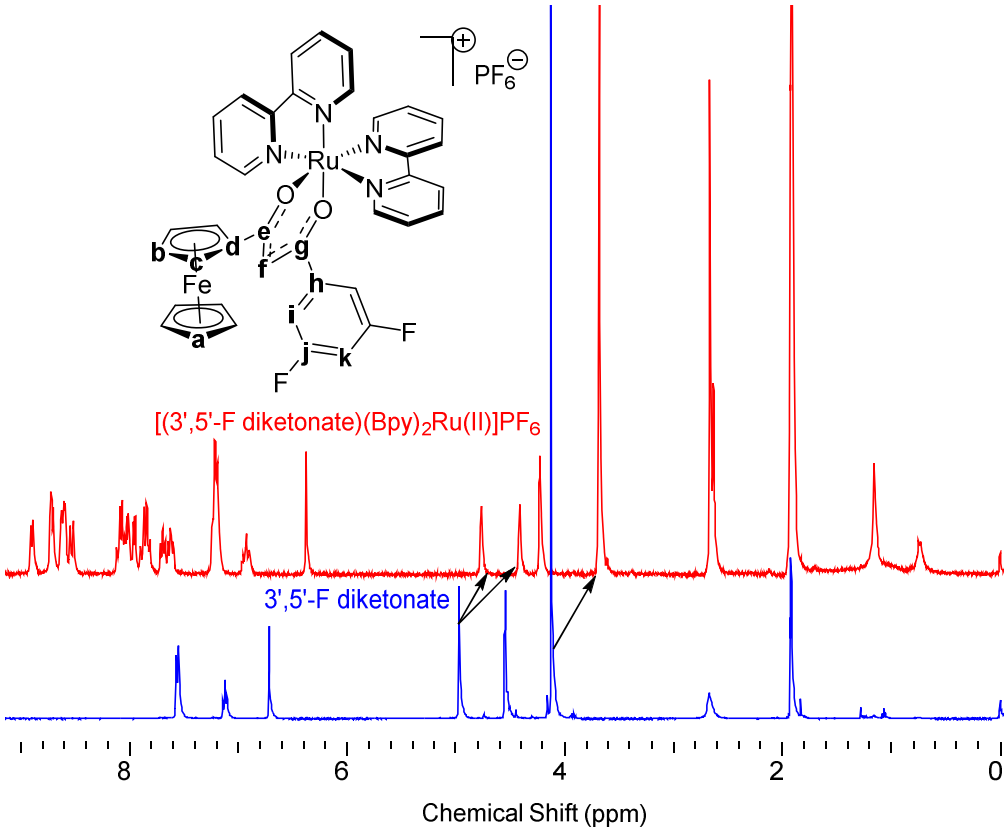

Figure 4.2 ^{1}H NMR (500 MHz, Acetone-d_6) for ruthenium complex (red) and free β-diketonate ligand (blue)

The ^{13}C [^{1}H] NMR spectra of all [(β-diketonate)Ru(II)(bpy)$_2$]PF$_6$ complexes show a slight upfield shift for β-diketonate carbon signals in the aromatic region upon complexation which are found, along with the bipyridine ligand carbon peaks, at approximately 100-165 ppm. The methine carbon (**f**) peak is also shifted slightly upfield during complexation but to a much lesser extent than that which is observed for the corresponding proton signal in the ^{1}H NMR. A considerable downfield shift can be observed from the quaternary Cp signal (**d**) in the region of 78-84 ppm. However, the other Cp signals were shifted upfield with the splitting of the Cp signals

(**c** and **b**) of the top face of ferrocene from two large double carbon peaks to four single peaks found between 65-75 ppm, again which arises from the loss of symmetry down the plane of the β-diketonate ligand. Full assignments given in Chapter 7.

4.1.2 X-Ray Characterisation of Ruthenium(II) Bipyridyl Complexes

X-ray crystallographic data was obtained for the complexes and solutions were performed in monoclinic (**C'1**, **C'7**, **C'8** and **C'12**) or triclinic cells (**C'2**, **C'4**, **C'10**, **C'11**, **C'13** and **C'14**). Bound ferrocene ligands display a planar structure unless an aromatic R substituent is present in which case torsion around that C23…C24 bond is observed. The ferrocene moiety adopts an eclipsed geometry as seen in the case of the free ligands. As in the case of the ruthenium arene complexes, the β-diketonate ligand centres become more symmetrical and similar in length upon complexation compared to the free ligands; this is attributed to the delocalisation of electrons around the β-diketonate centre. Again, there is a significant change in the bond angles around the β-diketonate ligand centres, increasing from 118-126˚ to 124-130˚, presumably due the electronic and steric effects upon binding to ruthenium. A typical labelling scheme is shown in **Figure 4.3.**

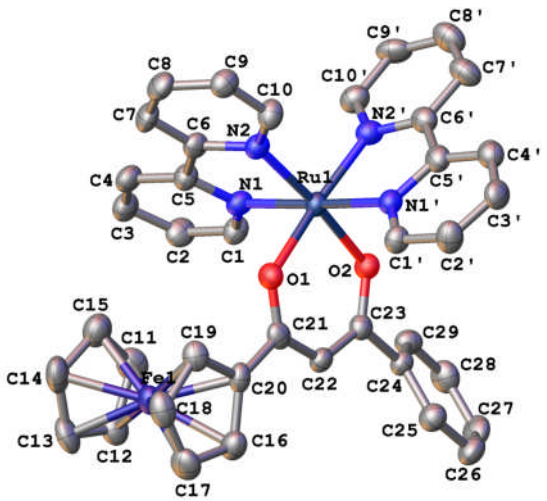

Figure 4.3 Typical labelling scheme for all complexes. Counter ion and hydrogen atoms are omitted for clarity. Thermal ellipsoids at the 50% probability level.

All complexes show a distorted octahedral geometry around the ruthenium centre with bond angles ranging between 81-90˚. Bonding interactions observed in the solid state have been noted due to the potential for these interactions to play a crucial role in the anticancer activity through processes such as DNA intercalation or enzyme binding. Intramolecular hydrogen bonding interactions (D…A 3.8-4.1 Å) are seen between the bottom Cp ring of ferrocene (C11-C15) and N1 for complexes **C'1**, **C'4**, **C'8**, **C'12, C'13** and **C'14.** As with the ruthenium arene complexes discussed in the previous chapter, this interaction could be a contributing factor to the upfield shift of the ferrocene Cp ring signals observed in the ^{1}H NMR spectra. Multiple intermolecular hydrogen bonding interactions (D…A 3.2-4.1 Å) are seen in all complexes typically between bipyridine/ferrocene C-H and bipyridine N and/or O2. Interactions with O1 are not observed, except in the case of **C'10**, due to the steric hindrance caused by the ferrocenyl group. Further intermolecular interactions can be observed in the form of π-π stacking for all complexes, except **C'2**, with bond distances in the range of 3.5-3.9 Å. The PF_6 counter ion is involved in both inter- and intra-molecular interactions.

4.1.2.1 X-Ray Characterisation of Complex C'1

Black single crystals of complex **C'1** were obtained by the slow evaporation of acetone. The molecular structure is shown in **Figure 4.4** with notable bond lengths and angles stated in **Table 4.1**. Intramolecular and intermolecular interactions are shown in **Figure 4.5** with bond lengths and angles stated in **Table 4.2**. Complex **C'1** crystallised in a monoclinic cell and structural solution performed in the *I*2/*a* space group with one molecule per asymmetric unit.

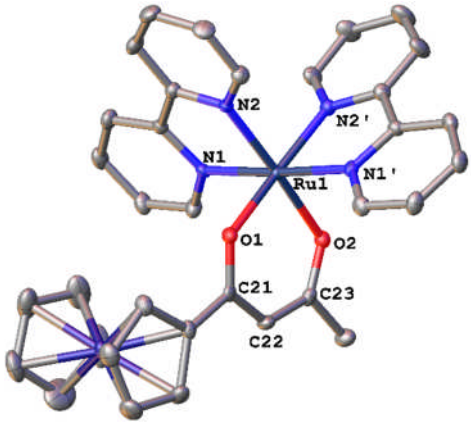

Figure 4.4 Molecular structure of complex **C'1**. Hydrogen atoms and counter ion are omitted for clarity and thermal ellipsoids at the 50% probability level.

Bond	Distance (Å)	Bond	Angle (˚)	Bond	Angle (˚)
Ru1-O1	2.057(2)	O1-Ru1-N1	87.75(10)	O1-Ru1-O2	92.45(10)
Ru1-O2	2.061(2)	O1-Ru1-N2	88.66(10)	Ru1-O1-C21	123.6(2)
Ru1-N1	2.045(3)	O2-Ru1-N1'	87.23(11)	Ru1-O2-C23	122.5(2)
Ru1-N2	2.026(3)	O2-Ru1-N2'	90.05(11)	O1-C21-C22	125.6(3)
Ru1-N1'	2.043(3)	N1-Ru1-N2	79.39(11)	O2-C23-C22	126.9(3)
Ru1-N2'	2.030(3)	N1'-Ru1-N2'	78.99(12)	C21-C22-C23	128.1(3)
O1-C21	1.282(4)				
O2-C23	1.288(4)				
C21-C22	1.404(5)				
C22-C23	1.392(5)				

Table 4.1 Bond lengths and angles for complex **C'1**. ESDs given in parentheses.

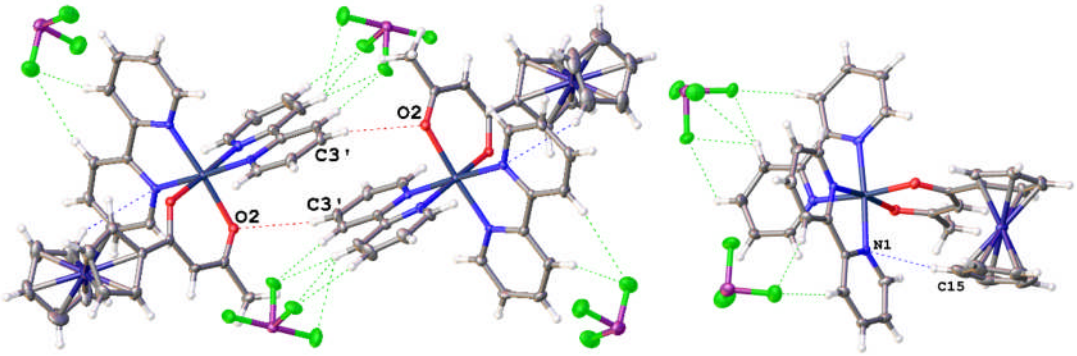

Figure 4.5 Intermolecular and intramolecular interactions for complex **C'1.** Only selected intermolecular interactions shown for charity.

Interaction	Bond D…A	Distance (Å)	Bond D…A	Distance (Å)
Intramolecular	**C15-H…N1**	**3.909(9)**		
Intermolecular	**C3-H…O2**	**3.372(1)**	**C3-H…N2'**	**4.004(12)**
	C3'-H…O2	**3.474(8)**	**π π**	**3.669(9)**
	C19-H…N1'	**3.920(13)**		

Table 4.2 Intermolecular and intramolecular bond lengths and angles for complex **C'1**. ESDs given in parentheses.

4.1.2.2 X-Ray Characterisation of Complex C'2

Black single crystals of complex **C'2** were obtained by the slow evaporation of acetone. The molecular structure is shown in **Figure 4.6** with notable bond lengths and angles stated in **Table 4.3**. Intramolecular interactions of feasible distances were not observed in this case. Intermolecular interactions are shown in **Figure 4.7** with bond lengths and angles stated in **Table 4.4**. Complex **C'2** crystallised in a triclinic cell and structural solution performed in the *P*-1 space group with one molecule per asymmetric unit. The structure showed disorder around the CF_3 group, with the F atoms being split across three partitions in a 0.55:0.56:0.61 ratio.

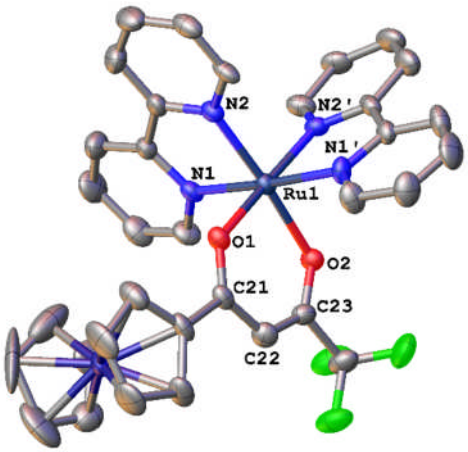

Figure 4.6 Molecular structure of complex **C'2**. Hydrogen atoms and counter ion are omitted for clarity and thermal ellipsoids at the 50% probability level.

Bond	Distance (Å)	Bond	Angle (˚)	Bond	Angle (˚)
Ru1-O1	2.054(4)	O1-Ru1-N1	88.79(19)	O1-Ru1-O2	91.79(18)
Ru1-O2	2.066(4)	O1-Ru1-N2	87.70(20)	Ru1-O1-C21	126.3(4)
Ru1-N1	2.043(6)	O2-Ru1-N1’	86.90(20)	Ru1-O2-C23	121.2(4)
Ru1-N2	2.040(6)	O2-Ru1-N2’	90.15(19)	O1-C21-C22	124.1(6)
Ru1-N1’	2.054(6)	N1-Ru1-N2	79.30(20)	O2-C23-C22	130.4(7)
Ru1-N2’	2.031(5)	N1’-Ru1-N2’	79.50(20)	C21-C22-C23	126.1(7)
O1-C21	1.271(8)				
O2-C23	1.283(8)				
C21-C22	1.430(10)				
C22-C23	1.374(9)				

Table 4.3 Bond lengths and angles for complex **C’2**. ESDs given in parentheses.

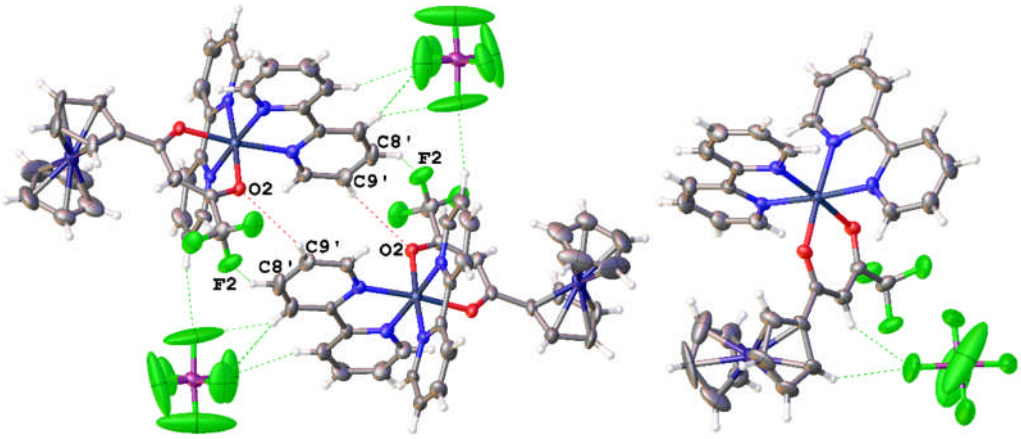

Figure 4.7 Intermolecular and intramolecular interactions for complex **C’2**. Only selected intermolecular interactions shown for charity.

Interaction	Bond D…A	Distance (Å)	Bond D…A	Distance (Å)
Intermolecular	C9’-H…O2	3.521(14)	C11-H…F2	3.356(15)
	C4-H…F1	3.661(2)	C1-H…F3	3.371(2)
	C8’-H…F2	3.288(14)		

Table 4.4 Intermolecular and intramolecular bond lengths and angles for complex **C’2**. ESDs given in parentheses.

4.1.2.3 X-Ray Characterisation of Complex C’4

Black single crystals of complex **C’4** were obtained by the slow evaporation of acetone. The molecular structure is shown in **Figure 4.8** with notable bond lengths and angles stated in **Table 4.5**. Intramolecular and intermolecular interactions are shown in **Figure 4.9** with bond lengths and angles stated in **Table 4.6**. Complex **C’4**

crystallised in a triclinic cell and structural solution performed in the *P*-1 space group with one molecule per asymmetric unit.

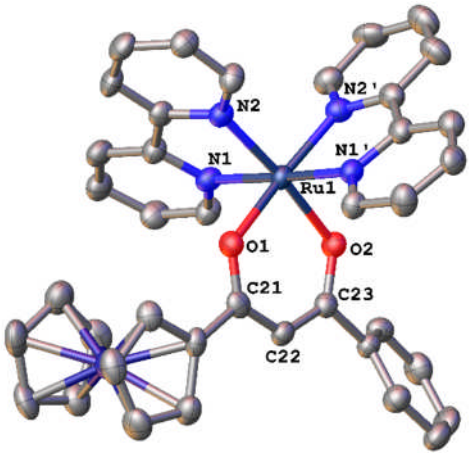

Figure 4.8 Molecular structure of complex **C'4**. Hydrogen atoms and counter ion are omitted for clarity and thermal ellipsoids at the 50% probability level.

Bond	Distance (Å)	Bond	Angle (˚)	Bond	Angle (˚)
Ru1-O1	2.042(5)	O1-Ru1-N1	85.8(2)	O1-Ru1-O2	92.2(2)
Ru1-O2	2.050(5)	O1-Ru1-N2	85.2(2)	Ru1-O1-C21	125.0(4)
Ru1-N1	2.050(6)	O2-Ru1-N1'	89.0(2)	Ru1-O2-C23	122.9(4)
Ru1-N2	2.017(6)	O2-Ru1-N2'	88.3(2)	O1-C21-C22	124.7(7)
Ru1-N1'	2.054(6)	N1-Ru1-N2	79.4(2)	O2-C23-C22	127.0(6)
Ru1-N2'	2.038(6)	N1'-Ru1-N2'	79.0(2)	C21-C22-C23	128.2(7)
O1-C21	1.285(9)				
O2-C23	1.291(9)				
C21-C22	1.401(10)				
C22-C23	1.383(10)				

Table 4.5 Bond lengths and angles for complex **C'4**. ESDs given in parentheses.

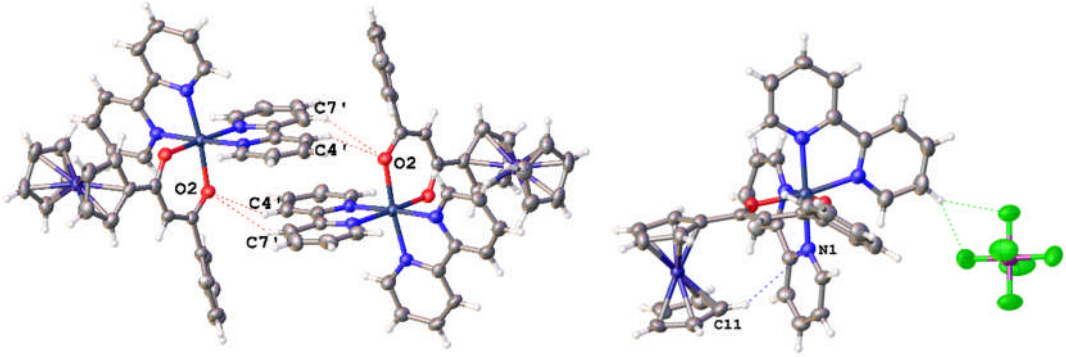

Figure 4.9 Intermolecular and intramolecular interactions for complex **C'4**. Only selected intermolecular interactions shown for charity.

Interaction	Bond D…A	Distance (Å)	Bond D…A	Distance (Å)
Intramolecular	C11-H…N1	4.106(11)		
Intermolecular	C4'-H…O2	3.404(9)	π π	3.798(13)
	C7'-H…O2	3.745(11)		

Table 4.6 Intermolecular and intramolecular bond lengths and angles for complex **C'4**. ESDs given in parentheses.

4.1.2.4 X-Ray Characterisation of Complex C'7

Black single crystals of complex **C'7** were obtained by the slow evaporation of acetone. The molecular structure is shown in **Figure 4.10** with notable bond lengths and angles stated in **Table 4.7**. Intramolecular interactions of feasible distances were not observed in this case. Intermolecular interactions are shown in **Figure 4.11** with bond lengths and angles stated in **Table 4.8**. Complex **C'7** crystallised in a monoclinic cell and structural solution performed in the $P2_1/n$ space group with one molecule per asymmetric unit.

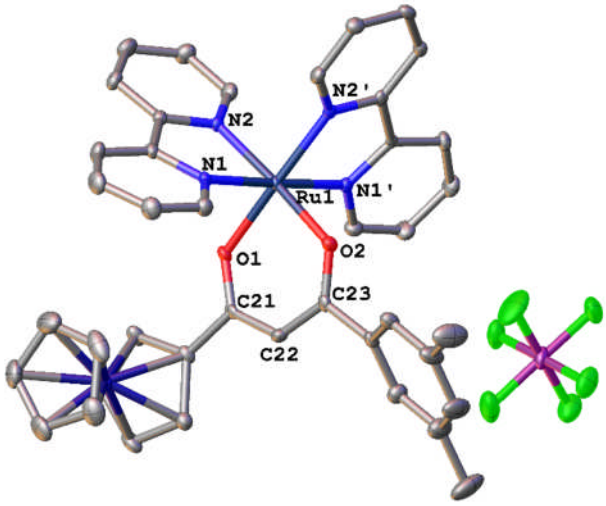

Figure 4.10 Molecular structure of complex **C'7**. Hydrogen atoms are omitted for clarity and thermal ellipsoids at the 50% probability level.

Bond	Distance (Å)	Bond	Angle (˚)	Bond	Angle (˚)
Ru1-O1	2.055(2)	O1-Ru1-N1	84.40(9)	O1-Ru1-O2	92.43(9)
Ru1-O2	2.056(2)	O1-Ru1-N2	86.89(9)	Ru1-O1-C21	123.9(2)
Ru1-N1	2.041(2)	O2-Ru1-N1’	86.05(9)	Ru1-O2-C23	122.9(2)
Ru1-N2	2.008(3)	O2-Ru1-N2’	89.86(9)	O1-C21-C22	125.1(3)
Ru1-N1’	2.050(2)	N1-Ru1-N2	79.34(10)	O2-C23-C22	126.5(3)
Ru1-N2’	2.025(3)	N1’-Ru1-N2’	78.85(10)	C21-C22-C23	128.6(3)
O1-C21	1.275(4)				
O2-C23	1.270(4)				
C21-C22	1.394(4)				
C22-C23	1.399(4)				

Table 4.7 Bond lengths and angles for complex **C’7**. ESDs given in parentheses.

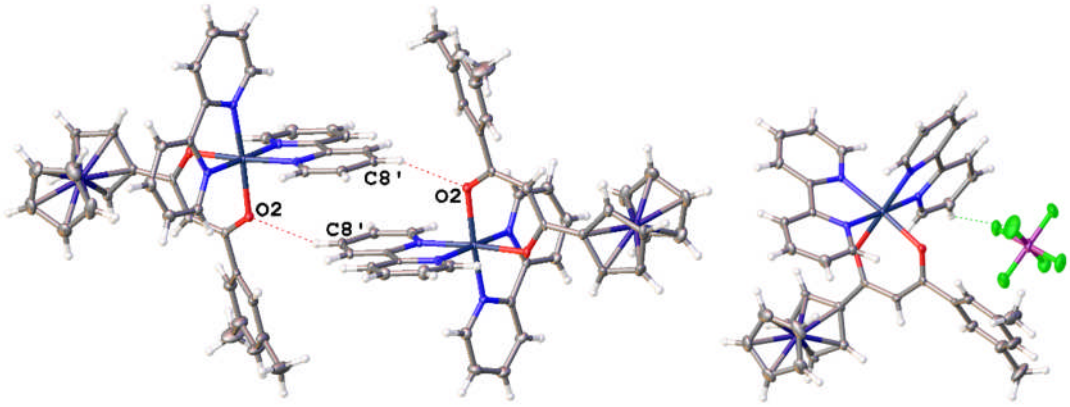

Figure 4.11 Intermolecular and intramolecular interactions for complex **C’7**. Only selected intermolecular interactions shown for charity.

Interaction	Bond D…A	Distance (Å)	Bond D…A	Distance (Å)
Intermolecular	C8’-H…O2	3.291(3)	C16-H…N1’	3.827(3)
	C14-H…N1	4.033(3)	π π	3.667(13)

Table 4.8 Intermolecular and intramolecular bond lengths and angles for complex **C’7**. ESDs given in parentheses.

4.1.2.5 X-Ray Characterisation of Complex C’8

Black single crystals of complex **C’8** were obtained by the slow evaporation of acetone. The molecular structure is shown in **Figure 4.12** with notable bond lengths and angles stated in **Table 4.9**. Intramolecular and intermolecular interactions are shown in **Figure 4.13** with bond lengths and angles stated in **Table 4.10**. Complex **C’8** crystallised in a monoclinic cell and structural solution performed in the $P2_1/c$ space group with one molecule per asymmetric unit.

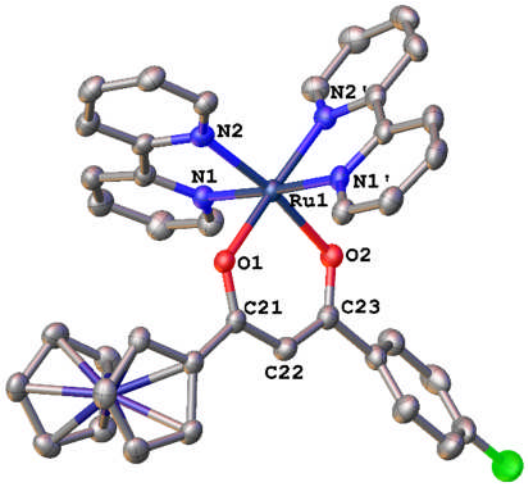

Figure 4.12 Molecular structure of complex **C'8**. Hydrogen atoms and counter ion are omitted for clarity and thermal ellipsoids at the 50% probability level.

Bond	Distance (Å)	Bond	Angle (˚)	Bond	Angle (˚)
Ru1-O1	2.042(2)	O1-Ru1-N1	87.50(9)	O1-Ru1-O2	92.09(8)
Ru1-O2	2.064(2)	O1-Ru1-N2	81.67(8)	Ru1-O1-C21	124.8(2)
Ru1-N1	2.043(2)	O2-Ru1-N1'	90.03(9)	Ru1-O2-C23	122.6(2)
Ru1-N2	2.029(2)	O2-Ru1-N2'	89.68(9)	O1-C21-C22	125.7(3)
Ru1-N1'	2.052(2)	N1-Ru1-N2	79.61(10)	O2-C23-C22	127.5(3)
Ru1-N2'	2.040(2)	N1'-Ru1-N2'	79.30(10)	C21-C22-C23	127.2(3)
O1-C21	1.274(4)				
O2-C23	1.288(4)				
C21-C22	1.408(4)				
C22-C23	1.385(4)				

Table 4.9 Bond lengths and angles for complex **C'8**. ESDs given in parentheses.

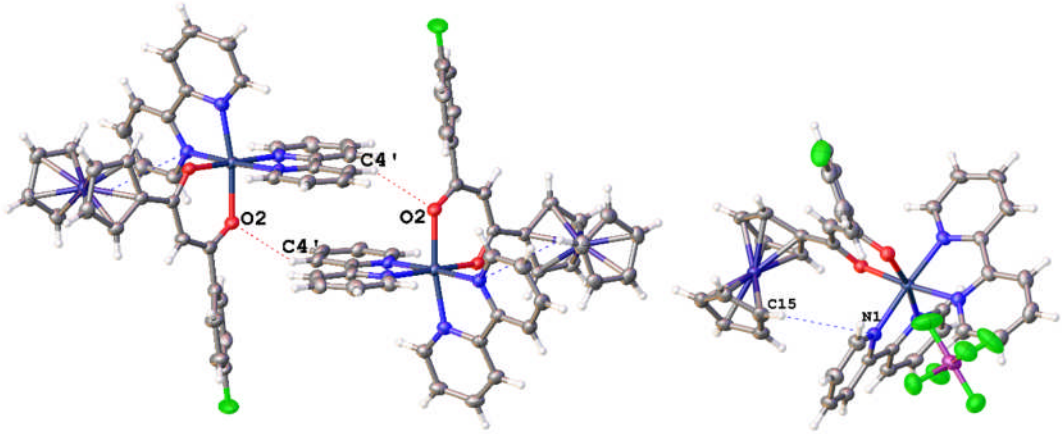

Figure 4.13 Intermolecular and intramolecular interactions for complex **C'8**. Only selected intermolecular interactions shown for charity.

Interaction	Bond D…A	Distance (Å)	Bond D…A	Distance (Å)
Intramolecular	C15-H…N1	3.964(7)		
Intermolecular	C4'-H…O2	3.213(5)	C17-H…F1	3.464(6)
	C2-H…N2'	4.071(7)	C22-H…F1	3.464(6)
	C11-H…F1	3.460(5)	π π	3.864(7)

Table 4.10 Intermolecular and intramolecular bond lengths and angles for complex **C'8**. ESDs given in parentheses.

4.1.2.6 X-Ray Characterisation of Complex C'10

Black single crystals of complex **C'10** were obtained by the slow evaporation of acetone. The molecular structure is shown in **Figure 4.14** with notable bond lengths and angles stated in **Table 4.11**. Intramolecular and intermolecular interactions are shown in **Figure 4.15** with bond lengths and angles stated in **Table 4.12**. Complex **C'10** crystallised in a triclinic cell and structural solution performed in the *P*-1 space group with one molecule and one molecule of acetone per asymmetric unit.

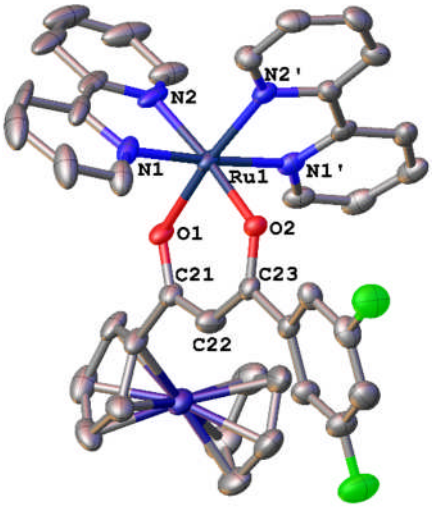

Figure 4.14 Molecular structure of complex **C'10**. Hydrogen atoms and counter ion are omitted for clarity and thermal ellipsoids at the 50% probability level.

Bond	Distance (Å)	Bond	Angle (˚)	Bond	Angle (˚)
Ru1-O1	2.054(4)	O1-Ru1-N1	90.00(16)	O1-Ru1-O2	92.80(14)
Ru1-O2	2.053(4)	O1-Ru1-N2	85.98(17)	Ru1-O1-C21	122.7(3)
Ru1-N1	2.047(5)	O2-Ru1-N1'	86.60(16)	Ru1-O2-C23	123.8(3)
Ru1-N2	2.037(5)	O2-Ru1-N2'	83.91(16)	O1-C21-C22	126.8(5)
Ru1-N1'	2.047(5)	N1-Ru1-N2	79.4(2)	O2-C23-C22	125.8(5)
Ru1-N2'	2.029(4)	N1'-Ru1-N2'	80.09(18)	C21-C22-C23	128.1(6)
O1-C21	1.277(7)				
O2-C23	1.273(7)				
C21-C22	1.404(5)				
C22-C23	1.392(5)				

Table 4.11 Bond lengths and angles for complex **C'10**. ESDs given in parentheses.

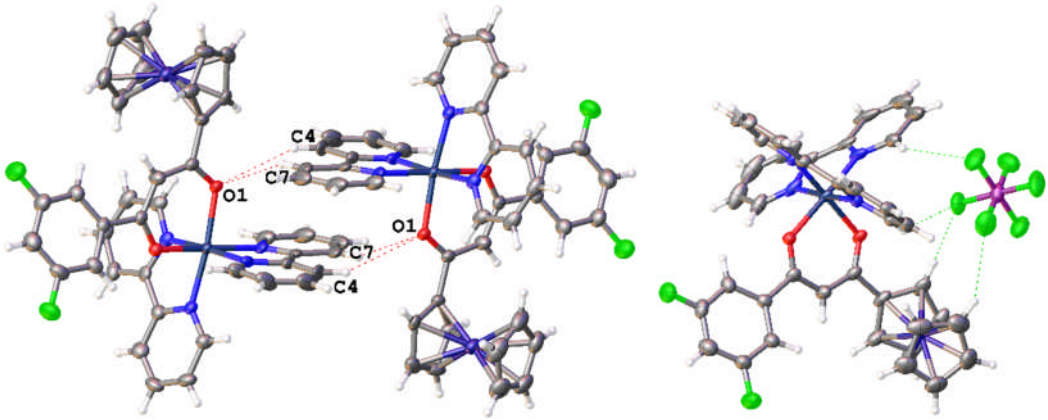

Figure 4.15 Intermolecular and intramolecular interactions for complex **C'10**. Only selected intermolecular interactions shown for charity.

Interaction	Bond D…A	Distance (Å)	Bond D…A	Distance (Å)
Intermolecular	C4-H…O1	3.715(8)	C2'-H…F2	4.135(7)
	C7-H…O1	3.695(14)	π π (Ph-Ph)	3.534(9)
	C13-H…N2	3.789(9)	π π	3.832(11)
	C13-H…N2'	3.784(9)		

Table 4.12 Intermolecular and intramolecular bond lengths and angles for complex **C'10**. ESDs given in parentheses.

4.1.2.7 X-Ray Characterisation of Complex C'11

Black single crystals of complex **C'11** were obtained by the slow evaporation of acetone. The molecular structure is shown in **Figure 4.16** with notable bond lengths and angles stated in **Table 4.13**. Intramolecular interactions of feasible distances were not observed in this case. Intermolecular interactions are shown in **Figure 4.17** with bond lengths and angles stated in **Table 4.14**. Complex **C'11** crystallised in a

triclinic cell and structural solution performed in the *P*-1 space group with two molecules and one molecule of water per asymmetric unit. Atoms corresponding to the second molecule in the asymmetric unit are marked by an asterisk.

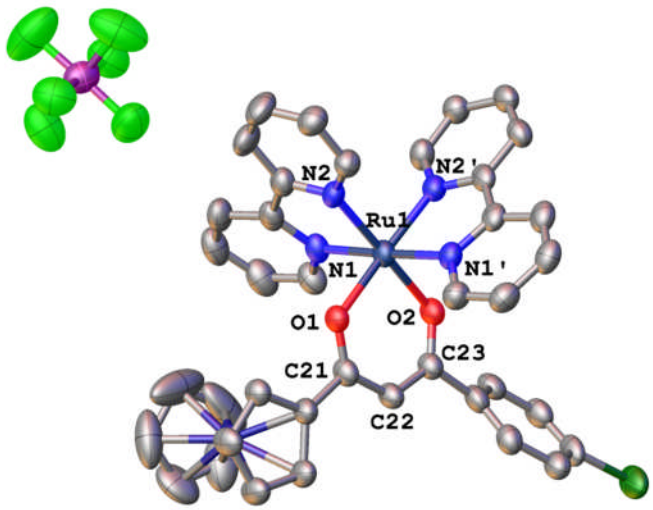

Figure 4.16 Molecular structure of complex **C'11**. Hydrogen atoms are omitted for clarity and thermal ellipsoids at the 50% probability level.

Bond	Distance (Å)	Bond	Angle (˚)	Bond	Angle (˚)
Ru1-O1	2.063(4)	O1-Ru1-N1	85.7(2)	O1-Ru1-O2	91.94(17)
Ru1-O2	2.072(5)	O1-Ru1-N2	90.1(2)	Ru1-O1-C21	123.6(4)
Ru1-N1	2.054(6)	O2-Ru1-N1'	86.1(2)	Ru1-O2-C23	122.7(4)
Ru1-N2	2.019(5)	O2-Ru1-N2'	89.8(2)	O1-C21-C22	126.2(6)
Ru1-N1'	2.060(6)	N1-Ru1-N2	79.5(2)	O2-C23-C22	126.8(6)
Ru1-N2'	2.029(6)	N1'-Ru1-N2'	79.1(2)	C21-C22-C23	127.5(7)
O1-C21	1.278(8)				
O2-C23	1.275(8)				
C21-C22	1.397(9)				
C22-C23	1.398(9)				

Table 4.13 Bond lengths and angles for complex **C'11**. ESDs given in parentheses.

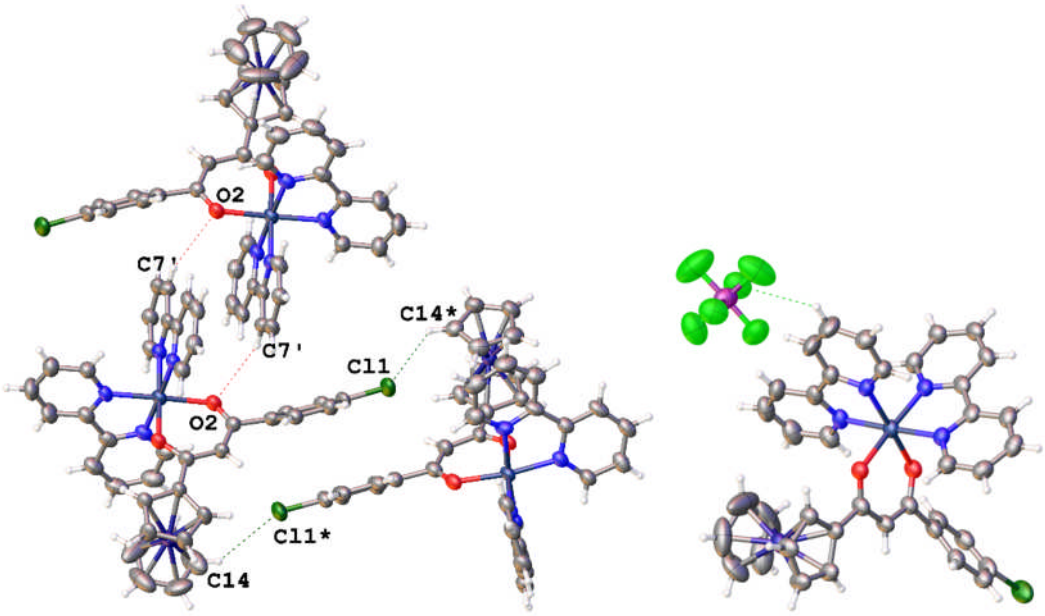

Figure 4.17 Intermolecular and intramolecular interactions for complex **C'11**. Only selected intermolecular interactions shown for charity.

Interaction	Bond D…A	Distance (Å)	Bond D…A	Distance (Å)
Intermolecular	**C4-H…N2'***	**3.372(1)**	**C7'-H…O2**	**3.465(2)**
	C17-H…Cl1	**3.805(2)**	**π π (Ph-Ph)**	**3.624(2)**
	C14*-H…Cl1	**3.708(2)**	**π π**	**3.993(2)**
	C18*-H…Cl1*	**3.706(2)**	**π π**	**3.594(2)**

Table 4.14 Intermolecular and intramolecular bond lengths and angles for complex **C'11**. ESDs given in parentheses.

4.1.2.8 X-Ray Characterisation of Complex C'12

Black single crystals of complex **C'12** were obtained by the slow evaporation of acetone. The molecular structure is shown in **Figure 4.18** with notable bond lengths and angles stated in **Table 4.15**. Intramolecular and intermolecular interactions are shown in **Figure 4.19** with bond lengths and angles stated in **Table 4.16**. Complex **C'12** crystallised in a monoclinic cell and structural solution performed in the $P2_1/c$ space group with one molecule and one water molecule per asymmetric unit.

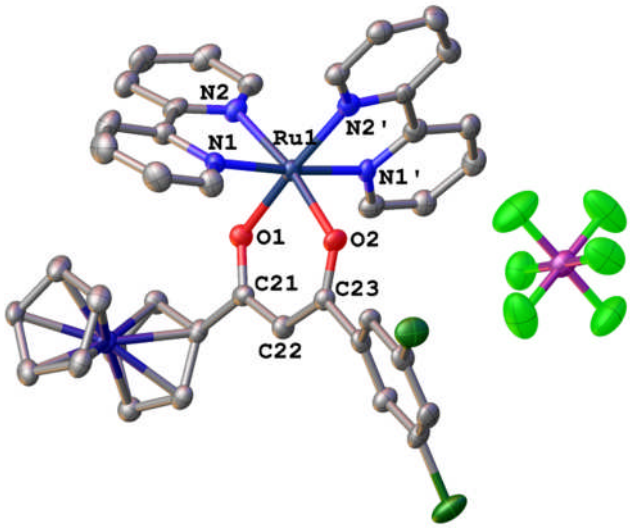

Figure 4.18 Molecular structure of complex **C'12**. Hydrogen atoms are omitted for clarity and thermal ellipsoids at the 50% probability level.

Bond	Distance (Å)	Bond	Angle (˚)	Bond	Angle (˚)
Ru1-O1	2.044(5)	O1-Ru1-N1	87.7(2)	O1-Ru1-O2	91.3(2)
Ru1-O2	2.078(5)	O1-Ru1-N2	81.4(2)	Ru1-O1-C21	125.9(5)
Ru1-N1	2.044(6)	O2-Ru1-N1'	89.6(2)	Ru1-O2-C23	122.7(4)
Ru1-N2	2.041(6)	O2-Ru1-N2'	89.0(2)	O1-C21-C22	125.4(7)
Ru1-N1'	2.046(6)	N1-Ru1-N2	79.5(2)	O2-C23-C22	128.1(6)
Ru1-N2'	2.044(6)	N1'-Ru1-N2'	79.3(2)	C21-C22-C23	126.4(7)
O1-C21	1.263(9)				
O2-C23	1.273(9)				
C21-C22	1.414(10)				
C22-C23	1.393(10)				

Table 4.15 Bond lengths and angles for complex **C'12**. ESDs given in parentheses.

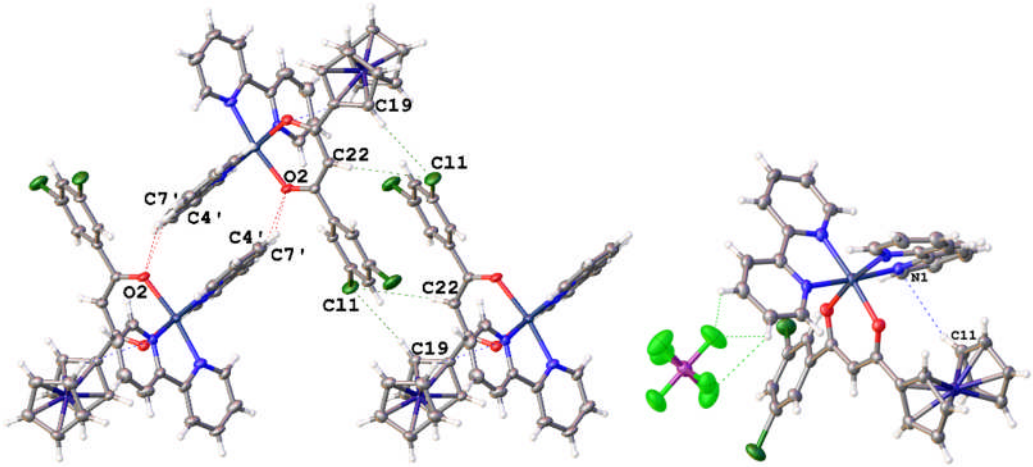

Figure 4.19 Intermolecular and intramolecular interactions for complex **C'12**. Only selected intermolecular interactions shown for charity.

Interaction	Bond D…A	Distance (Å)	Bond D…A	Distance (Å)
Intramolecular	C11-H…N1	3.822(10)		
Intermolecular	C4'-H…O2	3.395(9)	π π (Ph-Ph)	3.560(9)
	C7'-H…O2	3.520(7)	π π	3.629(9)
	C19-H…Cl1	3.882(11)		

Table 4.16 Intermolecular and intramolecular bond lengths and angles for complex **C'12**. ESDs given in parentheses.

4.1.2.9 X-Ray Characterisation of Complex C'13

Black single crystals of complex **C'13** were obtained by the slow evaporation of acetone. The molecular structure is shown in **Figure 4.20** with notable bond lengths and angles stated in **Table 4.17**. Intramolecular and intermolecular interactions are shown in **Figure 4.21** with bond lengths and angles stated in **Table 4.18**. Complex **C'13** crystallised in a triclinic cell and structural solution performed in the *P*-1 space group with two molecules per asymmetric unit. Atoms corresponding to the second molecule in the asymmetric unit are marked by an asterisk.

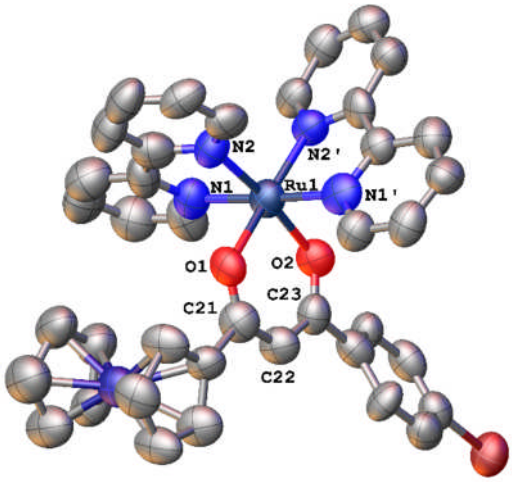

Figure 4.20 Molecular structure of complex **C'13**. Hydrogen atoms and counter ion are omitted for clarity and thermal ellipsoids at the 50% probability level.

Bond	Distance (Å)	Bond	Angle (˚)	Bond	Angle (˚)
Ru1-O1	2.053(7)	O1-Ru1-N1	86.9(3)	O1-Ru1-O2	92.2(3)
Ru1-O2	2.087(7)	O1-Ru1-N2	89.8(3)	Ru1-O1-C21	123.6(6)
Ru1-N1	2.061(9)	O2-Ru1-N1’	87.1(3)	Ru1-O2-C23	122.8(6)
Ru1-N2	2.045(8)	O2-Ru1-N2’	90.2(3)	O1-C21-C22	126.6(10)
Ru1-N1’	2.068(10)	N1-Ru1-N2	79.9(4)	O2-C23-C22	126.3(9)
Ru1-N2’	2.047(8)	N1’-Ru1-N2’	78.7(3)	C21-C22-C23	127.5(11)
O1-C21	1.286(13)				
O2-C23	1.279(12)				
C21-C22	1.400(15)				
C22-C23	1.384(13)				

Table 4.17 Bond lengths and angles for complex **C’13**. ESDs given in parentheses.

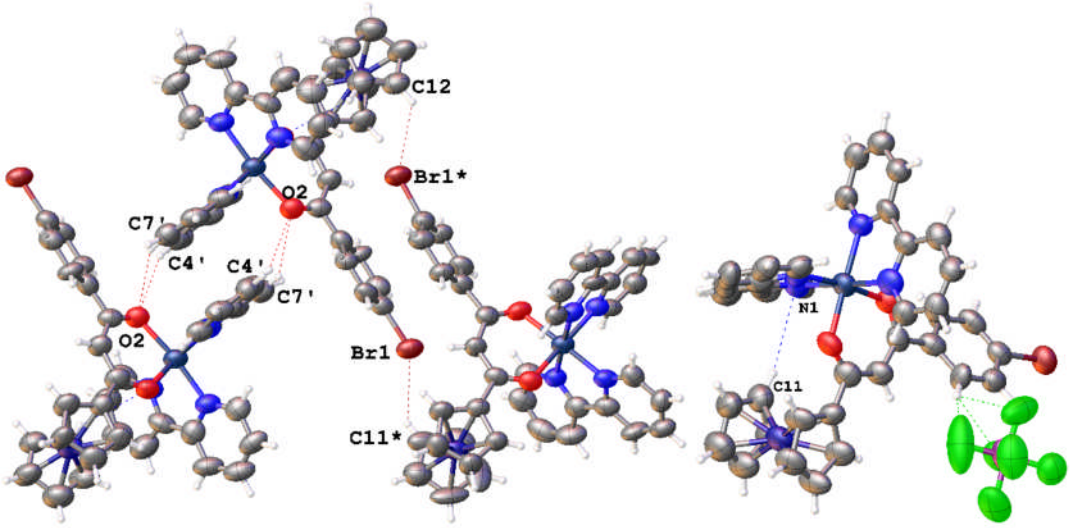

Figure 4.21 Intermolecular and intramolecular interactions for complex **C’13**. Only selected intermolecular interactions shown for charity.

Interaction	Bond D…A	Distance (Å)	Bond D…A	Distance (Å)
Intramolecular	C11-H…N1	3.975(9)		
Intermolecular	C4’-H…O2	3.584(6)	C12-H…Br1*	3.842(6)
	C7’-H…O2	3.526(11)	C17-H…Br1	3.991(9)
	C3*-H…Br1	4.125(10)	π π (Ph-Ph)	3.612(9)
	C11*-H…Br1	3.795(7)	π π	3.704(7)

Table 4.18 Intermolecular and intramolecular bond lengths and angles for complex **C’13**. ESDs given in parentheses.

4.1.2.10 X-Ray Characterisation of Complex C'14

Black single crystals of complex **C'14** were obtained by the slow evaporation of acetone. The molecular structure is shown in **Table 4.19** with notable bond lengths and angles stated in **Figure 4.22**. Intramolecular and intermolecular interactions are shown in **Figure 4.23** with bond lengths and angles stated in **Table 4.20**. Complex **C'14** crystallised in a triclinic cell and structural solution performed in the *P*-1 space group with two molecules per asymmetric unit. Atoms corresponding to the second molecule in the asymmetric unit are marked by an asterisk.

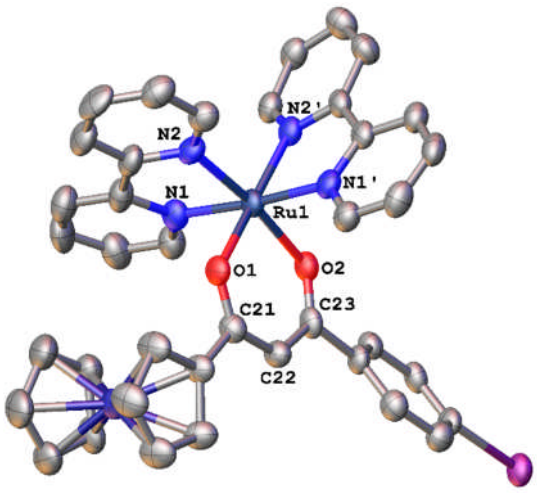

Figure 4.22 Molecular structure of complex **C'14**. Hydrogen atoms and counter ion are omitted for clarity and thermal ellipsoids at the 50% probability level.

Bond	Distance (Å)	Bond	Angle (˚)	Bond	Angle (˚)
Ru1-O1	2.041(5)	O1-Ru1-N1	87.1(2)	O1-Ru1-O2	92.18(19)
Ru1-O2	2.054(6)	O1-Ru1-N2	87.6(2)	Ru1-O1-C21	124.9(4)
Ru1-N1	2.040(7)	O2-Ru1-N1'	87.9(2)	Ru1-O2-C23	122.8(4)
Ru1-N2	2.030(6)	O2-Ru1-N2'	90.2(2)	O1-C21-C22	125.4(7)
Ru1-N1'	2.048(7)	N1-Ru1-N2	80.2(3)	O2-C23-C22	127.4(6)
Ru1-N2'	2.027(6)	N1'-Ru1-N2'	79.3(3)	C21-C22-C23	126.3(7)
O1-C21	1.272(9)				
O2-C23	1.275(9)				
C21-C22	1.421(10)				
C22-C23	1.402(9)				

Table 4.19 Bond lengths and angles for complex **C'14**. ESDs given in parentheses.

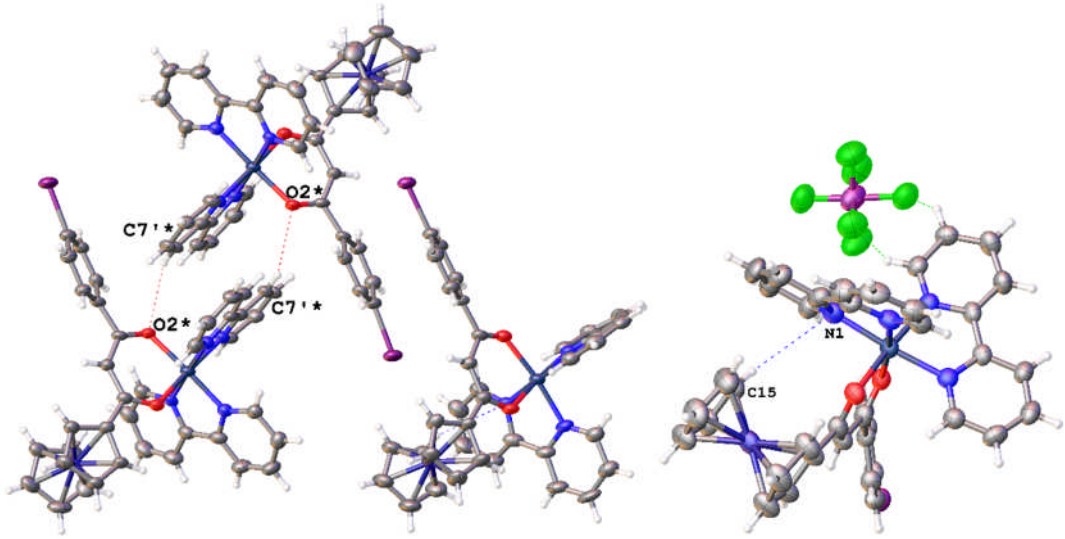

Figure 4.23 Intermolecular and intramolecular interactions for complex **C'14**. Only selected intermolecular interactions shown for charity.

Interaction	Bond D…A	Distance (Å)	Bond D…A	Distance (Å)
Intramolecular	**C15-H…N1**	**3.982(11)**		
Intermolecular	**C4'-H…O2**	**3.653(10)**	**π π**	**3.938(7)**
	C7'*-H…O2*	**3.449(8)**	**π π**	**3.896(7)**
	π π (Ph-Ph)	**3.807(6)**	**π π**	**3.598(7)**

Table 4.20 Intermolecular and intramolecular bond lengths and angles for complex **C'14.** ESDs given in parentheses.

4.2 Conclusion

A library of novel ruthenium(II) bipyridyl complexes containing functionalised ferrocene β-diketonate ligands possessing varying electronic and steric properties has been synthesised. Complexes have been fully characterised by ^{1}H NMR, ^{13}C [^{1}H] NMR, micro-analysis, mass spectrometry and X-ray crystallographic analysis (when possible). As seen in the previous chapter, ^{1}H NMR and ^{13}C [^{1}H] NMR spectra of the complexes show distinct shifts of the ligand peaks, particularly those associated with the ferrocene moiety and methine CH. Single crystals of these complexes were grown from the slow evaporation or vapour diffusion methods to give purple/black single crystals in all cases. Structural solutions were performed in triclinic cells in all cases except complex **C'1**, **C'7**, **C'8** and **C'12** which were monoclinic. Observed angles around the ruthenium metal centre are in the range of 81-90˚ showing that all complexes exist in a distorted octahedral geometry. The N1 of the bipyridine ligand and ferrocene Cp rings have been shown to be involved in intramolecular hydrogen bonding interactions in complexes **C'1**, **C'4**, **C'8**, **C'12, C'13** and **C'14**. Multiple intermolecular hydrogen bonding interactions are seen in all complexes with π-π stacking observed for all complexes except **C'2**. PF_6 counter ion is involved in both inter- and intra-molecular interactions. The bonding interactions which are observed in the solid state may help us to understand how these complexes interact with their biological targets.

As with the ruthenium arene complexes, the various steric and electronic properties of the functionalised ferrocene β-diketonate ligands facilitates the determination of any structural activity relationships. The biological activity of these complexes will be discussed in Chapter 5.

4.3 References

1. C.-W. Jiang, H. Chao, X.-L. Hong, H. Li, W.-J. Mei and L.-N. Ji, *Inorganic Chemistry Communications*, 2003, **6**, 773-775.
2. J.-G. Liu, B.-H. Ye, Q.-L. Zhang, X.-H. Zou, Q.-X. Zhen, X. Tian and L.-N. Ji, *JBIC Journal of Biological Inorganic Chemistry*, 2000, **5**, 119-128.
3. H.-L. Huang, Z.-Z. Li, Z.-H. Liang and Y.-J. Liu, *European Journal of Inorganic Chemistry*, 2011, **2011**, 5538-5547.
4. M. R. Gill and J. A. Thomas, *Chemical Society Reviews*, 2012, **41**, 3179-3192.
5. F. Dwyer, E. C. Gyarfas, W. Rogers and J. H. KOCH, *Nature*, 1952, **170**, 190.
6. A. Shulman and F. Dwyer, *Chelating Agents and Metal Chelates*, 1964, 383-439.
7. N. L. Kilah and E. Meggers, *Australian Journal of Chemistry*, 2012, **65**, 1325-1332.
8. F. Gao, H. Chao and L.-N. Ji, *Chemistry & Biodiversity*, 2008, **5**, 1962-1979.
9. M. R. Gill and J. A. Thomas, *Chemical Society Reviews*, 2012, **41**, 3179-3192.
10. Y. Y. Lee, D. B. Walker, J. J. Gooding and B. A. Messerle, *Dalton Transactions*, 2014, **43**, 12734-12742.

Chapter 5: Cytotoxicity and Antimicrobial Evaluation

5.0 *In vitro* Cytotoxicity Evaluation

Cytotoxicity and cell viability assays used during *in vitro* toxicology studies are based on a variety of cell functions such as enzyme activity, cell membrane permeability, cell adherence, ATP production, co-enzyme production, and nucleotide uptake activity.[1] These cell-based assays are used to measure metabolic biomarkers attributed to the aforementioned cellular activities and facilitate the screening of libraries of drug candidates to determine if the compounds produce any positive effects in the way of cell anti-proliferation or cytotoxicity.[2] There are many different assay methods which can be used to deduce the activity of a given compound but they all work with the same underlying premise, that the measured cell biomarker activities are relative to the number of viable cells and, therefore, a reduction in cell activity compared to a control is indicative of cell-cycle arrest or programmed cell death.[3]

5.0.1 MTT assay

The MTT (3-(4,5-diemthylthiazolyl-2)-2,5-diphenyltetrazolium bromide) assay is a sensitive and reliable colorimetric assay which is used as an indicator of cellular metabolic activity. Existing as a yellow water-soluble tetrazolium dye, MTT is able to be reduced to its water-insoluble purple formazan equivalent by NADPH or NADH dependent cellular oxidoreductase enzymes (**Scheme 5.1**). Therefore, this assay uses the enzymatic conversion of MTT to formazan, mainly from the reductive activity of dehydrogenases found in the mitochondria of living cells, as a measure of cell viability.[4, 5]

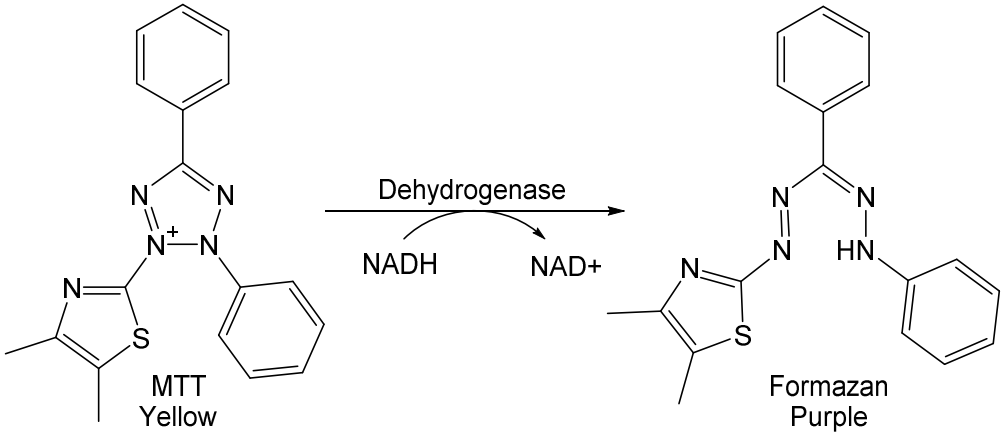

Scheme 5.1 Reduction of MTT to Formazan[4, 5]

Potential anticancer drugs are incubated with cancer cells at 37 ˚C for periods of 3-5 days. After this time the aqueous MTT solution is added to the cells followed by a further 3-4 hours of incubation time to allow for the reduction of MTT. The MTT solution/medium is removed from the incubation wells *via* pipette to leave behind the insoluble formazan crystals which are then dissolved in DMSO. The absorbance of the formazan solution is measured between 500 and 600 nm to calculate the concentration of converted MTT and hence, viable cells, allowing for the calculation of IC_{50} values.

5.1 Cytotoxicity Screening

5.1.1 Cytotoxicity Results & Discussion

Cytotoxic screening was conducted at the University of Huddersfield by Pablo Caramés-Méndez under the supervision of Samantha Sheppard and Prof. Roger Philips on the complexes described in Chapters 3 and 4, with cisplatin, carboplatin and oxaliplatin as controls. The cell lines used comprise of two cancerous cell lines, MIA PaCa-2 (human pancreatic carcinoma) and HCT116++ (human colon carcinoma), and a non-cancerous cell line, ARPE-19 (human retinal pigment epithelial cells). Assays were carried out over a 5-day period with 4-day drug exposure and incubation period at 37 °C, after which time the incubated cells were treated with MTT solution (5 mg/mL) with the concentration of the surviving cells being determined from the

measured absorbance at 540 nm. It should be noted that complexes were dissolved in DMSO for their use in cell line testing. Due to the potential for DMSO binding to the complexes, samples were frozen and prepared fresh if necessary. IC_{50} values were calculated for each complex by plotting a graph of percentage cell survival against drug concentration (μM) with the final value being found at 50% cell survival. An example of a concentration curve used in the determination of an IC_{50} value is shown in **Figure 5.1**.

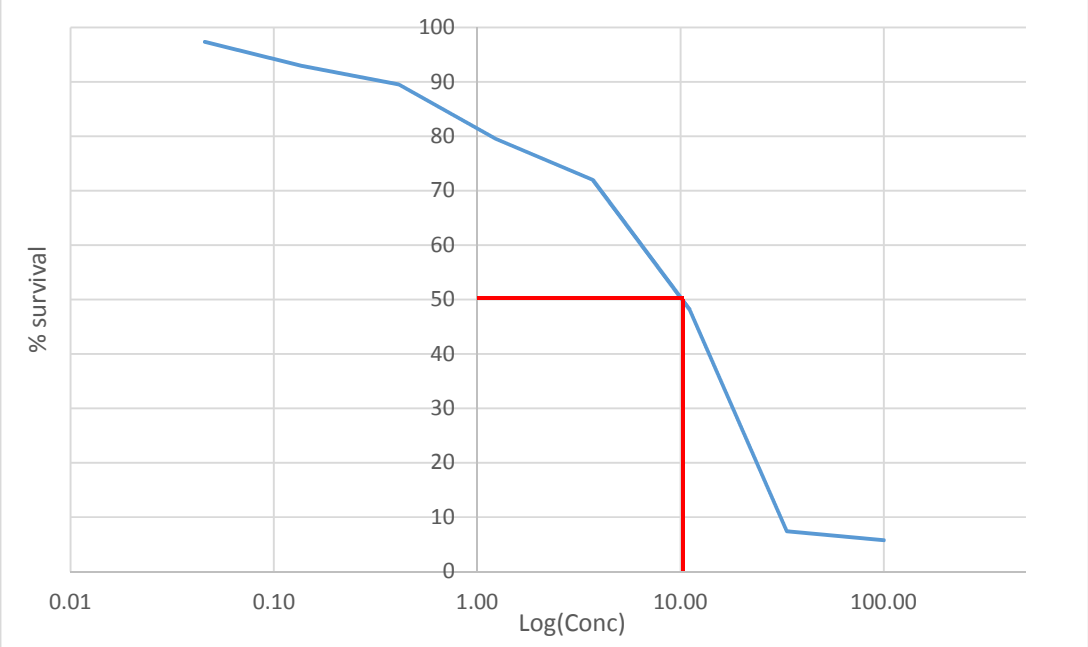

Figure 5.1 Logarithmic graph to show IC_{50} determination for complex **C5**

Cytotoxic results for the ruthenium arene piano stool complexes and bpy coordination complexes have been tabulated and summarised in the form of a bar chart in **Figure 5.2** and **Figure 5.3**, respectively.

Table 5.1 Summary of IC_{50} values for cisplatin, carboplatin, oxaliplatin and ruthenium arene complexes against MIA PaCa-2, HCT116++ and ARPE-19 averaged over 3 runs

Complex	MIA PaCa-2		HCT116++		ARPE-19	
	IC_{50} (μM)	±SD (μM)	IC_{50} (μM)	±SD (μM)	IC_{50} (μM)	±SD (μM)
Cisplatin	3.62	0.74	3.26	0.38	6.41	0.95
Carboplatin	35.59	7.91	32.37	11.14	-	-
Oxaliplatin	6.44	1.05	0.93	0.12	6.15	2.68
C1	93.33	11.55	91.72	7.18	100	-
C2	11.39	3.24	50.82	3.63	100	-
C3	100	-	94.84	8.94	100	-
C4	40.14	9.16	75.12	10.51	100	-
C5	7.9	2.32	72.41	18.65	100	-
C6	49.58	6.33	83.64	8.58	100	-
C7	100	-	100	-	100	-
C8	74.83	2.1	100	-	100	-
C9	100	-	83.84	14.25	100	-
C10	24.54	3.53	52.37	11.69	100	-
C11	32.61	2.9	84.67	12.94	100	-
C12	26.19	1.87	85.25	13.52	100	-
C13	100	-	92.9	6.16	100	-
C14	100	-	83.95	15.57	100	-
C15	28.51	3.29	78.38	17.34	100	-
C16	100	-	74.61	19.31	100	-
C17	26.26	7.99	53.25	16.11	100	-
C18	100	-	87.83	21.08	100	-
C19	100	-	64.88	18.93	100	-
C20	100	-	100	-	100	-
C21	25.14	7.44	88.83	19.35	100	-
C22	65.09	21.02	100	-	100	-
C23	40.44	10.29	87.98	16.64	100	-
C24	38.78	8.07	48.11	8.07	100	-

Note – No standard deviation is given for complexes with activity lower than the 100 μM limit

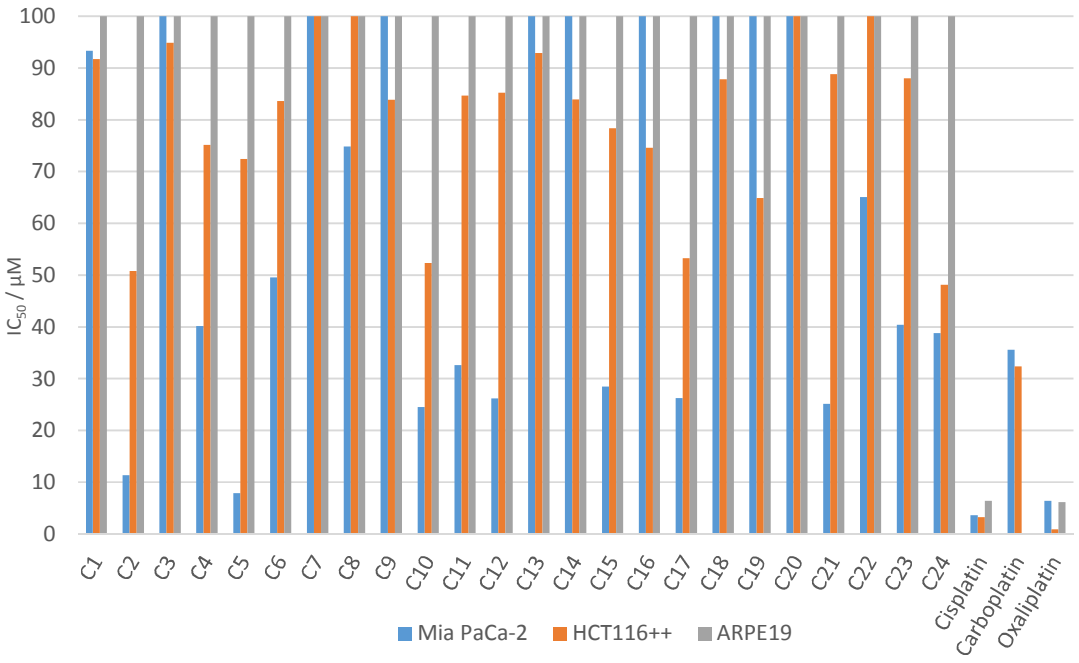

Figure 5.2 Chart to summarise the IC_{50} values for the ruthenium arene complexes

From the cell line data it is not possible to derive any general structural-activity relationships for these complexes against either cell line. However, what is evident is that these complexes are generally much more active towards the MIA PaCa-2 cell line than the HCT116++ cell line. *p*-Cymene ruthenium arene complexes previously reported in the McGowan group have similarly shown a lack of overall trend in activity.[6]

The most active arene complexes against the MIA PaCa-2 cell line were found to be **C2** (R = CF_3) and **C5** (R = 2-furan), with IC_{50} values of 11.39 µM and 7.90 µM respectively, compared to 3.62 µM for cisplatin. Interestingly, when the CF_3 group of **C2** is substituted for the CHF_2 group of **C3** the complex is rendered almost completely inactive towards both cancer cell lines and is, in fact, one of the least cytotoxic of all the tested complexes. Similarly, the substitution of the 2-furan substituent of **C5** to the 3-furan of **C4** gave a decrease of activity but to a much lesser extent than that observed between **C2** and **C3**.

Although complexes **C1**-**C24** may not be as active as the well-known platinum-based anticancer drugs, their selectivity towards cancerous cells is greatly increased. The obtained IC_{50} values for all the tested ruthenium arene complexes was found to

be > 100 μM for the ARPE-19 cell line, demonstrating the lack of toxicity towards healthy cells at concentrations lower than the experimental threshold. Therefore, it is plausible that these complexes will be tolerated much better by the body than the platinum-centred drugs and may present less severe side effects *in vivo*, allowing higher concentrations of these complexes to be administered during cancer chemotherapy to compensate for the lower cancer cell activity.[7, 8]

Table 5.2 Summary of IC_{50} values for cisplatin, carboplatin, oxaliplatin and ruthenium bipyridyl complexes against MIA PaCa-2, HCT116++ and ARPE-19 averaged over 3 runs

Complex	MIA PaCa-2		HCT116++		ARPE-19	
	IC_{50} (μM)	±SD (μM)	IC_{50} (μM)	±SD (μM)	IC_{50} (μM)	±SD (μM)
Cisplatin	3.62	0.74	3.26	0.38	6.41	0.95
Oxaliplatin	6.44	1.05	0.93	0.12	6.15	2.68
Carboplatin	35.59	7.91	32.37	11.14	-	-
C'1	0.43	0.1	0.34	0.03	0.74	0.04
C'2	2.41	0.25	2.95	0.12	2.71	0.52
C'3	0.11	0.01	0.23	0.07	0.10	0.03
C'4	0.13	0.01	0.30	0.04	0.32	0.07
C'5	0.09	0.02	0.11	0.03	0.11	0.03
C'6	0.13	0.03	0.21	0.03	0.21	0.02
C'7	0.12	0.01	0.30	0.04	0.25	0.08
C'8	0.25	0.03	0.32	0.04	0.18	0.06
C'9	0.33	0.01	0.72	0.05	0.27	0.03
C'10	0.35	0.02	0.82	0.07	0.35	0.06
C'11	0.16	0.04	0.32	0.04	0.13	0.02
C'12	0.1	0.02	0.11	0.00	0.13	0.01
C'13	0.12	0.01	0.30	0.07	0.13	0.03
C'14	0.12	0.02	0.19	0.04	0.11	0.02
C'15	0.22	0.03	0.25	0.06	0.13	0.03

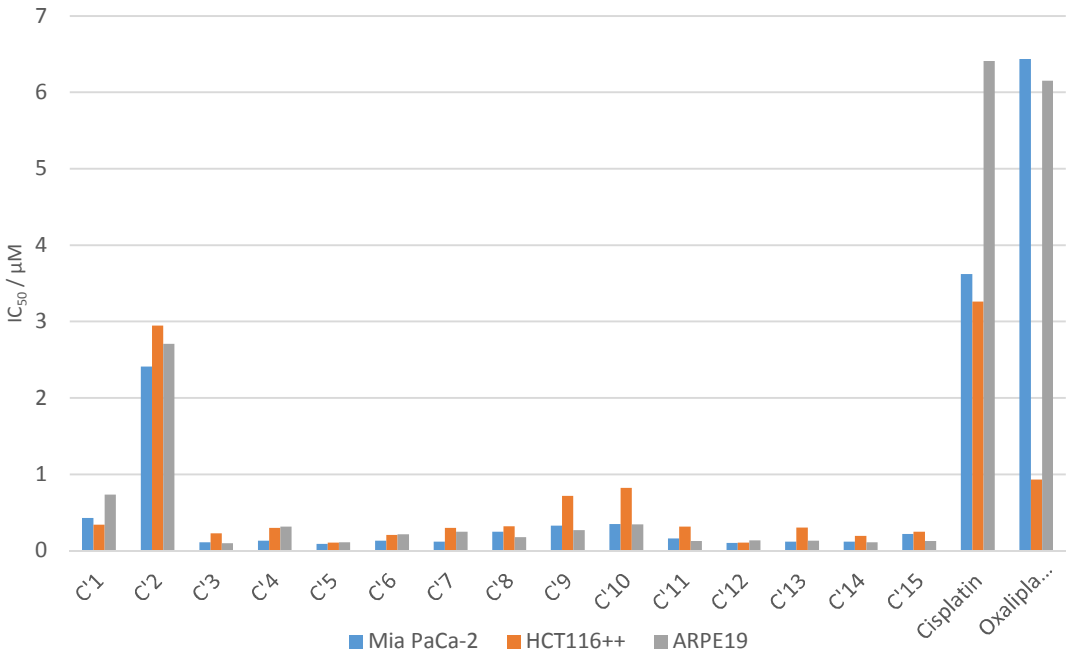

Figure 5.3 Chart to summarise the IC_{50} values for the ruthenium bpy complexes

The ruthenium coordination complexes were found to be highly cytotoxic towards all tested cell lines (**Figure 5.3**) with IC_{50} values in the nanomolar range, demonstrating cytotoxicity which is superior to that of cisplatin, a chemical attribute that still holds true even when the least active complex is taken into consideration. The most active complex **C'5** was found to be 40-fold more active than cisplatin against the MIA PaCa-2 cell line. Surprisingly, the least active complex (**C'2**) was found to contain the CF_3 moiety, a feature which has been shown in the literature to enhance the potency of many drug candidates.[9] This observation is also in contrast to the aforementioned arene complexes where the complex containing the same ligand was shown to possess high levels of activity. However, the lower activity in this case may be explained due to the electron withdrawing ability of the CF_3 group, removing electron density from the ruthenium/β-diketonate bonds and potentially leading to a reduced stability of the complex. As with the arene complexes, the observed activity towards the MIA PaCa-2 cell line is generally greater than towards the HCT116++ cell line.

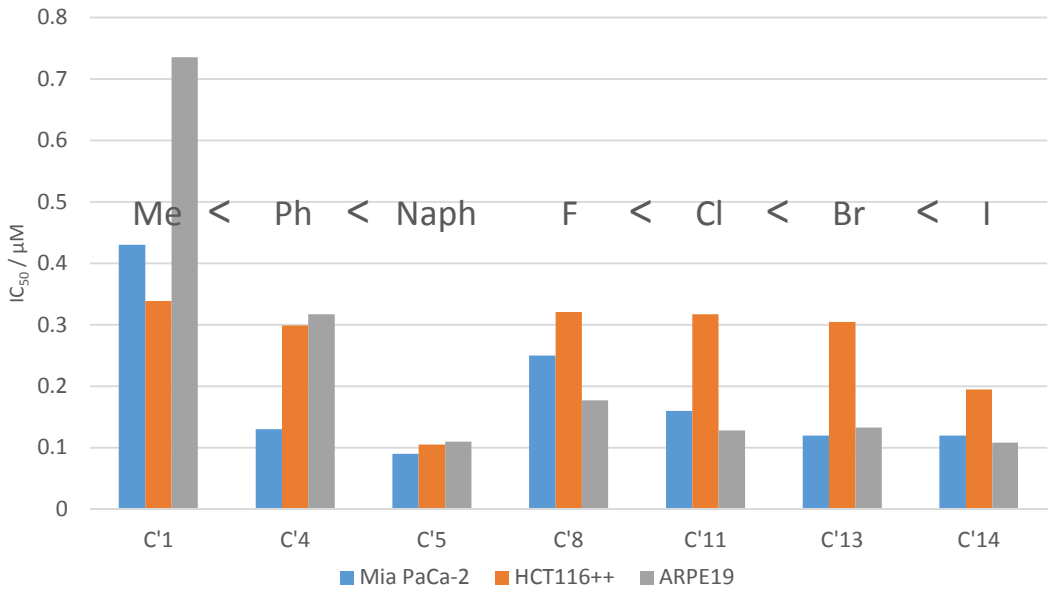

Figure 5.4 Chart to summarise the trends in IC_{50} values for the ruthenium bpy complexes

A clear correlation can be seen between the increasing aromaticity of the R substituent on the β-diketonate ligand and the cytotoxicity of the complexes across all cell lines tested (Me < Ph < Naph) (**Figure 5.4**), a finding which is common for ruthenium polypyridyl complexes.[10] One justification could be that the increasing hydrophobicity may be aiding in the passive transport through the cell membrane into the cell. Moreover, the increased aromaticity allows for greater overlap between the π systems of the complex and DNA bases during intercalation, increasing the binding affinity. Groove binding may also be increased with the increased size of the R group as the additional aromaticity and torsional freedom allows the complex to span more base pairs and increases the number of possible binding sites in the major and minor grooves of DNA. Another such correlation in the cytotoxic behaviour can be observed for the halogen substituents at the *para* position of the phenyl ring on the β-diketonate ligand, as moving down the halogen column of the periodic table resulted in an increase in the cytotoxicity of the complexes.

Table 5.3 Selectivity of ruthenium bipyridyl complexes

Complex	MIA PaCa-2	ARPE19	Selectivity
Cisplatin	3.62	6.41	1.77
C'1	0.43	0.74	1.72
C'2	2.41	2.71	1.12
C'3	0.11	0.10	0.91
C'4	0.13	0.32	2.46
C'5	0.09	0.11	1.22
C'6	0.13	0.21	1.62
C'7	0.12	0.25	2.08
C'8	0.25	0.18	0.72
C'9	0.33	0.27	0.82
C'10	0.35	0.35	1.00
C'11	0.16	0.13	0.81
C'12	0.1	0.13	1.30
C'13	0.12	0.13	1.08
C'14	0.12	0.11	0.92
C'15	0.22	0.13	0.59

Selectivity was calculated from ARPE19/MIA PaCa-2

An initial indicator of selectivity of the complexes is given as a ratio of IC_{50} values in ARPE-19 cells to cancer cells (in this case MIA PaCa-2), with a value of > 1 demonstrating increased response from cancer cells (**Table 5.3**). Compounds tested which showed preferential selectivity towards cancer cell lines are highlighted in yellow (selectivity between 1-1.5) and complexes with values highlighted in green were found to have comparable or superior selectivity to that of cisplatin (selectivity > 1.5).

A decrease in selectivity can be observed from **C'4** (R = Ph) to **C'5** (R = Naph), as the increasing activity with the larger aromaticity of the R substituent also increases activity of the complexes towards ARPE-19. A further, and more general, decrease can be seen with regards to the halogenated phenyl ring moieties in comparison to the unsubstituted ring or ones which contain alkyl substituents. However, the selectivity is not favoured by more electropositive polar effects, which this observation may indicate as **C'15,** containing an electron donating group (*p*-OMe), possesses the worst selectivity of all the coordination complexes studied. These

findings then suggest that preferential cytotoxicity is favoured towards complexes containing β-diketonate ligand with more neutral electronic proerties.

5.2 Cytotoxicity Studies under Hypoxic Conditions

5.2.1 Hypoxia in human tumours

Hypoxia, the result of an inadequate supply of oxygen, is a common feature of many solid tumours. The oxygen levels in healthy human tissue (normoxia/physoxia) ranges between 4.6 and 9.5 % but varies greatly between different organs due to the diverse blood vessel network and metabolic activity. Hypoxic tissue, on the other hand, experiences a decrease in oxygenation in comparison to healthy tissue and exists with average oxygen levels of between 1-2 %.[11] Growing past a diameter of 1mm, tumours must begin to develop their own blood supply by creating a vascular network from either pre-existing blood vessels or by forming new microvessels through angiogenesis. However, the network formed during the rapid growth phase of the tumour is usually quite inadequate and riddled with abnormalities, leading to a hindered flow of blood and as a result, a restricted supply of oxygen **Figure 5.5**.[12-16]

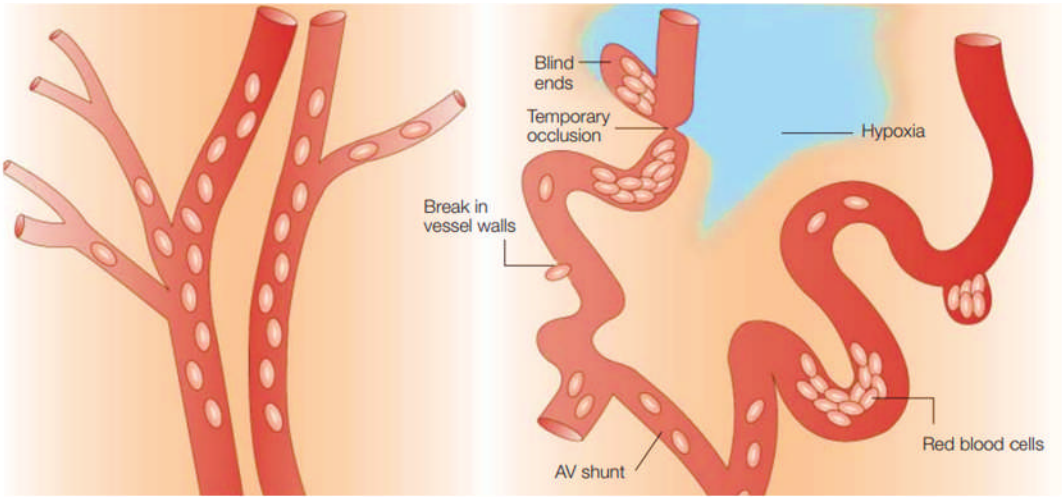

Figure 5.5 Examples of vascular networks inside normal and tumour tissue[17]

Hypoxic cells have been well known to cause resistance towards radiotherapy treatments from as early as the 1950s, when Gray *et al.* performed studies to

establish the effect of ionizing radiation on cells.[18] During the study they noted a remarkable reduction in the ionizing effects in the absence of oxygen, although this finding was not new. Earlier reports had demonstrated similar radioresistance in the absence of oxygen but were thought to be a product of lower metabolic rate of the cells rather than oxygen tension.[19-22] Rather, it has now been hypothesised that the high affinity of oxygen for the free radical on the irradiated DNA solidifies the radiation damage at a physicochemical level, preventing chemical restitution (**Scheme 5.2**).[23, 24]

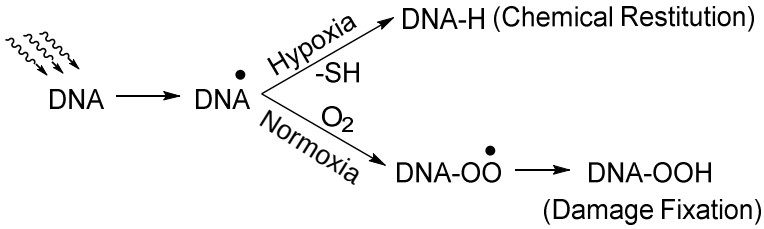

Scheme 5.2 Mechanism of radiation induced DNA damage in normoxia and hypoxia[22]

Furthermore, hypoxic cells are considered to be resistant to a multitude of chemotherapy drugs.[25] Clear links between chemotherapy resistance and hypoxia have been proven through preclinical studies which show that this occurrence arises for several reasons; hypoxic cells are located further away from a blood supply (blood vessel, capillary etc.) than most healthy cells, and hence they are not exposed to the same concentrations of anticancer compound as it travels around the cardiovascular system.[26-28] Cellular proliferation is another factor that also decreases with increasing distance from blood supply.[29] Hypoxia favours the formation of cells which are desensitised towards p53-mediated cell apoptosis, a common biological exploit during the mechanism of action of a number of anticancer compounds.[30] On a similar note, the cytotoxicity of some anticancer complexes is due to their ability to form reactive oxygen species inside a cell, leading to DNA damage and cell death. Evidently in hypoxia, this pathway is not as feasible as with cells in normoxic conditions.[31, 32] Upregulation of genes involved in drug resistance, such as p-glycoprotein and HIF-1, is common in hypoxia.[33, 34] Furthermore, the reducing environment associated with hypoxia can cause particular difficulties for transition

metals as a change in their oxidation state can lead to a change in their structure, binding mode, cellular drug uptake, metabolism, and even reduce the effectiveness of their cellular mechanism of action or change it completely.[6]

5.2.2 Responses to Hypoxia

Hypoxia has been shown to impair growth and provoke cell death through changes in the proteome of tumour cells. On the other hand, some of the proteomic changes actually help the tumour to successfully adapt and thrive in the low-oxygen, nutrient-deprived state.[35-39] Hypoxic cells undergo multiple adaptive responses to the low oxygen conditions which allow them to survive and proliferate.[40] The development of a more effective nutrient and oxygen supply is created through the changes in expression of genes for erythropoietin, transferring receptors, and the angiogenic vascular endothelial growth factor (VEGF), amongst other proteins. Cellular energy requirements are also met through the control of glycolytic enzymes and glucose transporters in the metabolic pathway by these adaptive response genes. Gene expression for a number of the aforementioned proteins is regulated by the transcriptional hypoxia-inducible factor (HIF-1α), a factor which also contributes to the aggressiveness of a tumour through the regulation of genes involved in invasion and metastasis, such as downregulation of adhesion molecules.[41-50]

5.2.3 HIF-1

HIF-1 is a heterodimeric transcription factor, comprising of HIF-1α and HIF-1β subunits, which mediates adaptive responses to hypoxia.[42] The HIF-1β subunit is a constitutively expressed nuclear protein which is independent of oxygen tension. Conversely, HIF-1α is an oxygen sensitive cytoplasmic protein whose expression and activity is regulated by cellular oxygen concentrations.[51, 52] In well oxygenated cells, HIF-1α is continuously degraded by the hydroxylation of select prolyl residues of the subunit by oxygen-dependant enzyme activity. These hydroxylated prolyl sites cause the HIF-1α to be recognised by the von Hippel-Lindau tumour suppressor protein

which further modifies HIF-1α, marking it for degradation by the proteasome.[53, 54] Under hypoxic conditions, the HIF-1α subunits do not undergo hydroxylation but instead migrate to the nucleus of the cell, where they are stabilised by the HIF-1β subunits and heterodimerise into the active HIF-1 protein.[55, 56] It is this active HIF-1 which goes on to bind to the core DNA and activates the transcription of hundreds of genes (transferrin, VEGF, glycotic enzymes etc.) which are over expressed in human tumour cells.[44, 57, 58]

5.2.4 Hypoxia Results and Discussion

In order to assess the influence of oxygen concentration upon chemosensitivity, the arene compounds which showed the highest activity against MIA PaCa-2 cells under normoxic conditions were selected. Complexes **C2** and **C5** were studied over a five day period *in vitro* using the MTT assay under hypoxic conditions at 0.1% O_2 against MIA PaCa-2 cells; cisplatin was also studied as a comparison.

The results show a decrease in cytotoxicity for all three tested complexes, including cisplatin, when the oxygen concentration is reduced to 0.1% (**Figure 5.6**). Complex **C2** experienced the least loss of activity from normoxia to hypoxia (11.39 ± 3.24 → 44.16 ± 7.17 μM) becoming the more active ruthenium complex of the two tested, where the opposite observation is true in normoxia. It is not possible to comment on the exact loss of activity of complex **C5** as the IC_{50} values concentration reached the threshold limit of 50 μM. Surprisingly, cisplatin's IC_{50} value rose from 3.62 ± 0.74 μM to > 50 μM under the hypoxic conditions, which is a significant decrease in cytotoxicity compared to complex **C2** under these conditions. Therefore, although there is a decrease in the activity of complexes **C2** and **C5**, complex **C2** remained much more cytotoxic than cisplatin against MIA PaCa-2 under 0.1% oxygen conditions.

Table 5.4 Summary of IC_{50} values for cisplatin, **C2** and **C5** under normoxic and hypoxic conditions against MIA PaCa-2 averaged over 3 runs

Complex	MIA PaCa-2			
	NORMOXIA		*HYPOXIA*	
	IC_{50} (μM)	±SD (μM)	IC_{50} (μM)	±SD (μM)
Cisplatin	3.62	0.74	50	-
C2	11.39	3.24	44.16	7.17
C5	7.9	2.32	50	-

Note – No standard deviation is given for complexes with activity lower than the 50 μM limit

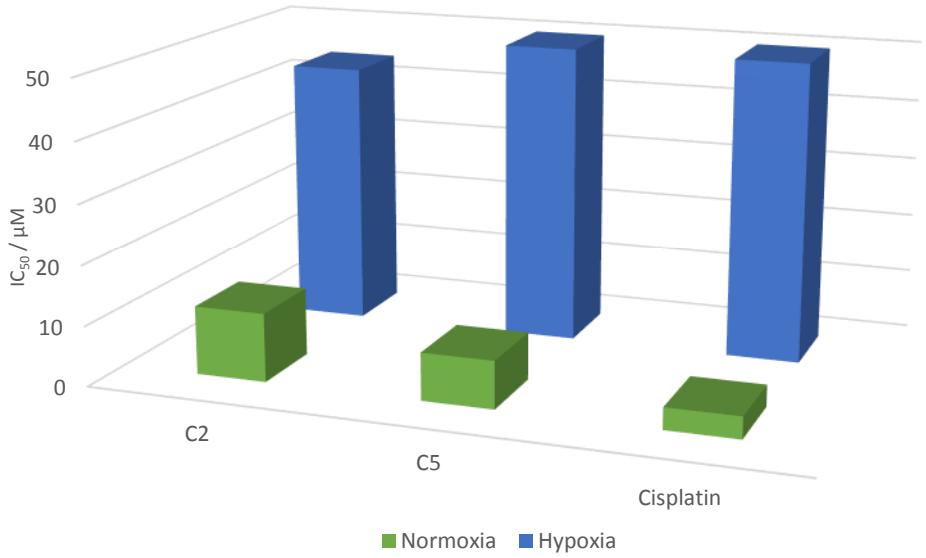

Figure 5.6 Chart to summarise the IC_{50} values of complexes **C2**, **C5** and cisplatin under differing oxygen concentrations

Coordination complexes were studied in the same manner to the aforementioned arene complexes over a five day period *in vitro* using the MTT assay at 0.1% O_2 against both HCT116++ and MIA PaCa-2 cells. Three platinum anticancer compounds, including cisplatin, were also studied as a comparison. Complexes **C'1**, **C'4**, **C'5**, **C'6**, **C'7** and **C'12** were selected for study, a larger cross section was chosen compared to the arene complexes due to the potent cytotoxicity of the whole library of coordination compounds on both cell lines in normoxia.

Results show that the reduction in oxygen concentration gave a decrease in activity for all complexes against both cell lines, although to a lesser degree for the MIA PaCa-2 cell line, but it should be noted that the platinum complexes were rendered completely inactive under the same conditions at the 50 μM threshold limit (**Figure**

5.7). For reasons yet unknown, complex **C'1** was also found to be inactive at the tested concentrations (IC_{50} > 50 μM) in hypoxia but solely towards the HCT116++ cell line. Complexes with a 3',5'- substituted phenyl ring at the R position (**C'7** and **C'12**) were the most active against both cell lines under hypoxia, with **C'7** (R = 3',5'-Me) being found to be approximately twice as cytotoxic than the mono-substituted *para* methyl **C'6**. With regards to the effect of increasing aromaticity, the same trend in cytotoxicity across the complexes observed in normoxia remained under hypoxia (**C'5** > **C'4** > **C'1**) although complex **C'1** experienced a greater loss of activity in comparison to the others. Remarkably, under hypoxic conditions, complex **C'5**, **C'7** and **C'12** (2.77 μM, 2.09 μM and 2.43 μM, respectively) were still more active than cisplatin under normoxic conditions (3.62 μM) against the MIA PaCa-2 cell line.

Table 5.5 Summary of IC_{50} values for cisplatin, carboplatin, oxaliplatin, **C'1**, **C'4**-**C'7** and **C'12** under normoxic and hypoxic conditions against MIA PaCa-2 and HTC116++ averaged over 3 runs

Complex	MIA PaCa-2				HTC116++			
	NORMOXIA		*HYPOXIA*		*NORMOXIA*		*HYPOXIA*	
	IC_{50} (μM)	±SD (μM)	IC_{50} (μM)	±SD (μM)	IC_{50} (μM)	±SD (μM)	IC_{50} (μM)	±SD (μM)
Cisplatin	3.62	0.74	50	-	3.26	0.38	50	-
Carboplatin	35.59	7.91	50	-	32.37	11.14	50	-
Oxaliplatin	6.44	1.05	50	-	0.93	0.12	50	-
C'1	0.43	0.10	12.55	4.02	0.34	0.03	50	-
C'4	0.13	0.01	6.41	2.55	0.30	0.04	10.20	2.11
C'5	0.09	0.02	2.77	0.66	0.11	0.03	9.96	2.33
C'6	0.13	0.03	4.84	0.80	0.21	0.03	9.03	2.52
C'7	0.12	0.01	2.09	0.42	0.30	0.04	4.97	0.77
C'12	0.1	0.02	2.43	0.28	0.11	0.004	5.26	0.17

Note – No standard deviation is given for complexes with activity lower than the 100 μM limit

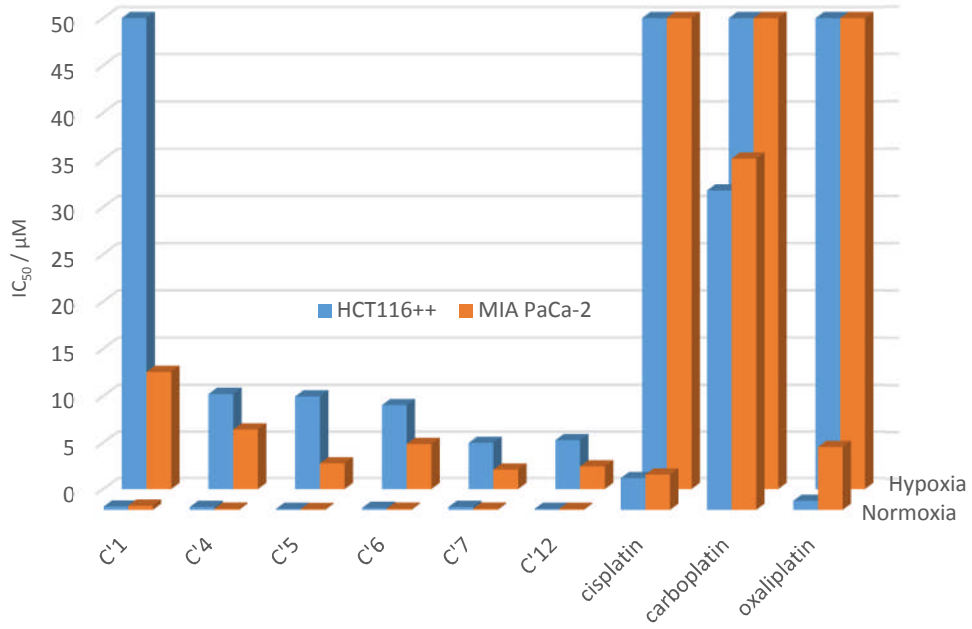

Figure 5.7 Chart to summarise the IC_{50} values of ruthenium bpy complexes under differing oxygen concentrations

5.3 Antibacterial Activity

There has been a vast expansion in the development of compounds which are used to treat bacterial infection since the discovery of the first antibiotic drug, penicillin. However, the often unnecessary and wide use of antibiotics has caused bacteria to grow increasingly resistant to common antibacterial agents, a problem which is fast becoming one of the great challenges of modern medicine.[59-62] Microorganisms develop drug resistance from a variety of genetically controlled biochemical processes, arising from either mutation of their intrinsic cellular genes or the transfer of genes from resistant bacteria.[63] These mutated genes yield several biochemical mechanisms of resistance including, but not limited to, drug inactivation/modification, target modification/repair, immunity, increased impermeability, and biofilm formation, amongst other unknown mechanisms.[64, 65] Consequently, the concern centred around antibiotic resistance has prompted the progress and production of novel antimicrobial therapies.

Numerous transition metal complexes have been shown to display antibacterial activity.[66-69] In some cases these complexes contain already existing antibacterial compounds as ligands, creating a synergistic effect which have been shown to

enhance the antimicrobial activity of the organic fragment and, notably, greatly increase their activity towards drug-resistant strains of bacteria.[70-72]

Silver and its complexes have long been used as antibacterial agents; silver nitrate is used in the clinical treatment of ophthalmia neonatorum and silver sulfadiazine is a widely used broad-spectrum antibiotic ointment applied to severely burnt skin.[73] More generally, silver complexes with oxygen donor ligands display a broad range of antibacterial activities which are independent from the ligand itself, but rather stems from the ease of ligand replacement with biological ligands due to the weaker Ag-O bond.[74] Anti-arthritic drugs containing gold, such as auranofin and several other related complexes, have been discovered to inhibit the growth of *Pseudomonas putida*. A further synergistic effect was discovered between Cu(II) compounds and the Au(I) complexes, as the co-administration caused an increase in their toxic effects towards strains of *P. putida*.[75]

As well as being widely studied for their anticancer properties, the therapeutic potential of ruthenium metal complexes as antimicrobial agents has also been explored.[76-87] The structural and electronic properties of the metal complexes which allow them to strongly interact with nucleic acids - and impart anticancer activity - also provide the basis for protein and enzyme targeting. For example, work by Meggers and Pandey on ruthenium arene and polypyridyl complexes has demonstrated their ability to bind and inhibit enzymes such as acetylcholinesterase and protein kinases that are involved in tumourgenisis and metastasis.[88-90]

Ruthenium polypyridyl complexes as antimicrobial agents is a growing area of interest but they have been studied in this role for over 60 years. Initial investigations were conducted by Dwyer *et al.* in the 1950s on ruthenium tris(bidentate) complexes containing derivatives of 1,10-phenanthroline and 2,2'-bipydridine against Gram positive, Gram negative and acid-fast bacteria.[83, 91, 92] During these investigations the authors were able to demonstrate the importance of the metal complexes' lipophilicity, dramatically increasing the activity of the inert $[Ru(phen)_3]^{2+}$ against all tested bacterial strains - in particular Gram positive bacteria and *Mycobacterium tuberculosis* - by the addition of methyl substituents to the phenanthroline ligands. More importantly, bacteria did not easily become resistant towards this type of

compound, after sub-culturing the highly virulent *Staphylococcus pyogenes* var. *Phillips* in the presence of $[Ru(Me_4phen)_2(acac)]^+$ every 48 hours for a total of 25 repeats, the bacteria only showed a two-fold increase in resistance in contrast with the antibiotic control penicillin, where there was an observed 10,000-fold decrease in activity.[74]

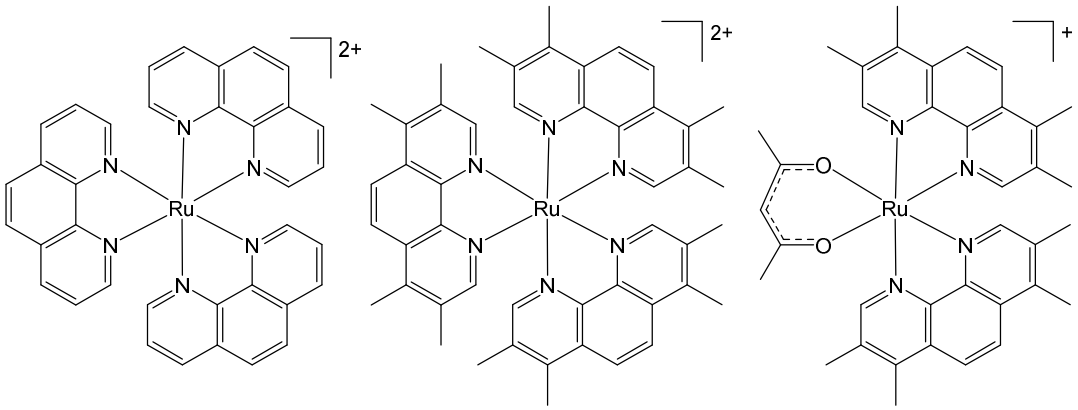

Figure 5.8 Molecular structure of $[Ru(phen)_3]^{2+}$, $[Ru(Me_4phen)_3]^{2+}$ and $[Ru(Me_4phen)_2(acac)]^+$ [74]

More recently, Aldrich-Wright *et al.* have reported significant antibacterial activity against *B. subtilis* and *S. aureus* (including several methicillin-resistant strains) from polypyridyl ruthenium(II) DNA binders. Although these complexes were found to be inactive against Gram negative bacteria, some of the complexes display particularly low minimum inhibitory concentrations (MIC) of as little as 2 μg ml^{-1} towards Gram positive strains.[87] Furthermore, their low toxicity towards eukaryotic systems was demonstrated by treating *S. aureus* infected *Caenorhabditis elegans* - a roundworm which is used as an infection model for human pathogens - with the most active compound $[Ru(2,9\text{-}Me_2phen)_2(dppz)]^{2+}$, resulting in an 80% increase in the survival population of the worms.[87] It is thought that this selectivity towards bacterial cells over eukaryotic cells is due to differences in the membrane composition, as the greater abundance of negatively charged components (phospholipids) in the bacterial membrane and cell wall will have a high affinity for the cationic ruthenium complexes.[93]

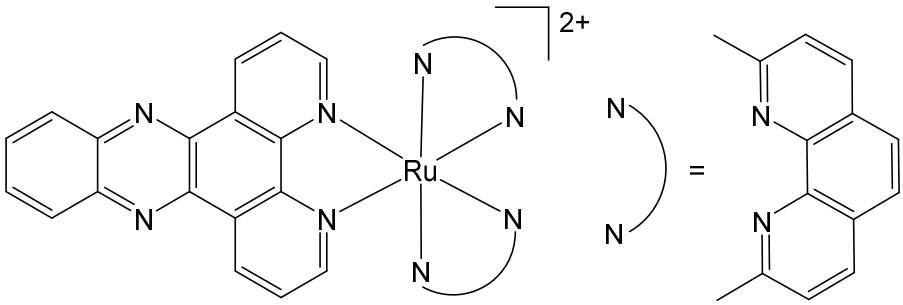

Figure 5.9 Molecular structure of $[Ru(2,9\text{-}Me_2phen)_2(dppz)]^{2+}$ [87]

Derivatives of ferrocene have also been explored for their potential antibacterial properties as far back as the 1970s when Marr *et al.* published antibacterial studies on ferrocene derivatives of the bactericides penicillin and cephalosporin.[94-96] Testing against a number of different bacterial strains the complexes exhibited moderate activity although some complexes were shown to exhibit comparable activity to that of the control molecules. Work in this area has increased in recent years, with the antibacterial properties of ferrocene derivatives being explored either as standalone complexes[69, 97-99] or incorporated into other metal complexes in the form of a ligand.[100-103]

5.3.1 Antibacterial Results and Discussion

Complexes were screened for their anti-bacterial activity against *Escherichia coli* (*E coli*), *Klebsiella pneumoniae* (*K. pneumoniae*), *Acinetobacter baumannii* (*A. baumannii*), *Pseudomonas aeruginosa* (*P. aeruginosa*) and *Staphylococcus aureus* (*S. aureus*) by The Community for Antimicrobial Drug Discovery (CO-ADD) at The University of Queensland. The complexes, at a single concentration of 32 μg mL^{-1}, were incubated with the bacterial strains at 37 °C for 18 hours without shaking. All growth inhibition assays were performed in duplicate. Growth inhibition was determined by measuring absorbance at 600 nm. Complexes with growth inhibition values greater than 80 % are classed as active and complexes with growth inhibition values in the range 50 - 80 % are classed as partially active.

Antibacterial screening results for the ruthenium arene piano stool complexes and bpy coordination complexes have been summarised in **Table 5.6** and **Table 5.7**, respectively. Active complexes have been highlighted for ease of observation.

Table 5.6 Growth inhibition for ruthenium arene complexes against bacterial strains

Complex	Inhibition / %				
	Sa	Ec	Kp	Pa	Ab
C01	34.22	-29.09	10.46	-22.97	30.61
C02	27.64	-15.35	8.87	-14.99	30.09
C03	23.53	-35.27	6.05	-16.69	13.58
C04	75.12	-20.02	0.46	-20.43	17.98
C05	29.52	-24.87	-1.68	-13.98	11.61
C06	93.65	-25.98	7.11	-33.19	18.91
C07	83.43	-49.1	0.52	-33.93	11.05
C08	94.64	-13	5.99	-24.77	7.47
C09	88.03	-22.03	2.7	-49.1	10.04
C10	85.24	-22.37	4.43	-33.05	22.24
C11	58.92	-37.82	2.56	-22.47	25.81
C12	31.77	-40.32	-1.28	-20.53	18.45
C13	12.06	-20.48	4.71	-19.35	2.95
C14	11.5	-45.46	-1.28	-32.88	9.73
C15	51.92	-44.24	6.09	-23.9	12.63
C16	49.6	-42.9	0.03	-29.13	15.11
C17	86.29	-31.94	2.17	-32.12	8.22
C18	43.52	-33.89	6.65	-40.78	21.16
C19	57.51	-34.73	0.92	-22.19	15.77
C20	24.07	-17.95	7.29	-38.57	18.12
C21	57.13	-27.9	6.54	-22.07	16.76
C22	90.91	-10.07	7.62	-22.57	28.15
C23	29.91	-23.77	-0.71	-40.74	9.38
C24	69.07	-22.29	0.38	-25.37	22.4

The ruthenium arene complexes showed considerably greater activity towards the Gram positive strain of bacteria, *S. aureus,* compared to the other four observed Gram negative bacterial strains, against which they proved inactive, an observation which is not uncommon for ruthenium complexes.[63] Of the seven complexes active against *S. aureus*, five of them contained a β-diketonate ligand with neutral inductive aromatic ring systems (**C6 – C10**). However, **C17** (R = 3',5'-Cl) and **C22** (R = 4'-OMe) were also shown to have comparable antibacterial activity to the previously

mentioned active complexes, despite containing electron withdrawing and donating moieties, respectively.

Considering only the *S. aureus* inhibition results, complex **C17** (R = 3',5'-Cl) has an almost two-fold increase in the inhibition of bacterial growth over complexes containing a mono-chlorinated β-diketonate ligand (**C15** and **C16**), which would suggest that the number of halogens plays a part in the active mechanism. Conversely, the equivalent fluorine containing complexes show a decrease in activity with the increase in fluorine atom substituents. In fact, **C14** (R = 3',5'-F) is the least active of all the complexes with fluorinated aromatic rings and is five times less active than the partially active **C11** (R = 4'-F). A trend in decreasing activity of the complexes can be seen with the position and number of fluorine atoms around the ring of the β-diketonate R substituent (**C11** > **C12** > **C13** > **C14**).

The electronic properties of the substituents at the *meta* and *para* position of the β-diketonate aromatic ring appears to have an interesting impact on the bacterial inhibition activity of the ruthenium arene complexes. The decreasing electronegativty of the halogen atoms F > Cl > Br > I causes a decrease in the activity of complexes when the halogen atom is located at the *para* position and an increase in activity of the complexes when the halogen atom is located at the *meta* position (**Figure 5.10**). The opposite observation is true for electron donating substituents (i.e R = Me/OMe) as the antibacterial activity is favoured for substituents in the *para* position. These observations suggest that the inductive effects around the aromatic ring may be responsible to some degree in imparting the bacterial inhibition properties to the complexes.

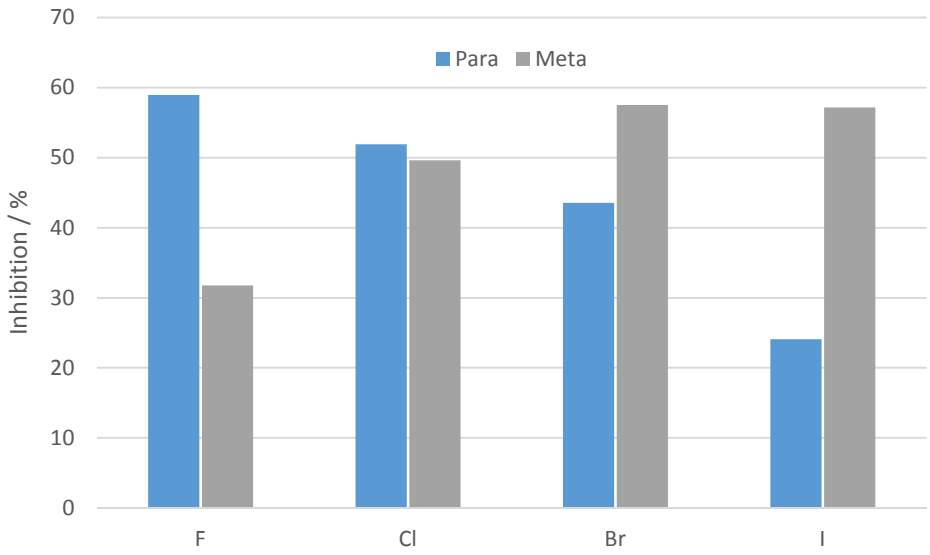

Figure 5.10 Chart to show how bacterial inhibition changes with *para* and *meta* halogen substituents

As with the ruthenium arene complexes, the ruthenium bpy coordination complexes were also considerably more active towards the Gram positive strain of bacteria, *S. aureus,* rather than the other Gram negative strains, although their activity towards *A. baumannii* is generally much improved with some of the coordination complexes entering the "partially active" region of inhibition (**C'8**, **C'9** and **C'15**). The inhibition percentages for *S. aureus* are also generally greater with all complexes being classed as at least partially active, demonstrating growth inhibition in the range of 66.35 – 87.15 %. These results are in agreement with other work stating that ruthenium polypyridyl complexes have superior activity towards Gram positive strains of bacteria in comparison to Gram negative strains.[63, 104, 105] A slight decrease in activity can be seen with the decreasing electronegativity of the halogen atoms at the *para* position of the β-diketonate (**C'8** > **C'11** > **C'13** > **C'14**). A further decrease in activity is observed between the *para* halogenated complexes and their *meta* dihalogenated counterparts (**C'8** > **C'10** and **C'11** > **C'12**). However, this observation is in contrast to the results shown from the equivalent methyl complexes which see better bacterial inhibition from the *meta* dimethyl moiety (**C'7** > **C'6**).

Table 5.7 Growth inhibition for ruthenium bipyridyl complexes against bacterial strains

Complex	Inhibition / %				
	Sa	Ec	Kp	Pa	Ab
C'01	85.24	-21.18	-4.5	-15.78	-4.11
C'02	73.83	-40.63	-16.41	-39.57	7.09
C'03	86.29	12.89	-8.66	3.29	9.26
C'04	73.41	10.63	-13.94	11.9	44.87
C'05	85.33	-0.09	-3.89	-14.08	34.28
C'06	66.35	2.98	-19.17	-19.16	42.08
C'07	77.26	-12.11	-13.9	-21.2	48.31
C'08	80.21	8.15	-10.85	-17.98	58.89
C'09	84.31	9.33	-8.47	13.86	52.55
C'10	74.54	-7.78	-14.81	-15.46	9.9
C'11	76.69	-3.32	-24.46	-21.2	43.91
C'12	68.66	-31.58	-23.66	-29.02	5.73
C'13	76.05	-5.68	-15.89	-28.95	42.22
C'14	71.57	-11.65	-15.31	-23.23	40.35
C'15	87.15	8.86	-1.68	-0.64	76.46

Complexes which were classed as active underwent hit confirmation to determine their minimum inhibitory concentration (MIC). MIC is the lowest drug concentration which prevents visible growth of the pathogen, in this case bacteria. The MIC values were determined against *E. coli, K. pneumoniae, A. baumannii, P. aeruginosa* and *S. aureus* by CO-ADD at The University of Queensland. The complexes, at eight concentrations, were incubated with the cell suspensions of the bacterial strains at 35 °C for 18 hours without shaking. All growth inhibition assays were performed in duplicate. Inhibition of bacterial growth was determined by measuring the absorbance at 600 nm. The MIC was determined as the lowest concentration at which the growth was fully inhibited, defined by an inhibition ≥ 80 %. Complexes with MIC less than 16 μg mL^{-1} are classed as confirmed active hits.

The cytotoxicity of these complexes was also determined against the HEK293 (human embryonic kidney) cell line. The complexes, at eight concentrations, were incubated with the cells at 37 °C for 20 hours in 5 % CO_2. Cytotoxicity was measured by fluorescence, with excitation at 560 nm and emission at 590 nm, after the addition of resazurin and further incubation for three hours under the same

conditions as previously stated. Cytotoxicity is expressed in terms of CC_{50}, which is defined as the concentration of drug required to produce 50 % of cell death.

Haemolysis assays were also conducted using human whole blood. The complexes, at eight concentrations, were shaken with the cells for ten minutes before incubation at 37 °C for one hour. Haemolysis was determined by measuring the supernatant absorbance at 405 nm of the centrifuged samples and is expressed in terms of HC_{10}, which is the concentration of the drug required to cause 10 % haemolysis.

The antibacterial MICs, cytotoxicity and haemolysis results for complexes **C6 – C10, C17** and **C22** are summarised in **Table 5.8**, with the results for complexes **C'1 – C'15** summarised in **Table 5.9**.

Table 5.8 Antibacterial toxicity and cytotoxicity of complexes **C6**-**C10**, **C17** and **C22**

Complex	MIC / µg mL^{-1}					CC_{50} / µg mL^{-1}	HC_{10} / µg mL^{-1}
	Sa	Ec	Kp	Pa	Ab	Hk	Hm
C06	16	>32	>32	>32	>32	21.38	>32
C07	32	>32	>32	>32	>32	11.94	>32
C08	32	>32	>32	>32	>32	20.45	>32
C09	32	>32	>32	>32	>32	14.79	>32
C10	16	>32	>32	>32	>32	5.79	>32
C17	32	>32	>32	>32	>32	6.27	>32
C22	32	>32	>32	>32	>32	28.37	>32

Despite the initial screening results for complexes **C6 – C10, C17** and **C22** displaying positive growth inhibition of *S. aureus* only complexes **C6** and **C10** display sufficient activity to be classed as active hits. All complexes also showed varying degrees of cytotoxicity towards HEK293 cells, with **C10** being shown to be the most toxic to eukaryotic cells (CC_{50} = 5.79 µg mL^{-1}) and **C6** being shown to be one of the least toxic (CC_{50} = 21.38 µg mL^{-1}) despite its antibacterial activity. These results are in contrast to the previous cytotoxicity studies performed on the ARPE19 human retinal pigment epithelial cells which showed no cytotoxicity at the tested 100 µM concentrations. Haemolysis results, on the other hand, were extremely positive and showed that the tested ruthenium arene complexes are non-toxic to human blood under 32 µg mL^{-1}.

Table 5.9 Antibacterial toxicity and cytotoxicity of complexes **C'1**-**C'15**

Complex	MIC / µg mL^{-1}					CC_{50} / µg mL^{-1}	HC_{10} / µg mL^{-1}
	Sa	Hk	Kp	Pa	Ab	Hk	Hm
C'01	8	>32	>32	>32	>32	9.494	>32
C'02	8	>32	>32	>32	>32	6.654	>32
C'03	4	>32	>32	>32	>32	4.659	17.58
C'04	0.5	>32	>32	>32	16	4.442	9.072
C'05	1	>32	>32	>32	>32	3.623	2.401
C'06	2	>32	>32	>32	>32	4.892	14.91
C'07	4	>32	>32	>32	>32	2.91	1.851
C'08	1	>32	>32	>32	>32	3.862	4.731
C'09	2	>32	>32	>32	>32	5.365	4.549
C'10	2	>32	>32	>32	>32	4.689	7.92
C'11	2	>32	>32	>32	16	2.749	2.608
C'12	2	>32	>32	>32	>32	4.652	4.482
C'13	4	>32	>32	>32	>32	5.828	11.72
C'14	2	>32	>32	>32	>32	6.906	16.05
C'15	2	>32	>32	>32	>32	2.865	<=0.25

Compared to the ruthenium arene complexes, the ruthenium coordination complexes gave considerably lower MIC values for *S. aureus*, which was to be expected considering their inhibitory activity results during the initial antibacterial screening. Their potential potency has also been demonstrated previously in the anticancer cytotoxicity results (**Table 5.2**). The most active complex **C'4** (MIC = 0.5 µg mL^{-1}) shares the same β-diketonate ligand (R = Ph) as one of the active arene complexes **C6**. Furthermore, **C'4** was one of only two complexes to show an active hit against the Gram negative *A. baumannii*, the other being **C'11**. However, with the keen potency of these complexes comes increased toxicity towards the HEK293 healthy cells and human blood cells, although **C'1** and **C'2** remained non-toxic during the haemolysis studies but possess the largest active MIC values of all the coordination complexes.

5.4 Antifungal Activity

Advances in modern medicine have granted us the ability to treat diseases which were previously beyond our medical and surgical capabilities. With these advances we delve deeper into the fundamental workings of the human body, bypassing or suppressing the body's natural defences in order to manage diseases which the immune system has failed to combat. Treatments of this kind, such as organ transplantation, cancer chemotherapy or immunosuppressive treatment for HIV/AIDS, which are associated with the more major health issues often leaves patients immunocompromised and vulnerable to severe fungal infections.[106]

Of the millions of different fungal species, only around 300 have been recorded to cause disease in humans, with approximately 25 of those responsible for 99% of reported infections.[107-110] These infections can be classified into two categories; superficial fungal infections (SFI) and invasive fungal infections (IFI), with the latter often being life-threatening and resulting in high mortality rates amongst immunocompromised individuals. The most common of these IFI pathogens are *Candida albicans* (mortality rate: 20-40%), *Cryptococcus neoformans* (mortality rate: 20-70%) and *Aspergillus fumigates* (mortality rate: 50-90%).[111]

Despite these considerable mortality rates, advances in the formation and discovery of new antifungal treatments have been slow. The main problems related to the treatment of fungal infections are similar to those faced during cancer therapy; both human and fungi are eukaryotic organisms comprised of cells which are similar in structure and function, and as a result, antifungal treatments can often exhibit high toxicity towards the closely related healthy mammalian cells.[112, 113] Furthermore, the increasing problem of drug resistance in fungal infections can be attributed in many cases to the over expression of multidrug resistant pumps, a property which has also been linked to the increased chemotherapy resistance of cancerous cells.[114, 115]

In spite of the desperate need for new fungal treatments, very few organometallic and coordination complexes have been explored for their potential antifungal effects. The first row transition metals (manganese, iron, cobalt, nickel, copper and zinc) are popular choices in the development of novel antifungal complexes.[116-120]

They possess the required redox and catalytic activities which enable them to serve as cofactors for a plethora of enzymes involved in the biological processes associated with the infections.[121]

Several ruthenium arene PTA complexes from the RAPTA series developed by Dyson *et al.* containing *p*-cymene and labile halogen and thiocyanate ligands, originally devolved for cancer therapy,[122] were subsequently explored for their antimicrobial activity.[123] During these studies the halogens proved to play an important role on the growth inhibition activity of the complexes. Compounds containing the heavier halogen atoms (I, Br) were practically inactive with non-specific antimicrobial action. The chloro- and thiocyan- complexes were found to selectively inhibit fungal growth, specifically *Trycophyton mentagrophytes* and *Cladosporium resinae*, over the tested bacteria and viruses.

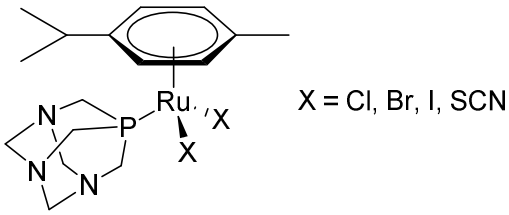

Figure 5.11 Ruthenium RAPTA complexes[123]

As well as being explored for their antibacterial properties as previously mentioned, many ferrocene derivatives have been simultaneously probed for their antifungal effects.[97, 98, 103] A common theme in the development of antifungal ferrocene derivatives is the incorporation of a ferrocene moiety into already well established fungicidal molecules such as triadimefon,[124] sedaxane[125] and fluconazole.[126] Although the antifungal toxicity of these ferrocene analogues varies considerably from case-to-case, the parent drug molecule often displays greater fungal growth inhibition than its ferrocenyl analogue.

5.4.1 Antifungal Results and Discussion

Complexes were screened for their anti-fungal activity against *Candida albicans* (*C. albicans*) and *Cryptococcus neoformans* (*C. neoformans*) by CO-ADD at The University of Queensland. The complexes, at a single concentration of 32 μg mL^{-1}, were incubated with the fungal strains at 35 °C for 24 hours without shaking. All growth inhibition assays were performed in duplicate. Growth inhibition of *C. albicans* was determined by measuring absorbance at 530 nm. Growth inhibition of *C. neoformans* was determined by measuring the difference in absorbance between 580 and 600 nm following the addition of resazurin and incubation at 35 °C for a further two hours. Complexes with growth inhibition values greater than 80 % are classed as active and complexes with growth inhibition values in the range 50 - 80 % are classed as partially active.

Antifungal screening results for the ruthenium arene piano stool complexes and bpy coordination complexes have been summarised in **Table 5.10** and **Table 5.11**, respectively. Active complexes have been highlighted for ease of observation.

Table 5.10 Growth inhibition of ruthenium arene complexes against fungal strains

Complex	Inhibition / %		Complex	Inhibition / %	
	Ca	Cn		Ca	Cn
C01	7.16	-18.91	**C13**	1.86	-6.95
C02	18.53	-21.78	**C14**	-0.84	-16.03
C03	11.06	-17.24	**C15**	9.99	-15.73
C04	30.27	-19.96	**C16**	2.67	-15.88
C05	46.13	-18.6	**C17**	8.98	-10.28
C06	25.32	116.19	**C18**	2.74	-18.15
C07	20.22	59.6	**C19**	13.02	-16.49
C08	4.27	-11.64	**C20**	3.39	-17.85
C09	7.77	-6.5	**C21**	8.71	-18.15
C10	12.81	119.73	**C22**	7.7	-13.91
C11	17.93	-19.81	**C23**	8.57	-14.67
C12	6.96	-21.63	**C24**	10	-13.61

Only two complexes were found to be active against the *C. neoformans* strain of fungus, complexes **C6** and **C10**. Interestingly, complexes **C6** and **C10** were also the only two complexes classed as active during the antibacterial hit confirmation studies (**Table 5.6**) and contain β-diketonate ligands with phenyl and 3', 5'-dimethyl

substituents, respectively. Complex **C7**, containing a naphthalene moiety, shows partial activity with 59.6 % growth inhibition of *C. neoformans.* All other complexes were found to be inactive towards *C. neoformans* and *C. albicans*, suggesting that a more electro-neutral aromatic substituent favours the inhibitive activity towards *C. neoformans*.

Table 5.11 Growth inhibition of ruthenium bipyridyl complexes against fungal strains

Compound	Inhibition / %		Compound	Inhibition / %	
	Ca	Cn		Ca	Cn
C'01	5.59	-11.34	**C'09**	26.95	118.48
C'02	8.44	123.67	**C'10**	16.79	116.82
C'03	10.66	115.99	**C'11**	100.37	129.28
C'04	96.71	123.46	**C'12**	100.3	116.19
C'05	99.96	120.14	**C'13**	100.44	124.29
C'06	99.96	121.59	**C'14**	100.03	120.76
C'07	99.96	120.14	**C'15**	89.8	119.52
C'08	96.91	127.2			

As was observed for the antibacterial and cytotoxicity studies, the ruthenium coordination complexes have superior fungal inhibition activity than the ruthenium arene complexes. All complexes except **C'1** were found to be excellent inhibitors in the growth of *C. neoformans.* With regards to *C. albicans*, complexes **C'4 – C'8**, **C'11 – C'15** were again highly active, with growth inhibition in the range of 89.8 – 100.44 %. Complexes **C'1 – C'3** which were inactive towards *C. albicans* are lacking an aromatic substituent on the β-diketonate ligand, suggesting that the aromatic group is essential for the *C. albicans* antifungal activity, possibly due to the increased potential for DNA binding by intercalation. However, **C'9** and **C'10** were also inactive to *C. albicans* and both of which contain phenyl substituents with fluorine at the *meta* positions.

Complexes which were classed as active underwent hit confirmation to determine their minimum inhibitory concentration (MIC). The MIC values were determined against *C. albicans* and *C. neoformans* by CO-ADD at The University of Queensland. The complexes, at eight concentrations, were incubated with the cell suspensions of the fungal strains at 35 °C for 36 hours without shaking. All growth inhibition assays

were performed in duplicate. Growth inhibition of *C. albicans* was determined by measuring absorbance at 630 nm. Growth inhibition of *C. neoformans* was determined by measuring the difference in absorbance between 570 and 600 nm following the addition of resazurin and incubation at 35 °C for a further two hours. The MIC was defined as the lowest concentration at which the growth was fully inhibited, set at ≥ 80% for *C. albicans* and inhibition ≥ 70% for *C. neoformans* (due to higher variance in growth and inhibition of *C. neoformans* compared to *C. albicans*). Complexes with MIC less than 16 μg mL^{-1} are classed as confirmed active hits. The cytotoxicity and haemolysis assays were conducted as previously described for the antibacterial hit confirmation.

The antifungal MICs, cytotoxicity and haemolysis results for complexes **C6 – C10, C17** and **C22** are summarised in **Table 5.12**, with the results for complexes **C'1 – C'15** summarised in **Table 5.13**. Despite displaying growth inhibition of *C. albicans* in the initial screening, complexes **C6** and **C10** did not display sufficient MICs to be classed as active hits.

Table 5.12 Antifungal toxicity and cytotoxicity of complexes **C6**-**C10**, **C17** and **C22**

Complex	MIC / μg mL^{-1}		CC_{50} / μg mL^{-1}	HC_{10} / μg mL^{-1}
	Ca	Cn	Hk	Hm
C06	>32	32	21.38	>32
C07	>32	32	11.94	>32
C08	32	32	20.45	>32
C09	32	32	14.79	>32
C10	32	32	5.794	>32
C17	>32	>32	6.27	>32
C22	>32	32	28.37	>32

As with the antibacterial hit confirmation, the ruthenium coordination complexes were found to possess much lower MIC values in general than the ruthenium arene complexes, although these is no correlation between their antibacterial MIC values and those obtained from the antifungal studies. Complexes were found to be more active towards *C. neoformans* than *C. albicans*, though this was to be expected from their initial fungal inhibition results. Antifungal activity of these complexes generally correlate with increased toxicity towards HEK293 kidney cells and human blood cells.

Table 5.13 Antibacterial toxicity and cytotoxicity of complexes **C'1**-**C'15**

Complex	MIC / µg mL^{-1}		CC_{50} / µg mL^{-1}	HC_{10} / µg mL^{-1}
	Ca	Cn	Hk	Hm
C'01	>32	32	9.494	>32
C'02	>32	16	6.654	>32
C'03	>32	16	4.659	17.58
C'04	16	8	4.442	9.072
C'05	8	8	3.623	2.401
C'06	8	8	4.892	14.91
C'07	8	8	2.91	1.851
C'08	16	16	3.862	4.731
C'09	32	8	5.365	4.549
C'10	32	8	4.689	7.92
C'11	16	8	2.749	2.608
C'12	8	8	4.652	4.482
C'13	16	8	5.828	11.72
C'14	16	16	6.906	16.05
C'15	16	16	2.865	≤0.25

5.5 Conclusions

Two libraries of ruthenium complexes have been screened for their anticancer activity under normoxic conditions (21 % O_2). Many of the ruthenium arene complexes were found to possess moderate to strong cytotoxicity against cancer cell lines, with increased activity towards the MIA PaCa-2 cell line. These complexes were shown to be highly selective for cancer cells, with IC_{50} values exceeding the tested threshold limit for healthy cells. The ruthenium coordination complexes were found to be highly cytotoxic towards all tested cell lines with IC_{50} values in the nanomolar range. Selected active complexes from each library were then studied under extreme hypoxia (0.1 % O_2) which saw a decrease in activity for all complexes, yet they were more active than cisplatin under the same conditions.

Both series of ruthenium complexes were screened for their antimicrobial activity against multiple bacterial and fungal strains. Against Gram positive bacteria, both sets of complexes showed elevated inhibition activity over the Gram negative strains, with the coordination complexes generally being far more active than the arene complexes. Hit confirmation was carried out on the active complexes to determine their MIC values and returned figures of as little as 0.5 μg mL^{-1} for the most active coordination complex. Only two arene complexes showed active inhibition of fungal growth but failed to be classed as active during hit confirmation stages of testing. Conversely, almost all the coordination complexes were extremely active growth inhibitors and gave MIC values or 8/16 μg mL^{-1}.

From both the cytotoxicity and antimicrobial results it is currently not possible to conclude any general structural activity relationship trends. The potential shown by both libraries of complexes promoted them to be taken forward and investigated further, the results of which are discussed in the following chapter.

5.6 References

1. A. Aysun, K. Yağmur and B. Yusuf, *Current Pharmaceutical Biotechnology*, 2016, **17**, 1213-1221.
2. T. L. Riss, R. A. Moravec, A. L. Niles, S. Duellman, H. A. Benink, T. J. Worzella and L. Minor, *Cell Viability Assays*, 2016.
3. A. L. Niles, R. A. Moravec and T. L. Riss, *Current Chemical Genomics*, 2009, **3**, 33.
4. V. Patravale, P. Dandekar and R. Jain, in *Nanoparticulate Drug Delivery*, Woodhead Publishing, 2012, pp. 123-155.
5. V. Kuete, O. Karaosmanoğlu and H. Sivas, in *Medicinal Spices and Vegetables from Africa*, Academic Press, 2017, pp. 271-297.
6. R. M. Lord, A. J. Hebden, C. M. Pask, I. R. Henderson, S. J. Allison, S. L. Shepherd, R. M. Phillips and P. C. McGowan, *Journal of Medicinal Chemistry*, 2015, **58**, 4940-4953.
7. U. Ndagi, N. Mhlongo and M. E. Soliman, *Drug Design, Development and Therapy*, 2017, **11**, 599-616.
8. S. Page and R. Wheeler, *Education in Chemistry*, 2012, **49**, 26.
9. W. K. Hagmann, *Journal of Medicinal Chemistry*, 2008, **51**, 4359-4369.
10. Z. Luo, L. Yu, F. Yang, Z. Zhao, B. Yu, H. Lai, K.-H. Wong, S.-M. Ngai, W. Zheng and T. Chen, *Metallomics*, 2014, **6**, 1480-1490.
11. B. Muz, P. de la Puente, F. Azab and A. K. Azab, *Hypoxia*, 2015, **3**, 83.
12. J. M. Brown and W. R. Wilson, *Nature Reviews Cancer*, 2004, **4**, 437-447.
13. J. M. Brown, *Cancer Biology & Therapy*, 2002, **1**, 453-458.
14. P. Vaupel, F. Kallinowski and P. Okunieff, *Cancer Research*, 1989, **49**, 6449-6465.
15. H. E. Ryan, M. Poloni, W. McNulty, D. Elson, M. Gassmann, J. M. Arbeit and R. S. Johnson, *Cancer Research*, 2000, **60**, 4010-4015.
16. J. Folkman, *JNCI: Journal of the National Cancer Institute*, 1990, **82**, 4-7.
17. J. M. Brown and W. R. Wilson, *Nature Reviews Cancer*, 2004, **4**, 437.
18. L. H. Gray, A. D. Conger, M. Ebert, S. Hornsey and O. C. A. Scott, *The British Journal of Radiology*, 1953, **26**, 638-648.

19. H. Crabtree and W. Cramer, *Proceedings of the Royal Society of London. Series B, Containing Papers of a Biological Character*, 1933, **113**, 238-250.
20. H. Holthusen, *Pflügers Archiv European Journal of Physiology*, 1921, **187**, 1-24.
21. J. Mottram, *The British Journal of Radiology*, 1935, **8**, 32-39.
22. E. Petry, *Biochem. Zeitschr*, 1923, **135**, 353.
23. E. J. Hall and A. J. Giaccia, *Radiobiology for the Radiologist*, Lippincott Williams & Wilkins, 2006.
24. R. Hodgkiss, I. Roberts, M. Watts and M. Woodcock, *International Journal of Radiation Biology and Related Studies in Physics, Chemistry and Medicine*, 1987, **52**, 735-744.
25. J. M. Brown, in *Methods in Enzymology*, Academic Press, 2007, vol. 435, pp. 295-321.
26. R. Durand, *In vivo (Athens, Greece)*, 1994, **8**, 691-702.
27. K. O. Hicks, F. B. Pruijn, T. W. Secomb, M. P. Hay, R. Hsu, J. M. Brown, W. A. Denny, M. W. Dewhirst and W. R. Wilson, *Journal of the National Cancer Institute*, 2006, **98**, 1118-1128.
28. I. F. Tannock, *The Lancet*, 1998, **351**, SII9-SII16.
29. I. Tannock, *British Journal of Cancer*, 1968, **22**, 258.
30. R. Welsh, F. Jensen, N. Cooper, M. Oldstone, B. Banapour, J. Sernatiriger, J. Levy, H. Hoshino, H. Tanaka and M. Miwa, *Nature*, 1996, **379**.
31. R. Batchelder, W. Wilson, M. Hay and W. Denny, *The British Journal of Cancer. Supplement*, 1996, **27**, S52.
32. B. A. Teicher, J. S. Lazo and A. C. Sartorelli, *Cancer Research*, 1981, **41**, 73-81.
33. K. M. Comerford, T. J. Wallace, J. Karhausen, N. A. Louis, M. C. Montalto and S. P. Colgan, *Cancer Research*, 2002, **62**, 3387-3394.
34. M. Wartenburg, F. C. Ling, M. Muschen, F. Klein, H. Acker, M. Gassmann, K. Petrat, V. Putz, J. Hescheler and H. Sauer, *The FASEB Journal*, 2003, **17**, 503-505.
35. J. E. Moulder and S. Rockwell, *Cancer and Metastasis Reviews*, 1987, **5**, 313-341.

36. R. E. Durand, *International Journal of Radiation Oncology, Biology, Physics*, 1991, **20**, 253-258.

37. A. J. Giaccia, Seminars in Radiation Oncology, 1996.

38. C. Riva, C. Chauvin, C. Pison and X. Leverve, *Anticancer Research*, 1998, **18**, 4729-4736.

39. Z. A. Haroon, J. A. Raleigh, C. S. Greenberg and M. W. Dewhirst, *Annals of Surgery*, 2000, **231**, 137.

40. P. Vaupel, *The Oncologist*, 2004, **9**, 10-17.

41. G. L. Semenza and G. L. Wang, *Molecular and Cellular Biology*, 1992, **12**, 5447-5454.

42. G. L. Wang, B.-H. Jiang, E. A. Rue and G. L. Semenza, *Proceedings of the National Academy of Sciences*, 1995, **92**, 5510-5514.

43. G. L. Wang and G. L. Semenza, *Journal of Biological Chemistry*, 1995, **270**, 1230-1237.

44. G. L. Semenza, *Critical Reviews in Biochemistry and Molecular Biology*, 2000, **35**, 71-103.

45. A. C. Koong, N. C. Denko, K. M. Hudson, C. Schindler, L. Swiersz, C. Koch, S. Evans, H. Ibrahim, Q. T. Le and D. J. Terris, *Cancer Research*, 2000, **60**, 883-887.

46. R.-P. Czekay, K. Aertgeerts, S. A. Curriden and D. J. Loskutoff, *The Journal of Cell Biology*, 2003, **160**, 781-791.

47. J. E. Ziello, I. S. Jovin and Y. Huang, *The Yale Journal of Biology and Medicine*, 2007, **80**, 51-60.

48. G. L. Semenza, *Physiology*, 2004, **19**, 176-182.

49. B. Krishnamachary, S. Berg-Dixon, B. Kelly, F. Agani, D. Feldser, G. Ferreira, N. Iyer, J. LaRusch, B. Pak and P. Taghavi, *Cancer Research*, 2003, **63**, 1138-1143.

50. S. Pennacchietti, P. Michieli, M. Galluzzo, M. Mazzone, S. Giordano and P. M. Comoglio, *Cancer Cell*, 2003, **3**, 347-361.

51. B.-H. Jiang, G. L. Semenza, C. Bauer and H. H. Marti, *American Journal of Physiology-Cell Physiology*, 1996, **271**, C1172-C1180.

52. B.-H. Jiang, J. Z. Zheng, S. W. Leung, R. Roe and G. L. Semenza, *Journal of Biological Chemistry*, 1997, **272**, 19253-19260.

53. C. J. Schofield and P. J. Ratcliffe, *Biochemical and Biophysical Research Communications*, 2005, **338**, 617-626.
54. W. G. Kaelin, *Clinical Cancer Research*, 2007, **13**, 680s-684s.
55. G. L. Semenza, B.-H. Jiang, S. W. Leung, R. Passantino, J.-P. Concordet, P. Maire and A. Giallongo, *Journal of Biological Chemistry*, 1996, **271**, 32529-32537.
56. J. L. Ruas and L. Poellinger, *Seminars in Cell & Developmental Biology*, 2005.
57. D. J. Manalo, A. Rowan, T. Lavoie, L. Natarajan, B. D. Kelly, Q. Y. Shui, J. G. Garcia and G. L. Semenza, *Blood*, 2005, **105**, 659-669.
58. G. P. Elvidge, L. Glenny, R. J. Appelhoff, P. J. Ratcliffe, J. Ragoussis and J. M. Gleadle, *Journal of Biological Chemistry*, 2006, **281**, 15215-15226.
59. D. J. Payne, M. N. Gwynn, D. J. Holmes and D. L. Pompliano, *Nature Reviews Drug Discovery*, 2006, **6**, 29.
60. G. D. Wright, *Chemistry & Biology*, 2000, **7**, R127-R132.
61. S. B. Levy and B. Marshall, *Nature Medicine*, 2004, **10**, S122-S129.
62. M. Martinez and P. Silley, in *Comparative and Veterinary Pharmacology*, Springer, 2010, pp. 227-264.
63. F. Li, J. G. Collins and F. R. Keene, *Chemical Society Reviews*, 2015, **44**, 2529-2542.
64. M. C. McManus, *American Journal of Health-System Pharmacy*, 1997, **54**, 1420-1433.
65. L. Silver and K. Bostian, *Antimicrobial Agents and Chemotherapy*, 1993, **37**, 377.
66. I. Turel, *Coordination Chemistry Reviews*, 2002, **232**, 27-47.
67. M. Rizzotto, in *A Search for Antibacterial Agents*, InTech, 2012.
68. J. Lemire, J. Harrison and R. Turner, *Antimicrobial Activity of Metals: Mechanisms, Molecular Targets and Applications*, 2013.
69. M. Patra, G. Gasser and N. Metzler-Nolte, *Dalton Transactions*, 2012, **41**, 6350-6358.
70. B. S. Sekhon, *Journal of Pharmaceutical Education and Research*, 2010, **1**, 1.
71. L. J. Ming, *Medicinal Research Reviews*, 2003, **23**, 697-762.

72. N. Metzler-Nolte, in *Medicinal Organometallic Chemistry*, Springer, 2010, pp. 195-217.
73. S. Rafique, M. Idrees, A. Nasim, H. Akbar and A. Athar, *Biotechnology and Molecular Biology Reviews*, 2010, **5**, 38-45.
74. V. Bobbarala, *InTech, Rijeka, Croatia*, 2012.
75. M. D. Rhodes, P. J. Sadler, M. D. Scawen and S. Silver, *Journal of Inorganic Biochemistry*, 1992, **46**, 129-142.
76. C. S. Allardyce and P. J. Dyson, *Platinum Metals Review*, 2001, **45**, 62-69.
77. B. Nordén, P. Lincoln and B. Akerman, *Metal Ions in Biological Systems: Volume 33: Probing of Nucleic Acids by Metal Ion Complexes of Small Molecules*, 1996, **33**, 177.
78. N. W. Luedtke, J. S. Hwang, E. Nava, D. Gut, M. Kol and Y. Tor, *Nucleic Acids Research*, 2003, **31**, 5732-5740.
79. C. Metcalfe and J. A. Thomas, *Chemical Society Reviews*, 2003, **32**, 215-224.
80. B. M. Zeglis, V. C. Pierre and J. K. Barton, *Chemical Communications*, 2007, 4565-4579.
81. F. R. Keene, J. A. Smith and J. G. Collins, *Coordination Chemistry Reviews*, 2009, **253**, 2021-2035.
82. M. R. Gill and J. A. Thomas, *Chemical Society Reviews*, 2012, **41**, 3179-3192.
83. J. Falk, J. Phillips, F. Dwyer and D. Mellor, *Academic Press, New York, NY*, 1964, 441.
84. C. A. Puckett and J. K. Barton, *Biochemistry*, 2008, **47**, 11711-11716.
85. M. R. Gill, J. Garcia-Lara, S. J. Foster, C. Smythe, G. Battaglia and J. A. Thomas, *Nature Chemistry*, 2009, **1**, 662-667.
86. M. Matson, F. R. Svensson, B. Nordén and P. Lincoln, *The Journal of Physical Chemistry B*, 2011, **115**, 1706-1711.
87. A. Bolhuis, L. Hand, J. E. Marshall, A. D. Richards, A. Rodger and J. Aldrich-Wright, *European Journal of Pharmaceutical Sciences*, 2011, **42**, 313-317.
88. E. Meggers, *Chemical Communications*, 2009, 1001-1010.
89. S. K. Singh and D. S. Pandey, *RSC Advances*, 2014, **4**, 1819-1840.
90. J. Maksimoska, L. Feng, K. Harms, C. Yi, J. Kissil, R. Marmorstein and E. Meggers, *Journal of the American Chemical Society*, 2008, **130**, 15764-15765.

91. F. Dwyer, I. Reid, A. Shulman, G. M. Laycock and S. Dixson, *The Australian Journal Experimental Biology and Medical Science*, 1969, **47**, 203-218.

92. F. Dwyer, E. C. Gyarfas, W. Rogers and J. H. KOCH, *Nature*, 1952, **170**, 190-191.

93. A. J. Mason, A. Marquette and B. Bechinger, *Biophysical Journal*, 2007, **93**, 4289-4299.

94. E. I. Edwards, R. Epton and G. Marr, *Journal of Organometallic Chemistry*, 1976, **107**, 351-357.

95. E. I. Edwards, R. Epton and G. Marr, *Journal of Organometallic Chemistry*, 1979, **168**, 259-272.

96. E. I. Edwards, R. Epton and G. Marr, *Journal of Organometallic Chemistry*, 1975, **85**, C23-C25.

97. Z. H. Chohan, *Applied organometallic Chemistry*, 2006, **20**, 112-116.

98. S. Yavuz and H. Yıldırım, *Journal of Chemistry*, 2013, **2013**.

99. M. Patra, G. Gasser, M. Wenzel, K. Merz, J. E. Bandow and N. Metzler-Nolte, *Organometallics*, 2010, **29**, 4312-4319.

100. Z. H. Chohan, *Applied Organometallic Chemistry*, 2002, **16**, 17-20.

101. K. Tahira, S. Ali, S. Shahzadi, S. K. Sharma and K. Qanungo, *Journal of Coordination Chemistry*, 2011, **64**, 1871-1884.

102. Z. H. Chohan, A. Scozzafava and C. T. Supuran, *Synthesis and Reactivity in Inorganic and Metal-Organic Chemistry*, 2003, **33**, 241-257.

103. Y.-T. Liu, G.-D. Lian, D.-W. Yin and B.-J. Su, *Spectrochimica Acta Part A: Molecular and Biomolecular Spectroscopy*, 2013, **100**, 131-137.

104. A. K. Gorle, M. Feterl, J. M. Warner, S. Primrose, C. C. Constantinoiu, F. R. Keene and J. G. Collins, *Chemistry: A European Journal*, 2015, **21**, 10472-10481.

105. A. K. Gorle, X. Li, S. Primrose, F. Li, M. Feterl, R. T. Kinobe, K. Heimann, J. M. Warner, F. R. Keene and J. G. Collins, *Journal of Antimicrobial Chemotherapy*, 2016, **71**, 1547-1555.

106. J. R. Perfect, *Nature Reviews Drug Discovery*, 2017.

107. G. D. Brown, D. W. Denning and S. M. Levitz, *Science*, 2012, **336**, 647-647.

108. G. E. Brzankalski, L. K. Najvar, N. P. Wiederhold, R. Bocanegra, A. W. Fothergill, M. G. Rinaldi, T. F. Pattterson and J. R. Graybill, *Journal of Antimicrobial Chemotherapy*, 2008, **62**, 1094-1100.

109. G. M. Gauthier and N. P. Keller, *Fungal Genetics and Biology*, 2013, **61**, 146-157.

110. M. C. Fisher, D. A. Henk, C. J. Briggs, J. S. Brownstein, L. C. Madoff, S. L. McCraw and S. J. Gurr, *Nature*, 2012, **484**, 186-194.

111. N. Liu, C. Wang, H. Su, W. Zhang and C. Sheng, *Future*, 2016, **8**, 1435-1454.

112. M. Mutz and T. Roemer, *Future Science*, 2016.

113. M. E. Cardenas, M. C. Cruz, M. Del Poeta, N. Chung, J. R. Perfect and J. Heitman, *Clinical Microbiology Reviews*, 1999, **12**, 583-611.

114. T. C. White, K. A. Marr and R. A. Bowden, *Clinical Microbiology Reviews*, 1998, **11**, 382-402.

115. B. D. Alexander and J. R. Perfect, *Drugs*, 1997, **54**, 657-678.

116. Z. H. Chohan, M. Arif, M. A. Akhtar and C. T. Supuran, *Bioinorganic Chemistry and Applications*, 2006, **2006**.

117. W. Raza, W. Hongsheng and S. Qirong, *Bioresource Technology*, 2010, **101**, 1904-1912.

118. W. Raza, X. Yang, H. Wu, Q. Huang, Y. Xu and Q. Shen, *Bioresource Technology*, 2010, **101**, 9264-9271.

119. Z. H. Chohan, H. Pervez, A. Rauf, K. M. Khan and C. T. Supuran, *Journal of Enzyme Inhibition and Medicinal Chemistry*, 2004, **19**, 417-423.

120. G. B. Bagihalli, P. G. Avaji, S. A. Patil and P. S. Badami, *European Journal of Medicinal Chemistry*, 2008, **43**, 2639-2649.

121. F. Gerwien, V. Skrahina, L. Kasper, B. Hube and S. Brunke, *FEMS Microbiology Reviews*, 2017, fux050-fux050.

122. P. Dyson, International Patent WO 02/40491 A1, March, 2002, 2002.

123. C. S. Allardyce, P. J. Dyson, D. J. Ellis, P. A. Salter and R. Scopelliti, *Journal of Organometallic Chemistry*, 2003, **668**, 35-42.

124. Z. Jin, Y. Hu, A. Huo, W. Tao, L. Shao, J. Liu and J. Fang, *Journal of Organometallic Chemistry*, 2006, **691**, 2340-2345.

125. R. Rubbiani, O. Blacque and G. Gasser, *Dalton Transactions*, 2016, **45**, 6619-6626.

126. C. Biot, N. François, L. Maciejewski, J. Brocard and D. Poulain, *Bioorganic & Medicinal Chemistry Letters*, 2000, **10**, 839-841.

Chapter 6: Mechanistic Studies

6.0 Biological Relevance

In the search for new potential cancer therapeutic drugs, conclusions of their success must not be based solely on their cytotoxic screening results. The assessment of new drug compounds is multi-layered and preclinical investigations must be undertaken in an attempt to determine their biological relevance. Through various in depth studies it is possible to determine, to some degree of certainty, how a drug molecule will behave *in vivo* (e.g. mode of transport, mechanism of action, cellular distribution) and from this data, we can establish important structural-activity relationships (SAR) between the molecular structure of a drug and its biological activity. As the majority of new drug compounds fail before clinical trials, the SAR information gathered at this stage of testing can be used to modify various physical traits of a molecule to improve its biocompatibility.

6.1 Hydrolysis Studies

Many of the successful metal-based anticancer drug compounds can be classed as "prodrugs", meaning that they are biologically inactive upon administration but can become active under certain biological conditions. As discussed in Chapter 1, the potent cytotoxic mode of action of cisplatin is strongly related to the drug's hydrolysis mechanism.[1-5] Upon entering the cell membrane, the drop in chloride concentration facilitates the ligand substitution reaction to form the active hydro-platinum species which can bind to DNA.

One of the possible modes of action for the successful ruthenium anticancer compounds NAMI-A and KP1019 is thought to involve the reduction of Ru(III) to Ru(II).[6-10] Such a reduction can be achieved in multiple ways under physiological conditions or *in vivo*, either through the aquation pathway to form a number of potentially active species,[11-14] or from interactions with an intracellular reducing agent such as ascorbate or glutathione within the cell.[15] Although these two complexes are rather similar, they undergo hydrolysis at very different rates. NAMI-A begins the process of hydrolysis within minutes of being administered to the body, whereas the more stable KP1019 is much slower, with a better cellular uptake,

resulting in much more of the ruthenium complex being delivered to the nucleus of cells.[16]

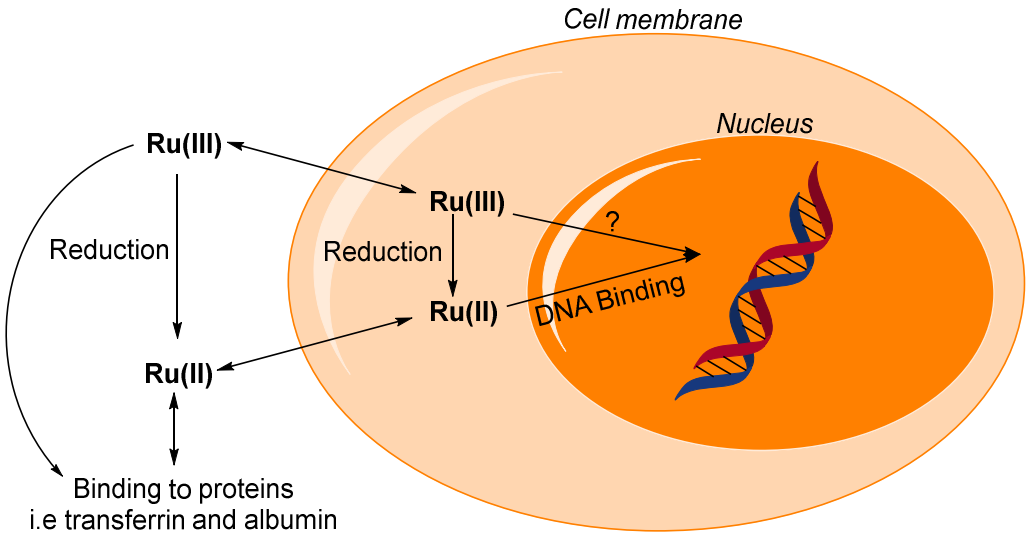

Figure 6.1 Reduction pathways of ruthenium(III) compounds *in vivo*

The strong connection between the hydrolysis pathway and the mechanism of action of these successful anticancer complexes demonstrates the importance of conducting hydrolysis studies on newly formed anticancer compounds. Anticancer ruthenium "piano stool" complexes containing ancillary ligands have also been shown to hydrolyse and bind to nucleobase through a mono- or di- hydrated intermediate species under physiological conditions.[17-19] Furthermore, previous work in the McGowan group on ruthenium(III) *bis*-picolinamide dihalide complexes found that the more cytotoxic dichloro complexes hydrolyse to a greater degree than their less active counterparts.[20]

6.1.1 Hydrolysis Results and Discussion

Hydrolysis studies were performed on all ruthenium complexes and monitored by UV-vis spectroscopy with ^{1}H NMR and electrospray mass spectrometry also conducted on selected complexes. UV-Vis samples were prepared in 90% acetonitrile/10% water to give a final concentration of 50 µM and ^{1}H NMR samples were prepared in 90% d_3-acetonitrile or d_6-acetone /10% D_2O to give final concentration of 5 mg ml^{-1}. Attempts to increase the water concentration of the

solvent solutions caused the complex to precipitate, affecting the overall concentration. Samples were analysed every 24 hours at 293 K over a period of four days to mimic the drug exposure time used during the *in vitro* MTT assay. UV-Vis spectra are assigned tentatively from TD-DFT calculations on similar structures.[21-25]

Over the four day study there was an observed change in the UV-Vis spectra for all of the ruthenium arene complexes **C1**-**C24** (**Table 6.1**) which is associated with the colour change of the sample solutions from red/purple to yellow/brown during the period of observation. UV-Vis absorption spectra for the complexes generally follow the same trend, an example of which is shown in **Figure 6.2**, with the arrows on the graph indicating the change in peak intensity. Intense ligand based absorbance (π-π*) can be observed at approximately 200 nm, followed by less intense metal-to-ligand charge transfer transitions, interligand and ligand-centred transitions at 250-330 nm and a weak d-d transition at 450-550 nm, all of which experience a loss in intensity over the four day period. Moreover, there is a hyperchromic shift of a newly formed metal-to-ligand charge-transfer band in the region of 330-370 nm and ligand based absorbance at 220-230nm, which appears as a shoulder in many but not all cases. These changes in the spectral properties of the complexes strongly suggest that they undergo a ligand substitution reaction in aqueous media to form hydrolysis products.

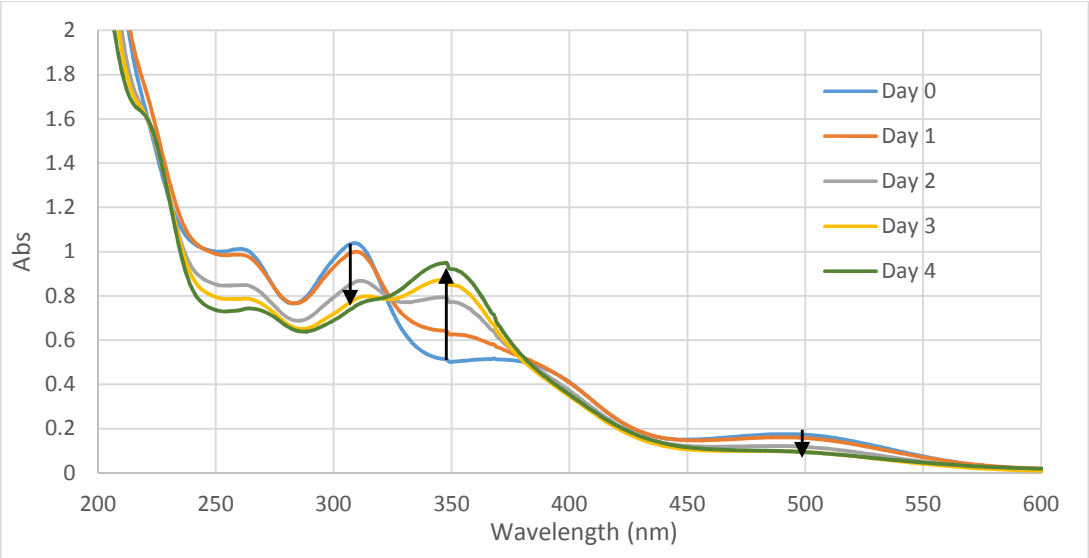

Figure 6.2 Typical changes in UV-Vis spectra for ruthenium arene complexes. Complex **C6** used as an example

Table 6.1 Table of wavelengths of absorption bands of ruthenium arene complexes

Complex	Wavelength / nm	
	Day 0	Day 4
C1	245(sh), 293, 348, 463	296, 348, 455
C2	337, 372(sh)	238(sh), 331
C3	330, 373(sh)	345
C4	255(sh), 310, 368, 487	274, 315(sh), 348
C5	274, 324, 387(sh), 492	221, 273, 347
C6	260, 309, 368, 489	264, 316(sh), 347
C7	252, 308(sh), 318, 378(sh), 487	277(sh), 285, 347
C8	267, 312, 377, 486	223, 266, 348
C9	263, 310, 384(sh), 490	223(sh), 272, 347
C10	266, 310, 368, 492	271, 347
C11	261, 309, 369(sh), 494	269, 347
C12	260, 311, 375(sh), 497	271, 348
C13	256, 307, 365(sh), 495	219(sh), 271, 348
C14	263(sh), 312, 353(sh), 396(sh), 503	272, 347
C15	265, 312, 358, 497	272, 348
C16	260, 311, 378(sh), 495	223(sh), 273, 348
C17	261, 311, 391(sh), 505	273, 349
C18	267, 312, 385(sh), 497	269, 347
C19	261, 311, 388(sh), 498	273, 351
C20	275, 315, 383(sh), 493	243, 272(sh), 347
C21	222(sh), 260, 311, 386(sh), 498	272, 347
C22	278, 320, 374, 485	247(sh), 273(sh), 343
C23	262, 309, 384(sh), 491	274, 347
C24	281, 321, 375, 483	245(sh), 273(sh), 346

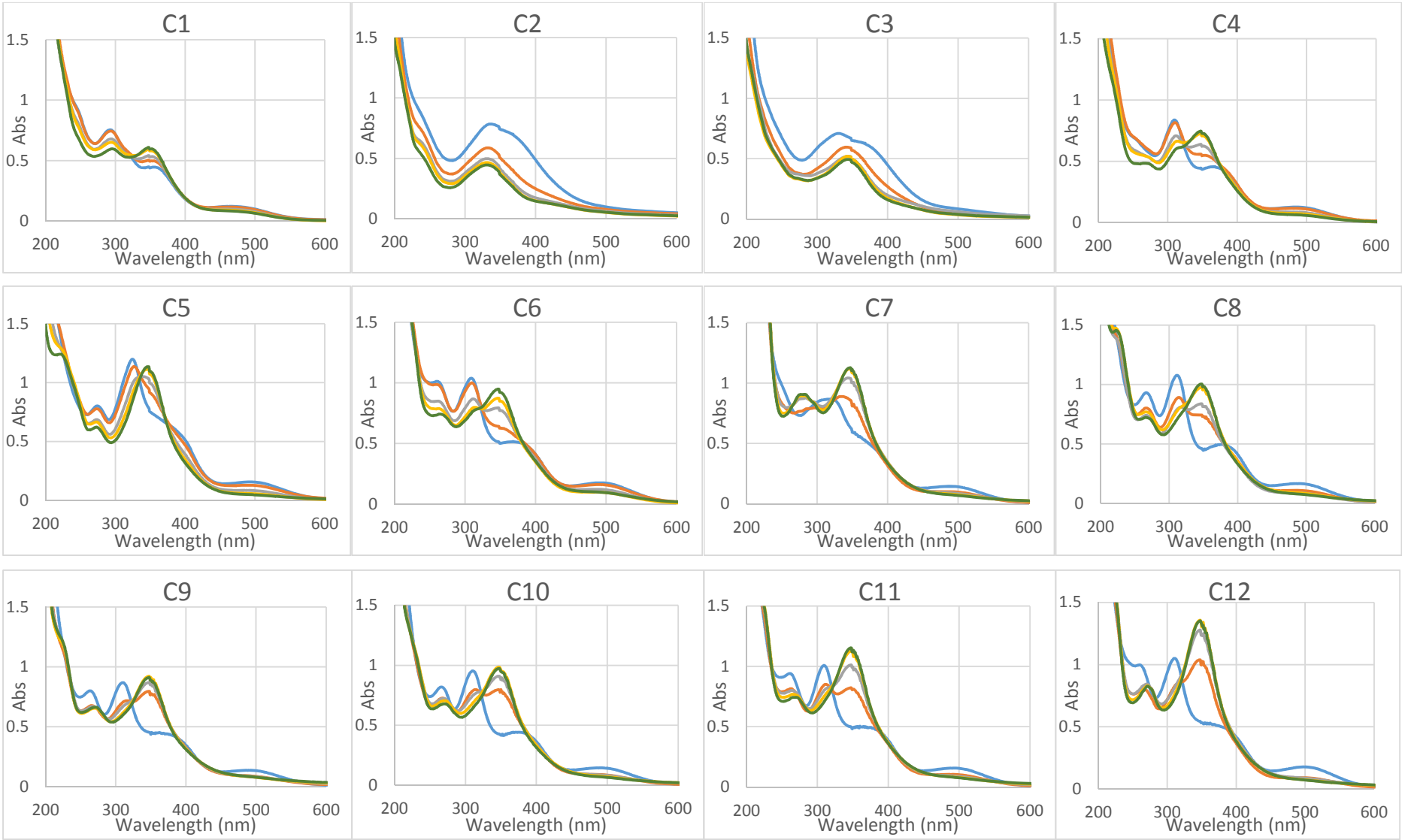
C1
C2
C3
C4
C5
C6
C7
C8
C9
C10
C11
C12
Abs
Wavelength (nm)
0
0.5
1
1.5
200
300
400
500
600

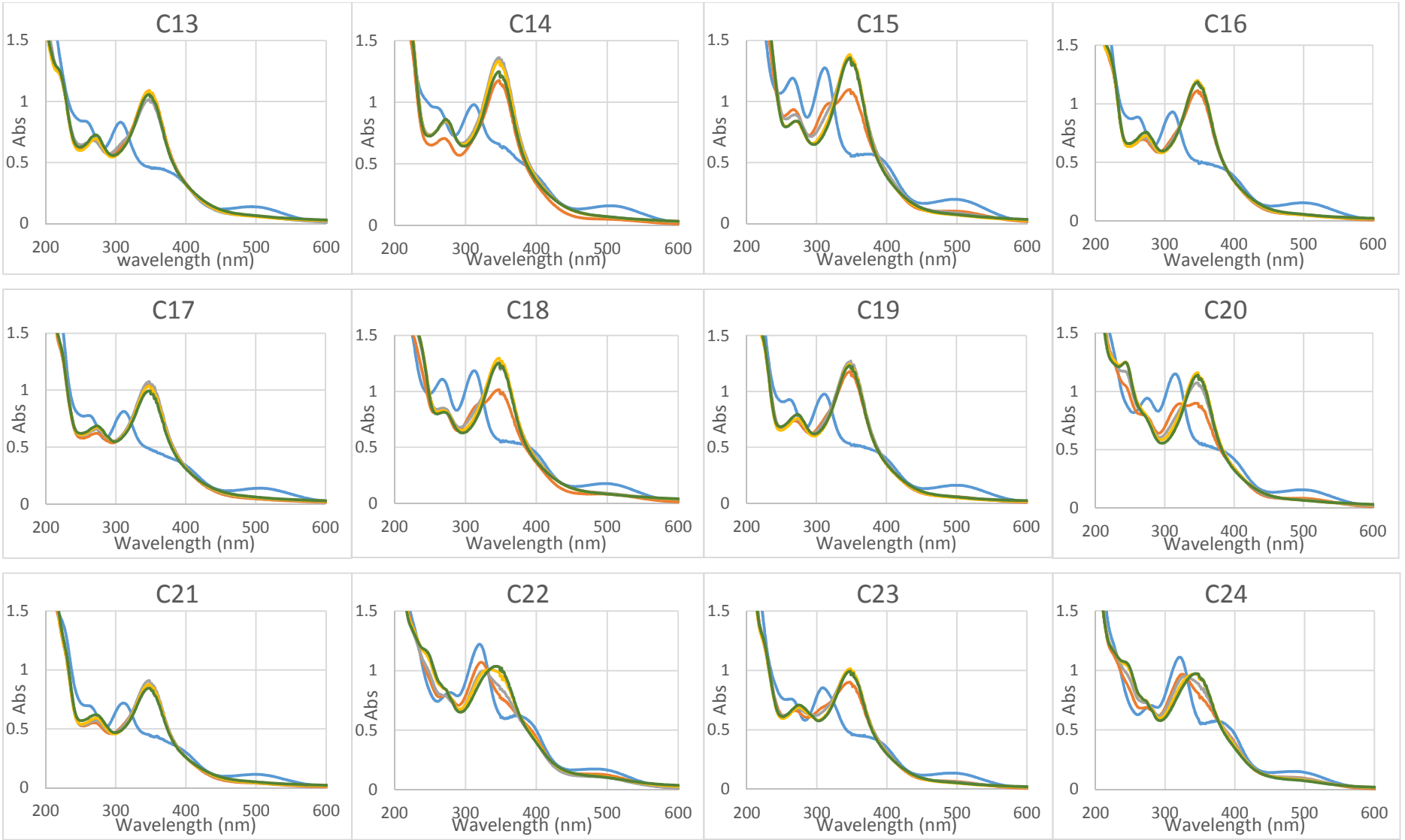

Figure 6.3 UV-Vis spectra for ruthenium arene complexes. Key: Day 0 = blue, Day 1 = orange, Day 2 = grey, Day 3 = yellow, Day 4 = green

The most active complexes against the MIA PaCa-2 cell line, **C2** and **C5**, and their less active but structurally similar counterparts, **C3** and **C4** respectively, were of particular interest in the search for links between hydrolysis and anticancer activity (**Figure 6.4**).

C2 and **C3** gave similar UV-Vis spectra, which is to be expected, with an intense ligand based absorbance (π-π*) at approximately 200 nm and a broad and less intense band at 300-400 nm arising from metal-to-ligand charge transfer transitions, coupled with some interligand and ligand-centered transitions. Over the four day period a hypochromic shift in the A_{Max} of both absorbance bands can be observed for both complexes, but to a greater extent in the case of the **C2**, especially over the first two days. As the relative hydrolysis rates can be inferred from the from the UV-Vis spectra, we can therefore conclude that the relative hydrolysis rates of these two complexes (**C2** > **C3**) correlate to their anticancer activity.

Complexes **C4** and **C5** also have similar UV-Vis absorption spectra to each other; both possess an intense ligand based absorbance (π-π*) at approximately 200 nm, a less intense band at 290-330 nm arising from metal-to-ligand charge transfer transitions, coupled with some interligand and ligand-centred transitions, and a weak d-d transition at 480-510 nm. A hypochromic shift in the A_{Max} of both the ligand based absorbance, metal-to-ligand charge-transfer and d-d transition band was observed over the four day period with a hyperchromic shift of a newly formed metal-to-ligand charge-transfer band in the region of 330-370 nm. In the case of complex **C5**, there was the formation of another band at 220-230 nm by the end of the four days. As with the case of the comparison of complex **C2** and **C3** but to a lesser extent, the more active complex **C5** hydrolyses at a slightly increased rate over **C4**, as the difference in the IC_{50} value between **C5** and **C4** is considerably less than that between complexes **C2** and **C5**. Again, the most active complex showed a greater rate of hydrolysis when compared to their less active equivalents (**C5** > **C4**), further suggesting that there is a correlation between the relative rate of hydrolysis and the anti-cancer activity of these particular complexes. However, it should be noted that the correlation between the hydrolysis rate and anticancer activity is not observed for all complexes.

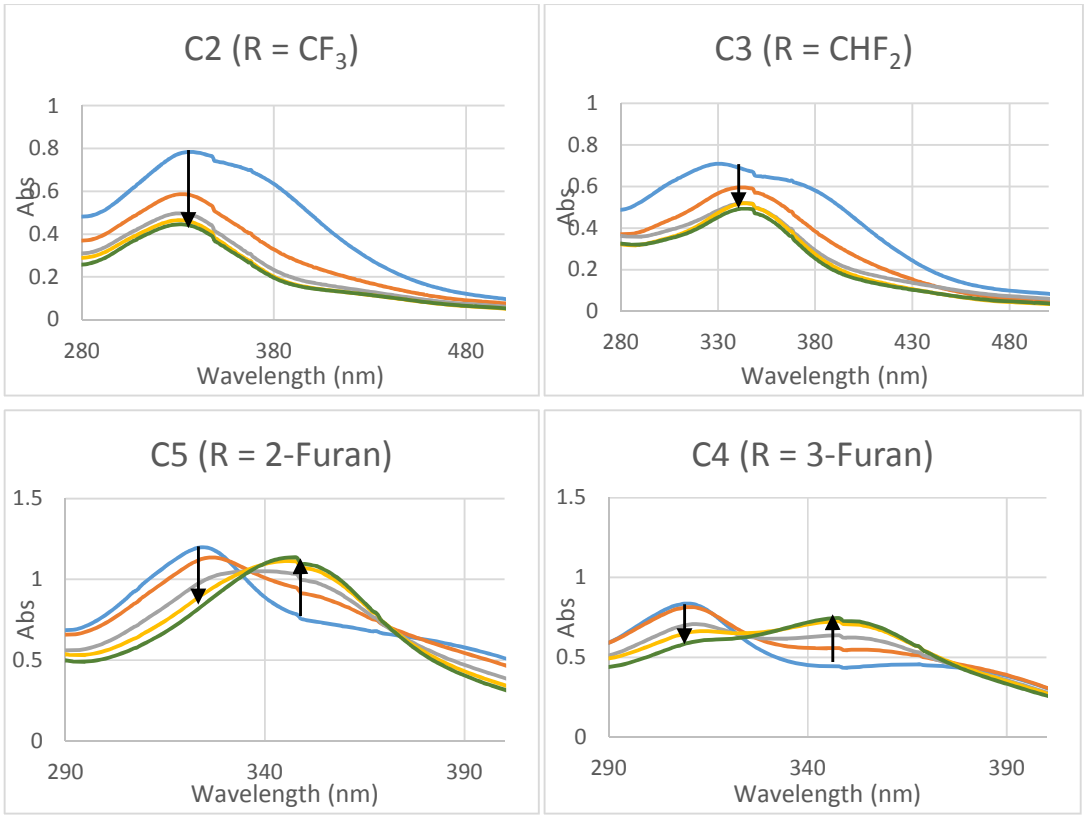

Figure 6.4 UV-vis spectra for the hydrolysis of complexes **C2-C5**

The formation of new species in the presence of water was further confirmed by ^{1}H NMR spectroscopy, an example of which is shown in **Figure 6.5**. In the NMR spectra, there is a change of the peaks at 5.3-6.5 ppm, the region associated with the aromatic *p*-cymene protons and methine proton, where there is a clear formation of multiple new proton environments. Further changes can be observed in the region of 3.0 ppm, again arising from the formation of new proton environments around the *p*-cymene ligand. However, this information alone brings us no closer to deciphering the structure of the hydrolysis products which are clearly forming under these conditions.

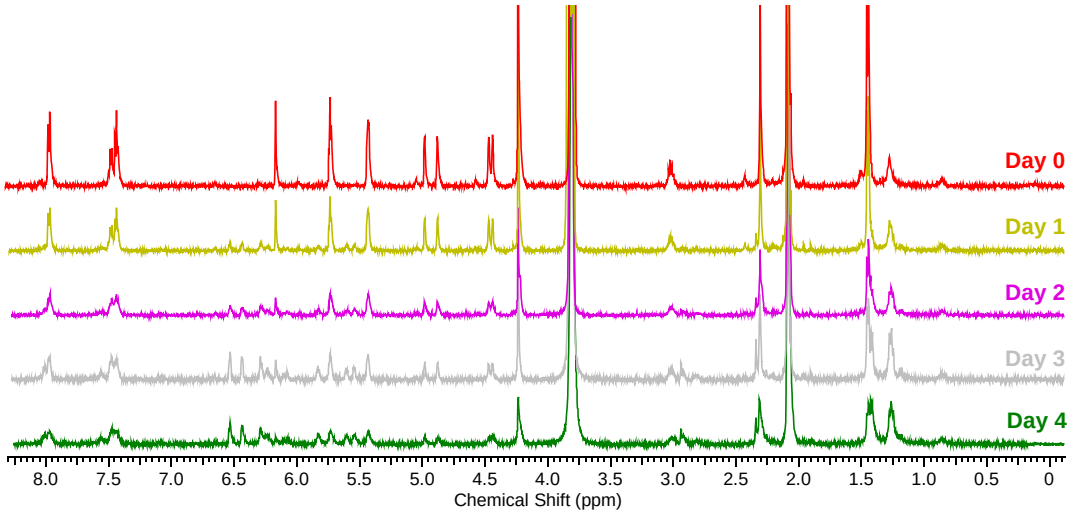

Figure 6.5 ^{1}H NMR (500 MHz, Acetone-d_6) spectra of complex **C6** under aqueous conditions over 4 days

ES-MS was collected for multiple hydrolysis samples, all of which gave peaks which correspond to structures analogous to those shown in **Figure 6.6**, although it should be noted that there is currently no further data to support the presence of these exact structures. Other hydrolysis products may form in the solutions that may be unstable and degrade when passed through the ES-MS, although these could also be important hydrolysis products. There is also the possibility that the proposed complexes in **Figure 6.6** may form inside the ES-MS device from unstable hydrolysed complexes. Attempts to try and isolate the hydrolysis products have proved futile.

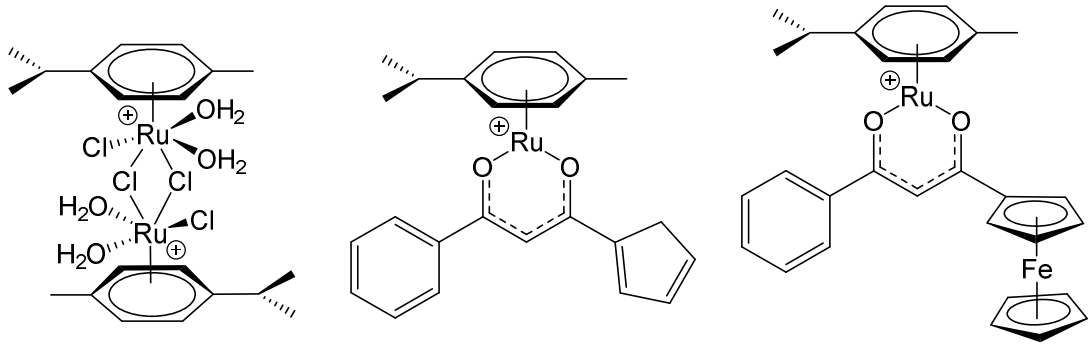

Found Mass $[M]^{2+}$: 341.0508
Exact Mass $[M]^{2+}$: 341.9722

Found Mass $[M]^{+}$: 448.0984
Exact Mass $[M]^{+}$: 447.0898

Found Mass $[M]^{+}$: 567.0584
Exact Mass $[M]^{+}$: 567.0560

Figure 6.6 Mass spectrometry peaks and assignments for complex **C6**

The formation of the additional peaks in the NMR spectra could arise from the breakdown of the ferrocene β-diketonate ligand into cyclopentadiene and β-diketonate (containing a Cp ring). These Cp protons will appear in the regions of the newly found proton environments in the ^{1}H NMR spectra. The possibility of the ferrocene present in these β-diketonate ligands breaking down under hydrolysis conditions has been previously observed by Dr. Laura Ghandhi in the McGowan group.[26] During hydrolysis studies on the isolated ligands in 20% water/acetonitrile over five days, there were changes in the UV-Vis, ^{1}H NMR and ES-MS spectra, but assignment of the hydrolysis products was not possible. Over time, dark brown crystals formed in the aqueous solutions of which it was possible to obtain single crystal x-ray data showing the presence of an iron centred complexes **Figure 6.7**.

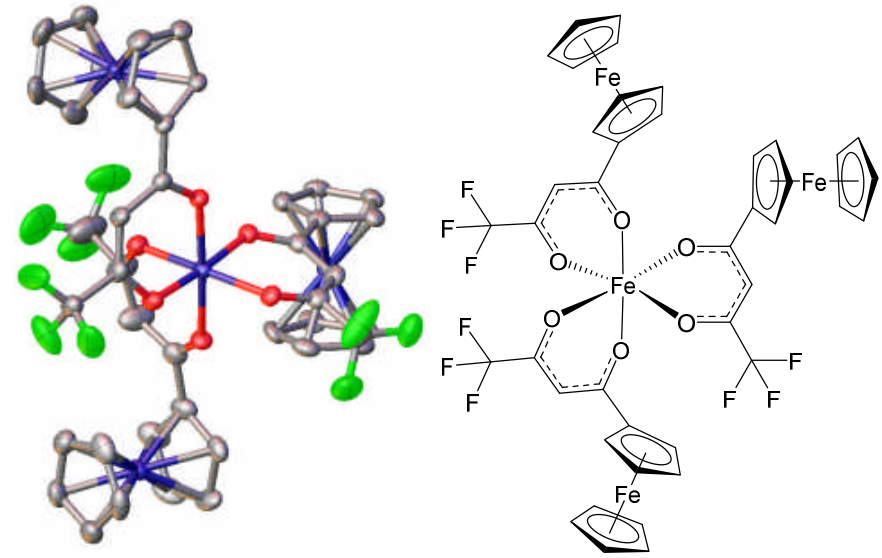

Figure 6.7 Molecular structure of the ferrocenyl β-diketonate ligand hydrolysis product. Displacement ellipsoids are at the 50 % probability level. Hydrogen atoms are omitted for clarity

The ruthenium coordination complexes were found to be highly stable under the previously mentioned hydrolysis condition. In both the NMR and UV-vis studies, there was found to be no notable change in the spectra over the four day observation window. The UV-Vis sample for complex **C'4** was retained and a spectra was obtained at 35 days on top of the four day study to demonstrate the degree of resistance to hydrolysis, a graph of the combined spectrum is shown in **Figure 6.8**. The UV-Vis absorption spectra of complex **C'4** displays an intense band at 245 and

295 nm which typically arise from bpy π → π_2* and π → π_1* intraligand transitions, respectively. A broad Ru(dπ) →bpy(π*) metal-to-ligand charge transfer band occurs centred around 500 nm.[27-32] Absorbance peaks at 205 and 330 nm likely arise from a ligand based absorbance and metal-to-ligand charge transfer transition from the ferrocene β-diketonate ligand.

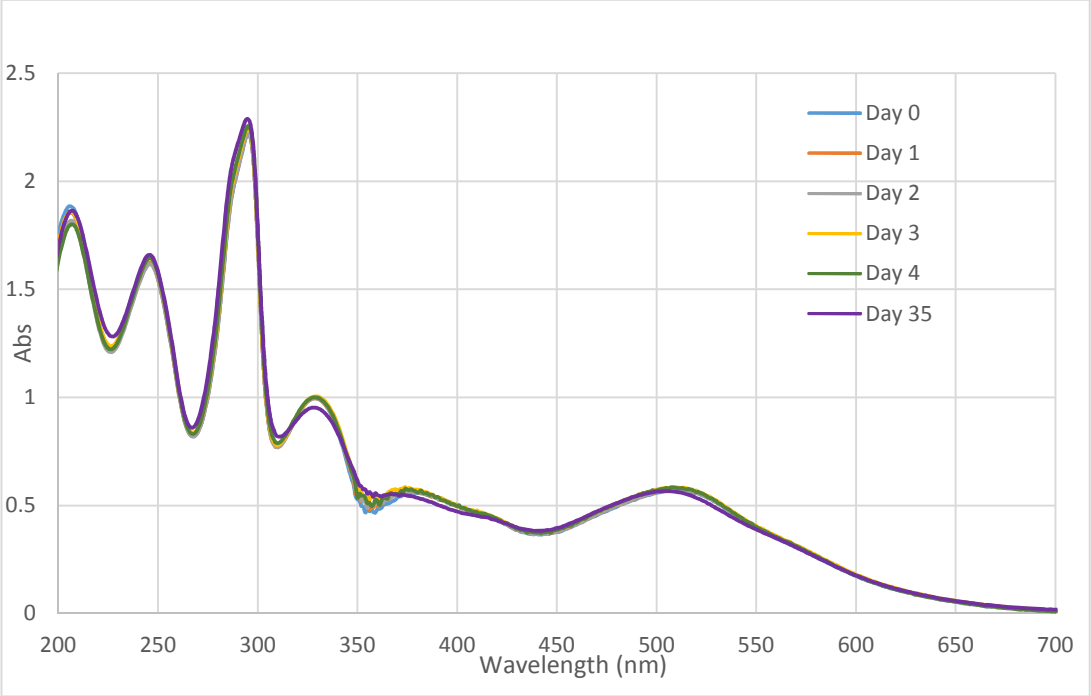

Figure 6.8 Changes in UV-Vis spectra for ruthenium bipyridyl complexes

Contrary to the proposed mechanism of cisplatin, NAMI-A and KP1019, not all metal complexes possess a ligand-substitution step during their mechanism of action. Work by Meggers *et al.* has demonstrated the biological potential of a variety of metal-based enzyme inhibitors, including substitutionally inert ruthenium(II) complexes.[33] Furthermore, the observed stability in aqueous conditions for these ruthenium coordination complexes is in agreement with findings from other ruthenium polypyridyl DNA binders.[34]

If hydrolysis of these complexes was observed in a similar manner to the mode of activation of cisplatin, their ability to bind through non-covalent interactions, such as intercalation, could potentially be hindered. This is to not say that hydrolysis of ruthenium polypyridyl complexes would cause a decrease in their anticancer

potency, but rather than the conditions required are more specific; incorporating sterically demanding ligands which cause distorted octahedral geometries around the ruthenium centre and therefore facilitates the photo-induced ligand loss of the sterically bulky ligand, forming bis-aqua complexes under aqueous conditions.[35-38]

These findings therefore suggest that any interactions which occur between the ruthenium bipyridyl complexes and DNA will be in the form of reversible binding interactions such as intercalation or electrostatics. It should be noted however, that the cytotoxic effects of ruthenium polypyridyl complexes may only be partially attributed to their non-covalent DNA binding interactions.[39] Further studies have provided evidence that their anticancer activity may also arise from intracellular enzyme inhibition and cell wall interactions amongst other biological processes.[40-44]

6.2 Hydrophobicity Studies

Hydrophobicity and hydrophobic interactions are some of the most important and extensively studied natural phenomenon.[45] Work which dates back to the late 19th century by Meyer and Overton first explores the importance of hydrophobic interactions in drug design by correlating the hydrophobic nature of anaesthetic gases to their biological potency.[46-48] Since then, hydrophobic interactions have been shown to be a key factor which is taken into account during the drug design, discovery and development phases, playing a crucial role in a multitude of computational modelling systems.[49-52] Furthermore, the significance of hydrophobicity is demonstrated in Lipinski's "rule of 5" which state that: absorption or permeation of a chemical entity is reduced when the octanol-water partition coefficient (LogP) is greater than 5, the molecule possess more than 5 H-bond donors and weighs more than 500 Da.[53, 54] These rules were later changed and extended by Lipinski in an attempt to improve predictions of "drug-likeness" with a new LogP range of -0.4 - +5.6 and then further refined to classify "lead-like" compounds with a LogP of less than 3.[55-57] The LogP range stated by Lipinski's rules allows a molecule to be orally administered through a balance of sufficient hydrophilicity, to dissolve in aqueous bodily fluids and enter the blood stream through the stomach or

intestines, and yet also sufficient hydrophobicity, to permeate lipophilic biological membranes.

6.2.1 Hydrophobicity Results and Discussion

The hydrophobicity of the ruthenium complexes was determined by their octanol-water partition coefficient obtained from the shaken-flask method which was conducted in the following manner; NaCl saturated deionised water and octanol in a 1:1 ratio was stirred overnight at room temperature and then separated into two layers of water-saturated octanol and octanol-saturated water. Complexes were found to be insoluble in the octanol-saturated water, which was to be expected. Complexes were therefore dissolved in water-saturated octanol, followed by the addition of an equal amount of octanol-saturated water and shaken at 1000 $gmin^{-1}$ for two hours. A minimum of six repeats were taken per complex. The organic layers of the solutions, before and after partitioning, were analysed by UV-vis spectroscopy to obtain the values of maximum absorbance (A_{max}). Using pre-prepared calibration graphs for each individual complex, it was possible to calculate the concentration of complex ($[C]_{org}$) in each sample from the A_{max} and hence, determine the partition coefficient **Equation 6.1**.[58-61]

$$\mathbf{Log}\boldsymbol{P} = \mathbf{Log_{10}}\left(\frac{[\boldsymbol{C}]_{\boldsymbol{final}}}{[\boldsymbol{C}]_{\boldsymbol{initial}} - [\boldsymbol{C}]_{\boldsymbol{final}}}\right)$$

Equation 6.1

When determining the hydrophobicity of a compound from the shaken-flask method, octanol acts as a model for the cell membrane, mimicking the lipophilic layers. In order for a complex to be classed as hydrophobic it must accumulate more readily in the organic phase rather than the aqueous phase, its LogP value will therefore be positive. If the opposite is true and the compound concentration is greater in the aqueous phase then the compound is hydrophilic and will produce a negative LogP value.

The hydrophobity for complexes **C1** – **C24** was studied using the aforementioned process and their obtained LogP values are summarised in **Table 6.2** and **Figure 6.1**. It was not possible to obtain the partition coefficient for complexes **C'1** – **C'15** due to their lack of solubility in water and only partial solubility in octanol.

Table 6.2 LogP values for ruthenium arene complexes

Complex	LogP	±SD	Complex	LogP	±SD
C1	1.11	0.09	**C14**	0.74	0.05
C2	1.76	0.18	**C15**	0.69	0.06
C3	1.13	0.09	**C16**	0.42	0.19
C4	0.97	0.1	**C17**	1.86	0.22
C5	1.02	0.11	**C18**	1.55	0.45
C6	0.8	0.1	**C19**	1.09	0.23
C7	1.04	0.2	**C20**	1.4	0.16
C8	0.33	0.08	**C21**	1.17	0.17
C9	0.64	0.22	**C22**	1.08	0.01
C10	0.55	0.13	**C23**	0.97	0.13
C11	0.79	0.09	**C24**	1.22	0.04
C12	1.26	0.05	**Cisplatin**	-2.2	0.2
C13	1.36	0.16			

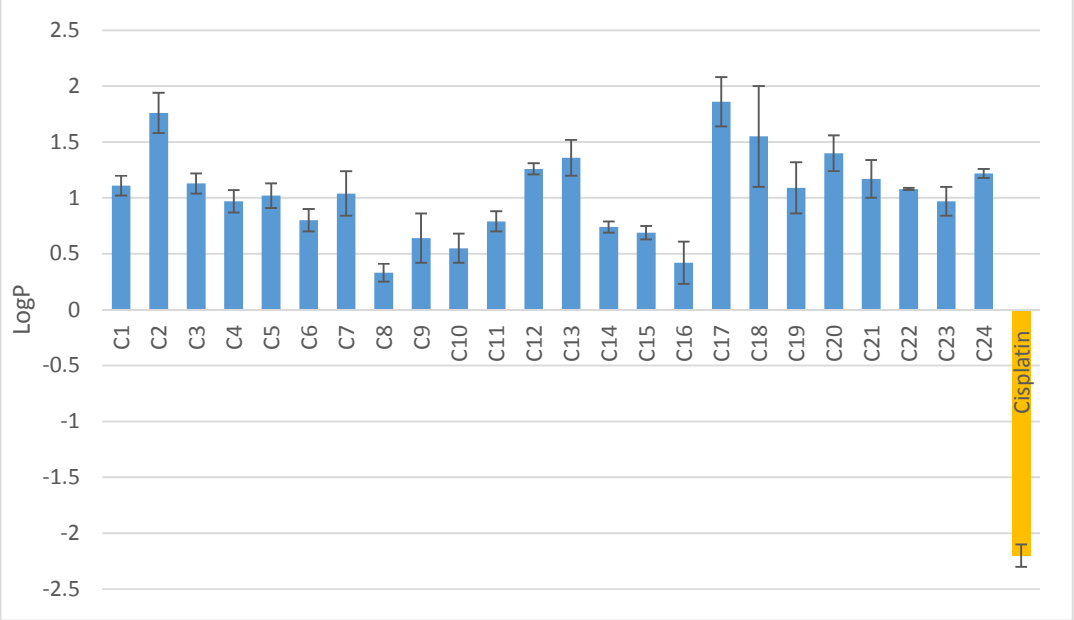

Figure 6.9 Graph of LogP values for ruthenium arene complexes

All complexes were found to possess positive LogP values in the range of 0.33-1.86 and are therefore hydrophobic, partitioning preferentially into the organic layer. This

result was unsurprising as their poor hydrophilicty was observed during attempts to solubilise the complexes in octanol-saturated water. The LogP values for all the complexes fall well within the range dictated by Lipinski's rules but these complexes do not obey the rules in their entirety, weighing considerable more than required. However, transition metal complexes are an exception when it comes to obeying some of Lipinski's rules as many metal complexes have a molecular weight above the proposed maximum of 500 Da. Furthermore, Cisplatin has a LogP value of -2.2,[62-64] well out of the acceptable ranges for a drug candidate set by Lipinski, and yet it is one of the most successful anticancer metal complexes to date.

The two most hydrophobic complexes, **C2** (LogP 1.76) and **C17** (LogP 1.86), were found to be two of the more potent cytotoxic complexes towards both tested cancer cell lines. In agreement with this, the complexes with the lowest LogP values, **C8** (LogP 0.33) and **C16** (LogP 0.42), were two of the least cytotoxic complexes observed. However, the same correlation between hydrophobicity and anticancer actively does not remain true when complexes with a LogP value in the middle of the obtained range are taken into consideration, an observation which has previously been seen for ruthenium piano-stool complexes in the McGowan group.[26, 65] As all the complexes were found to be hydrophobic, this suggests that the complexes will enter cells *via* passive diffusion due to their greater potential to cross the cell membrane of lipophilic layers.[66] However, it should be noted that LogP only describes the lipophilicity of compounds in their neutral form, and although it can be very useful for comparing overall trends it should be used carefully. To obtain a more accurate description of the partition coefficient of ionisable compounds the pH should be taken into consideration with the use of a buffer solution as the aqueous phase such as phosphate-buffered saline.

6.3 Biomembrane Studies

The human body contains a range of various biomembranes with various different functions, from guarding cells and tissues from harmful molecules, to acting as gateways for biomolecules to penetrate cells. After administration, a drug molecule

will come into contact and interact with many of these biomembranes before reaching its target site.[67] Biomembrane interactions are consequently a crucial factor in the distribution and bioavailability of drug molecules once inside the body, controlling both the rate of penetration and partitioning of the drug molecule.[68] Biomimetic model membrane systems - such as vesicles or liposomes, Langmuir monolayer, solid support bilayers and tethered bilayer lipid membranes – are designed to mimic the basic structural and functional properties of a natural membrane while at the same time being much more robust than membrane proteins. This offers the opportunity to observe drug-membrane interactions at preclinical stages of drug development under defined and controlled conditions.[69] Furthermore, recent work on ruthenium(II) complexes from well-established researchers has reported the induction of cell death *via* apoptosis, facilitated through the metal complexes interfering with the cell membrane potential.[42, 44, 70-72]

A unique biomembrane sensing device has been developed by Nelson *et al.* at the University of Leeds.[73-81] The intelligent design of this system utilises a dioleoyl phosphatidylcholine (DOPC) phospholipid monolayer deposited upon a microfabricated Pt/Hg sensing electrode (**Figure 6.10**) which acts as an excellent and effective artificial biomembrane model. This electrode is connected to an online high throughput flow system which allows for the rapid screening of mass amounts of compounds and records rapid cyclic voltammograms (RCVs) to show changes in the capacitance current peaks when a voltage of 40 Vs^{-1} is applied. Fluctuations in the RCV peaks are recorded by the electrode and show damage of the membrane caused by exposure to membrane active compounds. The mercury support facilitates the detection of any membrane interactions by allowing the formation of a self-healing and defect-free DOPC phospholipid monolayer.[77-79, 81]

This electrochemical setup has been previously used as a toxin detection device for water supplies,[77, 78, 80] however, it is currently being investigated as a fast, easy and inexpensive potential pre-screening technique for anti-cancer compounds as interactions with DOPC can help deduce the *in vivo* behaviour between a compound and the cell membrane.

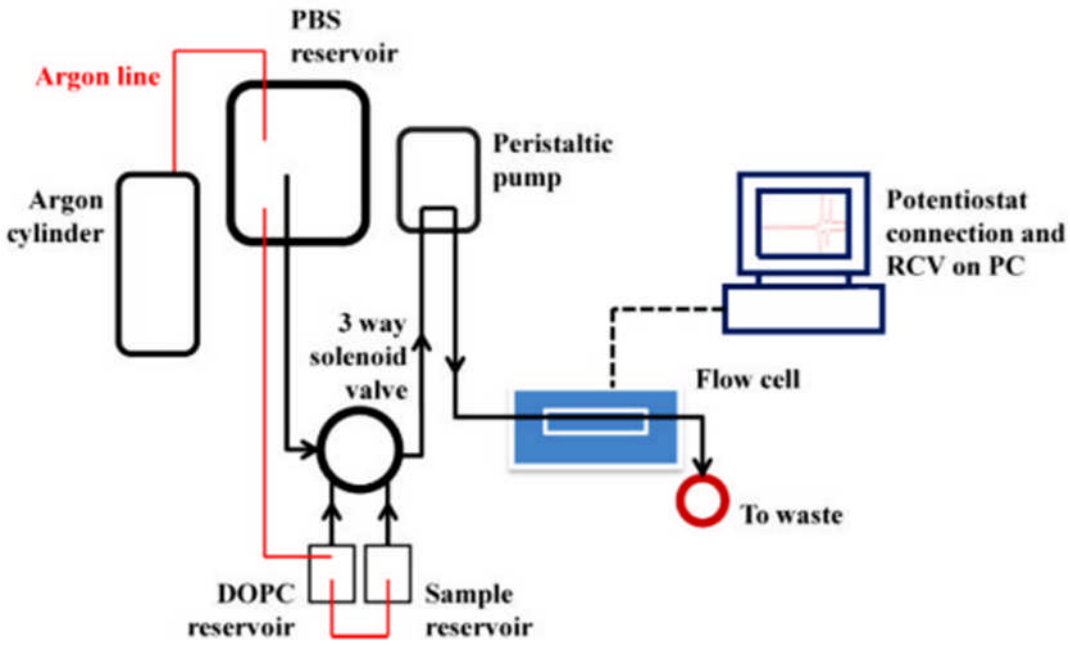

Figure 6.10 Schematic diagram of the electrochemical screening device[80]

The DOPC monolayer produces two sharp characteristic capacitance current peaks which correspond to two potential induced phase transitions which occur when a potential between 0.2-1.8 V is applied (**Figure 6.11**).[76] These peaks arise firstly from the passing of electrolytes into the DOPC layer and secondly from the formation of bilayers and micelles. Any interactions which occur between a biomembrane active compound and the phospholipids will lead to selective membrane damage and cause a change in the organisation and/or fluidity of the DOPC monolayer. If the DOPC monolayer becomes compromised in this manner, changes in the phase transitions will occur that can be detected electrochemically and consequently result in a change in the position, shape and height of the characteristic double peak configuration of the RCV.

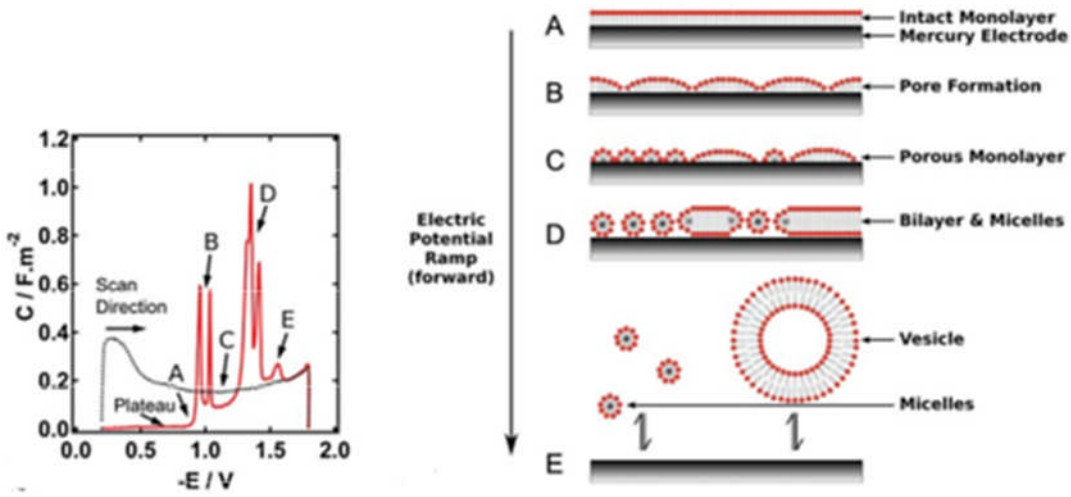

Figure 6.11 Predicted phase transitions of DOPC monolayer[76]

6.3.1 Biomembrane Results and Discussion

The experimental procedure was carried out by Danielle Marriott and Dr. Nicola William under the supervision of Professor Andrew Nelson at The University of Leeds. Solutions of the complexes were prepared by dissolving compounds **C1-C2, C6-C8, C11, C14-C15, C17-C18, C20** and Cisplatin in acetone to yield 15.6 µmol dm^{-3} solutions. Three solutions are introduced into the flow cell, separately, in the following order; control phospate-buffered saline (PBS), DOPC dispersion in PBS and the sample solution. Prior to and throughout each experiment an argon gas flow is maintained above the control and sample electrolytes and the DOPC layer to exclude oxygen. A constant flow of PBS is maintained over the electrode with a flow rate of 5-10 $cm^3\ min^{-1}$. A potential excursion is applied from -0.4V to -3.0V at a scan rate of 100Vs^{-1} during the introduction of the DOPC into the flow cell, which deposits the DOPC on the mercury chip. The potential excursion is altered to -0.4 to -1.2V and by repetitive cycling the characteristic capacitance current peaks of DOPC on mercury can be monitored. The solutions containing the complex is then introduced into the flow system with RCV monitoring the interactions of the sample with the DOPC monolayer while cycling the electrode potential from -0.4 to -3.0V.

As a proof of concept, cisplatin was screened first through the biomembrane sensing device and resulted in no change to RCV plot compared to the primary DOPC layer (**Figure 6.12**). This result was to be expected as cisplatin is hydrophilic and reported

to enter cells readily *via* active transport through copper transport channels and not by passive diffusion.[82-85] Therefore, cisplatin is not able to interact with the DOPC monolayer just as it is not able to interact and diffuse through a cell membrane.

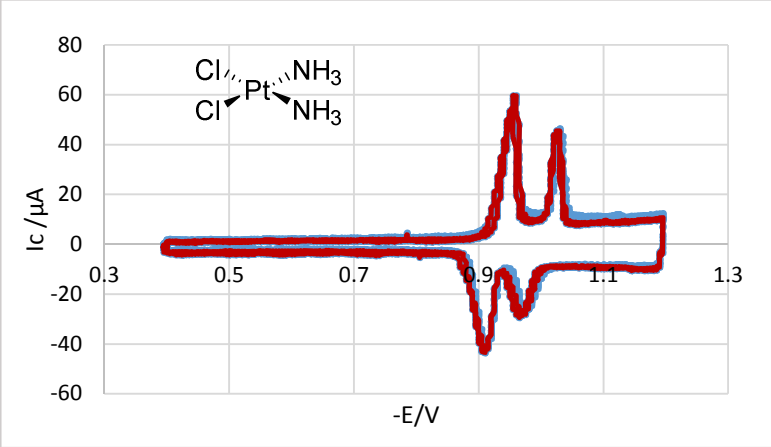

Figure 6.12 RCV plot of cispaltin

The RCVs of the tested complexes displayed varying, yet promising degrees of interaction with the DOPC layer depending on their electronic and steric properties (**Figure 6.14**). Both peaks show great deformation in the presence of the tested compounds with the second peak reducing more vastly in size than the former, suggesting the second DOPC phase transition (the nucleation and growth process) is affected to a greater extent than the first phase transition (movement of ions).

The increasing electronegativity of the halogens in the *para* position of the R substituent correlates to an obvious increase in the degree of DOPC damage (**C11** > **C15** > **C18** > **C20**). In the case of the iodo- containing complex the peaks in the RCV are well defined, gradually becoming less and less distinct with decreasing halogen atom size (**Figure 6.13**). This rise in monolayer disruption could be attributed to the increasing potential of the electronegative complexes to interact with the positively charged head group of DOPC. It could be argued that this is a size dependant SAR; the increasing size of the halogen atom may disrupt the transport of the complex into the DOPC monolayer, an observation that holds true for the bulky complexes **C7** (R = 1-Naph) and **C17** (R = 3',5'-Cl). However, complexes with much smaller R substituents, such as **C1** (R = Me) and **C2** (R = CF_3), have also been shown to cause

little disruption in the RCV plots in comparison to **C11** and **C14**, both of which contain fluoro-phenyl substituents.

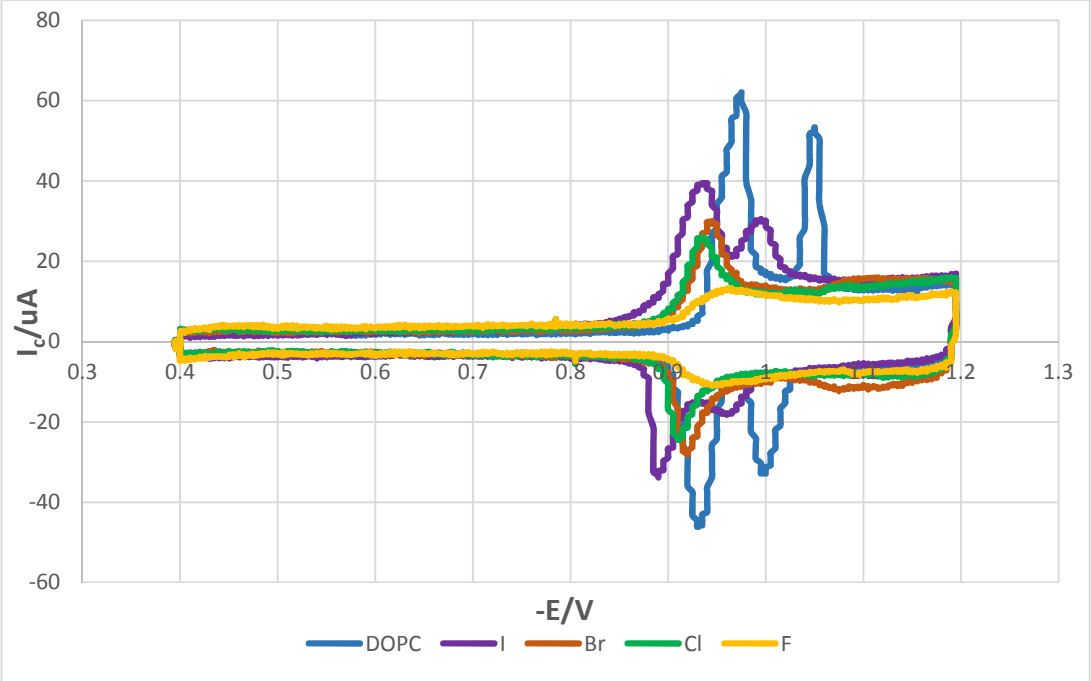

Figure 6.13 RCV graphs to show degree of DOPC monolayer disruption varying with halogen substituent

For several of the compounds (**C1, C2, C7, C17, C20**) partial recovery of the membrane was observed following the DOPC/complex interaction (**Figure 6.15**). This implies the mode of action of these molecules may not involve compromising the cell membrane itself, as they may penetrate the cell membrane with a lesser effect on its integrity and impart their cytotoxicity more internally within the cells. Again, the degree of recovery varies depending on the R substituent of the complex, although the recovery was found to be lesser extent in the complex **C17**.

Overall, these displayed changes in the RCV graphs clearly show the complexes ability to penetrate and interact with the DOPC layer. When applied to a biological system this may potentially translate to the complexes ability to enter and damage the cell membrane, unlimitedly leading to cellular apoptosis. However, there is no notable correlation between the complexes IC_{50} values and the degree of degradation of the DOPC monolayer peaks, an observation which is contrary to previous studies in the McGowan group on cobalt picolinamide anticancer

complexes using this exact biomembrane sensing device.[26] Therefore, even though the high membrane permeability displayed by this series of complexes suggests that their mode of cell entry is mainly, if not solely, *via* passive diffusion, the extent of which they passively diffuse into the cell has no bearing on their anticancer activity in this case, an observation which is in agreement with the previous mentioned hydrophobicty studies.

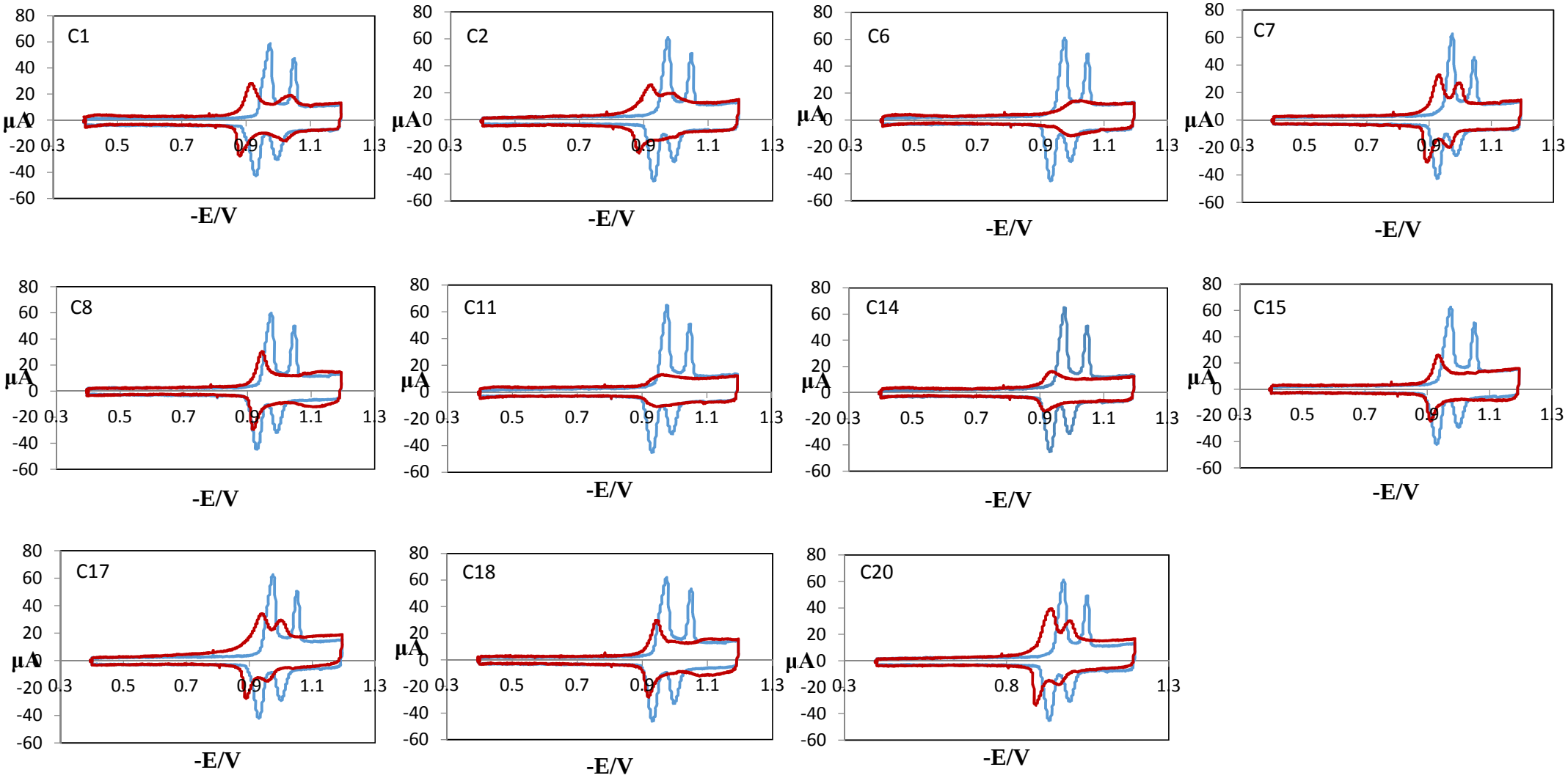

Figure 6.14 RCVs showing interaction of ruthenium/ferrocene complexes (**RED**) with DOPC (**BLUE**)

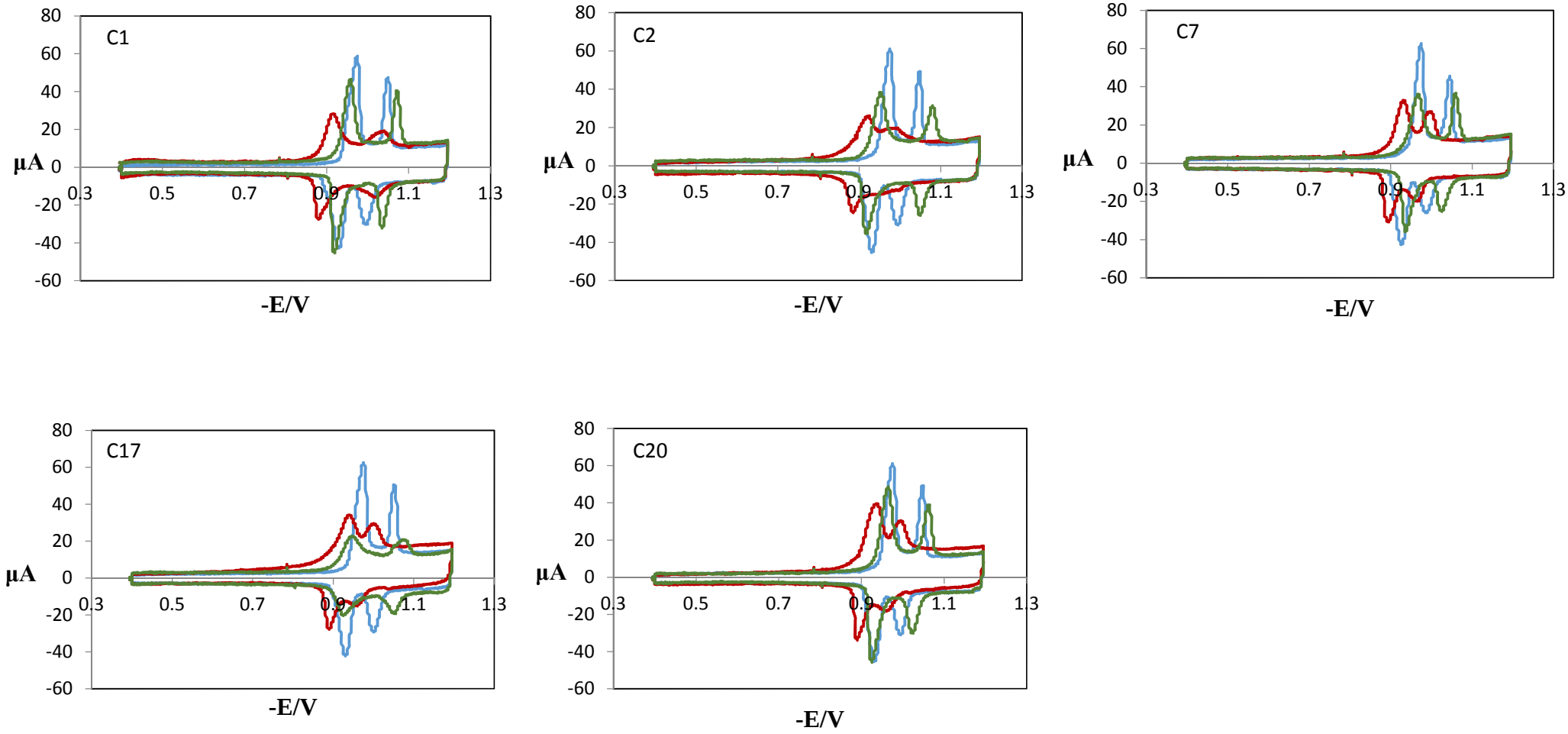

Figure 6.15 RCVs showing the recovery (**GREEN**) of DOPC (**BLUE**) with ruthenium/ferrocene complexes (**RED**)

6.4 Comet Assay

The comet assay, otherwise known as single-cell gel electrophoresis, is a simple method of determining DNA strand breakage in eukaryotic cells (**Figure 6.16**).[86] Microgel electrophoresis was first developed by Ostaling and Johanson in 1984 to measure single-strand breaks in DNA supercoils. This technique was later modified in 1988 by Singh *et al*. to incorporate alkaline conditions which has become the widespread method used to this day.[87]

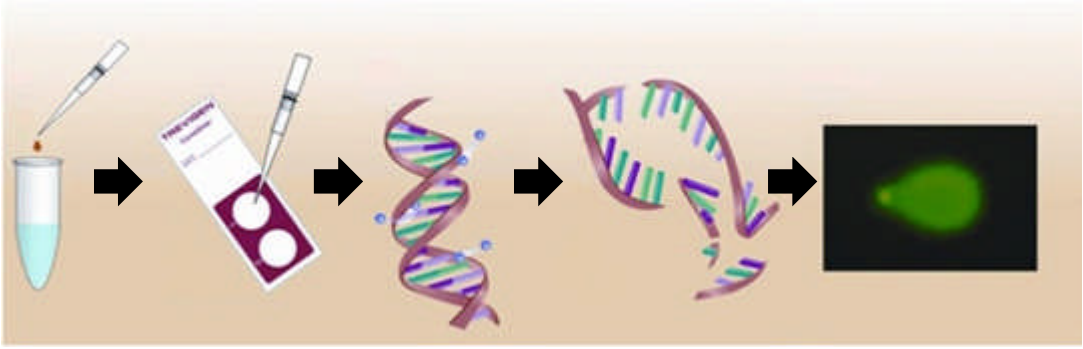

Figure 6.16 Comet assay procedure[88]

Eukaryotic cells are embedded in agarose, a polysaccharide gel, before being lysed with a buffer solution in order to break down the cell membrane. The remaining DNA is too large to diffuse into the agarose and is retained in the nucleoids created by the cells. Electrophoresis is then conducted in alkaline conditions which results in the flow towards the anode of broken and relaxed negatively charged DNA from the immobile DNA supercoils. This phenomenon creates a comet like image when observed with a fluorescent dye through a microscope. The degree of DNA damage is proportional to the amount of DNA in the comet "tail" compared to the comet "head".[86]

6.4.1 Comet Assay Results and Discussion

Comet assays were conducted by Dr. Rianne Lord at The University of Bradford. Complexes **C2**, **C5** and **C6** were tested for their ability to induce single strand breakage (SSB) of DNA, with varying concentrations of compound from 20 – 2.5 µM.

MIA PaCa-2 cells were chosen for this study due to their increased sensitivity to the complexes under observation. An incubation period of 48 hours was determined from shorter term MTT assay results which proved interesting and will be discussed later (**Table 6.3**). After harvesting the cells, they were added to pre-prepared slides containing an agarose layer. Neutral lysing solution was added to the slides followed by the alkaline electrophoresis buffer. The slides were then placed into the electrophoresis chamber where an electric field of 24 V was applied for 25 minutes before being washed and dried overnight. A staining solution was added to the slides and a minimum of 50 comets were analysed using Comet assay III software

Table 6.3 IC_{50} values for complexes **C2**, **C5** and **C6** over 24 and 48 hours averaged over 3 runs

Complex	IC_{50} Values ± SD	
	24 h	48 h
Cisplatin	>100	76 ± 3
C2	>100	29.6 ± 0.9
C5	>100	23 ± 2
C6	>100	>100

Complexes **C2** and **C6** only show a small degree of SSB (tail moments of 6.1 and 5.6 respectively) when incubated for 48 hours, but an increase in DNA damage is observed with respect to an increase in compound concentration. However, complex **C5** showed a significant degree of SSB (tail moment of 19.2) after 48 hours, and was similarly dose-dependent with respect to an increase in compound concentration. These values are in agreement with the IC_{50} values obtained in the short 48-hour exposure times, in which a low IC_{50} value corresponds to a higher degree of SSB and hence, increased DNA damage. These results therefore suggest a strong correlation between the amount of DNA SSB and activity of these complexes. Whilst the induction of SSB damage may not be the only cause of cell death, it provides a possible cause of the apoptotic phenotype induced by these compounds. Induction of single strand DNA breaks in a dose-dependent manner may suggest a different mechanism of action to cisplatin which primarily induces DNA cross-linking. However, to fully understand the mechanism of action, further investigations into Double Strand Breakages (DSB) and cross-linking assays must be undertaken.

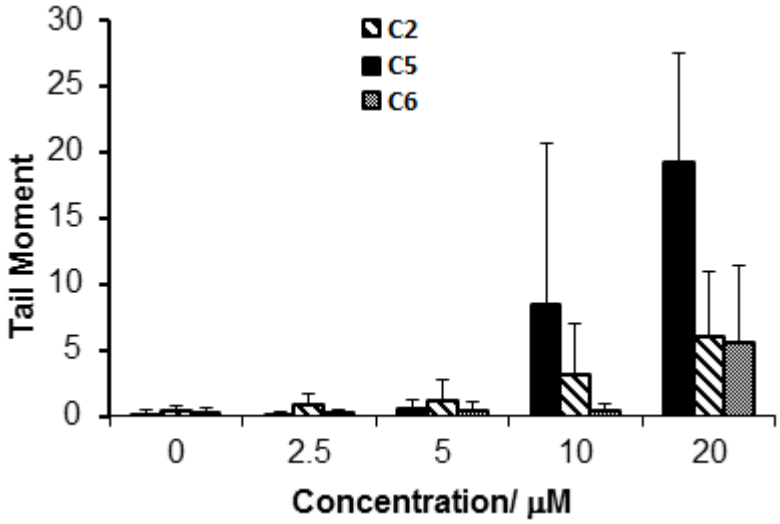

Figure 6.17 Bar-chart showing the tail moments after MIA-PaCa-2 cells were incubated with compounds **C2**, **C5** and **C6** for 48 hours.

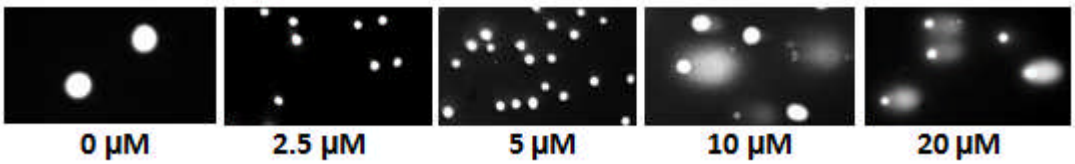

Figure 6.18 Images of 'Comets' observed for compound **C5**

The anticancer activity for the studied complexes was found to follow the order of **C5** > **C2** > **C6** for both the 48 hour and 4 day MTT cytotoxicity assays. However, complexes **C2** and **C5** were found to have superior anticancer activity than cisplatin over 48 hours, an observation which is not true for the longer incubation period. The mechanism of action for these complexes must therefore be much more rapid than that of cisplatin; or rather their window of action is narrower so that they are active only for a short period of time relative to cisplatin. Hydrolysis studies on these complexes discussed earlier in this chapter suggested a correlation between the hydrolysis rate and activity, with more active complexes hydrolysing faster, especially over the first couple of days of observation. However, this theory cannot be confirmed by the 48 hour cytotoxicity studies alone, other factors such as the rate of cellular uptake, biodistribution or protein interactions could be responsible for the greater rate of activity.

6.5 Conclusion

Hydrolysis studies were carried out on the ruthenium arene complexes and ruthenium coordination complexes in an attempt to understand the mechanism of action of these types of anticancer complexes. The ruthenium arene complexes were all shown to undergo hydrolysis with the most cytotoxic compounds hydrolysing at an increased rate than their structurally similar but less active equivalents. However, this trend in hydrolysis rate is not seen for the majority of the other complexes. Efforts to deduce the exact hydrolysis products of these complexes have proven unsuccessful, although potential hydrolysis products have been obtained through ES-MS and the breakdown of the ferrocene ring of the β-diketonate ligands seems likely. The ruthenium coordination compounds were shown to be extremely stable in aqueous conditions for up to 35 days. The structural stability of these complexes suggests that any DNA interactions will occur in a non-covalent manner through intercalation and/or electrostatic interactions.

Ruthenium arene complexes were all found to be hydrophobic, with positive LogP values obtained from the water-octanol partition coefficient that fall within the values set by Lipinski's rules. It was not possible to obtain the LogP values for the coordination complexes due to solubility issues in both water and octanol. A marginal trend was observed at the upper and lower limits of the obtained LogP range which corresponded to greater and lower cytotoxicity, respectively. However, no overall correlation was found between the hydrophobic properties of these complexes and their IC_{50} values. The hydrophobicty of the complexes suggests that their mode of entry into the cell is *via* passive diffusion, a theory which is supported by the biomembrane studies. Disruption of the RCV graphs shows clearly that these complexes are able interact with the artificial phospholipid biomembrane. As with the hydrophobicity studies, no general correlation can be found between the degree of biomembrane interaction and the IC_{50} values, suggesting that the mode of action for the arene complexes is not limited by their cell wall interactions.

The comet assay conducted on the two most active and one less active ruthenium arene complexes found a clear link between the amount of single strand DNA breakage and their cytotoxicity. Furthermore, a shorter term MTT assay (48 hours)

conducted as part of the Comet assay showed that their activity was superior to that of cisplatin over shorter incubation times.

6.6 References

1. Z. Guo and P. J. Sadler, *Angewandte Chemie*, 1999, **111**, 1610-1630.
2. M. Jakupec, M. Galanski and B. Keppler, in *Reviews of Physiology, Biochemistry and Pharmacology*, Springer, 2003, pp. 1-53.
3. V. Brabec and J. Kasparkova, *Drug Resistance Updates*, 2005, **8**, 131-146.
4. H. Zorbas and B. K. Keppler, *Chembiochem*, 2005, **6**, 1157-1166.
5. J. K.-C. Lau and B. Ensing, *Physical Chemistry Chemical Physics*, 2010, **12**, 10348-10355.
6. M. Pongratz, P. Schluga, M. A. Jakupec, V. B. Arion, C. G. Hartinger, G. Allmaier and B. K. Keppler, *Journal of Analytical Atomic Spectrometry*, 2004, **19**, 46-51.
7. F. Kratz, M. Hartmann, B. Keppler and L. Messori, *Journal of Biological Chemistry*, 1994, **269**, 2581-2588.
8. C. G. Hartinger, S. Zorbas-Seifried, M. A. Jakupec, B. Kynast, H. Zorbas and B. K. Keppler, *Journal of Inorganic Biochemistry*, 2006, **100**, 891-904.
9. C. G. Hartinger, M. A. Jakupec, S. Zorbas-Seifried, M. Groessl, A. Egger, W. Berger, H. Zorbas, P. J. Dyson and B. K. Keppler, *Chemistry & Biodiversity*, 2008, **5**, 2140-2155.
10. M. Brindell, D. Piotrowska, A. A. Shoukry, G. Stochel and R. van Eldik, *JBIC Journal of Biological Inorganic Chemistry*, 2007, **12**, 809-818.
11. M. Bacac, A. C. G. Hotze, K. v. d. Schilden, J. G. Haasnoot, S. Pacor, E. Alessio, G. Sava and J. Reedijk, *Journal of Inorganic Biochemistry*, 2004, **98**, 402-412.
12. M. Brindell, I. Stawoska, J. Supel, A. Skoczowski, G. Stochel and R. van Eldik, *JBIC Journal of Biological Inorganic Chemistry*, 2008, **13**, 909-918.
13. M. Bouma, B. Nuijen, M. T. Jansen, G. Sava, A. Bult and J. H. Beijnen, *Journal of Pharmaceutical and Biomedical Analysis*, 2002, **30**, 1287-1296.
14. M. I. Webb and C. J. Walsby, *Dalton Transactions*, 2011, **40**, 1322-1331.
15. A. Levina, A. Mitra and P. A. Lay, *Metallomics*, 2009, **1**, 458-470.
16. N. Graf and S. J. Lippard, *Advanced Drug Delivery Reviews*, 2012, **64**, 993-1004.

17. A. F. Peacock, M. Melchart, R. J. Deeth, A. Habtemariam, S. Parsons and P. J. Sadler, *Chemistry (Weinheim an der Bergstrasse, Germany)*, 2007, **13**, 2601-2613.
18. F. Wang, A. Habtemariam, E. P. L. van der Geer, R. Fernández, M. Melchart, R. J. Deeth, R. Aird, S. Guichard, F. P. A. Fabbiani, P. Lozano-Casal, I. D. H. Oswald, D. I. Jodrell, S. Parsons and P. J. Sadler, *Proceedings of the National Academy of Sciences of the United States of America*, 2005, **102**, 18269-18274.
19. S. H. van Rijt, A. J. Hebden, T. Amaresekera, R. J. Deeth, G. J. Clarkson, S. Parsons, P. C. McGowan and P. J. Sadler, *Journal of Medicinal Chemistry*, 2009, **52**, 7753-7764.
20. A. M. Basri, R. M. Lord, S. J. Allison, A. Rodríguez-Bárzano, S. J. Lucas, F. D. Janeway, H. J. Shepherd, C. M. Pask, R. M. Phillips and P. C. McGowan, *Chemistry-A European Journal*, 2017, **23**, 6341-6356.
21. M. Uršič, T. Lipec, A. Meden and I. Turel, *Molecules*, 2017, **22**, 326.
22. A. Habtemariam, C. Garino, E. Ruggiero, S. Alonso-de Castro, J. Mareque-Rivas and L. Salassa, *Molecules*, 2015, **20**, 7276.
23. S. Betanzos-Lara, L. Salassa, A. Habtemariam, O. Novakova, A. M. Pizarro, G. J. Clarkson, B. Liskova, V. Brabec and P. J. Sadler, *Organometallics*, 2012, **31**, 3466-3479.
24. J. G. Małecki, M. Jaworska, R. Kruszynski and J. Kłak, *Polyhedron*, 2005, **24**, 3012-3021.
25. J. G. Małecki, *Structural Chemistry*, 2012, **23**, 461-472.
26. L. Ghandhi, The University of Leeds 2017.
27. K. Rangan, S. M. Arachchige, J. R. Brown and K. J. Brewer, *Energy & Environmental Science*, 2009, **2**, 410-419.
28. L. J. Charbonnière, S. Faulkner, C. Platas-Iglesias, M. Regueiro-Figueroa, A. Nonat, T. Rodríguez-Blas, A. de Blas, W. S. Perry and M. Tropiano, *Dalton Transactions*, 2013, **42**, 3667-3681.
29. Y. Y. Lee, D. B. Walker, J. J. Gooding and B. A. Messerle, *Dalton Transactions*, 2014, **43**, 12734-12742.

30. A. Wu, J. Masland, R. D. Swartz, W. Kaminsky and J. M. Mayer, *Inorganic Chemistry*, 2007, **46**, 11190-11201.

31. G. Bryant, J. Fergusson and H. Powell, *Australian Journal of Chemistry*, 1971, **24**, 257-273.

32. P. Dongare, B. D. Myron, L. Wang, D. W. Thompson and T. J. Meyer, *Coordination Chemistry Reviews*, 2017, **345**, 86-107.

33. E. Meggers, *Chemical Communications*, 2009, 1001-1010.

34. M. S. Deshpande, A. A. Kumbhar and A. S. Kumbhar, *Inorganic Chemistry*, 2007, **46**, 5450-5452.

35. L. Salassa, T. Ruiu, C. Garino, A. M. Pizarro, F. Bardelli, D. Gianolio, A. Westendorf, P. J. Bednarski, C. Lamberti, R. Gobetto and P. J. Sadler, *Organometallics*, 2010, **29**, 6703-6710.

36. T. Sainuddin, M. Pinto, H. Yin, M. Hetu, J. Colpitts and S. A. McFarland, *Journal of Inorganic Biochemistry*, 2016, **158**, 45-54.

37. R. N. Garner, L. E. Joyce and C. Turro, *Inorganic Chemistry*, 2011, **50**, 4384-4391.

38. B. S. Howerton, D. K. Heidary and E. C. Glazer, *Journal of the American Chemical Society*, 2012, **134**, 8324-8327.

39. V. Pierroz, T. Joshi, A. Leonidova, C. Mari, J. Schur, I. Ott, L. Spiccia, S. Ferrari and G. Gasser, *Journal of the American Chemical Society*, 2012, **134**, 20376-20387.

40. U. Schatzschneider, J. Niesel, I. Ott, R. Gust, H. Alborzinia and S. Wölfl, *ChemMedChem*, 2008, **3**, 1104-1109.

41. J.-F. Kou, C. Qian, J.-Q. Wang, X. Chen, L.-L. Wang, H. Chao and L.-N. Ji, *JBIC Journal of Biological Inorganic Chemistry*, 2012, **17**, 81-96.

42. T. Chen, Y. Liu, W.-J. Zheng, J. Liu and Y.-S. Wong, *Inorganic Chemistry*, 2010, **49**, 6366-6368.

43. M. J. Pisani, P. D. Fromm, Y. Mulyana, R. J. Clarke, H. Körner, K. Heimann, J. G. Collins and F. R. Keene, *ChemMedChem*, 2011, **6**, 848-858.

44. S. P. Mulcahy, K. Gründler, C. Frias, L. Wagner, A. Prokop and E. Meggers, *Dalton Transactions*, 2010, **39**, 8177-8182.

45. A. Sarkar and G. E. Kellogg, *Current Topics in Medicinal Chemistry*, 2010, **10**, 67-83.
46. H. Meyer, *Naunyn-Schmiedeberg's Arch Exp Pathol Pharmakol*, 1899, **42**, 109-118.
47. K. H. Meyer, *Transactions of the Faraday Society*, 1937, **33**, 1062-1064.
48. E. Overton, Ziirieh, 1899.
49. P. Buchwald and N. Bodor, *Current Medicinal Chemistry*, 1998, **5**, 353-380.
50. R. Mannhold and H. van de Waterbeemd, *Journal of Computer-aided Molecular Design*, 2001, **15**, 337-354.
51. R. Mannhold, G. I. Poda, C. Ostermann and I. V. Tetko, *Journal of Pharmaceutical Sciences*, 2009, **98**, 861-893.
52. D. J. Livingstone, *Current Topics in Medicinal Chemistry*, 2003, **3**, 1171-1192.
53. C. A. Lipinski, F. Lombardo, B. W. Dominy and P. J. Feeney, *Advanced Drug Delivery Reviews*, 1997, **23**, 3-25.
54. C. A. Lipinski, *Journal of Pharmacological and Toxicological Methods*, 2000, **44**, 235-249.
55. A. K. Ghose, V. N. Viswanadhan and J. J. Wendoloski, *The Journal of Physical Chemistry A*, 1998, **102**, 3762-3772.
56. G. Vistoli, A. Pedretti and B. Testa, *Drug Discovery Today*, 2008, **13**, 285-294.
57. C. A. Lipinski, *Drug Discovery Today: Technologies*, 2004, **1**, 337-341.
58. A. Leo, C. Hansch and D. Elkins, *Chemical Reviews*, 1971, **71**, 525-616.
59. J. Sangster, *Octanol-water partition coefficients: Fundamentals and Physical Chemistry*, John Wiley & Sons, 1997.
60. M. P. Edwards and D. A. Price, in *Annual Reports in Medicinal Chemistry*, Elsevier, 2010, vol. 45, pp. 380-391.
61. P. D. Leeson and B. Springthorpe, *Nature Reviews Drug Discovery*, 2007, **6**, 881.
62. R. Raveendran, J. P. Braude, E. Wexselblatt, V. Novohradsky, O. Stuchlikova, V. Brabec, V. Gandin and D. Gibson, *Chemical Science*, 2016, **7**, 2381-2391.
63. V. Novohradsky, I. Zanellato, C. Marzano, J. Pracharova, J. Kasparkova, D. Gibson, V. Gandin, D. Osella and V. Brabec, *Scientific Reports*, 2017, **7**, 3751.

64. P. Yingchoncharoen, D. S. Kalinowski and D. R. Richardson, *Pharmacological Reviews*, 2016, **68**, 701-787.

65. R. Lord, The University of Leeds, 2014.

66. H. Lodish, A. Berk, S. Zipursky, P. Matsudaira, D. Baltimore and J. Darnell, *Molecular Cell Biology, 4th Edition WH Freeman, New York*, 2000.

67. R. Pignatello, T. Musumeci, L. Basile, C. Carbone and G. Puglisi, *Journal of Pharmacy and Bioallied Sciences*, 2011, **3**, 4.

68. G. P. van Balen, C. a. M. Martinet, G. Caron, G. Bouchard, M. Reist, P.-A. Carrupt, R. Fruttero, A. Gasco and B. Testa, *Medicinal Research Reviews*, 2004, **24**, 299-324.

69. J. Knobloch, D. K. Suhendro, J. L. Zieleniecki, J. G. Shapter and I. Köper, *Saudi Journal of Biological Sciences*, 2015, **22**, 714-718.

70. C. Tan, S. Wu, S. Lai, M. Wang, Y. Chen, L. Zhou, Y. Zhu, W. Lian, W. Peng and L. Ji, *Dalton Transactions*, 2011, **40**, 8611-8621.

71. C. Tan, S. Lai, S. Wu, S. Hu, L. Zhou, Y. Chen, M. Wang, Y. Zhu, W. Lian and W. Peng, *Journal of Medicinal Chemistry*, 2010, **53**, 7613-7624.

72. L. Li, Y.-S. Wong, T. Chen, C. Fan and W. Zheng, *Dalton Transactions*, 2012, **41**, 1138-1141.

73. A. Vakurov, M. Galluzzi, A. Podesta, N. Gamper, A. L. Nelson and S. D. Connell, *ACS nano*, 2014, **8**, 3242-3250.

74. A. Vakurov, R. Brydson and A. Nelson, *Langmuir*, 2011, **28**, 1246-1255.

75. D. Bizzotto and A. Nelson, *Langmuir*, 1998, **14**, 6269-6273.

76. A. V. Brukhno, A. Akinshina, Z. Coldrick, A. Nelson and S. Auer, *Soft Matter*, 2011, **7**, 1006-1017.

77. Z. Coldrick, A. Penezić, B. Gašparović, P. Steenson, J. Merrifield and A. Nelson, *Journal of Applied Electrochemistry*, 2011, **41**, 939-949.

78. Z. Coldrick, P. Steenson, P. Millner, M. Davies and A. Nelson, *Electrochimica Acta*, 2009, **54**, 4954-4962.

79. A. Nelson, *Journal of Electroanalytical Chemistry*, 2007, **601**, 83-93.

80. S. Mohamadi, D. J. Tate, A. Vakurov and A. Nelson, *Analytica Chimica Acta*, 2014, **813**, 83-89.

81. A. Nelson, *Current Opinion in Colloid & Interface Science*, 2010, **15**, 455-466.

82. F. Arnesano, S. Scintilla and G. Natile, *Angewandte Chemie*, 2007, **119**, 9220-9222.

83. S. Ishida, J. Lee, D. J. Thiele and I. Herskowitz, *Proceedings of the National Academy of Sciences*, 2002, **99**, 14298-14302.

84. I.-S. Song, N. Savaraj, Z. H. Siddik, P. Liu, Y. Wei, C. J. Wu and M. T. Kuo, *Molecular Cancer Therapeutics*, 2004, **3**, 1543-1549.

85. A. K. Holzer, G. Samimi, K. Katano, W. Naerdemann, X. Lin, R. Safaei and S. B. Howell, *Molecular Pharmacology*, 2004, **66**, 817-823.

86. A. R. Collins, *Molecular Biotechnology*, 2004, **26**, 249.

87. P. L. Olive and J. P. Banáth, *Nature Protocols*, 2006, **1**, 23.

88. T.Ricera, *https://www.temaricerca.com/entry2013new/ricerca/laboratorio_ricerca_diagnostica_prodotti/elenco_prodotti.php?id=24*, Accessed 14/03/2018, 2018.

Chapter 7: General Conclusions and Future Work

7.1 General Conclusions

This project has seen the formation of an array of ferrocene β-diketonate ligands with varying steric and electronic properties, and their use in the formation of two libraries of ruthenium metal complexes which have been explored for their biological potential. The first series of complexes consist of organometallic ruthenium(II) arene complexes and the second series comprising of ruthenium(II) *bis*-bipyridyl coordination complexes. All ligands and complexes have been fully characterised by ^{1}H NMR spectroscopy, ^{13}C [^{1}H] NMR spectroscopy, mass spectrometry and elemental analysis, with X-ray crystallographic data obtained when possible.

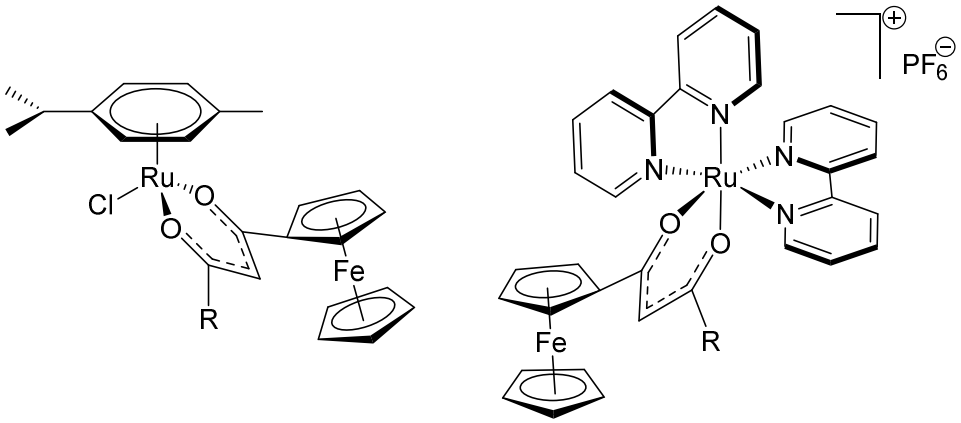

Figure 7.1 Ruthenium(II) arene complexes and ruthenium(II) *bis*-bipyridyl coordination complexes

Both sets of ruthenium complexes were screened for their anti-cancer activity against two cancerous cell lines and one healthy cell line; the ruthenium *bis*-bipyridyl complexes were found to express potent toxicity against all cell lines, including the healthy cell line, while the ruthenium arene complexes were found to be less toxic in comparison, they were highly selective towards the cancerous cell lines and showed no toxicity towards healthy cells at the used experimental concentrations. The most active complexes were studied under extreme hypoxia which resulted in a loss of anti-cancer activity for all complexes; however, all complexes were shown to be more active than cisplatin under the same conditions. The antimicrobial activity of these complexes was also probed through the screening against multiple bacterial and fungal strains. All ruthenium complexes showed elevated antibacterial effects

against Gram positive bacteria over Gram negative strains, with the *bis*-bipyridyl complexes showing greater activity than the arene complexes. The same observation holds true for the antifungal effects, but to a much greater extent, with almost all the *bis*-bipyridyl complexes being shown to be extremely potent growth inhibitors compared to only two of the arene complexes. However, from the cytotoxicity and antimicrobial results it is not possible to conclude any structural activity relationship trends.

To further try and establish any important structural activity relationships and possible mechanisms of action for these ruthenium complexes, several mechanistic studies were undertaken. The arene complexes were all found to undergo hydrolysis with the most cytotoxic complexes hydrolysing more rapidly than their structurally similar but less active equivalents. Potential hydrolysis products have been tentatively assigned and the degradation of the ferrocene moiety appears likely. The *bis*-bipyridyl complexes were found to be stable under the used hydrolysis conditions for up to 35 days, suggesting that these complexes will non-covalently interact with their target site. Hydrophobicity studies conducted on the arene complexes revealed that they were all hydrophobic with LogP values well within the values set by Lipinski's rules. A marginal trend was observed between the upper and lower limits of the obtained LogP values which correspond to greater and lower cytotoxicity, respectively. The hydrophobicity of the arene complexes, combined with the results from the biomembrane studies, suggests that their mode of cellular entry is *via* passive diffusion. Comet assay studies conducted on the most active arene complexes demonstrates a clear link between the DNA stand breakage and their cytotoxicity, suggesting DNA interaction is one of the possible mechanisms of action for these types of complexes.

Overall, this project has demonstrated the potential of ferrocene-containing ruthenium complexes in combating cancer and other microorganisms. Through several mechanistic studies it has been possible to suggest potential mechanisms of action for these complexes, however there still many pathways left to be explored in order to strengthen our understanding of how these complexes are imparting their biological activity.

7.2 Future Work

Moving forward with this project it would be appropriate to investigate the importance, if any, of the ferrocene moiety in the biological activity of these complexes. This could be achieved through cyclic voltammetry experiments to deduce any correlation between the activity and formal reduction potential of the complexes, allowing for conclusions to be made as to whether or not the redox properties of the complex are crucial to their interaction with cells. Furthermore, substitution of the ferrocene moiety for its isoelectronic ruthenium equivalent, ruthenocene, would facilitate this investigation as although they are structurally similar, they have very different redox properties.[1, 2]

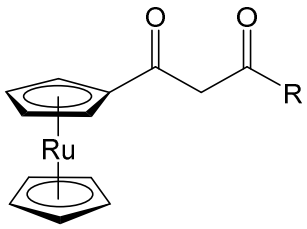

Figure 7.2 Ruthenocene β-diketonate ligand

The phototoxicity of the ruthenium *bis*-bipyridyl complexes should also be explored. Conducting cell line cytotoxicity assays under dark conditions and then comparing these results to their IC_{50} values obtained after exposure to light will allow for conclusions to be made as to whether these complexes are producing reactive oxygen species, a critical mode of action used in photodynamic therapy (PDT). If this same process is repeated under hypoxia it would then be possible to comment on the photoactivated chemotherapy (PACT) properties of these complexes. Unlike PDT, PACT does not require the presence of oxygen in its mode of action as the complex itself becomes activated after light exposure.[3] Moreover, modifications to the bipyridyl ligands in a way that extends their conjugated ring systems should permit the tuning of their photo-active properties, another future route for these complexes which would hopefully yield interesting results.

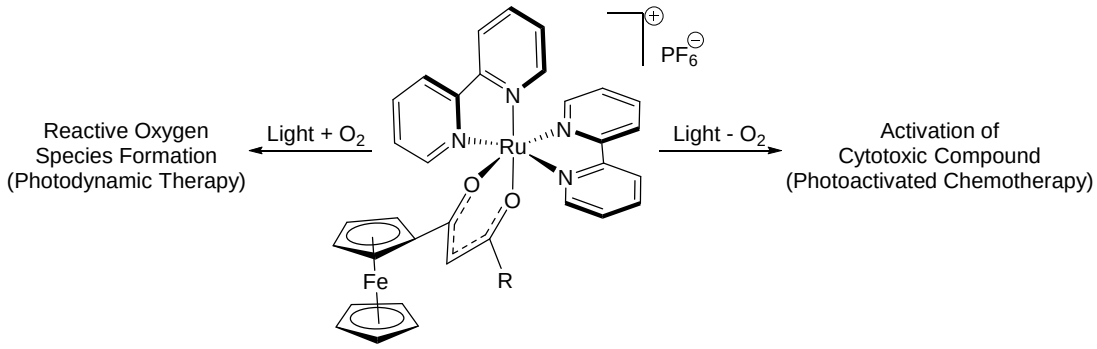

Figure 7.3 Photodynamic therapy vs photoactivated chemotherapy

Other mechanistic studies should be conducted in order to further our understanding of the mechanisms of action for both libraries of ruthenium complexes. Obtaining a greater comprehension of the complexes fluorescent properties would allow the use of confocal laser scanning microscopy (CLSM) in order to observe the cellular distribution and localisation of these complexes, something which could also be investigated *in vitro* through inductively coupled plasma mass spectrometry (ICP-MS).[4, 5] The possibility of enzyme inhibition could be explored through the thioredoxin reductase (TrxR) assay. As the TrxR enzyme is upregulated in many types of cancer, and is also essential for cell growth and survival, it is an excellent target for cancer therapeutic drugs.[6] Cell viability and cell cycle analysis will advance our interpretations of exactly how these complexes are imparting their biological activity, as the mode of action of a drug can be deduced to some degree from the phase of the cell cycle which it inhibits.[7]

7.3 References

1. S. P. Gubin, S. A. Smirnova, L. I. Denisovich and A. A. Lubovich, *Journal of Organometallic Chemistry*, 1971, **30**, 243-255.
2. T. Kuwana, D. E. Bublitz and G. Hoh, *Journal of the American Chemical Society*, 1960, **82**, 5811-5817.
3. C. Mari and G. Gasser, *CHIMIA International Journal for Chemistry*, 2015, **69**, 176-181.
4. C. A. Puckett and J. K. Barton, *Biochemistry*, 2008, **47**, 11711-11716.
5. S. H. van Rijt, A. Mukherjee, A. M. Pizarro and P. J. Sadler, *Journal of Medicinal Chemistry*, 2010, **53**, 840-849.
6. E. S. J. Arnér, L. Zhong and A. Holmgren, in *Methods in Enzymology*, Academic Press, 1999, vol. 300, pp. 226-239.
7. L. H. Hartwell and T. A. Weinert, *Science*, 1989, **246**, 629-634.

Chapter 8: Experimental

8.0 Experimental

8.1 General Experimental Procedures

Synthetic procedures were conducted under aerobic conditions unless stated otherwise. All chemicals were supplied by Sigma-Aldrich Chemical Co., Acros Organics, Alfa Aesar, Fisher Chemicals and BOC gases used without further purification. Deuterated NMR solvents were purchased from Sigma-Aldrich Chemical Co. or Acros Organics. Chromatography columns were prepared using Fisher Chemicals 60A 35–70 micron silica gel.

8.2 Instrumentation

Nuclear magnetic resonance spectra were recorded using Bruker Avance 300, 400, 500, DPX300 and DPX500 MHz spectrometers. Chemical shifts are reported in parts per million (δ) downfield relative to the internal reference tetramethylsilane or referenced to the solvent signal. Unless otherwise specified NMR spectra were recorded in deuterochloroform, deuteroacetone or deutroacetonitrile at room temperature. Abbreviations used: Ar = aromatic, dd = doublet of doublets, dt = doublet of triplets, m = multiplet, s = singlet, d = doublet, t = triplet, q = quartet. Mass spectra were recorded using a micromass ZMD 2000 spectrometer employing the electrospray (ES+/-) ionisation technique. Accurate molecular masses were obtained from Walters LCT, GCT or Bruker MicroTof spectrometers. Microanalyses were acquired either by Ms. Tanya Marinko-Covell at the University of Leeds Microanalytical Service using a Carlo Erba 1108 Elemental Analyser or by Mr. Stephen Boyer at the London Metropolitan University Elemental Analysis Service. UV/vis absorption spectra were acquired on a Cary Series UV-Vis spectrophotometer using 1 cm path length quartz cuvettes.

8.3 X-Ray Crystallography

Single crystal X-ray diffraction data were collected by the author or Dr Christopher Pask. A suitable single crystal was selected and immersed in inert oil. The crystal was then mounted to a goniometer head on an Agilent SuperNova X-ray diffractometer fitted with an Atlas area detector and a kappa-geometry 4-circle goniometer, using mirror monochromated Mo-Kα radiation (λ = 0.71073 Å) or Cu-Kα (λ = 1.54184 Å) radiation. The crystal was cooled to 120 K by an Oxford cryostream low temperature device.[1] The full data set was recorded and the images processed using CrysAlis Pro.[2] Structure solution by direct methods was achieved through the use of SHELXS86[3] SHELXL-2014[4] or SHELXT[5] programs, and the structural model refined by full matrix least squares on F^2 using SHELX97[6] interfaced through the program Olex2.[7] Molecular graphics were plotted, editing of CIFs and construction of tables of bond lengths and angles were achieved using Olex2. Unless otherwise stated, hydrogen atoms were placed using idealised geometric positions (with free rotation for methyl groups), allowed to move in a "riding model" along with the atoms to which they were attached, and refined isotropically. The SQUEEZE routine of Platon was used to refine structures where diffuse electron density could not be adequately modelled as solvent of crystallisation.[8] Complexes **C'13** and **C'14** were collected at diamond light source

8.4 Synthesis of β-diketonate Ferrocene and β-ketoiminate Ferrocene Ligands

Ligands have been synthesised from the following general procedure (unless stated otherwise) using methods adapted from Swarts *et al.* and Shi *et al.* and are fully characterised.[9,10]

General Procedure: Ethyl ester was added to a stirred solution of acetyl ferrocene (1.64 g, 7.2 mmol) and sodium ethoxide (0.89 g, 13 mmol) in ether (20 mL). The solution was stirred at reflux for 24-72 hours after which time the product was isolated by one of two methods;

1. The solid precipitate was isolated by filtration, dissolved in distilled water (150 mL) and acidified with 10% hydrochloric acid until pH 5 which caused a

red solid to precipitate out in solution. The solid was filtered and dried over night under vacuum before purification.

2. The solution was acidified with 10% hydrochloric acid until pH 5 and added to water (50 ml). The product was extracted with ether (3 x 20 mL) and the organic layers were combined, dried over $MgSO_4$ and filtered. Solvent was removed *in vacuo* to give a red solid product.

8.4.1 Synthesis of 1-Ferrocenylbutane-1,3-dione L1

Acetyl ferrocene (2.80 g, 12.3 mmol) was dissolved in ethyl acetate (25 mL) and stirred for a few minutes before the addition of sodium ethoxide (1.70 g, 25.0 mmol). The solution was stirred at reflux for 3 hours forming a yellow solid which was filtered and washed with ethyl acetate. The yellow solid was then dissolved in distilled water (150 mL) and acidified with 10% hydrochloric acid until pH 5 which caused a red solid to crash out in solution. Recrystallisation from hexane gave red crystals (2.70 g, 81 %).

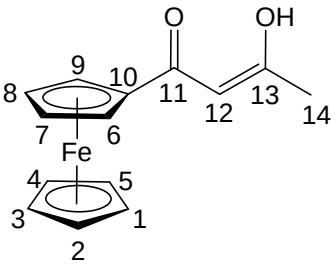

δ_H (500 MHz, $CDCl_3$); 5.63 (s, 0.67 H, enol CH, H_{12}), 4.77 (broad t, 2 H, *J* 6.82Hz, C_5H_4, $H_{6,9}$), 4.50 (d, 2 H, *J* 4.1 Hz, C_5H_4, $H_{7,8}$), 4.19 (s, 5 H, C_5H_5, $H_{1\text{-}5}$), 3.76 (s, 0.46 H, keto CH_2, H_{12}), 2.25 (s, 0.69 H, keto CH_3, H_{14}), 2.00 (s, 2.31 H, enol CH_3, H_{14}); **δ_C**{^{1}H}; (125 MHz, $CDCl_3$); 192.5 (quaternary CO, C_{11}), 186.4 (quaternary CO, C_{13}), 98.2 (CH, C_{12}), 77.7 (quaternary Cp, C_{10}), 73.1 (Cp CH, $C_{6/9}$), 72.1 (Cp CH, $C_{6/9}$), 70.3 (Cp ring, $C_{1\text{-}5}$), 70.1 (Cp CH, $C_{7/8}$), 68.7 (Cp CH, $C_{7/8}$), 24.2 (CH_3, C_{14}); **Analysis**: Calculated C 62.25, H 5.22 %, Found C 62.28, H 5.10 %; **H.R.M.S. [ES+]** found [MH^+] 271.041.

8.4.2 Synthesis of 1-Ferrocenyl-4,4,4-trifluorobutane-1,3-dione L2

Prepared using ethyl-trifluoroacetate (1.55 mL, 13.0 mmol), refluxed for 24 hours and worked up following method 1. The product was purified by column

chromatography, eluting 85:15 v/v hexane/ethyl acetate to give a red solid (1.63 g, 70 %).

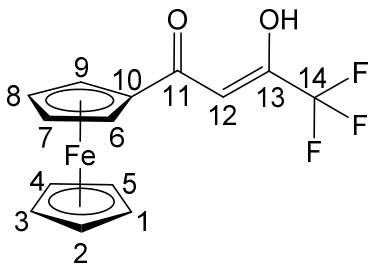

δ_H (500 MHz, $CDCl_3$); 6.01 (s, 1H, CH, H_{12}), 4.80 (t, 2H, *J 1.8* Hz, C_5H_4, $H_{6,9}$), 4.61 (t, 2H, *J 1.8* Hz, C_5H_4, $H_{7,8}$), 4.17 (s, 1H, C_5H_5, $H_{1\text{-}5}$); **δ_C**{^{1}H} (125 MHz, ($CDCl_3$); 194.6 (quaternary CO, C_{11}), 171.4 (q, quaternary CO, *J 35.8* Hz, C_{13}), 115.9 (q, CF_3, *J 281.1* Hz, C_{14}), 93.3 (CH, C_{12}), 75.4 (quaternary Cp, C_{10}), 73.7 (Cp CH, $C_{6,9}$), 70.9 (Cp ring, $C_{1\text{-}5}$), 69.2 (Cp CH, $C_{7,8}$); **Analysis**: Calculated C 51.89, H 3.42 %, Found C 51.73, H 3.49 %; **H.R.M.S. [ES+]** found [M-H$^+$] 322.999.

8.4.3 Synthesis of 1-Ferrocenyl-4,4-difluorobutane-1,3-dione L3

Prepared using ethyl difluoroacetate (1.37 mL, 13.0 mmol), refluxed for 24 hours and worked up following method 1. The product precipitated out as a pure red solid (2.13 g, 97 %).

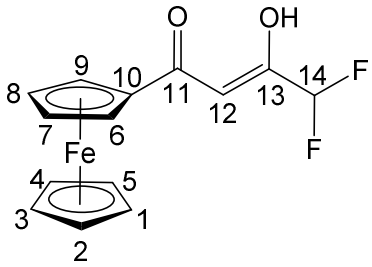

δ_H (500 MHz, $(CD_3)_2CO$); 6.17 (s, 1H, CH, H_{12}), 4.87 (t, 2H, *J 1.8* Hz, C_5H_4, $H_{6,9}$), 4.60 (t, 2H, *J 1.8* Hz, C_5H_4, $H_{7,8}$), 4.22 (s, 1H, CHF_2, H_{14}), 4.13 (s, 5H, C_5H_5, $H_{1\text{-}5}$); **δ_C**{^{1}H} (125 MHz, $(CD_3)_2CO$); 197.0 (quaternary CO, C_{11}), 163.6 (quaternary CO. C_{13}), 111.3 (t, CHF_2, *J 242.6* Hz, C_{14}), 95.8 (CH, C_{12}), 77.8 (quaternary Cp, C_{10}), 74.3 (Cp CH, $C_{6,9}$), 71.4 (Cp ring, $C_{1\text{-}5}$), 70.1 (Cp CH, $C_{7,8}$); **Analysis**: Calculated C 54.94, H 3.95 %, Found C 54.40, H 3.90 %; **H.R.M.S. [ES+]** found [MH$^+$] 307.022.

8.4.4 Synthesis of 1-Ferrocenyl-3-(3-furanyl)propane-1,3-dione L4

Prepared using ethyl-3-furoate (1.76 mL, 13.0 mmol), refluxed for 48 hours and worked up following method 1. The product was purified by column

chromatography, eluting 90:10 v/v hexane/ethyl acetate to give red solid (0.71 g, 31 %).

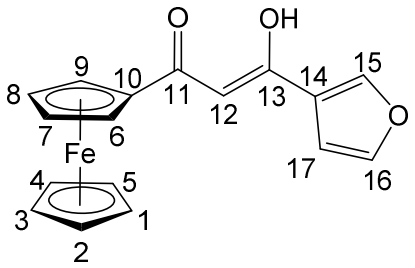

δ_H (500 MHz, $(CD_3)_2CO$); 8.17 (s, 1H, Furan CH, H_{15}), 7.57 (t, 1H, *J 1.6* Hz, Furan CH, H_{17}), 6.83 (d, 1H, *J 1.2* Hz, Furan CH, H_{16}), 6.35 (s, 1H, CH, H_{12}), 4.83 (t, 2H, *J 1.8* Hz, C_5H_4, $H_{6,9}$), 4.46 (t, 2H, *J 1.8* Hz, C_5H_4, $H_{7,8}$), 4.09 (s, 5H, C_5H_5, $H_{1\text{-}5}$); **δ_C**{^{1}H} (125 MHz, $(CD_3)_2CO$); 193.9 (quaternary CO, C_{11}), 176.7 (quaternary CO, C_{13}), 150.4 (quaternary Furan C, C_{14}), 146.3 (Furan CH, C_{15}), 145.5 (Furan CH, C_{17}), 109.0 (Furan CH, C_{16}), 95.4 (CH, C_{12}), 79.0 (quaternary Cp, C_{10}), 73.0 (Cp CH, $C_{6,9}$), 71.1 (Cp ring, $C_{1\text{-}5}$), 69.6 (Cp CH, $C_{7,8}$); **Analysis**: Calculated C 63.38, H 4.38 %, Found C 63.27, H 4.47 %; **H.R.M.S. [ES+]** found [MH^+] 322.029.

8.4.5 Synthesis of 1-Ferrocenyl-3-(2-furanyl)propane-1,3-dione L5

Prepared using ethyl-2-furroate (1.82 g, 13.0 mmol), refluxed for 24 hours and worked up following method 1. The product was purified by column chromatography, eluting 85:15 v/v hexane/ethyl acetate to give red solid (1.37 g, 59 %).

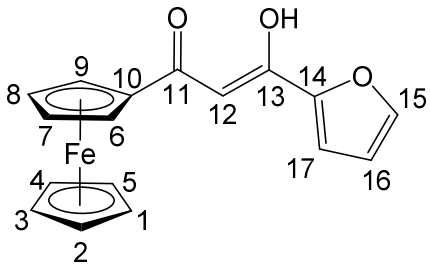

δ_H (500 MHz, $(CD_3)_2CO$); 7.71 (m, 1H, Furan CH, H_{17}), 7.12 (d, 1H, *J 3.4* Hz, Furan CH, H_{15}), 6.57 (m, 1H, Furan CH, H_{16}), 6.33 (s, 1H, CH, H_{12}), 4.83 (t, 2H, *J 1.8* Hz, C_5H_4, $H_{6,9}$), 4.49 (t, 2H, *J 1.8* Hz, C_5H_4, $H_{7,8}$), 4.11 (s, 5H, C_5H_5, $H_{1\text{-}5}$); **δ_C**{^{1}H} (125 MHz, $(CD_3)_2CO$); 192.8 (quaternary CO, C_{11}), 173.1 (quaternary CO. C_{13}), 151.3 (Furan quaternary C, C_{14}), 147.1 (Furan CH, C_{17}), 115.3 (Furan CH, C_{15}), 113.4 (Furan CH, C_{16}), 93.5 (CH, C_{12}), 78.6 (quaternary Cp, C_{10}), 73.1 (Cp CH, $C_{6,9}$), 71.1 (Cp ring, $C_{1\text{-}5}$), 69.5 (Cp CH, $C_{7,8}$); **Analysis**: Calculated C 63.38, H 4.38 %, Found C 63.50, H 4.45 %; **H.R.M.S. [ES+]** found [$M\text{-}H^+$] 321.022.

8.4.6 Synthesis of 1-Ferrocenyl-3-phenylpropane-1,3-dione L6

Prepaed using ethyl benzoate (1.87 mL, 13.0 mmol), refluxed for 24 hours and worked up following method 2. The product was purified by column chromatography, eluting 90:10 v/v hexane/ethyl acetate to give red solid (1.07 g, 45 %).

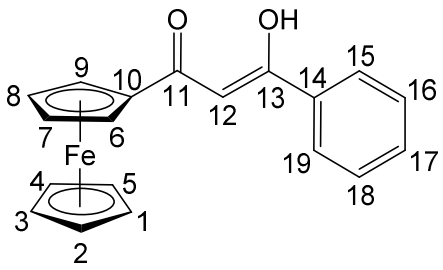

δ_H (500 MHz, $(CD_3)_2CO$); 7.93 (d, 2H, *J 7.3* Hz, ArH, $H_{15,19}$), 7.45 (t, 1H, *J 7.3* Hz, ArH, H_{17}), 7.39 (t, 2H, *J 7.3* Hz, ArH, $H_{16,18}$), 6.63 (s, 1H, CH, H_{12}), 4.92 (broad t, 2H, *J 1.8* Hz, C_5H_4, $H_{6,9}$), 4.49 (broad d, 2H, *J 1.8* Hz, C_5H_4, $H_{7,8}$), 4.10 (s, 5H, C_5H_5, $H_{1\text{-}5}$); **δ_C**$\{^1H\}$ (125 MHz, $(CD_3)_2CO$); 195.6 (quaternary CO, C_{11}), 180.2 (quaternary CO, C_{12}), 136.1 (quaternary ArC, C_{10}), 132.8 (ArCH, $C_{15/19}$), 129.5 (ArCH, $C_{16,18}$), 127.6 (ArCH, C_{17}), 94.6 (CH, C_{12}), 79.3 (quaternary Cp, C_{10}), 73.2 (Cp CH, $C_{6,9}$), 71.1 (Cp ring, $C_{1\text{-}5}$), 69.8 (Cp CH, $C_{7,8}$); **Analysis**: Calculated C 68.70, H 4.86 %, Found C 68.59, H 4.93 %; **H.R.M.S. [ES+]** found $[M\text{-}H^+]$ 331.042.

8.4.7 Synthesis of 1-Ferrocenyl-3-(1-naphthyl)propane-1,3-dione L7

Prepared using ethyl-1-naphthoate (2.35 mL, 13.0 mmol), refluxed for 48 hours and worked up following method 1. The product was purified by column chromatography, eluting 90:10 v/v hexane/ethyl acetate to give red solid (0.98 g, 28 %).

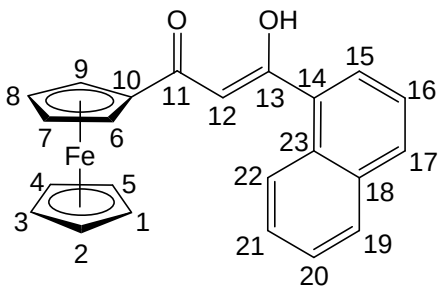

δ_H (500 MHz, $(CD_3)_2CO$); 8.41 (d, 1H, *J 8.5* Hz, ArH, H_{15}), 7.95 (d, 1H, *J 8.3* Hz, ArH, H_{16}), 7.88 (d, 1H, *J 7.6* Hz, ArH, H_{17}), 7.74 (dd, 1H, *J 7.2, 0.9* Hz, ArH, H_{19}), 7.52-7.41 (m, 3H, ArH, $H_{20\text{-}22}$), 6.34 (s, 1H, CH, H_{12}), 4.88 (t, 2H, *J 1.8* Hz, C_5H_4, $H_{6,9}$), 4.50 (t, 2H, *J 1.8* Hz, C_5H_4, $H_{7,8}$), 4.14 (s, 5H, C_5H_5, $H_{1\text{-}5}$); **δ_C**$\{^1H\}$ (125 MHz, $(CD_3)_2CO$); 194.7 (quaternary CO, C_{11}), 184.7 (quaternary CO, C_{13}), 135.3 (quaternary ArC, C_{14}), 134.9 (quaternary ArC, C_{23}), 132.1 (ArCH, C_{15}), 131.2 (quaternary ArC, C_{18}), 129.4 (ArCH,

C_{16}), 127.9 (ArCH, C_{17}), 127.9 (ArCH, C_{22}), 127.2 (ArCH, C_{19}), 126.6 (ArCH, C_{21}), 126.0 (ArCH, C_{20}), 99.7 (CH, C_{12}), 78.8 (quaternary Cp, C_{10}), 73.3 (Cp CH, $C_{6,9}$), 71.2 (Cp ring, $C_{1\text{-}5}$), 69.8 (Cp CH, $C_{7,8}$); **Analysis**: Calculated (+ 0.5H_2O) C 70.61, H 4.90 %, Found C 69.90, H 4.80 %; **H.R.M.S. [ES+]** found [MH^+] 383.073.

8.4.8 Synthesis of 1-Ferrocenyl-3-(4-methylphenyl)propane-1,3-dione L8

Prepared using ethyl *p*-toluate (2.07 mL, 13.0 mmol), refluxed for 24 hours and worked up following method 2. The product was purified by column chromatography, eluting 85:15 v/v hexane/ethyl acetate to give red solid (1.04 g, 42 %).

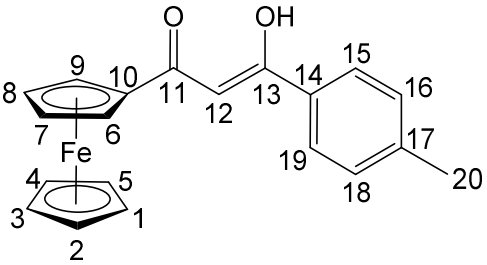

δ_H (500 MHz, $(CD_3)_2CO$); 7.82 (d, 2H, *J 8.3* Hz, ArH, $H_{15,19}$), 7.21 (d, 2H, *J 8.3* Hz, ArH, $H_{16,18}$), 6.60 (s, 1H, CH, H_{12}), 4.90 (broad t, 2H, *J 1.5* Hz, C_5H_4, $H_{6,9}$), 4.48 (braod t, 2H, *J 1.7* Hz, C_5H_4, $H_{7,8}$), 4.09 (s, 5H, C_5H_5, $H_{1\text{-}5}$), 2.28 (s, 3H, CH_3, H_{20}); **δ_C**{^{1}H} (125 MHz, $(CD_3)_2CO$); 194.9 (quaternary CO, C_{11}), 180.7 (quaternary CO, C_{13}), 143.4 (quaternary ArC, C_{14}), 133.4 (quaternary ArC, C_{17}), 130.2 (ArCH, $C_{15,19}$), 127.7 (ArCH, $C_{16,18}$), 94.1 (CH, C_{12}), 79.4 (quaternary Cp, C_{10}), 73.1 (Cp CH, $C_{6,9}$), 71.1 (Cp ring, $C_{1\text{-}5}$), 69.7 (Cp CH, $C_{7,8}$), 21.5 (CH_3, C_{20}); **Analysis**: Calculated C 69.39, H 5.24 %, Found C 69.20, H 5.25 %; **H.R.M.S. [ES+]** found [M-H^+] 345.058.

8.4.9 Synthesis of 1-Ferrocenyl-3-(3-methylphenyl)propane-1,3-dione L9

Prepared using ethyl-m-toluate (2.07 mL, 13.0 mmol), refluxed for 24 hours and worked up following method 2. The product was purified by column chromatography, eluting 85:15 v/v hexane/ethyl acetate to give red solid (1.73 g, 69 %).

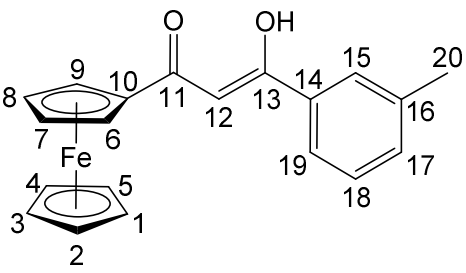

δ_H (500 MHz, $(CD_3)_2CO$); 7.91 (s, 1H, ArH, H_{15}), 7.87 (t, 1H, *J 3.6* Hz, ArH, H_{18}), 7.43 (d, 2H, *J 4.6* Hz, ArH, $H_{17,19}$), 6.77 (s, 1H, CH, H_{12}), 5.06 (t, 2H, *J 1.7* Hz, C_5H_4, $H_{6,9}$), 4.65 (t, 2H, *J 1.7* Hz, C_5H_4, $H_{7,8}$), 4.26 (s, 5H, C_5H_5, $H_{1\text{-}5}$), 2.45 (s, 3H, CH_3, H_{20}); **δ_C**{^{1}H} (125 MHz, $(CD_3)_2CO$); 195.4 (quaternary CO, C_{11}), 180.4 (quaternary CO, C_{13}), 139.2 (quaternary ArC, C_{14}), 136.0 (quaternary ArC, C_{16}), 133.5 (ArCH, C_{15}), 129.4 (ArCH, C_{19}), 128.1 (ArCH, C_{17}), 124.8 (ArCH, C_{18}), 94.6 (CH, C_{12}), 79.3 (quaternary Cp, C_{10}), 73.2 (Cp CH, $C_{6,9}$), 71.1 (Cp ring, $C_{1\text{-}5}$), 69.8 (Cp CH, $C_{7,8}$), 21.4 (CH_3, C_{20}); **Analysis**: Calculated C 69.39, H 5.24 %, Found C 69.28, H 5.31 %; **H.R.M.S. [ES+]** found [MH^+] 346.066.

8.4.10 Synthesis of 1-Ferrocenyl-3-(3,5-dimethylphenyl)propane-1,3-dione L10

Prepared using ethyl-3,5-dimethylbenzoate (2.08 mL, 13.0 mmol), refluxed for 24 hours and worked up following method 2. The product was purified by column chromatography, eluting 90:10 v/v hexane/ethyl acetate to give red solid (0.74 g, 28 %).

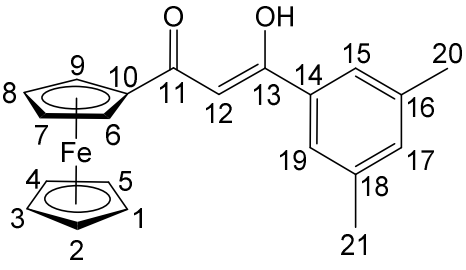

δ_H (500 MHz, $(CD_3)_2CO$); 7.54 (s, 2H, ArH, $H_{15,19}$), 7.08 (s, 1H, ArH, H17), 6.60 (s, 1H, CH, H_{12}), 4.89 (t, 2H, *J 1.8* Hz, C_5H_4, $H_{6,9}$), 4.47 (t, 2H, *J 1.8* Hz, C_5H_4, $H_{7,8}$), 4.09 (s, 5H, C_5H_5, $H_{1\text{-}5}$), 2.24 (s, 6H, CH_3, $H_{20,21}$); **δ_C**{^{1}H} (125 MHz, $(CD_3)_2CO$); 195.3 (quaternary CO, C_{11}), 180.7 (quaternary CO, C_{13}), 139.1 (ArCH, $C_{15,19}$), 136.0 (quaternary ArC, C_{14}), 134.3 (ArCH, C_{17}), 125.4 (quaternary ArC, $C_{16,18}$), 94.6 (CH, C_{12}), 79.4 (quaternary Cp, C_{10}), 73.1 (Cp CH, $C_{6,9}$), 71.1 (Cp ring, $C_{1\text{-}5}$), 69.7 (Cp CH, $C_{7,8}$), 21.3 (CH_3, $C_{20,21}$); **Analysis**: Calculated C 70.02, H 5.60 %, Found C 69.40, H 5.70 %; **H.R.M.S. [ES+]** found [MH^+] 361.088.

8.4.11 Synthesis of 1-Ferrocenyl-3-(4-fluorophenyl)propane-1,3-dione L11

Prepared using ethyl-4-flourobenzoate (1.90 mL, 13.0 mmol), refluxed for 24 hours and worked up following method 1. The product was purified by column chromatography, eluting 80:20 v/v hexane/ethyl acetate to give a red solid (1.59 g, 63 %).

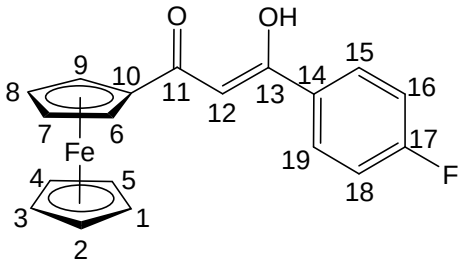

δ_H (500 MHz, $(CD_3)_2CO$); 8.10 (m, 2H, ArH, $H_{15,19}$), 7.29 (t, 2H, *J 8.7* Hz, ArH, $H_{16,18}$), 6.59 (s, 1H, CH, H_{12}), 5.00 (t, 2H, *J 1.8* Hz, C_5H_4, $H_{6,9}$), 4.66 (t, 2H, *J 1.8* Hz, C_5H_4, $H_{7,8}$), 4.26 (s, 5H, C_5H_5, $H_{1\text{-}5}$); **δ_C**{^{1}H} (125 MHz, $(CD_3)_2CO$); 195.0 (quaternary CO, C_{11}), 179.7 (quaternary CO, C_{13}), 165.8 (d, ArCF, *J 250.2* Hz, C_{17}), 132.6 (d, quaternary ArC, *J 2.1* Hz, C_{14}), 130.3 (d, ArCH, *J 9.3* Hz, $C_{15,19}$), 116.4 (d, ArCH, *J 21.8* Hz, $C_{16,18}$), 94.4 (CH, C_{12}), 73.5 (quaternary Cp, C_{10}), 73.2 (Cp CH, $C_{6/9}$), 71.1 (Cp ring, $C_{1\text{-}5}$), 70.8 (Cp CH, $C_{6/9}$), 70.6 (Cp CH, $C_{7/8}$), 69.8 (Cp CH, $C_{7/8}$); **Analysis**: Calculated C 65.17, H 4.32 %, Found C 65.00, H 4.40 %; **H.R.M.S. [ES+]** found [M-H$^+$] 3490.33.

8.4.12 Synthesis of 1-Ferrocenyl-3-(3-fluorophenyl)propane-1,3-dione L12

Prepared using ethyl-3-flourobenzoate (1.93 mL, 13.0 mmol), refluxed for 24 hours and worked up following method 1. The product was purified by column chromatography, eluting 83:17 v/v hexane/ethyl acetate to give red solid (2.00 g, 80 %).

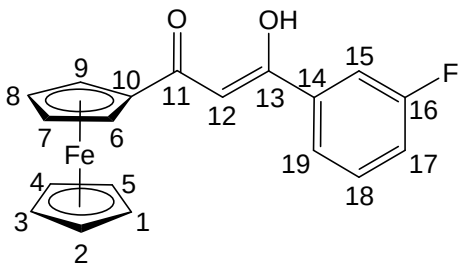

δ_H (500 MHz, $(CD_3)_2CO$); 7.77 (broad d, 1H, *J 7.8* Hz, ArH, H_{15}), 7.66 (broad d, 1H, *J 10.1* Hz, ArH, H_{19}), 7.44 (dt, 1H, *J 8.2, 6.0* Hz, ArH, H_{17}), 7.22 (td, 1H, *J 8.4, 1.8* Hz, ArH, H_{18}), 6.68 (s, 1H, CH, H_{12}), 4.95 (broad s, 2H, C_5H_4, $H_{6,9}$), 4.52 (broad s, 2H, C_5H_4, $H_{7,8}$), 4.11 (s, 5H, C_5H_5, $H_{1\text{-}5}$); **δ_C**{^{1}H} (125 MHz, $(CD_3)_2CO$); 196.0 (quaternary CO, C_{11}), 178.37 (quaternary CO, C_{13}), 163.9 (d, ArCF, *J 243.9* Hz, C_{16}),

138.6 (d, quaternary ArC, *J 7.8* Hz, C_{14}), 131.5 (d, ArCH, *J 8.3* Hz, C_{19}), 123.6 (d, ArCH, *J 2.1* Hz, C_{18}), 119.4 (d, ArCH, *J 21.8* Hz, C_{17}), 114.2 (d, ArCH, *J 23.9* Hz, C_{15}), 95.1 (CH, C_{12}), 79.0 (quaternary Cp, C_{10}), 73.5 (Cp CH, $C_{6,9}$), 71.2 (Cp ring, $C_{1\text{-}5}$), 69.9 (Cp CH, $C_{7,8}$); **Analysis**: Calculated C 65.17, H 4.32 %, Found C 65.10, H 4.30 %; **H.R.M.S. [ES+]** found [M-H^+] 349.032.

8.4.13 Synthesis of 1-Ferrocenyl-3-(2-fluorophenyl)propane-1,3-dione L13

Prepared using ethyl-2-fluorobenzoate (1.90 mL, 13.0 mmol), refluxed for 72 hours and worked up following method 2. The product was purified by column chromatography, eluting 90:10 v/v hexane/ethyl acetate to give red solid (1.17 g, 47 %).

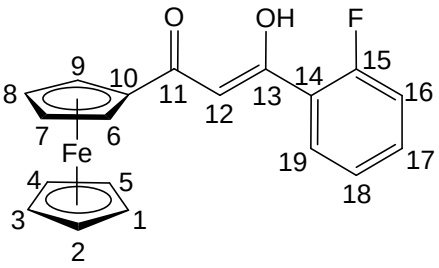

δ_H (500 MHz, $(CD_3)_2CO$); 7.84 (td, 1H, *J 7.8, 1.6* Hz, ArH, H_{19}), 7.47 (m, 1H, ArH, H_{16}), 7.22 (m, 1H, ArH, H_{18}), 7.16 (m, 1H, ArH, H_{17}), 6.47 (s, 1H, CH, H_{12}), 4.82 (q, 2H, *J 2.1* Hz, C_5H_4, $H_{6,9}$), 4.52 (q, 2H, *J 1.8* Hz, C_5H_4, $H_{7,8}$), 4.11 (s, 5H, C_5H_5, $H_{1\text{-}5}$); **δ_C**{^{1}H} (125 MHz, $(CD_3)_2CO$); 196.3 (quaternary CO, C_{11}), 175.4 (d, quaternary CO, *J 3.11* Hz, C_{13}), 161.7 (d, ArCF, *J 253.3* Hz, C_{15}), 134.2 (d, ArCH, *J 8.8* Hz, C_{17}), 130.6 (d, ArCH, *J 2.1* Hz, C_{19}), 125.6 (d, ArCH, *J 3.1* Hz, C_{18}), 124.2 (d, quaternary ArC, *J 10.4* Hz, C_{14}), 117.4 (d, ArCH, *J 23.4* Hz, C_{16}), 99.6 (d, CH, *J 11.9* Hz, C_{12}), 79.0 (quaternary Cp, C_{10}), 73.6 (Cp CH, $C_{6,9}$), 71.2 (Cp ring, $C_{1\text{-}5}$), 69.8 (Cp CH, $C_{7,8}$); **Analysis**: Calculated C 65.17, H 4.32 %, Found C 65.10, H 4.30 %; **H.R.M.S. [ES+]** found [MH^+] 351.049.

8.4.14 Synthesis of 1-Ferrocenyl-3-(3,5-difluorophenyl)propane-1,3-dione L14

Prepared using ethyl-3,5-difluorobenzoate (1.98 mL, 13.0 mmol), refluxed for 24 hours and worked up following method 2. The product was purified by column chromatography, eluting 90:10 v/v hexane/ethyl acetate to give red solid (2.56 g, 96 %).

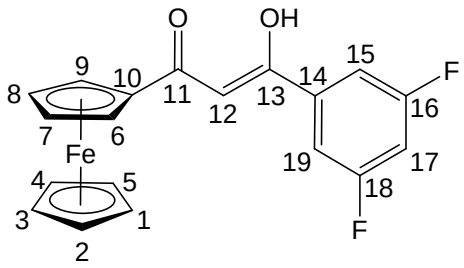

δ_H (500 MHz, $(CD_3)_2CO$); 7.56 (dd, 2H, *J 7.3, 2.1* Hz, ArH, $H_{15,19}$), 7.12 (tt, 1H, *J 8.9, 2.3* Hz, ArH, H_{17}), 6.72 (s, 1H, CH, H_{12}), 4.97 (t, 2H, *J 1.6* Hz, C_5H_4, $H_{6,9}$), 4.55 (t, 2H, *J 1.6* Hz, C_5H_4, $H_{7,8}$), 4.13 (s, 5H, C_5H_5, $H_{1\text{-}5}$); **δ_C**{^{1}H} (125 MHz, $(CD_3)_2CO$); 196.4 (quaternary CO, C_{11}), 176.7 (t, quaternary CO, *J 2.4* Hz, C_{13}), 165.1 (d, ArCF, *J 13.0* Hz, $C_{16/18}$), 163.4 (d, ArCF, *J 12.5* Hz, $C_{16/18}$), 139.9 (t, quaternary ArC, *J 9.1* Hz, C_{14}), 110.5 (dd, ArCH, *J 20.4, 6.5* Hz, $C_{15,19}$), 107.5 (t, ArCH, *J 26.0* Hz, C_{17}), 95.5 (CH, C_{12}), 78.8 (quaternary Cp, C_{10}), 73.7 (Cp CH, $C_{6,9}$), 71.2 (Cp ring, $C_{1\text{-}5}$), 70.0 (Cp CH, $C_{7,8}$); **Analysis**: Calculated C 61.99, H 3.83 %, Found C 61.60, H 3.80 %; **H.R.M.S. [ES+]** found [MH$^+$] 368.031.

8.4.15 Synthesis of 1-Ferrocenyl-3-(4-chlorophenyl)propane-1,3-dione L15

Prepared ethyl-4-chlorobenzoate (2.02 mL, 13.0 mmol), refluxed for 48 hours and worked up following method 1. The product was purified by column chromatography, eluting 83:17 v/v hexane/ethyl acetate to give a red solid (1.65 g, 63 %).

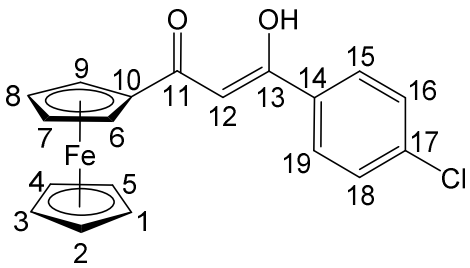

δ_H (500 MHz, $(CD_3)_2CO$); 7.95 (d, 2H, *J 8.7* Hz, ArH, $H_{15,19}$), 7.41 (d, 2H, *J 8.7* Hz, ArH, $H_{16,18}$), 6.36 (d, 1H, *J 5.5* Hz, CH, H_{12}), 4.92 (broad t, 2H, *J 1.7* Hz, C_5H_4, $H_{6,9}$), 4.51 (broad t, 2H, *J 1.7* Hz, C_5H_4, $H_{7,8}$), 4.11 (s, 5H, C_5H_5, $H_{1\text{-}5}$); **δ_C**{^{1}H} (125 MHz, $(CD_3)_2CO$); 195.7 (quaternary CO, C_{11}), 178.9 (quaternary CO, C_{13}), 134.9 (quaternary ArC, C_{14}), 131.4 (ArCCl, C_{17}), 129.7 (ArCH, $C_{15,19}$), 129.3 (ArCH, $C_{16,18}$), 94.8 (CH, C_{12}), 79.1 (quaternary Cp, C_{10}), 73.4 (Cp CH, $C_{6,9}$), 71.2 (Cp ring, $C_{1\text{-}5}$), 69.8 (Cp CH, $C_{7,8}$); **Analysis**: Calculated C 62.25, H 4.12, Cl 9.67 %, Found C 62.30, H 4.10, Cl 9.50 %; **H.R.M.S. [ES+]** found [MH$^+$] 366.011.

8.4.16 Synthesis of 1-Ferrocenyl-3-(3-chlorophenyl)propane-1,3-dione L16

Prepared using ethyl-3-chlorobenzoate (2.02 mL, 13.0 mmol), refluxed for 48 hours and worked up following method 1. The product was purified by column chromatography, eluting 90:10 v/v hexane/ethyl acetate to give red solid (1.89 g, 72 %).

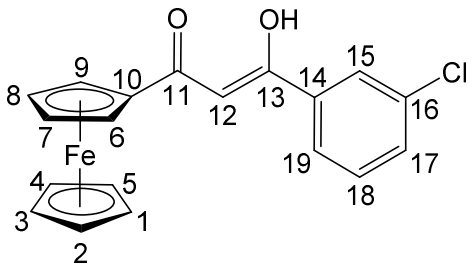

δ_H (500 MHz, $(CD_3)_2CO$); 7.92 (t, 1H, *J 1.8* Hz, ArH, H_{15}), 7.88 (dt, 1H, *J 7.8, 1.3* Hz, ArH, H_{19}), 7.48 (dq, 1H, *J 7.8, 1.0* Hz, ArH, H_{17}), 7.42 (t, 1H, *J 7.8* Hz, ArH, H_{18}), 6.70 (s, 1H, CH, H_{12}), 4.95 (t, 2H, *J 2.0* Hz, C_5H_4, $H_{7,8}$), 4.52 (t, 2H, *J 2.0* Hz, C_5H_4, $H_{6,9}$), 4.12 (s, 5H, C_5H_5, $H_{1\text{-}5}$); **δ_C**{^{1}H} (125 MHz, $(CD_3)_2CO$); 196.0 (quaternary CO, C_{11}), 178.3 (quaternary CO, C_{13}), 138.2 (quaternary ArC, C_{14}), 135.2 (ArCCl, C_{16}), 132.4 (ArCH, C_{15}), 131.3 (ArCH, C_{19}), 127.4 (ArCH, C_{17}), 126.1 (ArCH, C_{18}), 95.1 (CH, C_{12}), 79.0 (quaternary Cp, C_{10}), 73.5 (Cp CH, $C_{6,9}$), 71.2 (Cp ring, $C_{1\text{-}5}$), 69.9 (Cp CH, $C_{7,8}$); **Analysis**: Calculated C 62.15, H 4.12 %, Found C 62.18, H 4.13 %; **H.R.M.S. [ES+]** found [MH^+] 366.010.

8.4.17 Synthesis of 1-Ferrocenyl-3-(3,5-dichlorophenyl)propane-1,3-dione L17

Prepared using ethyl-3,5-dichlorobenzoate (2.85 g, 13.0 mmol), refluxed for 24 hours and worked up following method 2. The product precipitated out as a pure red solid (2.37 g, 83 %).

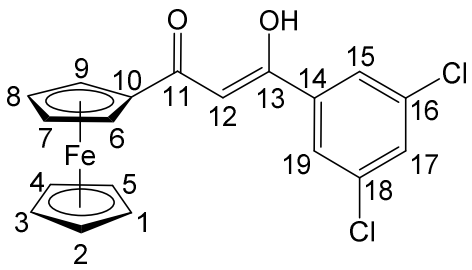

δ_H (500 MHz, $(CD_3)_2CO$); 7.92 (s, 1H, ArH, H_{17}), 7.59 (s, 1H, ArH, $H_{15/19}$), 7.50 (s, 1H, ArH, $H_{15/19}$), 6.79 (s, 1H, CH, H_{12}), 5.01 (t, 2H, *J 1.7* Hz, C_5H_4, $H_{6,9}$), 4.58 (t, 2H, *J 1.7* Hz, C_5H_4, $H_{7,8}$), 4.16 (s, 5H, C_5H_5, $H_{1\text{-}5}$); **δ_C**{^{1}H} (125 MHz, $(CDCl_3)$; 194.8 (quaternary CO, C_{11}), 176.4 (quaternary CO, C_{13}), 138.3 (ArCCl, $C_{16/18}$), 135.5 (ArCH, $C_{15/\ 19}$), 133.7 (ArCCl, $C_{16/18}$), 131.3 (ArCH, $C_{15/19}$), 128.8 (quaternary ArCH, C_{14}), 125.1 (ArCH, C_{17}), 94.2 (CH, C_{12}), 77.2 (quaternary Cp, $C_{6,9}$), 72.8 (Cp CH,

$C_{7/8}$), 70.5 (Cp ring $C_{1\text{-}5}$), 69.0 (Cp CH, $C_{7/8}$); **Analysis**: Calculated (+H_2O) C 54.45, H 3.85 %, Found C 53.80, H 3.20 %; **H.R.M.S. [ES+]** found [MH^+] 399.972.

8.4.18 Synthesis of 1-Ferrocenyl-3-(4-bromophenyl)propane-1,3-dione L18

Prepared using ethyl-4-bromobenzoate (2.12 mL, 13.0 mmol), refluxed for 24 hours and worked up following method 1. The product was purified by column chromatography, eluting 90:10 v/v hexane/ethyl acetate to give red solid (2.76 g, 93 %).

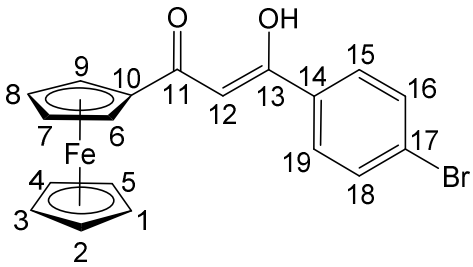

δ_H (500 MHz, $(CD_3)_2CO$); 7.87 (d, 2H, *J 8.0* Hz, ArH, $H_{15,19}$), 7.58 (d, 2H, *J 7.1* Hz, ArH, $H_{16,18}$), 6.66 (s, 1H, CH, H_{12}), 4.92 (Broad s, 2H, C_5H_4, $H_{6,9}$), 4.51 (Broad s, 2H, C_5H_4, $H_{7,8}$), 4.11 (s, 5H, C_5H_5, $H_{1\text{-}5}$); **δ_C**{^{1}H} (125 MHz, ($CDCl_3$); 194.3 (quaternary CO, C_{11}), 178.5 (quaternary CO, C_{13}), 134.2 (quaternary ArC, C_{14}), 131.9 (ArCH, $C_{15,19}$), 128.2 (ArCH, $C_{16,18}$), 126.5 (ArCBr, C_{17}), 93.6 (CH, C_{12}), 78.0 (quaternary Cp, C_{10}), 72.4 (Cp CH, $C_{6,9}$), 70.4 (Cp ring, $C_{1\text{-}5}$), 68.8 (Cp CH, $C_{7,8}$); **Analysis**: Calculated (+0.75 DCM) C 49.96, H 3.50 %, Found C 50.00, H 3.20 %; **H.R.M.S. [ES+]** found [MH^+] 409.960.

8.4.19 Synthesis of 1-Ferrocenyl-3-(3-Bromophenyl)propane-1,3-dione L19

Prepared using ethyl-3-bromobenzoate (2.08 mL, 13.0 mmol), refluxed for 24 hours and worked up following method 1. The product was purified by column chromatography, eluting 90:10 v/v hexane/ethyl acetate to give red solid (2.32 g, 78 %).

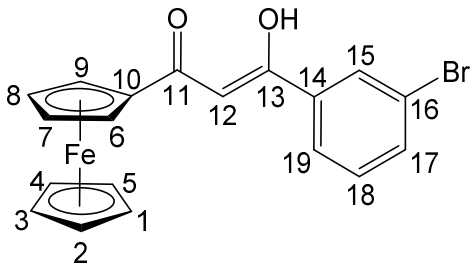

δ_H (500 MHz, $(CD_3)_2CO$); 8.07 (t, 1H, *J 1.6* Hz, ArH, H_{15}), 7.93 (dt, 1H, *J 7.8, 1.1* Hz, ArH, H_{19}), 7.62 (dt, 1H, *J 8.0, 0.8* Hz, ArH, H_{17}), 7.36 (t, 1H, *J 7.9* Hz, ArH, H_{18}), 6.69 (s, 1H, CH, H_{12}), 4.94 (t, 2H, *J 1.8* Hz, C_5H_4, $H_{6,9}$), 4.52 (t, 2H, *J 1.8* Hz, C_5H_4, $H_{7,8}$), 4.11 (s, 5H, C_5H_5, $H_{1\text{-}5}$); **δ_C**{^{1}H} (125 MHz, $(CD_3)_2CO$); 196.0 (quaternary CO, C_{11}), 178.3 (quaternary CO, C_{13}), 138.4 (quaternary ArC, C_{14}), 135.4 (ArCH, C_{15}), 131.5 (ArCH, C_{19}), 130.3 (ArCH, C_{17}), 126.5 (ArCH, C_{18}), 123.3 (ArCBr, C_{16}), 95.1 (CH, C_{12}), 79.0 (quaternary Cp, C_{10}), 73.5 (Cp CH, $C_{6,9}$), 71.2 (Cp ring, $C_{1\text{-}5}$), 69.9 (Cp CH, $C_{7,8}$); **Analysis**: Calculated C 55.52, H 3.68 %, Found C 55.54, H 3.77 %; **H.R.M.S. [ES+]** found [MH^+] 409.960.

8.4.20 Synthesis of 1-Ferrocenyl-3-(4-iodophenyl)propane-1,3-dione L20

Prepared using ethyl-4-iodobenzoate (2.19 mL, 13.0 mmol), refluxed for 48 hours and worked up following method 2. The product was purified by column chromatography, eluting 95:5 v/v hexane/ethyl acetate to give red solid (1.65 g, 50 %).

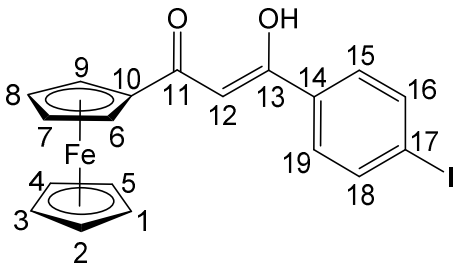

δ_H (500 MHz, $(CD_3)_2CO$); 7.79 (d, 2H, *J 8.3* Hz, ArH, $H_{15,19}$), 7.71 (d, 2H, *J 8.5* Hz, ArH, $H_{16,18}$), 6.65 (s, 1H, CH, H_{12}), 4.92 (t, 2H, *J 1.6* Hz, C_5H_4, $H_{6,9}$), 4.51 (t, 2H, *J 1.4* Hz, C_5H_4, $H_{7,8}$), 4.10 (s, 5H, C_5H_5, $H_{1\text{-}5}$); **δ_C**{^{1}H} (125 MHz, $(CD_3)_2CO$); 195.8 (quaternary CO, C_{11}), 179.0 (quaternary CO, C_{13}), 138.8 (ArCH, $C_{15,19}$), 135.7 (quaternary ArC, C_{14}), 129.5 (ArCl, C_{17}), 129.3 (ArCH, $C_{16,18}$), 94.7 (CH, C_{12}), 79.1 (quaternary Cp, C_{10}), 73.4 (Cp CH, $C_{6,9}$), 71.2 (Cp ring, $C_{1\text{-}5}$), 69.9 (Cp CH, $C_{7,8}$); **Analysis**: Calculated C 49.82, H 3.30, I 27.70 %, Found C 50.20, H 3.35, I 27.50 %; **H.R.M.S. [ES+]** found [MH^+] 457.947.

8.4.21 Synthesis of 1-Ferrocenyl-3-(3-iodophenyl)propane-1,3-dione L21

Prepared using ethyl-3-iodobenzoate (2.02 mL, 13.0 mmol), refluxed for 24 hours and worked up following method 1. The product was purified by column chromatography, eluting 90:10 v/v hexane/ethyl acetate to give red solid (1.02 g, 31 %).

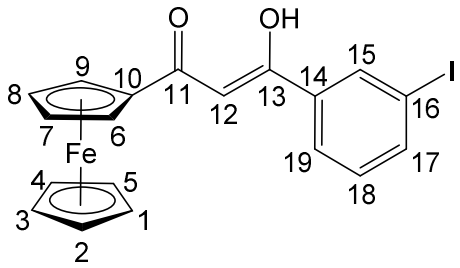

δ_H (500 MHz, $(CD_3)_2CO$); 8.41 (t, 1H, *J 1.4* Hz, ArH, H_{15}), 8.11 (dd, 1H, *J 7.8, 0.8* Hz, ArH, H_{19}), 7.98 (dt, 1H, *J 7.8, 0.8* Hz, ArH, H_{17}), 7.36 (t, 1H, *J 7.9* Hz, ArH, H_{18}), 6.83 (s, 1H, CH, H_{12}), 5.09 (t, 2H, *J 1.8* Hz, C_5H_4, $H_{6,9}$), 4.67 (t, 2H, *J 1.8* Hz, C_5H_4, $H_{7,8}$), 4.27 (s, 5H, C_5H_5, $H_{1\text{-}5}$); **$\delta_C\{^1H\}$** (125 MHz, $(CD_3)_2CO$); 195.9 (quaternary CO, C_{11}), 178.3 (quaternary CO, C_{13}), 142.9 (quaternary ArC, C_{14}), 141.5 ArCH, C_{15}), 138.3 (ArCI, C_{16}), 136.2 (ArCH, C_{19}), 131.5 (ArCH, C_{17}), 127.0 (ArCH, C_{18}), 94.8 (CH, C_{12}), 79.0 (quaternary Cp, C_{10}), 73.5 (Cp CH, $C_{6,9}$), 71.2 (Cp ring, $C_{1\text{-}5}$), 69.9 (Cp CH, $C_{7,8}$); **Analysis**: Calculated C 49.82, H 3.30 %, Found C 49.75, H 3.23 %; **H.R.M.S. [ES+]** found $[MH^+]$ 457.946.

8.4.22 Synthesis of 1-Ferrocenyl-3-(4-methoxyphenyl)propane-1,3-dione L22

Prepared using ethyl-4-methoxybenzoate (2.10 mL, 13.0 mmol), refluxed for 24 hours and worked up following method 1. The product was purified by column chromatography, eluting 80:20 v/v hexane/ethyl acetate to give a red solid (0.53 g, 21 %).

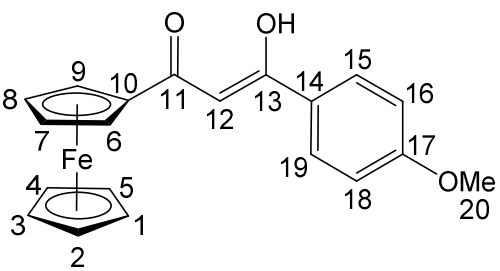

δ_H (500 MHz, $(CD_3)_2CO$); 7.90 (d, 2H, *J 8.3* Hz, ArH, $H_{15,19}$), 6.92 (d, 2H, *J 8.7* Hz, ArH, $H_{16,18}$), 6.56 (d, 1H, *J 6.9* Hz, CH, H_{12}), 4.89 (broad s, 2H, C_5H_4, $H_{6,9}$), 4.46 (broad s, 2H, C_5H_4, $H_{7,8}$), 4.09 (s, 5H, C_5H_5, $H_{1\text{-}5}$), 3.77 (s, 3H, OMe, H_{20}); **$\delta_C\{^1H\}$** (125 MHz, $(CD_3)_2CO$); 193.7 (quaternary CO, C_{11}), 181.4 (quaternary CO, C_{13}), 163.9 (ArCOMe, C_{17}), 132.0 (quaternary ArC, C_{14}), 129.7 (ArCH,

$C_{15,19}$), 114.8 (ArCH, $C_{16,18}$), 93.4 (CH, C_{12}), 79.4 (quaternary Cp, C_{10}), 72.9 (Cp CH, $C_{6,9}$), 71.0 (Cp ring, $C_{1\text{-}5}$), 69.6 (Cp CH, $C_{7,8}$), 55.9 (OCH_3, C_{20}); **Analysis**: Calculated C 66.32, H 5.01 %, Found C 66.10, H 5.00 %; **H.R.M.S. [ES+]** found [M-H^+] 361.053.

8.4.23 Synthesis of 1-Ferrocenyl-3-(3-methoxyphenyl)propane-1,3-dione L23

Prepared using ethyl-3-methoxybenzoate (2.15 mL, 13.0 mmol), refluxed for 24 hours and worked up following method 2. The product was purified by column chromatography, eluting 80:20 v/v hexane/ethyl acetate to give red solid (1.67 g, 64 %).

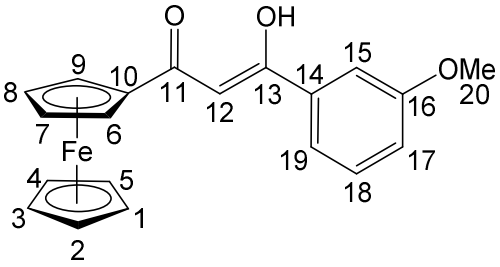

δ_H (500 MHz, $(CD_3)_2CO$); 7.66 (d, 1H, *J 7.6* Hz, ArH, H_{19}), 7.58 (s, 1H, ArH, H_{15}), 7.46 (t, 1H, *J 8.0* Hz, ArH, H_{18}), 7.17 (dd, 1H, *J 8.0, 2.3* Hz, ArH, H_{17}), 6.77 (s, 1H, CH, H_{12}), 5.08 (s, 2H, C_5H_4, $H_{6,9}$), 4.65 (s, 2H, C_5H_4, $H_{7,8}$), 4.26 (s, 5H, C_5H_5, $H_{1\text{-}5}$), 3.92 (s, 3H, OCH_3, H_{20}); **δ_C**{^{1}H} (125 MHz, $(CD_3)_2CO$); 195.4 (quaternary CO, C_{11}), 180.2 (quaternary CO, C_{13}), 161.0 (quaternary ArC-OMe, C_{16}), 137.5 (quaternary ArC, C_{14}), 130.6 (ArCH, C_{15}), 120.0 (ArCH, C_{19}), 118.4 (ArCH, C_{17}), 112.8 (ArCH, C_{18}), 94.8 (CH, C_{12}), 79.2 (quaternary Cp, C_{10}), 73.2 (Cp CH, $C_{6,9}$), 71.1 (Cp ring, $C_{1\text{-}5}$), 69.8 (Cp CH, $C_{7,8}$), 55.8 (OCH_3, C_{20}); **Analysis**: Calculated C 66.32, H 5.01 %, Found C 66.19, H 5.12 %; **H.R.M.S. [ES+]** found [MH^+] 362.061.

8.4.24 Synthesis of 1-Ferrocenyl-3-(4-ethoxyphenyl)propane-1,3-dione L24

Prepared using ethyl-4-ethoxybenzoate (2.36 mL, 13.0 mmol), refluxed for 24 hours and worked up following method 1. The product was purified by column chromatography, eluting 87:13 v/v hexane/ethyl acetate to give red solid (0.38 g, 14 %).

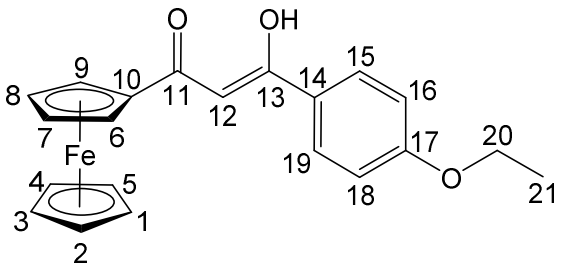

δ_H (500 MHz, $(CD_3)_2CO$); 8.04 (d, 2H, *J 2.1* Hz, ArH, $H_{15,19}$), 7.05 (d, 2H, *J 2.3* Hz, ArH, $H_{16,18}$), 6.72 (s, 1H, CH, H_{12}), 5.05 (Broad s, 2H, C_5H_4, $H_{6,9}$), 4.62 (Broad s, 2H, C_5H_4, $H_{7,8}$), 4.25 (s, 5H, C_5H_5, $H_{1\text{-}5}$), 4.18 (m, 2H, OCH_2, H_{20}), 1.43 (t, 3H, *J 3.3* Hz, CH_3, H_{21}); **δ_C**{^{1}H} (125 MHz, $(CD_3)_2CO$); 193.7 (quaternary CO, C_{11}), 181.4 (quaternary CO, C_{13}), 163.3 (ArCOEt, C_{17}), 132.1 (quaternary ArC, C_{14}), 129.7 (ArCH, $C_{15,19}$), 115.3 (ArCH, $C_{16,18}$), 93.4 (CH, C_{12}), 79.4 (quaternary Cp, C_{10}), 72.9 (Cp CH, $C_{6,9}$), 71.0 (Cp ring, $C_{1\text{-}5}$), 69.6 (Cp CH, $C_{7,8}$), 64.5 (OCH_2, C_{20}), 15.0 (CH_3, C_{21}); **Analysis**: Calculated C 67.04, H 5.36 %, Found C 67.10, H 5.40 %; **H.R.M.S. [ES+]** found [MH^+] 377.083.

8.4.25 Synthesis of 1-Ferrocenyl-3-(2-pyridinyl)propane-1,3-dione L25

Prepared using ethyl picolinate (1.76 mL, 13.0 mmol), refluxed for 24 hours and worked up following method 1. The product was purified by column chromatography, eluting 90:10 v/v hexane/ethyl acetate to give red solid (1.57 g, 66 %).

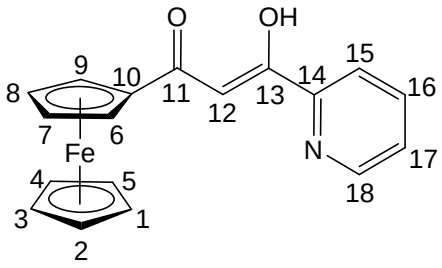

δ_H (500 MHz, $(CD_3)_2CO$); 8.60 (broad d, 1H, *J 3.9* Hz, ArH, H_{18}), 7.97 (d, 1H, *J 7.8* Hz, ArH, H_{15}), 7.87 (td, 1H, *J 7.6, 1.6* Hz, ArH, H_{17}), 7.44 (qd, 1H, *J 4.8, 2.8, 0.9* Hz, ArH, H_{16}), 7.01 (s, 1H, CH, H_{12}), 4.85 (broad t, 2H, *J 1.6* Hz, C_5H_4, $H_{6,9}$), 4.54 (broad t, 2H, *J 1.6* Hz, C_5H_4, $H_{7,8}$), 4.12 (s, 5H, C_5H_5, $H_{1\text{-}5}$); **δ_C**{^{1}H} (125 MHz, $(CD_3)_2CO$); 188.5 (quaternary CO, C_{11}), 178.4 (quaternary CO, C_{13}), 150.4 (ArCH, C_{18}), 138.1 (ArCH, C_{19}), 128.4 (quaternary ArC, C_{14}), 127.0 (ArCH, C_{15}), 122.2 (ArCH, C_{16}), 95.1 (CH, C_{12}), 78.9 (quaternary Cp, C_{10}), 73.5 (Cp CH, $C_{6,9}$), 71.2 (Cp ring, $C_{1\text{-}5}$), 69.8 (Cp CH, $C_{7,8}$); **Analysis**: Calculated C 64.89, H 4.54, N 4.20 %, Found C 65.10, H 4.60, N 4.10 %; **H.R.M.S. [ES+]** found [$M\text{-}H^+$] 332.037.

8.4.26 Synthesis of 1-Ferrocenyl-3-(4-pyridinyl)propane-1,3-dione L26

Prepared using ethyl isonicotinate (1.95 mL, 13.0 mmol), refluxed for 24 hours and worked up following method 1. The product precipitated out of solution as a pure solid (2.29 g, 96 %).

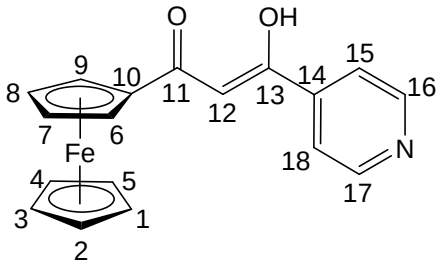

δ_H (500 MHz, $(CD_3)_2CO$); 8.78 (d, 2H, *J 5.7* Hz, ArH, $H_{16,17}$), 7.94 (d, 2H, *J 6.0* Hz, ArH, $H_{15,18}$), 6.90 (s, 1H, CH, H_{12}), 5.11 (broad t, 2H, C_5H_4, $H_{6,9}$), 4.71 (broad t, 2H, C_5H_4, $H_{7,8}$), 4.28 (s, 5H, C_5H_5, $H_{1\text{-}5}$); **$\delta_C\{^1H\}$** (125 MHz, $(CD_3)_2CO$); 197.6 (quaternary CO, C_{11}), 175.7 (quaternary CO, C_{13}), 151.5 (ArCH, $C_{16,\ 17}$), 142.8 (quaternary ArC, C_{14}), 120.9 (ArCH, $C_{15,18}$), 96.3 (CH, C_{12}), 79.0 (quaternary Cp, C_{10}), 73.8 (Cp CH, $C_{6,9}$), 71.2 (Cp ring, $C_{1\text{-}5}$) 70.1 (Cp CH, $C_{7,8}$); **Analysis**: Calculated C 64.89, H 4.54, N 4.20 %, Found C 65.10, H 4.60, N 4.10 %; **H.R.M.S. [ES+]** found $[MH^+]$ 334.053.

8.5 Synthesis of Ruthenium *p*-cymene Complexes

Complexes have been synthesised using the following general procedure adapted from methods previously used in the McGowan group.[95]

General Procedure: The required ligand was dissolved in dichloromethane (20 mL) followed by addition of triethylamine (0.05 mL, 0.392 mmol) and [*p*-cymRuCl$_2$]$_2$ (0.12 g, 0.196 mmol) and stirred at room temperature overnight. Solvent was removed *in vacuo* to give a red solid product.

8.5.1 Synthesis of (*p*-cymene)Ru(II)(1-Ferrocenylbutane-1,3-dione)Cl C1

Prepared using 1-ferrocenylbutane-1,3-dione (0.11 g, 0.392 mmol) and purified by column chromatography, eluting 3:2 v/v petrol/ethyl acetate to give orange solid (0.144 g, 68 %).

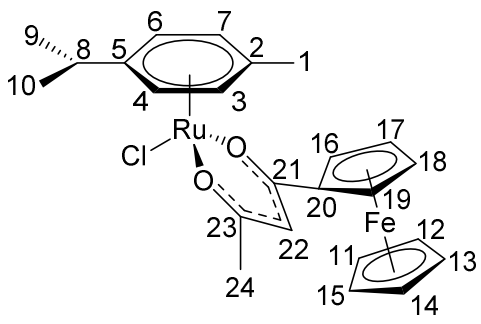

δ_H (500 MHz, $(CD_3)_2CO$); 5.47 (d, 1H, *J 6.0* Hz, *p*-cymene ArH, $H_{4/6}$), 5.45 (d, 1H, *J 6.0* Hz, *p*-cymene ArH, $H_{4/6}$), 5.32 (s, 1H, CH, H_{22}), 5.12 (d, 2H, *J 6.0* Hz, *p*-cymene ArH, $H_{3,7}$), 4.75 (t, 1H, *J 1.4* Hz, C_5H_4, $H_{16/19}$), 4.51 (t, 1H, *J 1.4* Hz, C_5H_4, $H_{16/19}$), 4.24 (q, 1H, *J 2.5, 1.3* Hz, C_5H_4, $H_{17/18}$), 4.20 (q, 1H, *J 2.5, 1.3* Hz, C_5H_4, $H_{17/18}$), 4.07 (s, 5H, C_5H_5, $H_{11\text{-}15}$), 2.83 (sept, 1H, *J 6.9* Hz, *p*-cymene $CH(Me)_2$, H_8), 2.07 (s, 3H, *p*-cymene $ArCH_3$, H_1), 1.79 (s, 3H, CH_3, H_{24}), 1.29 (dd, 6H, *J 6.9, 2.3* Hz, *p*-cymene $C(CH_3)_2$, $H_{9,10}$); **δ_C**{^{1}H} (125 MHz, $(CD_3)_2CO$); 184.9 (quaternary CO, C_{21}), 184.6 (quaternary CO, C_{23}), 99.2 (quaternary *p*-cymene, C_5), 97.7 (quaternary *p*-cymene, C_2), 95.9 (acac CH, C_{22}), 84.6 (*p*-cymene ArCH, $C_{3/4/6/7}$), 84.1 (*p*-cymene ArCH, $C_{3/4/6/7}$), 81.7 (quaternary Cp, C_{20}), 79.6 (*p*-cymene ArCH, $C_{3/4/6/7}$), 71.3 (Cp CH, $C_{19/16}$), 71.3 (Cp CH, $C_{16/19}$), 70.8 (Cp ring, $C_{11\text{-}15}$), 69.8 (Cp CH, $C_{17/18}$), 68.4 (Cp CH, $C_{17/18}$), 31.7 (*p*-cymene CH, C_8), 27.5 (acac CH_3, C_{24}) 22.6 (*p*-cymene $C(\underline{C}H_3)_2$, $C_{9,10}$), 17.7 (*p*-cymene CH_3, C_1); **Analysis**: Calculated C 53.40, H 5.04, Cl 6.57%, Found C 53.40, H 5.10, Cl 6.40%; **H.R.M.S. [ES+]** found [MH$^+$]-Cl 505.042.

8.5.2 Synthesis of (*p*-cymene)Ru(II)(1-Ferrocenyl-4,4,4-trifluorobutane-1,3-dione)Cl C2

Prepared using 1-ferrocenyl-4,4,4-trifluorobutane-1,3-dione (0.13 g, 0.392 mmol) and purified by column chromatography, eluting 3:2 v/v petrol/ethyl acetate to give orange solid (0.20 g, 85 %).

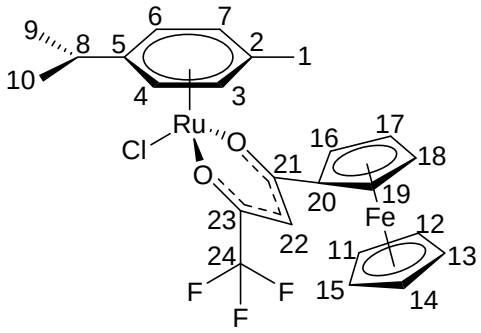

δ_H (500 MHz, $(CD_3)_2CO$); 5.63 (s, 1H, CH, H_{22}), 5.61 (t, 2H, *J 5.5* Hz, *p*-cymene ArH, $H_{4,6}$), 5.30 (d, 1H, *J 5.5* Hz, *p*-cymene ArH, $H_{3/7}$), 5.27 (d, 1H, *J 5.5* Hz, *p*-cymene ArH, $H_{3/7}$), 4.83 (t, 1H, *J 1.4* Hz, C_5H_4, $H_{16/19}$), 4.68 (t, 1H, *J 1.4* Hz, C_5H_4, $H_{16/19}$), 4.46 (m, 1H, C_5H_4, $H_{17/18}$), 4.41 (m, 1H, C_5H_4, $H_{17/18}$), 4.13 (s, 5H, C_5H_5, $H_{11\text{-}15}$), 2.83 (sept, 1H, *J 6.9* Hz, *p*-cymene $CH(Me)_2$, H_8), 2.10 (s, 3H, *p*-cymene $ArCH_3$, H_1), 1.17 (d, 6H, *J 7.3* Hz, *p*-cymene $C(CH_3)_2$, $H_{9,10}$); **δ_C**{^{1}H} (125 MHz, $(CD_3)_2CO$); 218.9 (quaternary CO, C_{21}), 191.8 (quaternary CO, C_{23}), 99.5 (quaternary *p*-cymene, C_5), 98.3 (quaternary *p*-cymene, C_2), 92.2 (acac CH, C_{22}), 84.8 (*p*-cymene ArCH, $C_{4/6}$), 84.2 (*p*-cymene ArCH, $C_{4/6}$), 80.1 (quaternary Cp, C_{20}), 79.5 (*p*-cymene ArCH, $C_{3/7}$), 79.5 (*p*-cymene ArCH, $C_{3/7}$), 73.5 (Cp CH, $C_{16/19}$), 73.1 (Cp CH, $C_{16/19}$), 71.3 (Cp ring, $C_{11\text{-}15}$), 70.9 (Cp CH, $C_{17/18}$), 67.5 (Cp CH, $C_{17/18}$), 31.8 (*p*-cymene CH, C_8), 22.5 (*p*-cymene $C(CH_3)$, $C_{9/10}$), 22.5 (*p*-cymene $C(CH_3)$, $C_{9/10}$), 17.7 (*p*-cymene CH_3, C_1); **Analysis**: Calculated C 48.54, H 4.07, Cl 5.97 %, Found C 48.90, H 4.10, Cl 6.00 %; **H.R.M.S. [ES+]** found $[MH^+]$-Cl 559.023.

8.5.3 Synthesis of (*p*-cymene)Ru(II)(1-Ferrocenyl-4,4-difluorobutane-1,3-dione)Cl C3

Prepared using 1-ferrocenyl-4,4-difluorobutane-1,3-dione (0.12 g, 0.392 mmol) and purified by column chromatography, eluting 3:2 v/v petrol/ethyl acetate to give orange solid (0.17 g, 77 %).

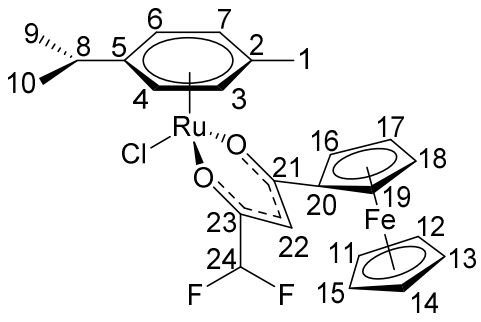

δ_H (500 MHz, $(CD_3)_2CO$); 5.86 (t, 1H, *J 55.2* Hz, CH, H_{22}), 5.57 (broad t, 2H, *J 6.2* Hz, *p*-cymene ArH, $H_{4,6}$), 5.56 (broad s, H, CHF_2, H_{24}), 5.22 (t, 2H, *J 5.6* Hz, *p*-cymene ArH, $H_{3/7}$), 4.80 (broad s, 1H, C_5H_4, $H_{16/19}$), 4.62 (broad s, 1H, C_5H_4, $H_{16/19}$), 4.40 (broad s, 1H, C_5H_4, $H_{17/18}$), 4.35 (broad s, 1H, C_5H_4, $H_{17/18}$), 4.11 (s, 5H, C_5H_5, $H_{11\text{-}15}$), 2.71 (sept, 1H, *J 5.9* Hz, *p*-cymene $CH(Me)_2$, H_8), 2.09 (s, 3H, *p*-cymene $ArCH_3$, H_1), 1.30 (t, 6H, *J 5.9* Hz, *p*-cymene $C(CH_3)_2$, $H_{9,10}$); **δ_C**{^{1}H} (125 MHz, $(CD_3)_2CO$); 190.1 (quaternary CO, C_{21}), 172.8 (t, quaternary CO, *J 22.1* Hz, C_{23}), 112.2 (t, CHF_2, *J 246.3* Hz, C_{24}), 99.5 (quaternary *p*-cymene, C_5), 98.2 (quaternary *p*-cymene, C_2), 92.6 (acac CH, C_{22}), 84.9 (*p*-cymene ArCH, $C_{4/6}$), 84.2 (*p*-cymene ArCH, $C_{4/6}$), 80.5 (quaternary Cp, C_{20}), 79.9 (*p*-cymene ArCH, $C_{3/7}$), 79.5 (*p*-cymene ArCH, $C_{3/7}$), 72.7 (Cp CH, $C_{16/19}$), 72.6 (Cp CH, $C_{16/19}$), 71.2 (Cp ring, $C_{11\text{-}15}$), 70.1 (Cp CH, $C_{17/18}$), 69.1 (Cp CH, $C_{17/18}$), 31.7 (*p*-cymene CH, C_8), 22.6 (*p*-cymene $C(CH_3)$, $C_{9/10}$), 22.5 (*p*-cymene $C(CH_3)$, $C_{9/10}$), 17.7 (*p*-cymene CH_3, C_1); **Analysis**: Calculated C 50.06, H 4.38, Cl 6.16 %, Found C 50.30, H 4.40, Cl 6.30 %; **H.R.M.S. [ES+]** found $[MH^+]$-Cl 541.023.

8.5.4 Synthesis of (*p*-cymene)Ru(II)(1-Ferrocenyl-3-(3-furanyl)propane-1,3-dione)Cl C4

Prepared using 1-ferrocenyl-3-(3-furanyl)propane-1,3-dione (0.13 g, 0.392 mmol) and purified by column chromatography, eluting 3:2 v/v petrol/ethyl acetate to give orange solid (0.19 g, 81 %).

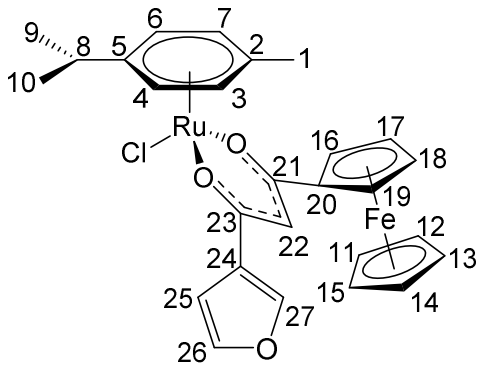

δ_H (500 MHz, $(CD_3)_2CO$); 8.19 (s, 1H, Furan CH, H_{27}), 7.60 (t, 1H, *J 1.6* Hz, Furan CH, H_{25}), 6.90 (d, 1H, *J 1.2* Hz, Furan CH, H_{26}), 5.97 (s, 1H, CH, H_{22}), 5.68 (t, 2H, *J 6.1* Hz, *p*-cymene ArH, $H_{4,6}$), 5.35 (t, 2H, *J 5.3* Hz, *p*-cymene ArH, $H_{3,7}$), 4.96 (d, 1H, *J 1.2* Hz, C_5H_4, $H_{16/19}$), 4.84 (d, 1H, *J 1.2* Hz, C_5H_4, $H_{16/19}$), 4.44 (m, 1H,

C_5H_4, $H_{17/18}$), 4.40 (m, 1H, C_5H_4, $H_{17/18}$), 4.25 (s, 5H, C_5H_5, $H_{11\text{-}15}$), 3.04 (sept, 1H, *J 6.9* Hz, *p*-cymene $CH(Me)_2$, H_8), 2.29 (s, 3H, *p*-cymene $ArCH_3$, H_1), 1.49 (dd, 6H, *J 6.9, 0.9* Hz, *p*-cymene $C(CH_3)_2$, $H_{9,10}$); **δ_C**{^{1}H} (125 MHz, $(CD_3)_2CO$); 186.0 (quaternary CO, C_{21}), 173.6 (quaternary CO, C_{23}), 145.0 (Furan CH, C_{27}), 144.4 (Furan CH, C_{26}), 128.8 (quaternary Furan C, C_{24}), 109.8 (Furan CH, C_{25}), 99.2 (quaternary *p*-cymene, C_5), 97.8 (quaternary *p*-cymene, C_2), 94.0 (acac CH, C_{22}), 84.7 (*p*-cymene ArCH, $C_{4/6}$), 84.5 (*p*-cymene ArCH, $C_{4/6}$), 82.0 (quaternary Cp, C_{20}), 79.9 (*p*-cymene ArCH, $C_{3/7}$), 79.8 (*p*-cymene ArCH, $C_{3/7}$), 71.5 (Cp CH, $C_{16/19}$), 71.5 (Cp CH, $C_{16/19}$), 70.9 (Cp ring, $C_{11\text{-}15}$), 69.8 (Cp CH, $C_{17/18}$), 68.6 (Cp CH, $C_{17/18}$), 31.7 (*p*-cymene CH, C_8), 22.7 (*p*-cymene $C(CH_3)$, $C_{9/10}$), 22.6 (*p*-cymene $C(CH_3)$, $C_{9/10}$), 17.7 (*p*-cymene CH_3, C_1); **Analysis**: Calculated C 54.79, H 4.60 %, Found C 54.72, H 4.55 %; **H.R.M.S. [ES+]** found [MH^+]-Cl 557.043.

8.5.5 Synthesis of (*p*-cymene)Ru(II)(1-Ferrocenyl-3-(2-furanyl)propane-1,3-dione)Cl C5

Prepared using 1-ferrocenyl-3-furanylpropane-1,3-dione (0.13 g, 0.392 mmoland purified by column chromatography, eluting 3:2 v/v petrol/ethyl acetate to give orange solid (0.20 g, 86 %).

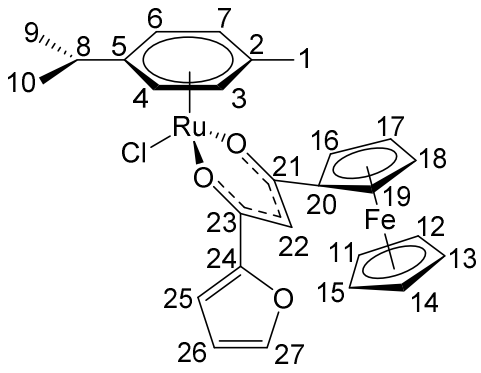

δ_H (500 MHz, $(CD_3)_2CO$); 7.53 (broad d, 1H, *J 0.9* Hz, Furan CH, H_{25}), 6.96 (broad d, 1H, *J 3.4* Hz, Furan CH, H_{27}), 6.44 (dd, 1H, *J 3.7, 1.6* Hz, Furan CH, H_{26}), 5.92 (s, 1H, CH, H_{22}), 5.53 (t, 2H, *J 6.3* Hz, *p*-cymene ArH, $H_{4,6}$), 5.20 (t, 2H, *J 5.7* Hz, *p*-cymene ArH, $H_{3,7}$), 4.79 (broad t, 1H, *J 1.2* Hz, C_5H_4, $H_{16/19}$), 4.60 (broad t, 1H, *J 1.2* Hz, C_5H_4, $H_{16/19}$), 4.32 (broad q, 1H, *J 2.5, 1.2* Hz, C_5H_4, $H_{17/18}$), 4.28 (broad q, 1H, *J 2.5, 1.2* Hz, C_5H_4, $H_{17/18}$), 4.11 (s, 5H, C_5H_5, $H_{11\text{-}15}$), 2.88 (sept, 1H, *J 6.9* Hz, *p*-cymene $CH(Me)_2$, H_8), 2.14 (s, 3H, *p*-cymene $ArCH_3$, H_1), 1.33 (d, 6H, *J 6.9* Hz, *p*-cymene $C(CH_3)_2$, $H_{9,10}$); **δ_C**{^{1}H} (125 MHz, $(CD_3)_2CO$); 186.6 (quaternary CO, C_{21}), 168.6 (quaternary CO, C_{23}), 163.6 (quaternary Furan C, C_{24}), 145.0 (Furan CH, C_{25}), 113.3

(Furan CH, C_{27}), 112.9 (Furan CH, C_{26}), 99.2 (quaternary *p*-cymene, C_5), 97.9 (quaternary *p*-cymene, C_2), 92.3 (acac CH, C_{22}), 84.8 (*p*-cymene ArCH, $C_{4/6}$), 84.5 (*p*-cymene ArCH, $C_{4/6}$), 81.9 (quaternary Cp, C_{20}), 79.9 (*p*-cymene ArCH, $C_{3/7}$), 79.8 (*p*-cymene ArCH, $C_{3/7}$), 71.7 (Cp CH, $C_{16/19}$), 71.7 (Cp CH, $C_{16/19}$), 70.9 (Cp ring, $C_{11\text{-}15}$), 69.9 (Cp CH, $C_{17/18}$), 68.6 (Cp CH, $C_{17/18}$), 31.7 (*p*-cymene CH, C_8), 22.7 (*p*-cymene $C(CH_3)$, $C_{9/10}$), 22.6 (*p*-cymene $C(CH_3)$, $C_{9/10}$), 17.7 (*p*-cymene CH_3, C_1); **Analysis**: Calculated C 54.79, H 4.60, Cl 5.99 %, Found C 55.05, H 4.60, Cl 5.70 %; **H.R.M.S. [ES+]** found $[MH^+]$-Cl 557.036.

8.5.6 Synthesis of (*p*-cymene)Ru(II)(1-Ferrocenyl-3-phenylpropane-1,3-dione)Cl C6

Prepared using 1-ferrocenyl-3-phenylpropane-1,3-dione (0.13 g, 0.392 mmol) and purified by column chromatography, eluting 2:3 v/v petrol/ethyl acetate to give orange solid (0.21 g, 89 %).

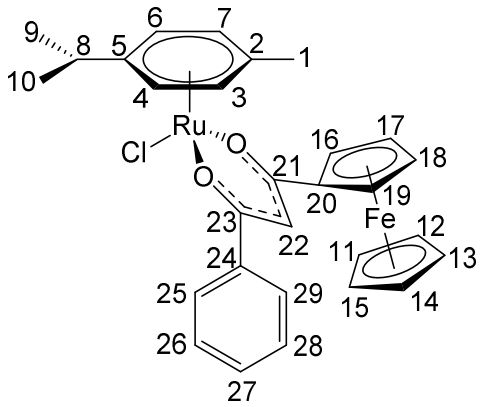

δ_H (500 MHz, $(CD_3)_2CO$); 7.84 (broad d, 2H, *J 7.3* Hz, ArH, $H_{25,29}$), 7.33 (t, 1H, *J 7.3* Hz, ArH, H_{27}), 7.28 (t, 2H, *J 7.3* Hz, ArH, $H_{26,28}$), 6.04 (s, 1H, CH, H_{22}), 5.55 (d, 2H, *J 6.4* Hz, *p*-cymene ArH, $H_{4,6}$), 5.24 (dd, 2H, *J 6.0, 1.8* Hz, *p*-cymene ArH, $H_{3,7}$), 4.83 (t, 1H, *J 1.2* Hz, C_5H_4, $H_{16/19}$), 4.73 (t, 1H, *J 1.2* Hz, C_5H_4, $H_{16/19}$), 4.32 (broad q, 1H, *J 2.2, 1.4* Hz, C_5H_4, $H_{17/18}$), 4.28 (broad q, 1H, *J 2.3, 1.4* Hz, C_5H_4, $H_{17/18}$), 4.11 (s, 5H, C_5H_5, $H_{11\text{-}15}$), 2.91 (sept, 1H, *J 6.9* Hz, *p*-cymene $CH(Me)_2$, H_8), 2.16 (s, 3H, *p*-cymene $ArCH_3$, H_1), 1.34 (d, 6H, *J 7.3* Hz, *p*-cymene $C(CH_3)_2$, $H_{9,10}$); **$\delta_C\{^1H\}$** (125 MHz, $(CD_3)_2CO$); 186.8 (quaternary CO, C_{21}), 178.4 (quaternary CO, C_{23}), 140.5 (quaternary ArC, C_{24}), 131.2 (ArCH, $C_{25,29}$), 128.9 (ArCH, $C_{26,28}$), 127.9 (ArCH, C_{27}), 99.4 (quaternary *p*-cymene, C_5), 97.8 (quaternary *p*-cymene, C_2), 93.4 (acac CH, C_{22}), 84.6 (*p*-cymene ArCH, $C_{4/6}$), 84.5 (*p*-cymene ArCH, $C_{4/6}$), 82.1 (quaternary Cp, C_{20}), 80.0 (*p*-cymene ArCH, $C_{3/7}$), 80.0 (*p*-cymene ArCH, $C_{3/7}$), 71.7 (Cp CH, $C_{16/19}$), 71.6 (Cp CH, $C_{16/19}$), 70.9 (Cp ring, $C_{11\text{-}15}$), 69.9 (Cp CH,

$C_{17/18}$), 68.7 (Cp CH, $C_{17/18}$), 31.7 (*p*-cymene CH, C_8), 22.7 (*p*-cymene C(CH_3), $C_{9/10}$), 22.6 (*p*-cymene C(CH_3), $C_{9/10}$), 17.9 (*p*-cymene CH_3, C_1); **Analysis**: Calculated C 57.87, H 4.86, Cl 5.89 %, Found C 57.70, H 5.20, Cl 5.75 %; **H.R.M.S. [ES+]** found [MH^+]-Cl 567.058.

8.5.7 Synthesis of (*p*-cymene)Ru(II)(1-Ferrocenyl-3-(1-naphthyl)propane-1,3-dione)Cl C7

Prepared using 1-ferrocenyl-3-(1-naphthyl)propane-1,3-dione (0.15 g, 0.392 mmol) and purified by column chromatography, eluting 3:2 v/v petrol/ethyl acetate to give orange solid (0.21 g, 82 %).

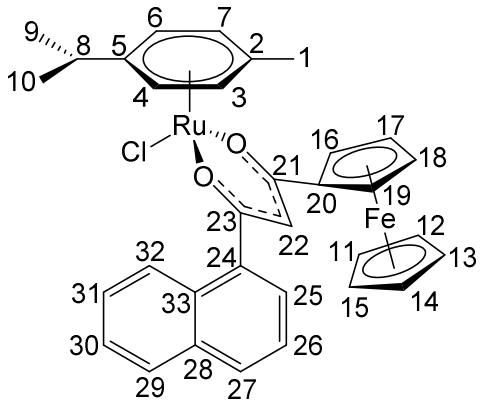

δ_H (500 MHz, $(CD_3)_2CO$); 8.54 (d, 1H, *J 7.8* Hz, ArH, H_{25}), 7.82 (d, 1H, *J 8.0* Hz, ArH, H_{26}), 7.78 (dd, 1H, *J 7.1, 2.1* Hz, ArH, H_{27}), 7.45 (d, 1H, *J 7.1* Hz, ArH, H_{32}), 7.37 (m, 3H, ArH, $H_{29\text{-}31}$), 5.72 (s, 1H, CH, H_{22}), 5.57 (d, 1H, *J 5.7* Hz, *p*-cymene ArH, $H_{4/6}$), 5.53 (d, 1H, *J 5.9* Hz, *p*-cymene ArH, $H_{4/6}$), 5.25 (t, 2H, *J 4.9* Hz, *p*-cymene ArH, $H_{3,7}$), 4.83 (d, 1H, *J 0.7* Hz, C_5H_4, $H_{16/19}$), 4.62 (d, 1H, *J 0.9* Hz, C_5H_4, $H_{16/19}$), 4.33 (m, 1H, C_5H_4, $H_{17/18}$), 4.27 (m, 1H, C_5H_4, $H_{17/18}$), 4.14 (s, 5H, C_5H_5, $H_{11\text{-}15}$), 2.86 (sept, 1H, *J 6.9* Hz, *p*-cymene $CH(Me)_2$, H_8), 2.09 (s, 3H, *p*-cymene $ArCH_3$, H_1), 1.30 (t, 6H, *J 6.7* Hz, *p*-cymene $C(CH_3)_2$, $H_{9,10}$); **δ_C**{^{1}H} (125 MHz, $(CD_3)_2CO$); 186.9 (quaternary CO, C_{21}), 176.0 (quaternary CO, C_{23}), 156.4 (quaternary ArC, C_{24}), 140.5 (quaternary ArC, C_{33}), 134.9 (quaternary ArC, C_{28}), 132.0 (ArCH, C_{25}), 130.2 (ArCH, C_{26}), 128.6 (ArCH, C_{27}), 128.4 (ArCH, C_{32}), 126.8 (ArCH, C_{329}), 125.7 (ArCH, C_{31}), 125.6 (ArCH, C_{30}), 99.7 (quaternary *p*-cymene, C_5), 98.3 (acac CH, C_{22}), 97.7 (quaternary *p*-cymene, C_2), 84.4 (*p*-cymene ArCH, $C_{4/6}$), 84.2 (*p*-cymene ArCH, $C_{4/6}$), 81.5 (quaternary Cp, C_{20}), 80.1 (*p*-cymene ArCH, $C_{3/7}$), 80.1 (*p*-cymene ArCH, $C_{3/7}$), 71.9 (Cp CH, $C_{16/19}$), 71.9 (Cp CH, $C_{16/19}$), 71.0 (Cp ring, $C_{11\text{-}15}$), 69.9 (Cp CH, $C_{17/18}$), 68.8 (Cp CH, $C_{17/18}$), 31.6 (*p*-cymene CH, C_8), 22.7 (*p*-cymene C(CH_3), $C_{9/10}$), 22.6 (*p*-cymene C(CH_3), $C_{9/10}$), 17.8 (*p*-cymene CH_3, C_1); **Analysis**: Calculated C 60.79,

H 4.79, Cl 5.44 %, Found C 60.70, H 4.90, Cl 5.20 %; **H.R.M.S. [ES+]** found [MH^+]-Cl 617.074.

8.5.8 Synthesis of (*p*-cymene)Ru(II)(1-Ferrocenyl-3-(4-methylphenyl)propane-1,3-dione)Cl C8

Prepared using 1-ferrocenyl-3-(4-methylphenyl)propane-1,3-dione (0.14 g, 0.392 mmol) and purified by column chromatography, eluting 3:2 v/v petrol/ethyl acetate to give orange solid (0.18 g, 75 %).

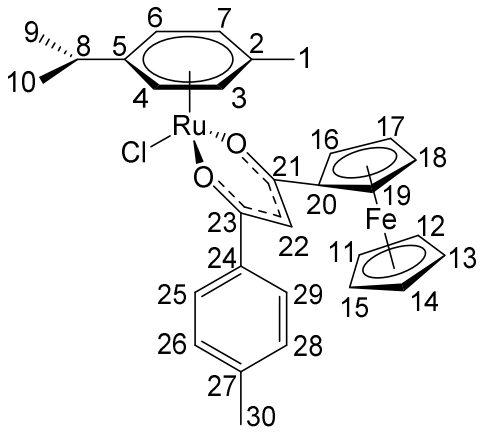

δ_H (500 MHz, $(CD_3)_2CO$); 7.74 (d, 2H, *J 8.3* Hz, ArH, $H_{25,29}$), 7.10 (d, 2H, *J 7.8* Hz, ArH, $H_{26,28}$), 6.02 (s, 1H, CH, H_{22}), 5.54 (broad d, 2H, *J 6.0* Hz, *p*-cymene ArH, $H_{4,6}$), 5.22 (d, 2H, *J 6.0* Hz, *p*-cymene ArH, $H_{3,7}$), 4.82 (t, 1H, *J 1.2* Hz, C_5H_4, $H_{16/19}$), 4.71 (t, 1H, *J 1.2* Hz, C_5H_4, $H_{16/19}$), 4.30 (m, 1H, C_5H_4, $H_{17/18}$), 4.27 (m, 1H, C_5H_4, $H_{17/18}$), 4.11 (s, 5H, C_5H_5, $H_{11\text{-}15}$), 2.90 (sept, 1H, *J 6.9* Hz, *p*-cymene $CH(Me)_2$, H_8), 2.24 (s, 3H, $ArCH_3$, H_{30}), 2.16 (s, 3H, *p*-cymene $ArCH_3$, H_1), 1.34 (d, 6H, *J* 6.9 Hz, *p*-cymene $C(CH_3)_2$, $H_{9,10}$); **δ_C**{^{1}H} (125 MHz, $(CD_3)_2CO$); 186.4 (quaternary CO, C_{21}), 178.4 (quaternary CO, C_{23}), 141.4 (quaternary ArC, C_{24}), 137.7 (quaternary ArC, C_{27}), 129.6 (ArCH, $C_{25,29}$), 127.9 (ArCH, $C_{26,28}$), 99.4 (quaternary *p*-cymene, C_5), 97.8 (quaternary *p*-cymene, C_2), 93.0 (acac CH, C_{22}), 84.7 (*p*-cymene ArCH, $C_{4/6}$), 84.5 (*p*-cymene ArCH, $C_{4/6}$), 82.2 (quaternary Cp, C_{20}), 79.9 (*p*-cymene ArCH, $C_{3,7}$), 71.6 (Cp CH, $C_{16/19}$), 71.5 (Cp CH, $C_{16/19}$), 70.9 (Cp ring, $C_{11\text{-}15}$), 69.9 (Cp CH, $C_{17/18}$), 68.6 (Cp CH, $C_{17/18}$), 31.7 (*p*-cymene CH, C_8), 22.7 (*p*-cymene $C(CH_3)$, $C_{9/10}$), 22.6 (*p*-cymene $C(CH_3)$, $C_{9/10}$), 21.4 (PhMe, C_{30}), 17.8 (*p*-cymene CH_3, C_1); **Analysis**: Calculated C 58.50, H 5.07, Cl 5.76 %, Found C 58.60, H 5.10, Cl 5.80 %; **H.R.M.S. [ES+]** found [MH^+]-Cl 581.072.

8.5.9 Synthesis of (*p*-cymene)Ru(II)(1-Ferrocenyl-3-(3-methylphenyl)propane-1,3-dione)Cl C9

Prepared using 1-ferrocenyl-3-(3-methylphenyl)propane-1,3-dione (0.14 g, 0.392 mmol) and purified by column chromatography, eluting 1:1 v/v petrol/ethyl acetate to give orange solid (0.23 g, 93 %).

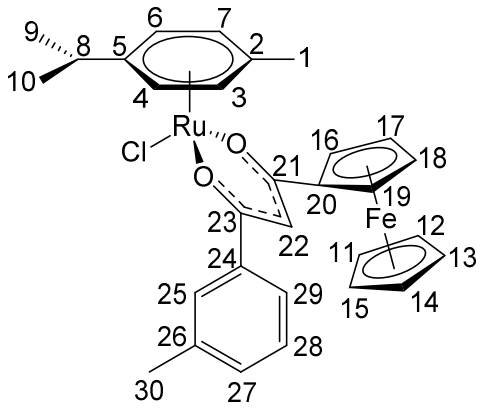

δ_H (500 MHz, $(CD_3)_2CO$); 7.79 (s, 1H, ArH, H_{25}), 7.75 (m, 1H, ArH, H_{29}), 7.29 (m, 2H, ArH, $H_{27,28}$), 6.15 (s, 1H, CH, H_{22}), 5.68 (dt, 2H, *J 4.9, 1.5* Hz, *p*-cymene ArH, $H_{4,6}$), 5.36 (dt, 2H, *J 4.9, 1.5* Hz, *p*-cymene ArH, $H_{3,7}$), 4.96 (t, 1H, *J 1.2* Hz, C_5H_4, $H_{16/19}$), 4.84 (t, 1H, *J 1.2* Hz, C_5H_4, $H_{16/19}$), 4.44 (m, 1H, C_5H_4, $H_{17/18}$), 4.40 (m, 1H, C_5H_4, $H_{17/18}$), 4.24 (s, 5H, C_5H_5, $H_{11\text{-}15}$), 3.04 (sept, 1H, *J 6.9* Hz, *p*-cymene $CH(Me)_2$, H_8), 2.42 (s, 3H, $ArCH_3$, H_{30}), 2.29 (s, 3H, *p*-cymene $ArCH_3$, H_1), 1.47 (d, 6H, *J 7.1* Hz, *p*-cymene $C(CH_3)_2$, $H_{9,10}$); **δ_C**{^{1}H} (125 MHz, $(CD_3)_2CO$); 186.6 (quaternary CO, C_{21}), 178.6 (quaternary CO, C_{23}), 140.5 (quaternary ArC, C_{24}), 138.4 (quaternary ArC, C_{26}), 131.8 (ArCH, C_{25}), 128.8 (ArCH, C_{29}), 128.5 (ArCH, C_{27}), 125.1 (ArCH, C_{28}), 99.4 (quaternary *p*-cymene, C_5), 97.8 (quaternary *p*-cymene, C_2), 93.4 (acac CH, C_{22}), 84.6 (*p*-cymene ArCH. $C_{4/6}$), 84.5 (*p*-cymene ArCH, $C_{4/6}$), 82.1 (quaternary Cp, C_{20}), 80.0 (*p*-cymene ArCH, $C_{3/7}$), 80.0 (*p*-cymene ArCH, $C_{3/7}$), 71.6 (Cp CH, $C_{16/19}$), 71.6 (Cp CH, $C_{16/19}$), 70.9 (Cp ring, $C_{11\text{-}15}$), 69.9 (Cp CH, $C_{17/18}$), 68.7 (Cp CH, $C_{17/18}$), 31.7 (*p*-cymene CH, C_8), 22.7 (*p*-cymene $C(CH_3)$, $C_{9/10}$), 22.6 (*p*-cymene $C(CH_3)$, $C_{9/10}$), 21.5 ($ArCH_3$, C_{30}), 17.8 (*p*-cymene CH_3, C_1); **Analysis**: Calculated C 58.50, H 5.07 %, Found C 57.91, H 5.06 %; **H.R.M.S. [ES+]** found [MH^+]-Cl 581.072.

8.5.10 Synthesis of (*p*-cymene)Ru(II)(1-Ferrocenyl-3-(3,5-dimethylphenyl)propane-1,3-dione)Cl C10

Prepared using 1-ferrocenyl-3-(3,5-dimethylphenyl)propane-1,3-dione (0.14 g, 0.392 mmol) and purified by column chromatography, eluting 3:2 v/v petrol/ethyl acetate to give orange solid (0.20 g, 80 %).

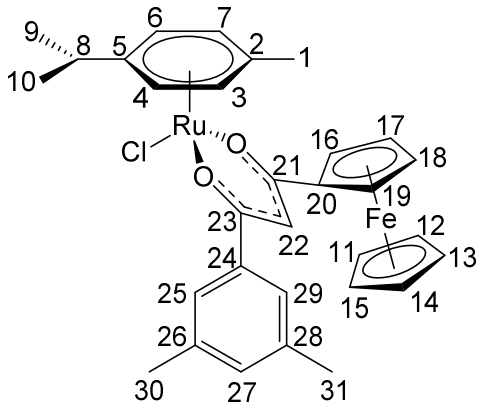

δ_H (500 MHz, $(CD_3)_2CO$); 7.45 (s, 2H, ArH, $H_{25,29}$), 6.98 (s, 1H, ArH, H_{27}), 6.01 (s, 1H, CH, H_{22}), 5.54 (t, 2H, *J 4.0* Hz, *p*-cymene ArH, $H_{4,6}$), 5.22 (d, 2H, *J 4.4* Hz, *p*-cymene ArH, $H_{3,7}$), 4.82 (broad s, 1H, C_5H_4, $H_{16/19}$), 4.69 (broad s, 1H, C_5H_4, $H_{16/19}$), 4.30 (broad s, 1H, C_5H_4, $H_{17/18}$), 4.26 (broad s, 1H, C_5H_4, $H_{17/18}$), 4.10 (s, 5H, C_5H_5, $H_{11\text{-}15}$), 2.90 (sept, 1H, *J 6.9* Hz, *p*-cymene $CH(Me)_2$, H_8), 2.21 (s, 6H, $ArCH_3$, $C_{30,31}$), 2.16 (s, 3H, *p*-cymene $ArCH_3$, H_1), 1.34 (d, 6H, *J 6.9* Hz, *p*-cymene $C(CH_3)_2$, $H_{9,10}$); **δ_C**{^{1}H} (125 MHz, $(CD_3)_2CO$); 185.5 (quaternary CO, C_{21}), 178.0 (quaternary CO, C_{23}), 139.6 (quaternary ArC, C_{24}), 137.4 (quaternary ArC, $C_{26,28}$), 131.7 (ArCH, C_{27}), 124.9 (ArCH, $C_{25/29}$), 124.5 (ArCH, $C_{25/29}$), 98.5 (quaternary *p*-cymene, C_5), 96.9 (quaternary *p*-cymene, C_2), 92.5 (acac CH, C_{22}), 83.8 (*p*-cymene ArCH, $C_{4/6}$), 83.6 (*p*-cymene ArCH, $C_{4/6}$), 81.3 (quaternary Cp, C_{20}), 79.1 (*p*-cymene ArCH, $C_{3/7}$), 79.0 (*p*-cymene ArCH, $C_{3/7}$), 70.7 (Cp CH, $C_{16/19}$), 70.6 (Cp CH, $C_{16/19}$), 70.0 (Cp ring, $C_{11\text{-}15}$), 69.0 (Cp CH, $C_{17/18}$), 67.8 (Cp CH, $C_{17/18}$), 30.8 (*p*-cymene CH, C_8), 22.7 (*p*-cymene $C(CH_3)$, $C_{9/10}$), 22.6 (*p*-cymene $C(CH_3)$, $C_{9/10}$), 20.6 ($ArCH_3$, $C_{30,31}$), 17.9 (*p*-cymene CH_3, C_1); **Analysis**: Calculated C 59.01, H 5.28, Cl 5.63 %, Found C 59.30, H 5.30, Cl 5.50 %; **H.R.M.S. [ES+]** found $[MH^+]$-Cl 595.090.

8.5.11 Synthesis of (*p*-cymene)Ru(II)(1-Ferrocenyl-3-(4-fluorophenyl)propane-1,3-dione)Cl C11

Prepared using 1-ferrocenyl-3-(4-fluorophenyl)propane-1,3-dione (0.14 g, 0.392 mmol) and purified by column chromatography, eluting 3:2 v/v petrol/ethyl acetate to give orange solid (0.12 g, 82 %).

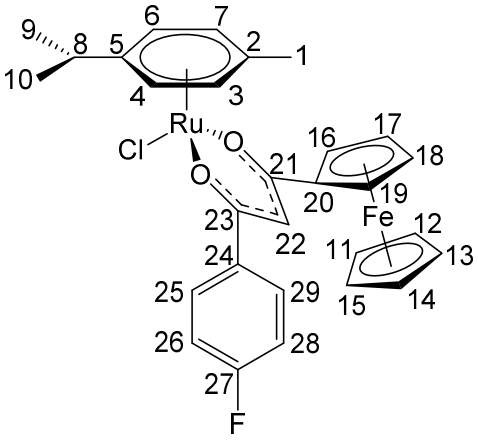

δ_H (500 MHz, $(CD_3)_2CO$); 7.91 (q, 2H, *J 5.5, 3.2* Hz, ArH, $H_{28/26}$), 7.04 (t, 2H, *J 8.7* Hz, ArH, $H_{26,28}$), 6.02 (s, 1H, CH, H_{22}), 5.56 (d, 2H, *J 6.4* Hz, *p*-cymene ArH, $H_{4,6}$), 5.24 (t, 2H, *J 4.4* Hz, *p*-cymene ArH, $H_{3,7}$), 4.83 (t, 1H, *J 1.2* Hz, C_5H_4 $H_{16/19}$), 4.73 (t, 1H, *J 1.2* Hz, C_5H_4, $H_{16/19}$), 4.32 (broad q, 1H, *J 2.4, 1.1* Hz, C_5H_4, $H_{17/18}$), 4.28 (broad q, 1H, *J 2.4, 1.1* Hz, C_5H_4, $H_{17/18}$), 4.11 (s, 5H, C_5H_4, $H_{11\text{-}15}$), 2.90 (sept, 1H, *J 6.9* Hz, *p*-cymene $CH(Me)_2$, H_8), 2.16 (s, 3H, *p*-cymene $ArCH_3$, H_1), 1.33 (d, 6H, *J 6.9* Hz, *p*-cymene $C(CH_3)_2$, $H_{9,10}$); **δ_C**{^{1}H} (125 MHz, $(CD_3)_2CO$); 187.0 (quaternary CO, C_{21}), 177.0 (quaternary CO, C_{23}), 165.0 (d, ArCF, *J 248.6* Hz, C_{27}), 136.9 (d, quaternary ArC, *J 3.1* Hz, C_{24}), 130.3 (d, ArCH, *J 8.8* Hz, $C_{25,29}$), 115.6 (d, ArCH *J 21.8* Hz, $C_{26,28}$), 99.5 (quaternary *p*-cymene, C_5), 97.8 (quaternary *p*-cymene, C_2), 93.2 (acac CH, C_{22}), 84.6 (*p*-cymene ArCH, $C_{4/6}$), 84.5 (*p*-cymene ArCH, $C_{4/6}$), 82.0 (quaternary Cp, C_{20}), 80.0 (*p*-cymene ArCH, $C_{3,7}$), 71.7 (Cp CH, $C_{16/19}$), 71.7 (Cp CH, $C_{16/19}$), 70.9 (Cp ring, $C_{11\text{-}15}$), 69.9 (Cp CH, $C_{17/18}$), 68.8 (Cp CH, $C_{17/18}$), 31.7 (*p*-cymene CH, C_8), 22.7 (*p*-cymene $C(CH_3)$, $C_{9/10}$), 22.6 (*p*-cymene $C(CH_3)$ $C_{9/10}$), 17.9 (*p*-cymene CH_3, C_1); **Analysis**: Calculated C 56.19, H 4.55, Cl 5.72 %, Found C 56.20, H 4.95, Cl 5.95 %; **H.R.M.S. [ES+]** found $[MH^+]$-Cl 585.047.

8.5.12 Synthesis of (*p*-cymene)Ru(II)(1-Ferrocenyl-3-(3-fluorophenyl)propane-1,3-dione)Cl C12

Prepared using 1-ferrocenyl-3-(3-fluorophenyl)propane-1,3-dione (0.14 g, 0.392 mmol) and purified by column chromatography, eluting 3:2 v/v petrol/ethyl acetate to give orange solid (0.19 g, 78 %).

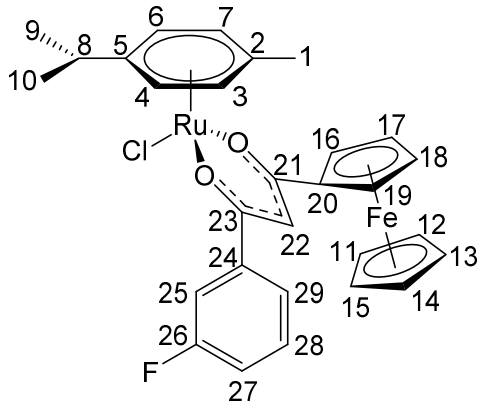

δ_H (500 MHz, $(CD_3)_2CO$); 7.70 (broad dt, 1H, *J 7.8* Hz, ArH, H_{25}), 7.61 (dq, 1H, *J 10.4, 1.6, 0.9* Hz, ArH, H_{29}), 7.36 (m, 1H, ArH, H_{27}), 7.14 (td, 1H, *J 8.3, 2.3* Hz, ArH, H_{28}), 6.08 (s, 1H, CH, H_{22}), 5.62 (d, 2H, *J 6.2* Hz, *p*-cymene ArH, $H_{4,6}$), 5.29 (t, 2H, *J 4.7* Hz, *p*-cymene ArH, $H_{3,7}$), 4.89 (quintet, 1H, *J 1.2* Hz, C_5H_4, $H_{16/19}$), 4.81 (quintet, 1H, *J 1.2* Hz, C_5H_4, $H_{16/19}$), 4.37 (m, 1H, C_5H_4, $H_{17/18}$), 4.34 (m, 1H, C_5H_4, $H_{17/18}$), 4.15 (s, 5H, C_5H_5, $H_{11\text{-}15}$), 2.94 (sept, 1H, *J 6.9* Hz, *p*-cymene $CH(Me)_2$, H_8), 2.20 (s, 3H, *p*-cymene $ArCH_3$, H_1), 1.38 (d, 6H, *J 7.1* Hz, *p*-cymene $C(CH_3)_2$, $H_{9,10}$); **δ_C**{^{1}H} (125 MHz, $(CD_3)_2CO$); 187.6 (quaternary CO, C_{21}), 179.1 (quaternary CO, C_{23}), 164.6 (d, quaternary ArCF, *J 243.9* Hz, C_{26}), 143.0 (d, quaternary ArC, *J 6.7* Hz, C_{24}), 130.8 (d, ArCH, *J 8.3* Hz, C_{28}), 123.6 (d ArCH *J 2.6* Hz, C_{29}), 117.7 (d, ArCH *J 21.3* Hz, C_{25}), 114.5 (d, ArCH *J 22.8* Hz, C_{27}), 99.5 (quaternary *p*-cymene, C_5), 97.9 (quaternary *p*-cymene, C_2), 93.6 (acac CH, C_{22}), 84.6 (*p*-cymene ArCH, $C_{4/6}$), 84.5 (*p*-cymene ArCH, $C_{4/6}$), 81.8 (quaternary Cp, C_{20}), 80.0 (*p*-cymene ArCH, $C_{3/7}$), 80.0 (*p*-cymene ArCH, $C_{3/7}$), 71.9 (Cp CH, $C_{16/19}$), 71.8 (Cp CH, $C_{16/19}$), 71.0 (Cp ring, $C_{11\text{-}15}$), 70.0 (Cp CH, $C_{17/18}$), 68.9 (Cp CH, $C_{17/18}$), 31.7 (*p*-cymene CH, C_8), 22.7 (*p*-cymene $C(CH_3)$, $C_{9/10}$), 22.6 (*p*-cymene $C(CH_3)$, $C_{9/10}$), 17.9 (*p*-cymene CH_3, C_1); **Analysis**: Calculated C 56.19, H 4.55, Cl 5.72 %, Found C 56.30, H 4.85, Cl 5.30 %; **H.R.M.S. [ES+]** found $[MH^+]$-Cl 585.048.

8.5.13 Synthesis of (*p*-cymene)Ru(II)(1-Ferrocenyl-3-(2-fluorophenyl)propane-1,3-dione)Cl C13

Prepared using 1-ferrocenyl-3-(2-fluorophenyl)propane-1,3-dione (0.14 g, 0.392 mmol) and purified by column chromatography, eluting 3:2 v/v petrol/ethyl acetate to give orange solid (0.18 g, 72 %).

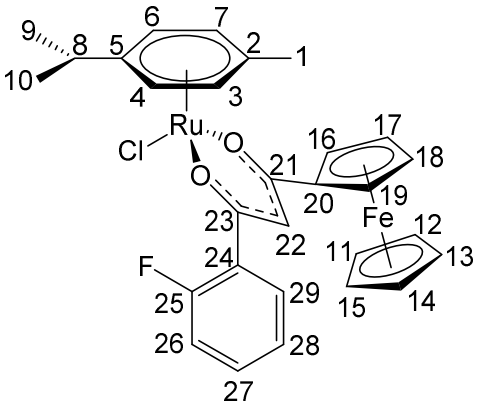

δ_H (500 MHz, $(CD_3)_2CO$); 7.87 (td, 1H, *J 7.7, 1.2* Hz, ArH, H_{29}), 7.49 (m, 1H, ArH, H_{26}), 7.28 (t, 1H, *J 7.6* Hz, ArH, H_{28}), 7.19 (dd, 1H, *J 11.8, 1.2* Hz, ArH, H_{27}), 6.02 (s, 1H, CH, H_{22}), 5.71 (d, 2H, *J 4.8* Hz, *p*-cymene ArH, $H_{4,6}$), 5.39 (t, 2H, *J 4.8* Hz, *p*-cymene ArH, $H_{3,7}$), 4.93 (d, 1H, *J 0.8* Hz, C_5H_4, $H_{16/19}$), 4.75 (d, 1H, *J 0.9* Hz, C_5H_4, $H_{16/19}$), 4.49 (broad t, 1H, C_5H_4, $H_{17/18}$), 4.45 (broad t, 1H, C_5H_4, $H_{17/18}$), 4.27 (s, 5H, C_5H_5, $H_{11\text{-}15}$), 3.04 (sept, 1H, *J 6.9* Hz, *p*-cymene $CH(Me)_2$, H_8), 1.99 (s, 3H, *p*-cymene $ArCH_3$, H_1), 1.48 (d, 6H, *J 6.9* Hz, *p*-cymene $C(CH_3)_2$, $H_{9,10}$); **δ_C**{^{1}H} (125 MHz, $(CD_3)_2CO$); 187.1 (quaternary CO, C_{21}), 174.8 (d, quaternary CO, *J 3.6* Hz, C_{22}), 160.6 (d, ArCF, *J 250.1* Hz, C_{25}), 132.3 (d, ArCH, *J 8.8* Hz, C_{29}), 131.7 (d, ArCH, *J 3.1* Hz, C_{28}), 129.3 (d, quaternary ArC, *J 11.9* Hz, C_{24}), 125.1 (d, ArCH, *J 3.6* Hz, C_{27}), 116.9 (d, ArCH, *J 23.9* Hz, C_{26}), 99.5 (quaternary *p*-cymene, C_5), 97.9 (d, acac CH, *J 5.2* Hz, C_{22}), 97.8 (quaternary *p*-cymene, C_2), 84.5 (*p*-cymene ArCH, $c_{4/6}$), 84.4 (*p*-cymene ArCH, $C_{4/6}$), 81.7 (quaternary Cp, C_{20}), 79.9 (*p*-cymene ArCH, $C_{3,7}$), 71.9 (Cp CH, $C_{16/19}$), 71.9 (Cp CH, $C_{16/19}$), 71.1 (Cp ring, $C_{11\text{-}15}$), 69.9 (Cp CH, $C_{17/18}$), 68.8 (Cp CH, $C_{17/18}$), 31.7 (*p*-cymene CH, C_8), 22.7 (*p*-cymene $C(CH_3)$, $C_{9/10}$), 22.6 (*p*-cymene $C(CH_3)$, $C_{9/10}$), 17.9 (*p*-cymene CH_3, C_1); **Analysis**: Calculated C 56.19, H 4.55, Cl 5.72 %, Found C 55.90, H 4.70, Cl 5.90 %; **H.R.M.S. [ES+]** found $[MH^+]$-Cl 585.049.

8.5.14 Synthesis of (*p*-cymene)Ru(II)(1-Ferrocenyl-3-(3,5-difluorophenyl)propane-1,3-dione)Cl C14

Prepared using 1-ferrocenyl-3-(3,5-difluorophenyl)propane-1,3-dione (0.15 g, 0.392 mmol) and purified by column chromatography, eluting 3:2 v/v petrol/ethyl acetate to give orange solid (0.19 g, 76 %).

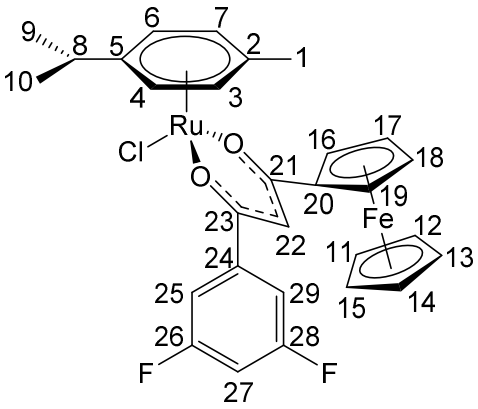

δ_H (500 MHz, $(CD_3)_2CO$); 7.45 (d, 2H, *J 6.9* Hz, ArH, $H_{25,29}$), 6.99 (tt, 1H, *J 8.9, 2.1* Hz, ArH, H_{27}), 6.05 (s, 1H, CH, H_{22}), 5.60 (d, 2H, *J 6.0* Hz, *p*-cymene ArH, $H_{4,6}$), 5.28 (t, 2H, *J 5.0* Hz, *p*-cymene ArH, $H_{3,7}$), 4.87 (broad s, 1H, C_5H_4, $H_{16/19}$), 4.83 (broad s, 1H, C_5H_4, $H_{16/19}$), 4.36 (broad s, 1H, C_5H_4, $H_{17/18}$), 4.32 (broad s, 1H, C_5H_4, $H_{17/18}$), 4.12 (s, 5H, C_5H_5, H_{11-15}), 2.90 (sept, 1H, *J 7.0* Hz, *p*-cymene $CH(Me)_2$, H_8), 2.17 (s, 3H, $ArCH_3$, H_1), 1.34 (d, 6H, *J 6.9* Hz, *p*-cymene $C(CH_3)_2$, $H_{9,10}$); **δ_C**{^{1}H} (125 MHz, $(CD_3)_2CO$); 188.4 (quaternary CO, C_{21}), 174.6 (quaternary CO, C_{23}), 163.7 (dd, ArCF, *J 264.0, 12.8* Hz, $C_{26,28}$), 144.3 (quaternary ArC, *J 8.3* Hz, C_{24}), 110.7 (dd, ArCH, *J 20.2, 6.2* Hz, $C_{25,29}$), 105.9 (t, ArCH, *J 26.0* Hz, C_{27}), 99.6 (quaternary *p*-cymene, C_5), 98.0 (quaternary *p*-cymene, C_2), 93.7 (acac CH, C_{22}), 84.6 (*p*-cymene ArCH, $C_{4/6}$), 84.5 (*p*-cymene ArCH, $C_{4/6}$), 81.6 (quaternary Cp, C_{20}), 80.0 (*p*-cymene ArCH, $C_{3,7}$), 72.1 (Cp CH, $C_{16/19}$), 72.0 (Cp CH, $C_{16/19}$), 71.0 (Cp ring, C_{11-15}), 70.0 (Cp CH, $C_{17/18}$), 69.1 (Cp CH, $C_{17/18}$), 31.7 (*p*-cymene CH, C_8), 22.7 (*p*-cymene $C(CH_3)$, $C_{9/10}$), 22.6 (*p*-cymene $C(CH_3)$, $C_{9/10}$), 17.9 (*p*-cymene CH_3, C_1); **Analysis**: Calculated C 54.60, H 4.27, Cl 5.56 %, Found C 55.20, H 4.40, Cl 5.57 %; **H.R.M.S. [ES+]** found $[MH^+]$-Cl 603.040.

8.5.15 Synthesis of (*p*-cymene)Ru(II)(1-Ferrocenyl-3-(4-chlorophenyl)propane-1,3-dione)Cl C15

Prepared using 1-ferrocenyl-3-(4-chlorophenyl)propane-1,3-dione (0.14 g, 0.392 mmol) and purified by column chromatography, eluting 3:2 v/v petrol/ethyl acetate to give orange solid (0.23 g, 91 %).

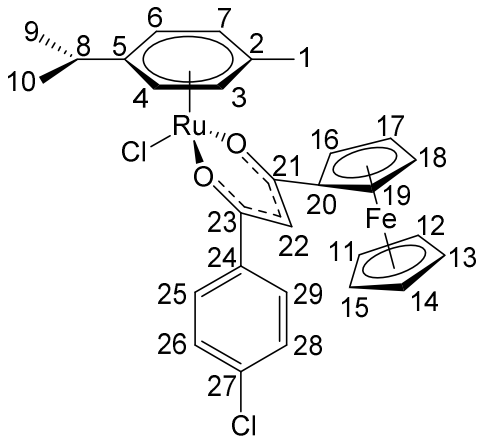

δ_H (500 MHz, $(CD_3)_2CO$); 7.86 (broad d, 2H, *J 8.7* Hz, ArH, $H_{25,29}$), 7.31 (broad d, 2H, *J 8.7* Hz, ArH, $H_{26,28}$), 6.03 (s, 1H, CH, H_{22}), 5.56 (d, 2H, *J 6.0* Hz, *p*-cymene ArH, $H_{4,6}$), 5.24 (t, 2H, *J 4.6* Hz, *p*-cymene ArH, $H_{3,7}$), 4.84 (t, 1H, *J 1.4* Hz, C_5H_4, $H_{16/16}$), 4.74 (t, 1H, *J 1.2* Hz, C_5H_4, $H_{16/19}$), 4.33 (q, 1H, *J 2.3, 1.2* Hz, C_5H_4, $H_{17/18}$), 4.29 (q, 1H, *J 2.3, 1.4* Hz, C_5H_4 $H_{17/18}$), 4.11 (s, 5H, C_5H_5, $H_{11\text{-}15}$), 2.90 (sept, 1H, *J 6.9* Hz, $CH(Me)_2$, H_8), 2.16 (s, 3H, *p*-cymene $ArCH_3$, H_1), 1.33 (d, 6H, *J 6.9* Hz, *p*-cymene $C(CH_3)_2$, $H_{9,10}$); **$\delta_C\{^1H\}$** (125 MHz, $(CD_3)_2CO$); 187.3 (quaternary CO, C21), 176.8 (quaternary CO, C_{23}), 139.2 (quaternary ArC, C_{24}), 136.6 (quaternary ArC, C_{27}), 129.6 (ArCH. $C_{25,29}$), 129.0 (ArCH, $C_{26,28}$), 99.5 (quaternary *p*-cymene, C_5), 97.8 (quaternary *p*-cymene, C_2), 93.4 (acac CH, C_{22}), 84.6 (*p*-cymene ArCH, $C_{4/6}$), 84.5 (*p*-cymene ArCH, $C_{4/6}$), 81.9 (quaternary Cp, C_{20}), 80.0 (*p*-cymene ArCH, $C_{3,7}$), 71.9 (Cp CH, $C_{16/19}$), 71.8 (Cp CH. $C_{16/19}$), 71.0 (Cp ring, $C_{11\text{-}15}$), 70.0 (Cp CH, $C_{17/18}$), 68.8 (Cp CH, $C_{17/18}$), 31.74 (*p*-cymene CH, C_8), 22.7 (*p*-cymene $C(CH_3)$, $C_{9/10}$), 22.6 (*p*-cymene $C(CH_3)$, $C_{9/10}$), 17.9 (*p*-cymene CH_3, C1); **Analysis**: Calculated C 54.74, H 4.44, Cl 11.14 %, Found C 54.90, H 4.50, Cl 11.10 %; **H.R.M.S. [ES+]** found $[MH^+]$-Cl 601.016.

8.5.16 Synthesis of (*p*-cymene)Ru(II)(1-Ferrocenyl-3-(3-chlorophenyl)propane-1,3-dione)Cl C16

Prepared using 1-ferrocenyl-3-(3-chlorophenyl)propane-1,3-dione (0.14 g, 0.392 mmol) and purified by column chromatography, eluting 3:2 v/v petrol/ethyl acetate to give orange solid (0.23 g, 92 %).

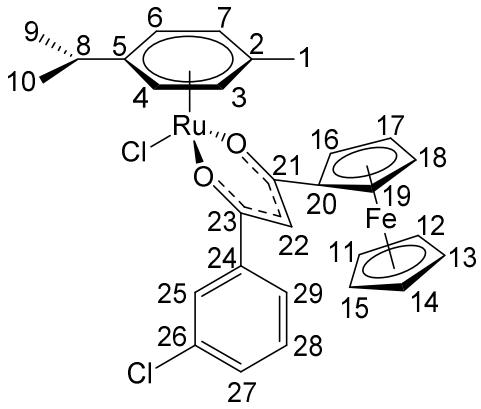

δ_H (500 MHz, $(CD_3)_2CO$); 7.99 (t, 1H, *J 1.8* Hz, ArH, H_{25}), 7.93 (dt, 1H, *J 7.8, 1.4* Hz, ArH, H_{29}), 7.52 (dq, 1H, *J 8.0, 1.1* Hz, ArH, H_{27}), 7.46 (t, 1H, *J 7.8* Hz, ArH, H_{29}), 6.20 (s, 1H, CH, H_{22}), 5.73 (dd, 2H, *J 4.8, 1.4* Hz, *p*-cymene ArH, $H_{4,6}$), 5.42 (t, 2H, *J 5.0* Hz, *p*-cymene ArH, $H_{3,7}$), 5.01 (quin, 1H, *J 1.3* Hz, C_5H_4, $H_{16/19}$), 4.93 (pent, 1H, *J 1.3* Hz, C_5H_4, $H_{16/19}$), 4.49 (m, 1H, C_5H_4, $H_{17/18}$), 4.45 (m, 1H, C_5H_4, $H_{17/18}$), 4.27 (s, 5H, C_5H_5, $H_{11\text{-}15}$), 3.06 (sept, 1H, *J 6.9* Hz, *p*-cymene $CH(Me)_2$, H_8), 2.32 (s, 3H, *p*-cymene $ArCH_3$, H_1), 1.50 (d, 6H, *J 7.1* Hz, *p*-cymene $C(CH_3)_2$, $H_{9,10}$); **δ_C**{^{1}H} (125 MHz, $(CD_3)_2CO$); 187.7 (quaternary CO, C_{21}), 176.3 (quaternary CO, C_{23}), 142.6 (ArCCl, C_{26}), 134.6 (quaternary ArC, C_{24}), 130.9 (ArCH, C_{25}), 130.7 (ArCH, C_{29}), 127.8 (ArCH, C_{27}), 126.2 (ArCH, C_{28}), 99.5 (quaternary *p*-cymene, C_5), 97.6 (quaternary *p*-cymene, C_2), 93.6 (acac CH, C_{22}), 84.6 (*p*-cymene ArCH, $C_{4/6}$), 84.5 (*p*-cymene ArCH, $C_{4/6}$), 81.8 (quaternary Cp, C_{20}), 80.0 (*p*-cymene ArCH, $C_{3/7}$), 80.0 (*p*-cymene ArCH), 71.9 (Cp CH, $C_{16/19}$), 71.9 (Cp CH, $C_{16/19}$), 71.0 (Cp ring, $C_{11\text{-}15}$), 70.0 (Cp CH, $C_{17/18}$), 68.9 (Cp CH, $C_{17/18}$), 31.7 (*p*-cymene CH, C_8), 22.7 (*p*-cymene $C(CH_3)$, $C_{9/10}$), 22.6 (*p*-cymene $C(CH_3)$, $C_{9/10}$), 17.9 (*p*-cymene CH_3, C_1); **Analysis**: Calculated C 54.74, H 4.44 %, Found C 53.95, H 4.51 %; **H.R.M.S. [ES+]** found $[MH^+]$-Cl 601.0183.

8.5.17 Synthesis of (*p*-cymene)Ru(II)(1-Ferrocenyl-3-(3,5-dichlorophenyl)propane-1,3-dione)Cl C17

Prepared using 1-ferrocenyl-3-(3,5-dichlorophenyl)propane-1,3-dione (0.16 g, 0.392 mmol) and purified by column chromatography, eluting 3:2 v/v petrol/ethyl acetate to give orange solid (0.16 g, 61 %).

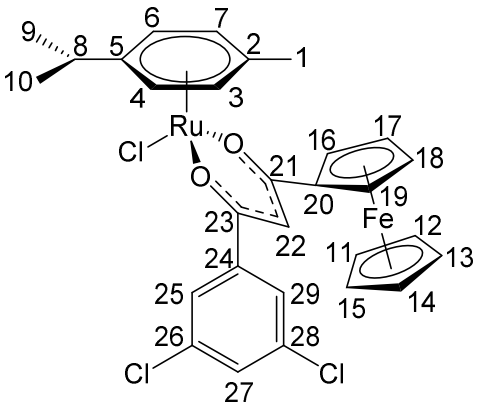

δ_H (500 MHz, $(CD_3)_2CO$); 7.94 (d, 2H, *J 1.8* Hz, ArH, $H_{25,29}$), 7.59 (t, 1H, *J 1.8* Hz, ArH, H_{27}), 6.21 (s, 1H, CH, H_{22}), 5.75 (d, 2H, *J 5.7* Hz, *p*-cymene ArH, $H_{4,6}$), 5.44 (t, 2H, *J 5.7* Hz, *p*-cymene ArH, $H_{3,7}$), 5.03 (d, 1H, *J 0.9* Hz, C_5H_4, $H_{16/19}$), 4.98 (d, 1H, *J 1.1* Hz, C_5H_4, H16/19), 4.52 (broad t, 1H, C_5H_4, $H_{17/18}$), 4.47 (broad t, 1H, C_5H_4, $H_{17/18}$), 4.27 (s, 5H, C_5H_5, $H_{11\text{-}15}$), 3.05 (sept, 1H, *J 6.9* Hz, *p*-cymene $CH(Me)_2$, H_8), 2.32 (s, 3H, *p*-cymene $ArCH_3$, H_1), 1.49 (d, 6H, *J 7.1* Hz, *p*-cymene $C(CH_3)_2$, $H_{9,10}$); **δ_C**{^{1}H} (125 MHz, $(CD_3)_2CO$); 187.7 (quaternary CO, C_{21}), 173.5 (quaternary CO, C_{23}), 143.0 (ArCCl, $C_{26,28}$), 134.6 (quaternary ArC, C_{24}), 129.4 (ArCH, $C_{25,29}$), 125.5 (ArCH, C_{27}), 98.7 (quaternary *p*-cymene, C_5), 97.0 (quaternary *p*-cymene, C_2), 92.9 (acac CH, C_{22}), 83.7 (*p*-cymene ArCH, $C_{4/6}$), 83.6 (*p*-cymene ArCH, $C_{4/6}$), 80.6 (quaternary Cp, C_{20}), 79.2 (*p*-cymene ArCH, $C_{3/7}$), 79.1 (*p*-cymene ArCH, $C_{3/7}$), 71.3 (Cp CH, $C_{16/19}$), 71.2 (Cp CH, $C_{16/19}$), 70.1 (Cp ring, $C_{11\text{-}15}$), 69.2 (Cp CH, $C_{17/18}$), 68.2 (Cp CH, $C_{17/18}$), 30.9 (*p*-cymene CH, C_8), 21.8 (*p*-cymene $C(CH_3)$, $C_{9/10}$), 21.7 (*p*-cymene $C(CH_3)$, $C_{9/10}$), 17.0 (*p*-cymene CH_3, C_1); **Analysis**: Calculated C 51.92, H 4.06, Cl 15.86 %, Found C 51.00, H 3.90, Cl 15.86 %; **H.R.M.S. [ES+]** found $[MH^+]$-Cl 634.979.

8.5.18 Synthesis of (*p*-cymene)Ru(II)(1-Ferrocenyl-3-(4-bromophenyl)propane-1,3-dione)Cl C18

Prepared using 1-ferrocenyl-3-(4-bromophenyl)propane-1,3-dione (0.16 g, 0.392 mmol) and purified by column chromatography, eluting 3:2 v/v petrol/ethyl acetate to give orange solid (0.17 g, 64 %).

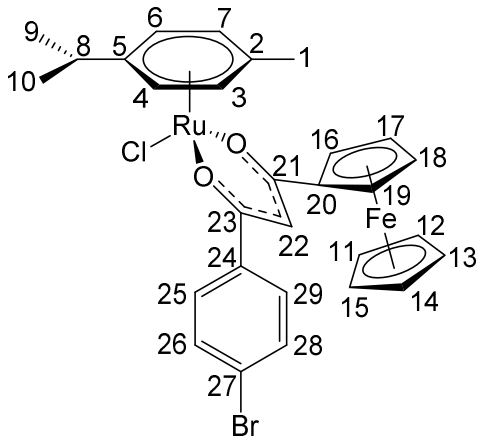

δ_H (500 MHz, $(CD_3)_2CO$); 7.78 (d, 2H, *J 8.7* Hz, ArH, $H_{25,29}$), 7.46 (d, 2H, *J 8.7* Hz, ArH, $H_{26,28}$), 6.03 (s, 1H, CH. H_{22}), 5.56 (d, 2H, *J 6.2* Hz, *p*-cymene ArH, $H_{4,6}$), 5.24 (t, 2H, *J 4.7* Hz, *p*-cymene ArH, $H_{3,7}$), 4.83 (q, 1H, *J 1.3* Hz, C_5H_4, $H_{16/19}$), 7.47 (q, 1H, *J 1.3* Hz, C_5H_4, $H_{16/19}$), 4.33 (m, 1H, C_5H_4, $H_{17/18}$), 4.29 (m, 1H, C_5H_4, $H_{17/18}$), 4.11 (s, 5H, C_5H_5, $H_{11\text{-}15}$), 2.90 (sept, 1H, *J 6.9* Hz, *p*-cymene $CH(Me)_2$, H_8), 2.16 (s, 3H, *p*-cymene $ArCH_3$, H_1), 1.33 (d, 6H, *J 6.9* Hz, *p*-cymene $C(CH_3)_2$, $H_{9,10}$), **δ_C**$\{^1H\}$ (125 MHz, $(CD_3)_2CO$); 194.4 (quaternary CO, C_{21}), 189.7 (quaternary CO, C_{23}), 139.7 (quaternary ArC, C_{24}), 132.0 (ArCH, $C_{25,29}$), 129.8 (ArCH, $C_{26,28}$), 106.7 (ArCBr, C_{27}), 99.5 (quaternary *p*-cymene, C_5), 97.8 (quaternary *p*-cymene, C_2), 93.4 (acac CH, C_{22}), 84.6 (*p*-cymene ArCH, $C_{4/6}$), 84.5 (*p*-cymene ArCH, $C_{4/6}$), 81.9 (quaternary Cp, C_{20}), 80.0 (*p*-cymene ArCH, $C_{3/7}$), 80.0 (*p*-cymene ArCH, $C_{3/7}$), 71.9 (Cp CH, $C_{16/19}$), 71.8 (Cp CH, $C_{16/19}$), 71.0 (Cp ring, $C_{11\text{-}15}$), 69.9 (Cp CH, $C_{17/18}$), 68.8 (Cp CH, $C_{17/18}$), 31.7 (*p*-cymene CH, C_8), 22.7 (*p*-cymene $C(CH_3)$, $C_{9/10}$), 22.6 (*p*-cymene $C(CH_3)$, $C_{9/10}$), 17.9 (*p*-cymene CH_3, C_1); **Analysis**: Calculated C 51.16, H 4.15 %, Found C 51.20, H 4.20 %; **H.R.M.S. [ES+]** found $[MH^+]$-Cl 644.968.

8.5.19 Synthesis of (*p*-cymene)Ru(II)(1-Ferrocenyl-3-(3-bromophenyl)propane-1,3-dione)Cl C19

Prepared using 1-ferrocenyl-3-(3-bromophenyl)propane-1,3-dione (0.16 g, 0.392 mmol) and purified by column chromatography, eluting 3:2 v/v petrol/ethyl acetate to give orange solid (0.23 g, 84 %).

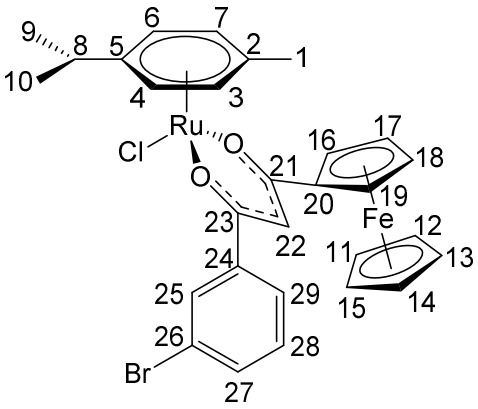

δ_H (500 MHz, $(CD_3)_2CO$); 7.99 (t, 1H, *J 1.7* Hz, ArH, H_{25}), 7.81 (dt, 1H, *J 7.8, 1.1* Hz, ArH, H_{29}), 7.51 (dq, 1H, *J 7.8, 0.9* Hz, ArH, H_{27}), 7.24 (t, 1H, *J 7.8* Hz, ArH, H_{28}), 6.03 (s, 1H, CH, H_{22}), 5.57 (dd, 2H, *J 5.0, 1.4* Hz, *p*-cymene ArH, $H_{4,6}$), 5.26 (t, 2H, *J 5.0* Hz, *p*-cymene ArH, $H_{3,7}$), 4.85 (quin, 1H, *J 1.2* Hz, C_5H_4, $H_{16/19}$), 4.77 (quin, 1H, *J 1.2* Hz, C_5H_4, $H_{16/19}$), 4.34 (m, 1H, C_5H_4, $H_{17/18}$), 4.30 (m, 1H, C_5H_4, $H_{17/18}$), 4.11 (s, 5H, C_5H_5, $H_{11\text{-}15}$), 2.90 (sept, 1H, *J 6.9* Hz, *p*-cymene $CH(Me)_2$, H_8), 2.16 (s, 3H, *p*-cymene $ArCH_3$, H_1), 1.33 (d, 6H, *J 7.1* Hz, *p*-cymene $C(CH_3)_2$, $H_{9,10}$); **δ_C**{^{1}H} (125 MHz, $(CD_3)_2CO$); 187.7 (quaternary CO, C_{21}), 176.2 (quaternary CO, C_{23}), 142.8 (quaternary ArC, C_{24}), 133.8 (ArCH, C_{25}), 130.9 (ArCH, C_{29}), 130.8 (ArCH, C_{28}), 126.6 (ArCH, C_{27}), 122.8 (ArCBr, C_{26}), 99.5 (quaternary *p*-cymene, C_5), 97.9 (quaternary *p*-cymene, C_2), 93.6 (acac CH, C_{22}), 84.6 (*p*-cymene ArCH, $C_{4/6}$), 84.5 (*p*-cymene ArCH, $C_{4/6}$), 81.7 (quaternary Cp, C_{20}), 80.1 (*p*-cymene ArCH, $C_{3/7}$), 80.0 (*p*-cymene ArCH, $C_{3/7}$), 72.0 (Cp CH, $C_{16/19}$), 71.9 (Cp CH, $C_{16/19}$), 71.0 (Cp ring, $C_{11\text{-}15}$), 70.0 (Cp CH, $C_{17/18}$), 68.9 (Cp CH, $C_{17/18}$), 31.7 (*p*-cymene CH, C_8), 22.7 (*p*-cymene $C(CH_3)$, $C_{9/10}$), 22.6 (*p*-cymene $C(CH_3)$, $C_{9/10}$), 17.9 (*p*-cymene CH_3, C_1); **Analysis**: Calculated C 51.16, H 4.15 %, Found C 51.06, H 4.18 %; **H.R.M.S. [ES+]** found $[MH^+]$-Cl 646.967.

8.5.20 Synthesis of (*p*-cymene)Ru(II)(1-Ferrocenyl-3-(4-iodophenyl)propane-1,3-dione)Cl C20

Prepared using 1-ferrocenyl-3-(4-iodophenyl)propane-1,3-dione) (0.18 g, 0.392 mmol) and purified by column chromatography, eluting 3:2 v/v petrol/ethyl acetate to give orange solid (0.29 g, 79 %).

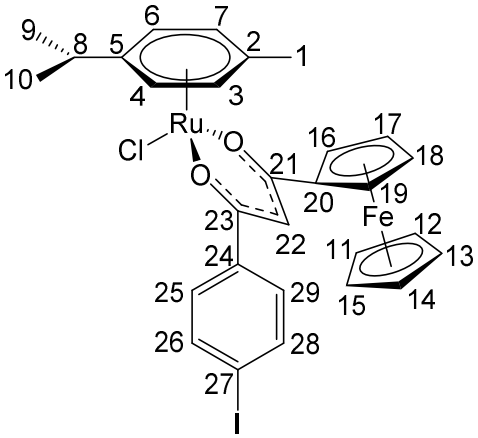

δ_H (500 MHz, $(CD_3)_2CO$); 7.66 (broad d, 4H, *J 12.8* Hz, ArH, $H_{25,26,28,29}$), 6.02 (s, 1H, CH, H_{22}), 5.56 (broad s, 2H, *p*-cymene ArH, $H_{4,6}$), 5.24 (broad s, 2H, *p*-cymene ArH, $H_{3,7}$), 4.83 (broad m, 1H, C_5H_4, $H_{16/19}$), 4.73 (broad m, 1H, C_5H_4, $H_{16/19}$), 4.31 (broad d, 2H, *J 18.6* Hz, C_5H_4, $H_{17,18}$), 4.11 (s, 5H, C_5H_5, $H_{11\text{-}51}$), 2.90 (sept, 1H, *J 6.8* Hz, *p*-cymene $CH(Me)_2$, H_8), 2.15 (s, 3H, *p*-cymene $ArCH_3$, H_1), 1.34 (d, 6H, *J 6.2* Hz, *p*-cymene $C(CH_3)_2$, $H_{9,10}$); **δ_C**{^{1}H} (125 MHz, $(CD_3)_2CO$); 187.1 (quaternary CO, C_{21}), 178.8 (quaternary CO, C_{23}), 140.2 (quaternary ArC, C_{24}), 138.2 (ArCH, $C_{25,29}$), 129.8 (ArCH, $C_{26,28}$), 105.9 (ArCl, C_{27}), 99.5 (quaternary *p*-cymene, C_5), 97.8 (quaternary *p*-cymene, C_2), 93.3 (acac CH, C_{22}), 84.6 (*p*-cymene ArCH, $C_{4/6}$), 84.5 (*p*-cymene ArCH, $C_{4/6}$), 81.9 (quaternary Cp, C_{20}), 80.0 (*p*-cymene ArCH, $C_{3/7}$), 80.0 (*p*-cymene ArCH, $C_{3/7}$), 71.9 (Cp CH, $C_{16/19}$), 71.8 (Cp CH, $C_{16/19}$), 71.0 (Cp ring, $C_{11\text{-}15}$), 69.9 (Cp CH, $C_{17/18}$), 68.8 (Cp CH, $C_{17/18}$), 31.7 (*p*-cymene CH, C_8), 22.7 (*p*-cymene $C(CH_3)$, $C_{9/10}$), 22.6 (*p*-cymene $C(CH_3)$, $C_{9/10}$), 17.9 (*p*-cymene CH_3, C_1); **Analysis**: Calculated C 47.86, H 3.88 %, Found C 48.00, H 3.90 %; **H.R.M.S. [ES+]** found $[MH^+]$-Cl 692.955.

8.5.21 Synthesis of (*p*-cymene)Ru(II)(1-Ferrocenyl-3-(3-iodophenyl)propane-1,3-dione)Cl C21

Prepared using 1-ferrocenyl-3-(3-iodophenyl)propane-1,3-dione (0.18 g, 0.392 mmol) and purified by column chromatography, eluting 3:2 v/v petrol/ethyl acetate to give orange solid (0.23 g, 80 %).

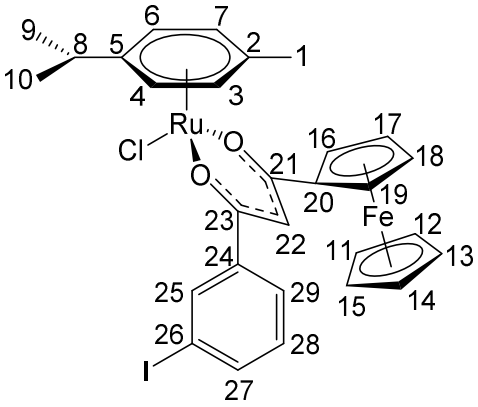

δ_H (500 MHz, $(CD_3)_2CO$); 8.20 (t, 1H, *J 1.6* Hz, ArH, H_{25}), 7.83 (dt, 1H, *J 8.0, 1.2* Hz, ArH, H_{29}), 7.71 (dt, 1H, *J 7.8, 0.7* Hz, ArH, H_{27}), 7.10 (t, 1H, *J 7.8* Hz, ArH, H_{28}), 6.01 (s, 1H, CH, H_{22}), 5.57 (dt, 2H, *J 4.81, 1.3* Hz, *p*-cymene ArH, $H_{4,6}$), 5.26 (t, 2H, *J 5.0* Hz, *p*-cymene ArH, $H_{3,7}$), 4.85 (t, 1H, *J 1.2* Hz, C_5H_4, $H_{16/19}$), 4.76 (t, 1H, *J 1.2* Hz, C_5H_4, $H_{16/19}$), 4.34 (m, 1H, C_5H_4, $H_{17/18}$), 4.30 (m, 1H, C_5H_4, $H_{17/18}$), 4.11 (s, 5H, C_5H_5, $H_{11\text{-}15}$), 2.90 (sept, 1H, *J 6.9* Hz, *p*-cymene $CH(Me)_2$, H_8), 2.16 (s, 3H, *p*-cymene $ArCH_3$, H_1), 1.34 (d, 6H, *J 7.1* Hz, *p*-cymene $C(CH_3)_2$, $H_{9,10}$); **δ_C**{^{1}H} (125 MHz, $(CD_3)_2CO$); 187.6 (quaternary CO, C_{21}), 176.3 (quaternary CO, C_{23}), 142.7 (quaternary ArC, C_{24}), 139.9 (ArCH, C_{25}), 136.9 (ArCH, C_{29}), 131.0 (ArCH, C_{28}), 127.0 (ArCH, C_{27}), 105.9 (ArCl, C_{26}), 99.5 (quaternary *p*-cymene, C_5), 97.8 (quaternary *p*-cymene, C_2), 93.5 (acac CH, C_{22}), 84.5 (*p*-cymene ArCH, $C_{4/6}$), 84.5 (*p*-cymene ArCH, $C_{4/6}$), 81.8 (quaternary Cp, C_{20}), 80.1 (*p*-cymene ArCH, $C_{3/7}$), 80.0 (*p*-cymene ArCH, $C_{3/7}$), 71.9 (Cp CH, $C_{16/19}$), 71.9 (Cp CH, $C_{16/19}$), 71.0 (Cp ring, $C_{11\text{-}15}$), 70.0 (Cp CH, $C_{17/18}$), 68.9 (Cp CH, $C_{17/18}$), 31.7 (*p*-cymene CH, C_8), 22.7 (*p*-cymene $C(CH_3)$, $C_{9/10}$), 22.6 (*p*-cymene $C(CH_3)$, $C_{9/10}$), 17.8 (*p*-cymene CH_3, C_1); **Analysis**: Calculated C 47.86, H 3.88 %, Found C 47.89, H 3.72 %; **H.R.M.S. [ES+]** found $[MH^+]$-Cl 692.954.

8.5.22 Synthesis of (*p*-cymene)Ru(II)(1-Ferrocenyl-3-(4-methoxyphenyl)propane-1,3-dione)Cl C22

Prepared using 1-ferrocenyl-3-(4-methoxyphenyl)propane-1,3-dione (0.14 g, 0.392 mmol) and purified by column chromatography, eluting 3:2 v/v petrol/ethyl acetate to give orange solid (0.22 g, 89 %).

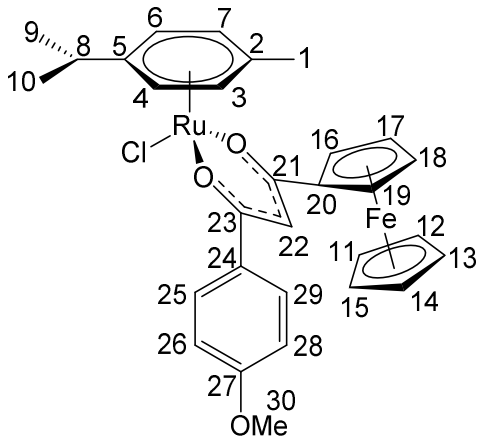

δ_H (500 MHz, $(CD_3)_2CO$); 7.83 (dt, 2H, *J 9.2, 2.8* Hz, ArH, $H_{25,29}$), 6.82 (dt, 2H, *J 9.2, 2.8* Hz, ArH, $H_{26,28}$), 6.01 (s, 1H, CH, H_{22}), 5.53 (dd, 2H, *J 6.0, 0.9* Hz, *p*-cymene ArH, $H_{4,6}$), 5.21 (d, 2H, *J 6.4* Hz, *p*-cymene ArH, $H_{3,7}$), 4.82 (t, 1H, *J 1.2* Hz, C_5H_4, $H_{16/19}$), 4.71 (t, 1H, *J 1.2* Hz, C_5H_4, $H_{16/19}$), 4.92 (m, 1H, C_5H_4, $H_{17/18}$), 4.25 (m, 1H, C_5H_4, $H_{17/18}$), 4.10 (s, 5H, C_5H_5, H_{11-15}), 3.73 (s, 3H, OMe, H_{30}), 2.91 (sept, 1H, *J 6.9* Hz, *p*-cymene $CH(Me)_2$, H_8), 2.16 (s, 3H, *p*-cymene $ArCH_3$, H_1), 1.34 (d, 6H, *J 7.3* Hz, *p*-cymene $C(CH_3)_2$, $H_{9,10}$); **δ_C**{^{1}H} (125 MHz, $(CD_3)_2CO$); 185.9 (quaternary CO, C_{21}), 178.0 (quaternary CO, C_{23}), 162.7 (quaternary ArC, C_{27}), 132.8 (quaternary ArC, C_{24}), 129.7 (ArCH, $C_{25,29}$), 114.2 (ArCH, $C_{26,28}$), 99.3 (quaternary *p*-cymene, C_5), 97.8 (quaternary *p*-cymene, C_2), 92.6 (acac CH, C_{22}), 84.6 (*p*-cymene ArCH, $C_{4/6}$), 84.5 (*p*-cymene ArCH, $C_{4/6}$), 82.4 (quaternary Cp, C_{20}), 79.9 (*p*-cymene ArCH, $C_{3/7}$), 79.9 (*p*-cymene ArCH, $C_{3/7}$), 71.4 (Cp CH, $C_{16/19}$), 71.4 (Cp CH, $C_{16/19}$), 70.9 (Cp ring, C_{11-15}), 69.9 (Cp CH, $C_{17/18}$), 68.6 (Cp CH, $C_{17/18}$), 55.8 (OMe, C_{30}), 31.7 (*p*-cymene CH, C_8), 22.7 (*p*-cymene $C(CH_3)$, $C_{9/10}$), 22.6 (*p*-cymene $C(CH_3)$, $C_{9/10}$), 17.8 (*p*-cymene CH_3, C_1); **Analysis**: Calculated C 57.02, H 4.94, Cl 5.60 %, Found C 57.00, H 5.00, Cl 5.50 %; **H.R.M.S. [ES+]** found [MH^+]-Cl 597.066.

8.5.23 Synthesis of (*p*-cymene)Ru(II)(1-Ferrocenyl-3-(3-methoxyphenyl)propane-1,3-dione)Cl C23

Prepared using 1-ferrocenyl-3-(3-methoxyphenyl)propane-1,3-dione (0.14 g, 0.392 mmol) and purified by column chromatography, eluting 1:1 v/v petrol/ethyl acetate to give orange solid (0.20 g, 80 %).

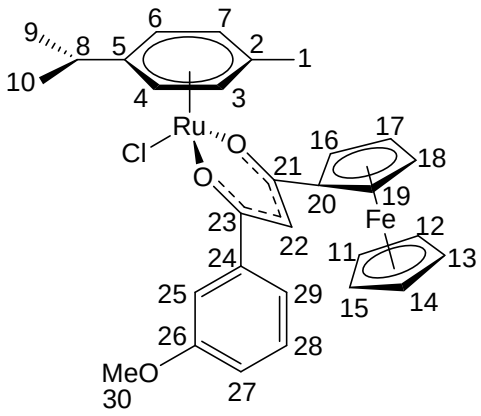

δ_H (500 MHz, $(CD_3)_2CO$); 7.55 (s, 1H, ArH, H_{25}), 7.54 (d, 1H, *J 7.8* Hz, ArH, H_{29}), 7.34 (t, 1H, *J 8.1* Hz, ArH, H_{28}), 7.06 (dt, 1H, *J 7.3, 1.7* Hz, ArH, H_{27}), 6.17 (s, 1H, CH, H_{22}), 5.72 (q, 2H, *J 2.4* Hz, *p*-cymene ArH, $H_{4,6}$), 5.39 (q, 2H, *J 2.4* Hz, *p*-cymene ArH, $H_{3,7}$), 4.99 (broad s, 1H, C_5H_4, $H_{16/19}$), 4.89 (broad s, 1H, C_5H_4, $H_{16/19}$), 4.47 (broad d, 1H, *J 0.9* Hz, C_5H_4, $H_{17/18}$), 4.43 (broad d, 1H, *J 0.9* Hz, C_5H_4, $H_{17/18}$), 4.27 (s, 5H, C_5H_5, $H_{11\text{-}15}$), 3.89 (s, 3H, $ArOCH_3$, H_{30}), 3.07 (sept, 1H, *J 6.7* Hz, *p*-cymene $CH(Me)_2$, H_8), 2.33 (s, 3H, *p*-cymene $ArCH_3$, H_1), 1.50 (dd, 6H, *J 6.9, 1.6* Hz, *p*-cymene $C(CH_3)_2$, $H_{9,10}$); **δ_C**$\{^1H\}$ (125 MHz, $(CD_3)_2CO$); 186.9 (quaternary CO, C_{21}), 178.1 (quaternary CO, C_{23}), 160.6 (quaternary ArCOMe, C_{26}), 142.0 (quaternary ArC, C_{24}), 129.9 (ArCH, C_{25}), 120.1 (ArCH, C_{29}), 116.9 (ArCH, C_{27}), 113.3 (ArCH, C_{28}), 99.3 (quaternary *p*-cymene, C_5), 97.9 (quaternary *p*-cymene, C_2), 93.5 (acac CH, C_{22}), 84.7 (*p*-cymene ArCH, $C_{4/6}$), 84.7 (*p*-cymene ArCH, $C_{4/6}$), 82.1 (quaternary Cp, C_{20}), 79.9 (*p*-cymene ArCH, $C_{3/7}$), 79.9 (*p*-cymene ArCH, $C_{3/7}$), 71.7 (Cp CH, $c_{16/19}$), 71.7 (Cp CH, $C_{16/19}$), 70.9 (Cp ring, $C_{11\text{-}15}$), 69.9 (Cp CH, $C_{17/18}$), 68.8 (Cp CH, $C_{17/18}$), 55.6 ($ArOCH_3$, C_{30}), 31.7 (*p*-cymene CH, C_8), 22.8 (*p*-cymene $C(CH_3)$, $C_{9/10}$), 22.6 (*p*-cymene $C(CH_3)$, $C_{9/10}$), 17.8 (*p*-cymene CH_3, C_1); **Analysis**: Calculated C 57.02, H 4.94 %, Found C 57.09, H 4.90 %; **H.R.M.S. [ES+]** found $[MH^+]$-Cl 597.068.

8.5.24 Synthesis of (*p*-cymene)Ru(II)(1-Ferrocenyl-3-(4-ethoxyphenyl)propane-1,3-dione)Cl C24

Prepared using 1-ferrocenyl-3-(4-ethoxyphenyl)propane-1,3-dione (0.15 g, 0.392 mmol) and purified by column chromatography, eluting 3:2 v/v petrol/ethyl acetate to give orange solid (0.19 g, 75 %).

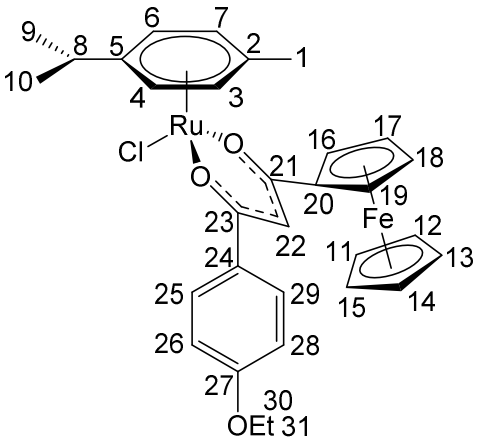

δ_H (500 MHz, $(CD_3)_2CO$); 7.82 (d, 2H, *J 8.9* Hz, ArH, $H_{25,29}$), 6.80 (d, 2H, *J 8.9* Hz, ArH, $H_{26,28}$), 6.00 (s, 1H, CH, H_{22}), 5.53 (dt, 2H, *J 4.8, 1.2* Hz, *p*-cymene ArH, $H_{4,6}$), 5.21 (d, 2H, *J 5.2* Hz, *p*-cymene ArH, $H_{3,7}$), 4.82 (t, 1H, *J 1.2* Hz, C_5H_4, $H_{16/19}$), 4.70 (t, 1H, *J 1.2* Hz, C_5H_4, $H_{16/19}$), 4.29 (m, 1H, C_5H_4, $H_{17/18}$), 4.25 (m, 1H, C_5H_4, $H_{17/18}$), 4.10 (s, 5H, C_5H_5, H_{11-15}), 3.99 (q, 2H, *J 6.9* Hz, OCH_2, H_{30}), 2.90 (sept, 1H, *J 6.9* Hz, $CH(Me)_2$, H_8), 2.16 (s, 3H, *p*-cymene $ArCH_3$, H_1), 1.33 (d, 6H, *J 6.9* Hz, *p*-cymene $C(CH_3)_2$, $H_{9,10}$) 1.26 (t, 3H, *J 6.9* Hz, CH_3, H_{31}); **δ_C**$\{^1H\}$ (125 MHz, $(CD_3)_2CO$); 185.8 (quaternary CO, C_{21}), 178.0 (quaternary CO, C_{23}), 162.1 (ArCOEt, C_{27}), 132.6 (quaternary ArC, C_{24}), 129.7 (ArCH, $C_{25,29}$), 114.7 (ArCH, $C_{26,28}$), 99.3 (quaternary *p*-cymene, C_5), 97.7 (quaternary *p*-cymene, C_2), 92.5 (acac CH, C_{22}), 84.6 (*p*-cymene ArCH, $C_{4/6}$), 84.5 (*p*-cymene ArCH, $C_{4/6}$), 82.4 (quaternary Cp, C_{20}), 79.9 (*p*-cymene ArCH, $C_{3/7}$), 79.9 (*p*-cymene ArCH, $C_{3/7}$), 71.4 (Cp CH, $C_{16/19}$), 71.4 (Cp CH, $C_{16/19}$), 70.9 (Cp ring, C_{11-15}), 69.8 (Cp CH, $C_{17/18}$), 68.6 (Cp CH, $C_{17/18}$), 64.2 (OCH_2Me, C_{30}), 31.7 (*p*-cymene CH, C_8), 22.8 (*p*-cymene $C(CH_3)$, $C_{9/10}$), 22.6 (*p*-cymene $C(CH_3)$, $C_{9/10}$), 17.9 (*p*-cymene CH_3, C_1), 15.0 (CH_3, C_{31}); **Analysis**: Calculated C 57.64, H 5.15, Cl 5.49 %, Found C 57.65, H 5.25, Cl 5.40 %; **H.R.M.S. [ES+]** found $[MH^+]$-Cl 611.085.

8.6 Synthesis of Ruthenium Bipyridine Complexes

Ruthenium bipyridine complexes were prepared using the following general procedure from an adapted literature method.[11]

General Procedure: The required ligand was dissolved in ethanol (20 mL) followed by addition of triethylamine (0.05 mL, 0.3 mmol) and bis(2,2′-bipyridine)dichlororuthenium (0.15 g, 0.3 mmol). The solution was stirred at reflux for 48 hours. Solvent was reduced *in vacuo* and red solid crashed out with the addition of aq NH_4PF_6. The mixture was filtered and the solid was washed with water and ether before being dried overnight in a desiccator.

8.6.1 Synthesis of (1-Ferrocenylpropane-1,3-dione)bis(bipyridine)Ru(II)PF_6 C'1

Prepared using 1-ferrocenylpropane-1,3-dione (0.09 g, 0.3 mmol) and purified by column chromatography, eluting 1:9 v/v acetonitrile/dichloromethane to give dark red solid (0.05 g, 21 %).

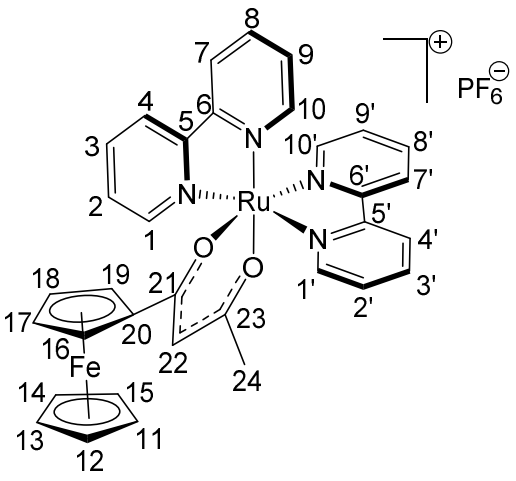

δ_H (500 MHz, $(CD_3)_2CO$); 8.93 (d, 1H, *J 5.7* Hz, bpyH, $H_{1'}$), 8.70 (m, 2H, bpyH, $H_{1,4'}$), 8.65 (d, 1H, *J 8.3* Hz, bpyH, H_4), 8.60 (d, 1H, *J 8.0* Hz, bpyH, $H_{7'}$), 8.53 (d, 1H, *J 8.0* Hz, bpyH, H_7), 8.10 (q, 2H, *J 8.5* Hz, bpyH, $H_{3',3}$), 7.97 (d, 1H, *J 5.5* Hz, bpyH, $H_{10'}$), 7.90 (d, 1H, *J 5.3* Hz, bpyH, H_{10}), 7.86 (t, 1H, *J 7.6* Hz, bpyH, $H_{8'}$), 7.82 (t, 1H, *J 8.0* Hz, bpyH, H_8), 7.74 (t, 1H, *J 6.2* Hz, bpyH, $H_{2'}$), 7.66 (t, 1H, *J 6.4* Hz, bpyH, H_2), 7.21 (q, 2H, *J 6.4* Hz, bpyH, $H_{9',9}$), 5.71 (s, 1H, CH, H_{22}), 4.49 (broad s, 1H, Cp CH, $H_{16/19}$), 4.31 (broad s, 1H, Cp CH, $H_{16/19}$), 4.17 (broad s, 2H, Cp CH, $H_{17,18}$), 3.66 (s, 5H, Cp ring, $H_{11\text{-}15}$), 1.78 (s, 3H, Me, H_{24}); **δ_C**{^{1}H} (125 MHz, $(CD_3)_2CO$); 185.7 (quaternary CO, C_{21}), 178.0 (quaternary CO, C_{23}), 160.4 (quaternary bpyC, $C_{5'}$), 160.3 (quaternary bpyC, C_5), 159.1 (quaternary bpyC, $C_{6'}$), 159.0 (quaternary bpyC, C_6), 154.3 (bpyC, $C_{1'}$), 154.2 (bpyC, C_1), 151.5 (bpyC, $C_{10'}$), 151.0 (bpyC, C_{10}), 137.4 (bpyC, $C_{3'}$), 137.2 (bpyC, C_3), 135.7 (bpyC, $C_{8'}$), 135.7 (bpyC, C_8),

127.3 (bpyC, $C_{2,}$), 127.1 (bpyC, C_2), 126.3 (bpyC, $C_{9'}$), 126.2 (bpyC, C_9), 124.1 (bpyC, $C_{4',4}$), 124.0 (bpyC, $C_{7',7}$), 97.3 (CH, C_{22}), 83.1 (quaternary Cp, C_{20}), 71.3 (Cp CH, $C_{16/19}$), 71.2 (Cp CH, $C_{16/19}$), 70.5 (Cp ring, $C_{11\text{-}15}$), 69.7 (Cp CH, $C_{17/18}$), 68.0 (Cp CH, $C_{17/18}$), 28.3 (CH_3, C_{24}); **Analysis**: Calculated (+2H_2O) C 47.79, H 3.28, N 6.49 %, Found C 47.79, H 3.28, N 6.49 %; **H.R.M.S. [ES+]** found [MH^+]-PF_6 683.066.

8.6.2 Synthesis of (1-Ferrocenyl-4,4,4-trifluorobutane-1,3-dione)bis(bipyridine)Ru(II)PF_6 C'2

Prepared using 1-ferrocenyl-4,4,4-trifluorobutane-1,3-dione (0.1 g, 0.3 mmol) and purified by column chromatography, eluting 1:9 v/v acetonitrile/dichloromethane to give dark red solid (0.06 g, 21 %).

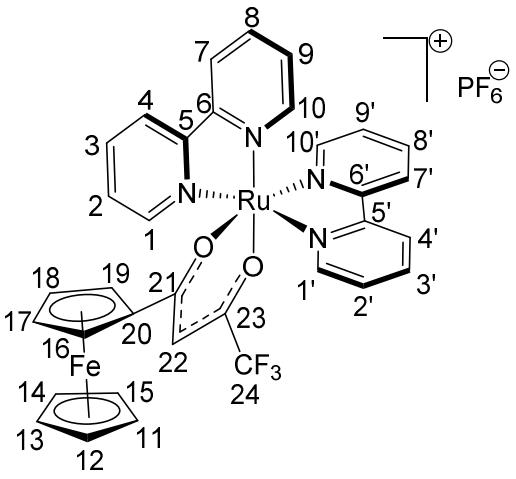

δ_H (500 MHz, $(CD_3)_2CO$); 8.99 (d, 1H, *J 5.0* Hz, bpyH, $H_{1'}$), 8.90 (d, 1H, *J 8.5* Hz, bpyH, H_1), 8.81 (m, 2H, bpyH, $H_{4',4}$), 8.77 (d, 1H, *J 8.0* Hz, bpyH, $H_{7'}$), 8.67 (d, 1H, *J 7.8* Hz, bpyH, H_7), 8.30 (q, 2H, *J 7.1* Hz, bpyH, $H_{3',3}$), 8.11 (broad s, 2H, bpyH, $H_{10',10}$), 8.04 (t, 1H, *J 7.1* Hz, bpyH, $H_{8'}$), 7.98 (m, 2H, bpyH, $H_{8,2'}$), 7.83 (t, 1H, *J 6.4* Hz, bpyH, H_2), 7.37 (dq, 2H, *J 18.3, 6.4* Hz, bpyH, $H_{9',9}$), 6.14 (s, 1H, CH, H_{22}), 4.79 (broad s, 1H, Cp CH, $H_{16/19}$), 4.51 (broad s, 1H, Cp CH, $H_{16/19}$), 4.48 (broad s, 2H, Cp CH, $H_{17,18}$), 3.86 (s, 5H, Cp ring, $H_{11\text{-}15}$); **δ_C**{^{1}H} (125 MHz, $(CD_3)_2CO$); 190.9 (quaternary CO, C_{23}), 160.3 (quaternary bpyC, $C_{5'}$), 160.2 (quaternary bpyC, C_5), 159.1 (quaternary bpyC, $C_{6'}$), 158.9 (quaternary bpyC, C_6), 154.8 (bpyC, $C_{1'}$), 154.7 (bpyC, C_1), 151.1 (bpyC, $C_{10'}$), 151.0 (bpyC, C_{10}), 138.3 (bpyC, $C_{3'}$), 138.1 (bpyC, C_3), 136.6 (bpyC, $C_{8'}$), 136.5 (bpyC, C_8), 127.9 (bpyC, $C_{2'}$), 127.5 (bpyC, C_2), 126.6 (bpyC, $C_{9'}$), 126.5 (bpyC, C_9), 124.4 (bpyC, $C_{4',4}$), 124.3 (bpyC, $C_{7',7}$), 93.7 (d, *J 2.08* Hz, CH, C_{22}), 81.8 (quaternary Cp, C_{20}), 73.0 (Cp CH, $C_{16/19}$), 72.9 (Cp CH, $C_{16/19}$), 70.9 (Cp ring, $C_{11\text{-}15}$), 69.9 (Cp CH, $C_{17/18}$), 68.8 (Cp CH, $C_{17/18}$), 15.6 (CF_3, C_{24}); **Analysis**: Calculated C

46.33, H 2.97, N 6.36 %, Found C 46.27, H 2.89, N 6.28 %; **H.R.M.S. [ES+]** found [MH^+]-PF_6 737.041.

8.6.3 Synthesis of (1-Ferrocenyl-3-(2-furanyl)propane-1,3-dione)bis(bipyridine)Ru(II)PF_6 C'3

Prepared using 1-ferrocenyl-3-(2-furanyl)propane-1,3-dione (0.1 g, 0.3 mmol) and column chromatography, eluting 1:9 v/v acetonitrile/dichloromethane to give dark red solid (0.08 g, 31 %).

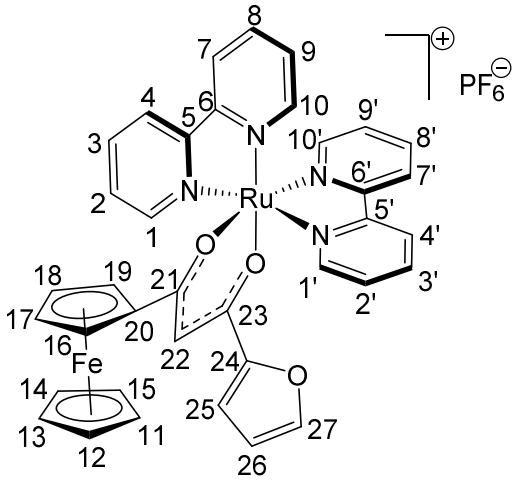

δ_H (500 MHz, $(CD_3)_2CO$); 8.88 (d, 1H, *J 5.3* Hz, bpyH, $H_{1'}$), 8.71 (m, 2H, bpyH, $H_{1,4'}$), 8.60 (t, 2H, *J 7.3* Hz, bpyH, $H_{4,7'}$), 8.52 (d, 1H, *J 8.0* Hz, bpyH, H_7), 8.06 (q, 2H, *J 8.7* Hz, bpyH, $H_{3',3}$), 7.98 (d, 1H, *J 5.5* Hz, bpyH, $H_{10'}$), 7.91 (d, 1H, *J 5.3* Hz, bpyH, H_{10}), 7.84 (quin, 2H, *J 7.8* Hz, bpyH, $H_{8',8}$), 7.70 (t, 1H, *J 6.6* Hz, bpyH, $H_{2,}$), 7.61 (t, 1H, *J 6.6* Hz, bpyH, H_2), 7.47 (s, 1H, Furan H, H_{25}), 7.21 (m, 2H, bpyH, $H_{9',9}$), 6.63 (d, 1H, *J 3.2* Hz, Furan H, H_{27}), 6.34 (m, 1H, Furan H, H_{26}), 6.25 (s, 1H, CH, H_{22}), 4.55 (broad s, 1H, Cp CH, $H_{16/19}$), 4.34 (broad s, 1H, Cp CH, $H_{16/19}$), 4.20 (broad d, 2H, *J 7.3* Hz, Cp CH, $H_{17,18}$), 3.66 (s, 5H, Cp ring, $H_{11\text{-}15}$); **δ_C**{^{1}H} (125 MHz, $(CDCl_3)$); 212.3 (quaternary CO, C_{21}) C 185.0 (quaternary CO, C_{23}), 168.0 (quaternary Furan C, C_{24}), 158.9 (quaternary bpyC, $C_{5'/5}$), 158.8 (quaternary bpyC, $C_{5'/5}$), 157.7 (quaternary bpyC, $C_{6'/6}$), 153.5 (quaternary bpyC, $C_{6'/6}$), 153.1 (bpyC, $C_{1'}$), 153.0 (bpyC, C_1), 151.4 (bpyC, $C_{10'}$), 149.8 (bpyC, C_{10}), 143.1 (Furan C, C_{27}), 136.4 (bpyC, $C_{3'}$), 136.3 (bpyC, C_3), 134.9 (bpyC, $C_{8'}$), 134.8 (bpyC, C_8), 126.1 (bpyC, $C_{2'}$), 125.9 (bpyC, C_2), 125.4 (bpyC, $C_{9'/9}$), 122.9 (bpyC, $C_{4'/4}$), 122.9 (bpyC, $C_{7',7}$), 112.2 (Furan C, C_{25}), 112.0 (Furan C, C_{26}), 93.0 (CH, C_{22}), 82.7 (quaternary Cp, C_{20}), 71.3 (Cp CH, $C_{16/19}$), 71.2 (Cp CH, $C_{16/19}$), 70.3 (Cp ring, $C_{11\text{-}15}$), 69.9 (Cp CH, $C_{17/18}$), 67.7 (Cp CH, $C_{17/18}$); **Analysis**: Calculated C 50.53, H 3.32, N 6.37 %, Found C 50.64, H 3.19, N 6.28 %; **H.R.M.S. [ES+]** found [MH^+]-PF_6 735.064.

8.6.4 Synthesis of (1-Ferrocenyl-3-phenylpropane-1,3-dione)bis(bipyridine)Ru(II)PF_6 C'4

Prepared using 1-ferrocenyl-3-phenylpropane-1,3-dione (0.1 g, 0.3 mmol) and purified by column chromatography, eluting 1:9 v/v acetonitrile/dichloromethane to give dark red solid (0.06 g, 23 %).

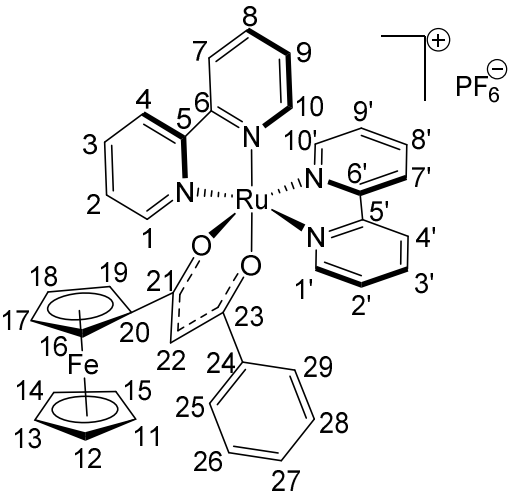

δ_H (500 MHz, $(CD_3)_2CO$); 9.03 (d, 1H, *J 5.3* Hz, bpyH, $H_{1'}$), 8.87 (m, 2H, bpyH, $H_{1,4'}$), 8.75 (d, 2H, *J 7.8* Hz, bpyH, $H_{4,7'}$), 8.68 (d, 1H, *J 7.6* Hz, bpyH, H_7), 8.21 (quin, 2H, *J 7.6* Hz, bpyH, $H_{3',3}$), 8.17 (d, 1H, *J 5.0* Hz, bpyH, H_{10}), 8.11 (d, 1H, *J 5.0* Hz, bpyH, H_{10}), 8.00 (quin, 2H, *J 6.5* Hz, bpyH, $H_{8',8}$), 7.84 (t, 1H, *J 6.4* Hz, bpyH, $H_{2'}$), 7.75 (m, 3H, bpyH and ArH, $H_{2,25,29}$), 7.43 (t, 1H, *J 6.6* Hz, ArH, H_{27}), 7.37 (t, 2H, *J 6.6* Hz, bpyH, $H_{9',9}$), 7.33 (t, 2H, *J 7.3* Hz, ArH, $H_{26,28}$), 6.52 (s, 1H, CH, H_{22}), 4.83 (broad s, 1H, Cp CH, $H_{16/16}$), 4.55 (broad s, 1H, Cp CH, $H_{16/19}$), 4.36 (broad s, 2H, Cp CH, $H_{17,18}$), 3.83 (s, 5H, Cp ring, $H_{11\text{-}15}$); **δ_C**{^{1}H} (125 MHz, CD_3CN); 185.2 (quaternary CO, C_{21}), 177.8 (quaternary CO, C_{23}), 158.9 (quaternary bpyC, $C_{5'}$), 158.8 (quaternary bpyC, C_5), 157.7 (quaternary bpyC, $C_{6'}$), 157.6 (quaternary bpyC, C_6), 153.1 (bpyC, $C_{1',1}$), 150.0 (bpyC, $C_{10'}$), 149.8 (bpyC, C_{10}), 139.6 (quaternary ArC, C_{24}), 136.2 (bpyC, $C_{3'}$), 136.1 (bpyC, C_3), 134.5 (ArC, C_{27}), 129.8 (bpyC, $C_{8',8}$), 127.9 (ArC, $C_{25,29}$), 126.0 (ArC, $C_{26,28}$), 125.8 (bpyC, $C_{2'}$), 125.8 (bpyC, C_2), 124.9 (bpyC, $C_{9'}$), 124.9 (bpyC, C_9), 122.8 (bpyC, $C_{4',4}$), 122.7 (bpyC, $C_{7'}$), 122.7 (bpyC, C_7), 93.7 (CH, C_{22}), 82.3 (quaternary Cp, C_{20}), 70.5 (Cp CH, $C_{16/19}$), 70.4 (Cp CH, $C_{16/19}$), 69.4 (Cp ring, $C_{11\text{-}15}$), 68.4 (Cp CH, $C_{17/18}$), 67.0 (Cp CH, $C_{17/18}$); **Analysis**: Calculated C 52.66, H 3.51, N 6.30 %, Found C 52.67, H 3.47, N 6.26 %; **H.R.M.S. [ES+]** found $[MH^+]$-PF_6 745.084.

8.6.5 Synthesis of (1-Ferrocenyl-3-(1-naphthyl)propane-1,3-dione)bis(bipyridine)Ru(II)PF_6 C'5

Prepared using 1-ferrocenyl-3-(1-naphthyl)propane-1,3-dione (0.12 g, 0.3 mmol) and purified by column chromatography, eluting 1:9 v/v acetonitrile/dichloromethane to give dark red solid (0.11 g, 39 %).

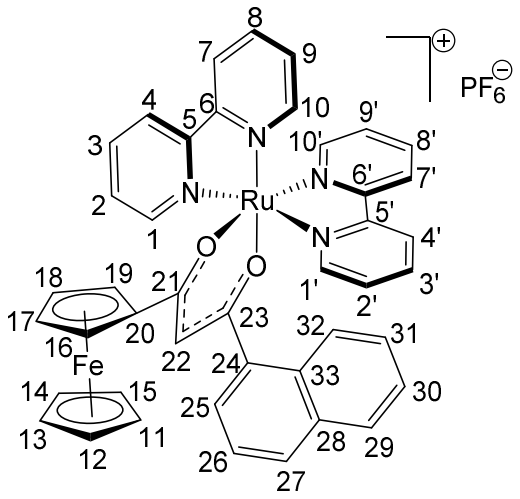

δ_H (500 MHz, $(CD_3)_2CO$); 8.98 (d, 1H, *J 5.3* Hz, bpyH, $H_{1'}$), 8.92 (d, 1H, *J 5.1* Hz, bpyH, H_1), 8.74 (t, 2H, *J 8.5* Hz, bpyH, $H_{3',3}$), 8.61 (d, 1H, *J 8.1* Hz, bpyH, $H_{4'}$), 8.49 (d, 1H, *J 8.48* Hz, bpyH, H_4), 8.24 (t, 1H, *J 7.6* Hz, ArH, H_{25}), 8.12 (m, 2H, bpyH, $H_{7',7}$), 7.88 (m, 2H, bpy H, $H_{8',8}$), 7.72 (m, 5H, ArH and bpyH, $H_{10',10,2',2,26}$), 7.46 (d, 1H, *J 6.6* Hz, ArH, H27), 7.29 (m, 3H, ArH and bpyH, $H_{9',9,29}$), 7.05 (m, 3H, ArH, $H_{30\text{-}32}$), 6.03 (s, 1H, CH, H_{22}), 4.55 (broad s, 1H, Cp CH, $H_{16/19}$), 4.37 (broad s, 1H, Cp CH, $H_{16/19}$), 4.19 (broad s, 2H, Cp CH, $H_{17/18}$), 3.74 (s, 5H, Cp ring, $H_{11\text{-}15}$); **δ_C**$\{^1H\}$ (125 MHz, $(CD_3)_2CO$); 186.4 (quaternary CO, C_{21}), 183.0 (quaternary CO, C_{23}), 160.3 (quaternary bpyC, $C_{5'}$), 160.3 (quaternary bpyC, C_5), 159.5 (quaternary bpyC, $C_{6'}$), 159.2 (quaternary bpyC, C_6), 154.6 (bpyC, $C_{1'}$), 154.5 (bpyC, C_1), 154.4 (quaternary ArC, C_{24}), 151.5 (bpyC, $C_{10'}$), 151.4 (bpyC, C_{10}), 140.9 (quaternary ArC, C_{33}), 137.8 (bpyC, $C_{3'}$), 137.7 (bpyC, C_3), 136.0 (bpyC, $C_{8'}$), 135.8 (bpyC, C_8), 134.7 (quaternary ArC, C_{28}), 131.3 (ArC, C_{27}), 129.9 (ArC, C_{25}), 129.0 (ArC, C_{26}), 127.5 (ArC, C_{32}), 127.3 (ArC, C_{29}), 126.7 (bpyC, $C_{2'}$), 126.6 (bpyC, C_2), 126.3 (bpyC, $C_{9'}$), 126.3 (bpyC, C_9), 126.0 (bpyC, $C_{4'}$), 126.0 (bpyC, C_4), 125.1 (ArC, C_{31}), 124.2 (ArC, C_{30}), 124.1 (bpyC, $C_{7'}$), 124.0 (bpyC, C_7), 99.8 (CH, C_{22}), 83.1 (quaternary Cp, C_{20}), 71.8 (Cp CH, $C_{16/19}$), 71.7 (Cp CH, $C_{16/19}$), 70.7 (Cp ring, $C_{11\text{-}15}$), 69.7 (Cp CH, $C_{17/18}$), 68.4 (Cp CH, $C_{17/18}$); **Analysis**: Calculated C 54.96, H 3.54, N 5.96 %, Found C 54.86, H 3.44, N 5.91 %; **H.R.M.S. [ES+]** found $[MH^+]$-PF_6 735.064.

8.6.6 Synthesis of (1-Ferrocenyl-3-(4-methylphenyl)propane-1,3-dione)bis(bipyridine)Ru(II)PF_6 C'6

Prepared using 1-ferrocenyl-3-(4-methylphenyl)propane-1,3-dione (0.1 g, 0.3 mmol) and purified by column chromatography, eluting 1:9 v/v acetonitrile/dichloromethane to give dark red solid (0.08 g, 28 %).

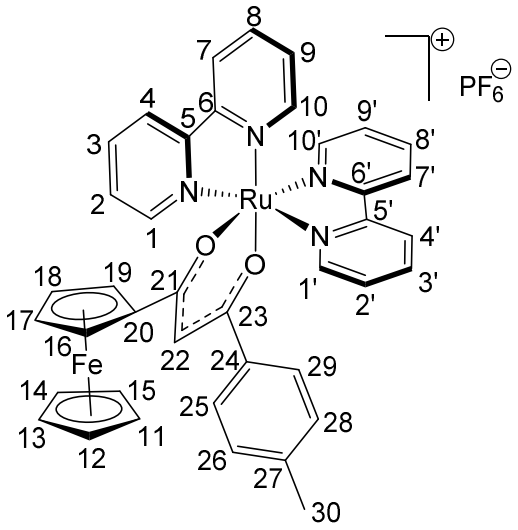

δ_H (500 MHz, $(CD_3)_2CO$); 8.85 (d, 1H, *J 5.7* Hz, bpyH, $H_{1'}$), 8.73 (d, 1H, *J 5.3* Hz, bpyH, H_1), 8.70 (d, 1H, *J 8.3* Hz, bpyH, $H_{4'}$), 8.60 (d, 2H, *J 8.0* Hz, bpyH, $H_{7',7}$), 8.52 (d, 1H, *J 8.0* Hz, bpyH, H_4), 8.05 (m, 2H, bpyH, $H_{3',3}$), 8.01 (d, 1H, *J 5.5* Hz, bpyH, $H_{10'}$), 7.95 (d, 1H, *J 5.7* Hz, bpyH, H_{10}), 7.86 (dt, 1H, *J 7.8, 1.2* Hz, bpyH, $H_{8'}$), 7.83 (dt, 1H, *J 7.8, 1.2* Hz, bpyH, H_8), 7.68 (t, 1H, *J 6.2* Hz, bpyH, $H_{2'}$), 7.60 (t, 1H, *J 6.2* Hz, bpyH, H_2), 7.49 (d, 2H, *J 8.3* Hz, ArH, $H_{25,29}$), 7.21 (t, 2H, *J 6.7* Hz, bpyH, $H_{9',9}$), 6.99 (d, 2H, *J 8.0* Hz, ArH, $H_{26,28}$), 6.35 (s, 1H, CH, H_{22}), 4.65 (broad t, 1H, *J 1.2* Hz, Cp CH, $H_{16/19}$), 4.38 (broad t, 1H, *J 1.2* Hz, Cp CH, $H_{16/19}$), 4.19 (m, 2H, Cp CH, $H_{17,18}$), 3.66 (s, 5H, Cp ring, $H_{11\text{-}15}$), 2.16 (s, 3H, $ArCH_3$, H_{30}); **δ_C**{^{1}H} (125 MHz, $(CD_3)_2CO$); 186.0 (quaternary CO, C_{21}), 178.8 (quaternary CO, C_{23}), 160.3 (quaternary bpyC, $C_{5'/5/6'/6}$), 160.3 (quaternary bpyC, $C_{5'/5/6'/6}$), 154.3 (bpyC, $C_{1'}$), 154.3 (bpyC, C_1), 151.3 (bpyC, $C_{10'}$), 151.0 (bpyC, C_{10}), 141.3 (quaternary ArC, C_{24}), 138.0 (bpyC, $C_{3',3}$), 137.5 (bpyC, $C_{8'}$), 137.4 (bpyC, C_8), 135.8 (ArC, C_{27}), 129.7 (ArC, $C_{25,29}$), 127.4 (bpyC, $C_{2'}$), 127.3 (ArC, $C_{26,28}$), 127.1 (bpyC, C_2), 126.3 (bpyC, $C_{9'}$), 126.3 (bpyC, C_9), 124.1 (bpyC, $C_{4'}$), 124.1 (bpyC, C_4), 124.0 (bpyC, $C_{7'}$), 124.0 (bpyC, C_9), 94.3 (CH, C_{22}), 83.7 (quaternary Cp, C_{20}), 71.5 (Cp CH, $C_{16/19}$), 71.4 (Cp CH, $C_{16/19}$), 70.6 (Cp ring, $C_{11\text{-}15}$), 69.8 (Cp CH, $C_{17/18}$), 68.2 (Cp CH, $C_{17/18}$), 21.3 ($ArCH_3$, C_{30}); **Analysis**: Calculated C 53.17, H 3.68, N 6.20 %, Found C 53.09, H 3.55, N 6.18 %; **H.R.M.S. [ES+]** found $[MH^+]$-PF_6 759.102.

8.6.7 Synthesis of (1-Ferrocenyl-3-(3,5-dimethylphenyl)propane-1,3-dione)bis(bipyridine)Ru(II)PF_6 C'7

Prepared using 1-ferrocenyl-3-(3,5-dimethylphenyl)propane-1,3-dione (0.11 g, 0.3 mmol) and purified by column chromatography, eluting 1:9 v/v acetonitrile/dichloromethane to give dark red solid (0.1 g, 35 %).

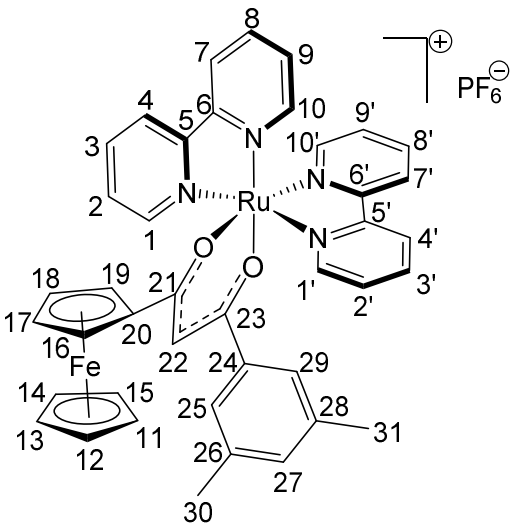

δ_H (500 MHz, $(CD_3)_2CO$); 8.87 (d, 1H, *J 5.5* Hz, bpyH, $H_{1'}$), 8.72 (t, 2H, *J 8.5* Hz, bpyH, $H_{3',3}$), 8.60 (d, 2H, *J 7.9* Hz, bpyH, $H_{4',4}$), 8.52 (d, 1H, *J 7.9* Hz, bpyH, H_1), 8.04 (m, 3H, bpyH, $H_{7',7,10'}$), 7.94 (d, 1H, *J 5.5* Hz, bpyH, H_{10}), 7.84 (q, 2H, *J 8.0* Hz, bpyH, $H_{8',8}$), 7.69 (t, 1H, *J 6.2* Hz, bpyH, $H_{2'}$), 7.61 (t, 1H, *J 6.2* Hz, bpyH, H_2), 7.21 (m, 4H, ArH and bpyH, $H_{9',9,25,29}$), 6.92 (s, 1H, ArH, H_{27}), 6.33 (s, 1H, CH, H_{22}), 4.63 (broad s, 1H, Cp CH, $H_{16/19}$), 4.37 (broad s, 1H, Cp CH, $H_{16/19}$), 4.19 (broad s, 2H, Cp CH, $H_{17,18}$), 3.66 (s, 5H, Cp ring, $H_{11\text{-}15}$), 2.10 (s, 6H, $ArCH_3$, $H_{30,31}$); **δ_C**{^{1}H} (125 MHz, $(CD_3)_2CO$); 185.9 (quaternary CO, C_{21}), 179.5 (quaternary CO, C_{23}), 159.1 (quaternary bpyC, $C_{5',5}$), 159.0 (quaternary bpyC, $C_{6',6}$), 154.4 (bpyC, $C_{1'}$), 154.3 (bpyC, C_1), 151.3 (bpyC, $C_{10'}$), 151.0 (bpyC, C_{10}), 140.9 (quaternary ArC, C_{24}), 138.4 (ArC, C_{27}), 137.5 (bpyC, $C_{3'}$), 137.4 (bpyC, C_3), 135.8 (bpyC, $C_{8',8}$), 132.5 (quaternary ArC, $C_{26,28}$), 127.4 (bpyC, $C_{2'}$), 127.1 (bpyC, C_2), 126.3 (bpyC, $C_{9'}$), 126.3 (bpyC, C_9), 125.1 (ArC, $C_{25,29}$), 124.1 (bpyC, $C_{4'}$), 124.0 (bpyC, C_4), 124.0 (bpyC, $C_{7'}$), 124.0 (bpyC, C_7), 94.8 (CH, C_{22}), 83.6 (quaternary Cp, C_{20}), 71.5 (Cp CH, $C_{16/19}$), 71.3 (Cp CH, $C_{16/19}$), 70.5 (Cp ring, $C_{11\text{-}15}$), 69.8 (Cp CH, $C_{17/18}$), 68.2 (Cp CH, $C_{17/18}$), 21.3 ($ArCH_3$, $C_{30,31}$); **Analysis**: Calculated C 53.67, H 3.84, N 6.11 %, Found C 53.73, H 3.81, N 5.98 %; **H.R.M.S. [ES+]** found [MH^+]-PF_6 773.117.

8.6.8 Synthesis of (1-Ferrocenyl-3-(4-fluorophenyl)propane-1,3-dione)bis(bipyridine)Ru(II)PF_6 C'8

Prepared using 1-ferrocenyl-3-(4-fluorophenyl)propane-1,3-dione (0.1 g, 0.3 mmol) and purified by column chromatography, eluting 1:9 v/v acetonitrile/dichloromethane to give dark red solid (0.06 g, 20 %).

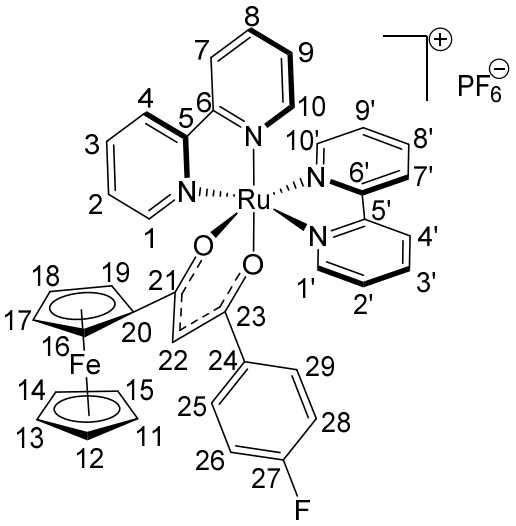

δ_H (500 MHz, $(CD_3)_2CO$); 8.87 (d, 1H, *J 5.5* Hz, bpyH, $H_{1'}$), 8.73 (d, 1H, *J 5.5* Hz, bpyH, H_1), 8.70 (d, 1H, *J 8.3* Hz, bpyH, $H_{4'}$), 8.60 (broad d, 2H, *J 8.3* Hz, bpyH, $H_{7',7}$), 8.52 (d, 1H, *J 8.0* Hz, bpyH, H_4), 8.06 (m, 2H, bpyH, $H_{3',3}$), 8.01 (d, 1H, *J 5.7* Hz, bpyH, $H_{10'}$), 7.94 (d, 1H, *J 5.5* Hz, bpyH, H_{10}), 7.86 (t, 1H, *J 7.8* Hz, bpyH, $H_{8'}$), 7.83 (t, 1H, *J 7.8* Hz, bpyH, H_8), 7.67 (m, 3H, ArH and bpyH, $H_{2',25,29}$), 7.61 (t, 1H, *J 6.6* Hz, bpyH, H_2), 7.21 (t, 2H, *J 6.6* Hz, bpyH, $H_{9',9}$), 6.92 (t, 2H, *J 8.7* Hz, ArH, $H_{26,28}$), 6.35 (s, 1H, CH, H_{22}), 4.67 (broad s, 1H, Cp CH, $H_{16/19}$), 4.39 (broad s, 1H, Cp CH, $H_{16/19}$), 4.20 (broad t, 2H, *J 2.4* Hz, Cp CH, $H_{17,18}$), 3.67 (s, 5H, Cp ring, $H_{11\text{-}15}$); **δ_C**$\{^1H\}$ (125 MHz, $(CD_3)_2CO$); 186.6 (quaternary CO, C_{21}), 177.3 (quaternary CO, C_{23}), 164.8 (d, *J 248.6* Hz, ArCF, C_{27}), 160.3 (quaternary bpyC, $C_{5'}$), 160.3 (quaternary bpyC, C_5), 159.1 (quaternary bpyC, $C_{6'}$), 159.0 (quaternary bpyC, C_6), 154.4 (bpyC, $C_{1'}$), 154.4 (bpyC, C_1), 151.3 (bpyC, C_{10}), 151.0 (bpyC, $C_{10'}$), 137.6 (bpyC, $C_{3'}$), 137.5 (bpyC, C_3), 137.1 (d, *J 3.1* Hz, quaternary ArC, C_{24}), 135.9 (bpyC, $C_{8',8}$), 139.7 (d, *J 8.3* Hz, ArC, $C_{25,29}$), 127.5 (bpyC, $C_{2'}$), 127.1 (bpyC, C_2), 126.4 (bpyC, $C_{9'}$), 126.3 (bpyC, C_9), 124.2 (bpyC, $C_{4'}$), 124.1 (bpyC, C_4), 124.1 (bpyC, $C_{7'}$), 124.0 (bpyC, C_7), 115.7 (d, *J 21.8* Hz, ArC, $C_{26,28}$), 94.5 (CH, C_{22}), 83.2 (quaternary Cp, C_{20}), 71.6 (Cp CH, $C_{16/19}$), 71.5 (Cp CH, $C_{16/19}$), 70.6 (Cp ring, $C_{11\text{-}15}$), 69.8 (Cp CH, $C_{17/18}$), 68.3 (Cp CH, $C_{17/18}$); **Analysis**: Calculated C 51.61, H 3.33, N 6.17 %, Found C 51.55, H 3.25, N 6.12 %; **H.R.M.S. [ES+]** found $[MH^+]$-PF_6 763.075.

8.6.9 Synthesis of (1-Ferrocenyl-3-(3-fluorophenyl)propane-1,3-dione)bis(bipyridine)Ru(II)PF_6 C'9

Prepared using 1-ferrocenyl-3-(3-fluorophenyl)propane-1,3-dione (0.1 g, 0.3 mmol) and purified by column chromatography, eluting 1:9 v/v acetonitrile/dichloromethane to give dark red solid (0.08 g, 28 %).

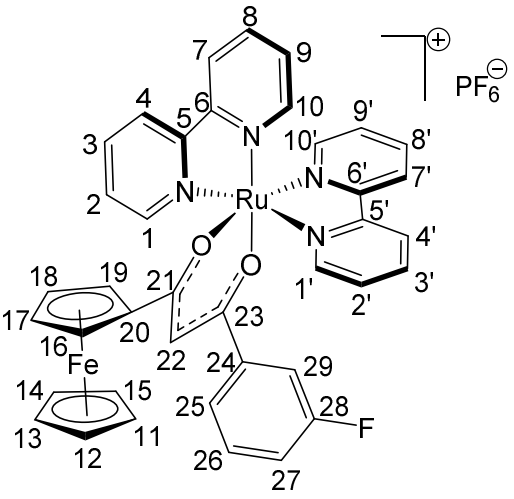

δ_H (500 MHz, $(CD_3)_2CO$); 8.89 (d, 1H, *J 5.7* Hz, bpyH, $H_{1'}$), 8.73 (d, 1H, *J 5.5* Hz, bpyH, H_1), 8.70 (d, 1H, *J 8.5* Hz, bpyH, $H_{4'}$), 8.61 (d, 2H, *J 7.9* Hz, bpyH, $H_{7',7}$), 8.53 (d, 1H, *J 8.3* Hz, bpyH, H_4), 8.05 (m, 3H, bpyH, $H_{10',3',3}$), 7.96 (d, 1H, *J 5.3* Hz, bpyH, H_{10}), 7.85 (q, 2H, *J 7.8* Hz, bpyH, $H_{8',8}$), 7.70 (t, 1H, *J 6.5* Hz, bpyH, $H_{2'}$), 7.61 (t, 1H, *J 6.5* Hz, bpyH, H_2), 7.47 (d, 1H, *J 8.1* Hz, ArH, H_{29}), 7.24 (m, 4H, ArH and bpyH, $H_{9',9,25,26}$), 7.04 (td, 1H, *J 8.1, 2.6* Hz, ArH, H_{27}), 6.38 (s, 1H, CH, H_{22}), 4.72 (broad s, 1H, Cp CH, $H_{16/19}$), 4.40 (broad s, 1H, Cp CH, $H_{16/19}$), 4.22 (broad s, 2H, Cp CH, $H_{17,18}$), 3.68 (s, 5H, Cp ring, $H_{11\text{-}15}$); **δ_C**$\{^1H\}$ (125 MHz, $(CD_3)_2CO$); 187.0 (quaternary CO, C_{21}), 180.0 (quaternary CO, C_{23}), 160.3 (quaternary bpyC, $C_{5'}$), 160.2 (quaternary bpyC, C_5), 159.0 (quaternary bpyC, $C_{6'}$), 159.0 (quaternary bpyC, C_6), 154.4 (bpyC, $C_{1'}$), 154.4 (bpyC, C_1), 151.3 (bpyC, $C_{10'}$), 151.0 (bpyC, C_{10}), 142.8 (quaternary ArCF, C_{28}), 137.6 (bpyC, $C_{3'}$), 137.5 (bpyC, C_3), 135.9 (bpyC, $C_{8',8}$), 130.9 (quaternary ArC, C_{24}), 127.5 (bpyC, $C_{2'}$), 127.2 (bpyC, C_2), 126.4 (bpyC, $C_{9'}$), 126.3 (bpyC, C_9), 124.2 (bpyC, $C_{4'}$), 124.1 (bpyC, C_4), 124.1 (bpyC, $C_{7'}$), 124.1 (bpyC, C_7), 123.0 (d, *J 2.5* Hz, ArC, C_{26}), 117.5 (d, *J 21.2* Hz, ArC, C_{29}), 114.5 (d, *J 22.4* Hz, ArC, C_{27}), 94.9 (CH, C_{22}), 83.4 (quaternary Cp, C_{20}), 71.8 (Cp CH, $C_{16/19}$), 71.7 (Cp CH, $C_{16/19}$), 70.6 (Cp ring, $C_{11\text{-}15}$), 69.8 (Cp CH, $C_{17/18}$), 68.4 (Cp CH, $C_{17/18}$); **Analysis**: Calculated C 51.61, H 3.33, N 6.17 %, Found C 51.57, H 3.40, N 6.18 %; **H.R.M.S. [ES+]** found $[MH^+]$-PF_6 763.076.

8.6.10 Synthesis of (1-Ferrocenyl-3-(3,5-difluorophenyl)propane-1,3-dione)bis(bipyridine)bis(bipyridine)Ru(II)PF_6 C'10

Prepared using 1-ferrocenyl-3-(3,5-difluorophenyl)propane-1,3-dione (0.11 g, 0.3 mmol) and purified by column chromatography, eluting 1:9 v/v acetonitrile/dichloromethane to give dark red solid (0.06 g, 23 %).

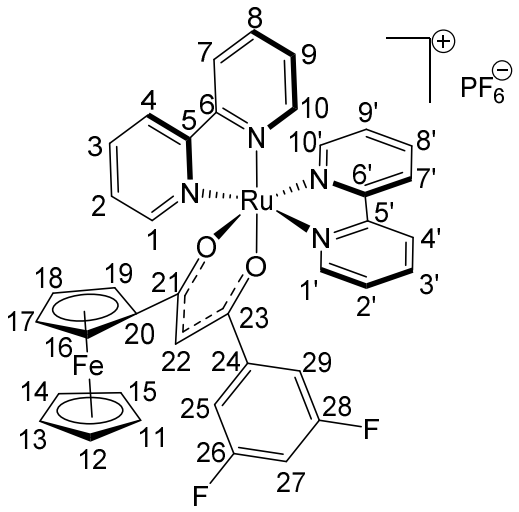

δ_H (500 MHz, $(CD_3)_2CO$); 8.90 (d, 1H, *J 5.1* Hz, bpyH, $H_{1'}$), 8.71 (m, 2H, bpyH, $H_{1,4'}$), 8.61 (m, 2H, bpyH, $H_{4,7'}$), 8.53 (d, 1H, *J 8.1* Hz, bpyH, H_7), 8.08 (q, 2H, *J 7.2* Hz, bpyH, $H_{3',3}$), 8.02 (d, 1H, *J 5.7* Hz, bpyH, $H_{10'}$), 7.96 (d, 1H, *J 5.7* Hz, bpyH, H_{10}), 7.85 (q, 2H, *J 8.1* Hz, bpyH, $H_{8',8}$), 7.69 (t, 1H, *J 6.4* Hz, bpyH, $H_{2'}$), 7.62 (t, 1H, *J 6.6* Hz, bpyH, H_2), 7.22 (m, 4H, ArH and bpyH, $H_{9',9,25,29}$), 6.93 (tt, 1H, *J 9.1, 2.2* Hz, ArH, H_{27}), 6.38 (s, 1H, CH, H_{22}), 4.77 (broad s, 1H, Cp CH, $H_{16/19}$), 4.41 (broad s, 1H, Cp CH, $H_{16/19}$), 4.22 (broad s, 2H, Cp CH, $H_{17,18}$), 3.68 (s, 5H, Cp ring, $H_{11\text{-}15}$); **δ_C**{^{1}H} (125 MHz, $(CD_3)_2CO$); 187.7 (quaternary CO, C_{21}), 177.4 (quaternary CO, C_{23}), 164.7 (quaternary ArCF, $C_{26,28}$), 160.3 (quaternary bpyC, $C_{5'}$), 160.2 (quaternary bpyC, C_5), 159.0 (quaternary bpyC, $C_{6'}$), 158.9 (quaternary bpyC, C_6), 154.5 (bpyC, $C_{1'}$), 154.5 (bpyC, C_1), 151.4 (bpyC, $C_{10'}$), 151.0 (bpyC, C_{10}), 137.7 (bpyC, $C_{3'}$), 137.7 (bpyC, C_3), 136.0 (bpyC, $C_{8',8}$), 127.6 (quaternary ArC, C_{24}), 127.2 (bpyC, $C_{2',2}$), 126.4 (bpyC, $C_{9'}$), 126.3 (bpyC, C_9), 124.2 (bpyC, $C_{4',4}$), 124.1 (bpyC, $C_{7'}$), 124.1 (bpyC, C_7), 109.6 (d, *J 25.5* Hz, ArC, $C_{25,29}$), 105.4 (d, *J 25.5* Hz, ArC, C_{27}), 95.0 (CH, C_{22}), 83.2 (quaternary Cp, C_{20}), 71.9 (Cp CH, $C_{16/19}$), 71.8 (Cp CH, $C_{16/19}$), 70.6 (Cp ring, $C_{11\text{-}15}$), 69.8 (Cp CH, $C_{17/18}$), 68.5 (Cp CH, $C_{17/18}$); **Analysis**: Calculated C 50.61, H 3.16, N 6.05 %, Found C 50.05, H 2.72, N 6.08 %; **H.R.M.S. [ES+]** found $[MH^+]$-PF_6 781.067.

8.6.11 Synthesis of (1-Ferrocenyl-3-(4-chlorophenyl)propane-1,3-dione)bis(bipyridine)Ru(II)PF_6 C'11

Prepared using 1-ferrocenyl-3-(4-chlorophenyl)propane-1,3-dione (0.11 g, 0.3 mmol) and purified by column chromatography, eluting 1:9 v/v acetonitrile/dichloromethane to give dark red solid (0.06 g, 22 %).

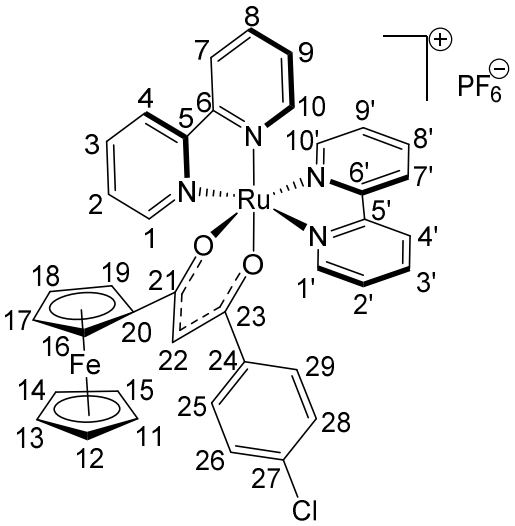

δ_H (500 MHz, $(CD_3)_2CO$); 9.00 (dq, 1H, *J 5.5, 0.7* Hz, bpyH, $H_{1'}$), 8.86 (dq, 1H, *J 5.6, 0.7* Hz, bpyH, H_1), 8.83 (d, 1H, *J 8.1* Hz, bpyH, $H_{4'}$), 8.73 (d, 2H, *J 8.1* Hz, bpyH, $H_{7',7}$), 8.65 (d, 1H, *J 8.66* Hz, bpyH, H_4), 8.21 (td, 1H, *J 8.1, 1.5* Hz, bpyH, $H_{3'}$), 8.18 (td, 1H, *J 8.1, 1.5* Hz, bpyH, H_3), 8.14 (dd, 1H, *J 5.6, 0.7* Hz, bpyH, $H_{10'}$), 8.07 (dd, 1H, *J 5.6, 0.6* Hz, bpyH, H_{10}), 7.99 (td, 1H, *J 7.8, 1.3* Hz, bpyH, $H_{8'}$), 7.96 (td, 1H, *J 7.8, 1.4* Hz, bpyH, H_8), 7.81 (ddd, 1H, *J 5.6, 1.2, 0.6* Hz, bpyH, $H_{2'}$), 7.75 (dt, 2H, *J 8.7, 2.3* Hz, ArH, $H_{25,29}$), 7.73 (m, 1H, bpyH, H_2), 7.34 (ddt, 2H, *J 7.4, 1.5, 1.4* Hz, bpyH, $H_{9',9}$), 7.32 (dt, 2H, *J 8.8, 2.2* Hz, ArH, $H_{26,28}$), 6.50 (s, 1H, CH, H_{22}), 4.80 (quin, 1H, *J 1.3* Hz, Cp CH, $H_{16/19}$), 4.52 (quin, 1H, *J 1.2* Hz, Cp CH, $H_{16/19}$), 4.34 (m, 2H, Cp CH, $H_{17,18}$), 3.81 (s, 5H, Cp ring, $H_{11\text{-}15}$); **δ_C**{^{1}H} (125 MHz, $(CD_3)_2CO$); 186.8 (quaternary CO, C_{21}), 177.1 (quaternary CO, C_{23}), 160.3 (quaternary bpyC, $C_{5'}$), 160.3 (quaternary bpyC, C_5), 159.1 (quaternary bpyC, $C_{6'}$), 159.0 (quaternary bpyC, C_6), 154.4 (bpyC, $C_{1'}$), 154.4 (bpyC, C_1), 151.3 (bpyC, $C_{10'}$), 151.0 (bpyC, C_{10}), 139.4 (quaternary ArC, C_{24}), 137.6 (bpyC, $C_{3'}$), 137.5 (bpyC, C_3), 136.4 (quaternary ArCCl, C_{27}), 135.9 (bpyC$_{8',8}$), 129.1 (ArC, $C_{25,29}$), 129.0 (ArC, $C_{26,28}$), 127.5 (bpyC, $C_{2'}$), 127.2 (bpyC, C_2), 126.4 (bpyC, $C_{9'}$), 126.3 (bpyC, C_9), 124.2 (bpyC, $C_{4'}$), 124.1 (bpyC, C_4), 124.1 (bpyC, $C_{7'}$), 124.0 (bpyC, C_7), 94.7 (CH, C_{22}), 83.4 (quaternary Cp, C_{20}), 71.7 (Cp CH, $C_{16/19}$), 71.6 (Cp CH, $C_{16/19}$), 70.6 (Cp ring, $C_{11\text{-}15}$), 69.8 (Cp CH, $C_{17/18}$), 68.3 (Cp CH, $C_{17/18}$); **Analysis**: Calculated C 50.69, H 3.27, N 6.06 %, Found C 50.52, H 3.19, N 6.01 %; **H.R.M.S. [ES+]** found $[MH^+]$-PF_6 779.046.

8.6.12 Synthesis of (1-Ferrocenyl-3-(3,5-dichlorophenyl)propane-1,3-dione)bis(bipyridine)bis(bipyridine)Ru(II)PF_6 C'12

Prepared using 1-ferrocenyl-3-(3,5-dichlorophenyl)propane-1,3-dione (0.12 g, 0.3 mmol) and purified by column chromatography, eluting 1:9 v/v acetonitrile/dichloromethane to give dark red solid (0.09 g, 32 %).

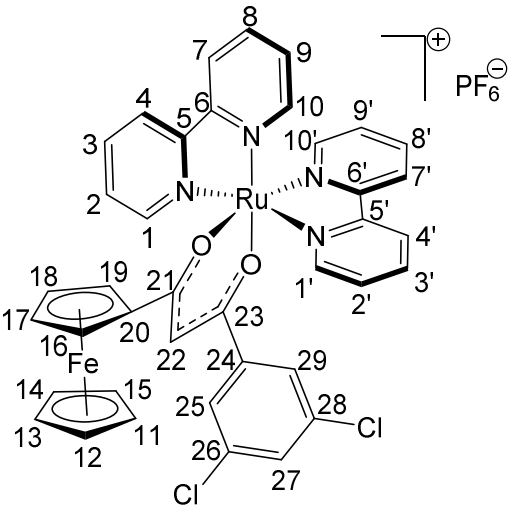

δ_H (500 MHz, $(CD_3)_2CO$); 8.93 (d, 1H, *J 8.9* Hz, bpyH, $H_{1'}$), 8.71 (m, 2H, bpyH, $H_{1,4'}$), 8.61 (dd, 2H, *J 8.1, 2.2* Hz, bpyH, $H_{7',7}$), 8.53 (d, 1H, *J 7.7* Hz, bpyH, H_4), 8.08 (q, 2H, *J 7.2* Hz, bpyH, $H_{3',3}$), 8.01 (d, 1H, *J 5.7* Hz, bpyH, $H_{10'}$), 7.94 (d, 1H, *J 5.5* Hz, bpyH, H_{10}), 7.85 (q, 2H, *J 8.5* Hz, bpyH, $H_{8',8}$), 7.70 (t, 1H, *J 6.6* Hz, bpyH, $H_{2'}$), 7.62 (t, 1H, *J 6.4* Hz, bpyH, H_2), 7.53 (d, 2H, *J 1.7* Hz, ArH, $H_{25,29}$), 7.37 (broad s, 1H, ArH, H_{27}), 7.22 (t, 2H, *J 6.6* Hz, bpyH, $H_{9',9}$), 6.39 (s, 1H, CH, H_{22}), 4.76 (broad s, 1H, Cp CH, $H_{16/19}$), 4.41 (broad s, 1H, Cp CH, $H_{16/19}$), 4.23 (broad s, 2H, Cp CH, $H_{17,18}$), 3.68 (s, 5H, Cp ring, $H_{11\text{-}15}$); **δ_C**{^{1}H} (125 MHz, $(CD_3)_2CO$); 187.8 (quaternary CO, C_{21}), 174.6 (quaternary CO, C_{23}), 160.3 (quaternary bpyC, $C_{5'}$), 160.2 (quaternary bpyC, C_5), 159.0 (quaternary bpyC, $C_{6'}$), 159.0 (quaternary bpyC, C_6), 154.5 (bpyC, $C_{1'}$), 154.4 (bpyC, C_1), 151.5 (bpyC, $C_{10'}$), 151.0 (bpyC, C_{10}), 144.0 (quaternary ArC, C_{24}), 137.7 (bpyC, $C_{3'}$), 137.7 (bpyC, C_3), 136.0 (bpyC, $C_{8'}$), 135.5 (bpyC, C_8), 134.8 (quaternary ArCCl, $C_{26,28}$), 130.1 (ArC, C_{27}), 127.6 (bpyC, $C_{2'}$), 127.2 (bpyC, C_2), 126.4 (bpyC, $C_{9'}$), 126.3 (bpyC, C_9), 125.8 (ArC, $C_{26,28}$), 124.2 (bpyC, $C_{4'}$), 124.1 (bpyC, C_4), 124.1 (bpyC, $C_{7'}$), 124.1 (bpyC, C_7), 95.2 (CH, C_{22}), 83.2 (quaternary Cp, C_{20}), 72.0 (Cp CH, $C_{16/19}$), 71.8 (Cp CH, $C_{16/19}$), 70.6 (Cp ring, $C_{11\text{-}15}$), 69.9 (Cp CH, $C_{17/18}$), 68.5 (Cp CH, $C_{17/18}$); **Analysis**: Calculated C 48.87, H 3.05, N 5.85 %, Found C 48.66, H 2.99, N 5.76 %; **H.R.M.S. [ES+]** found $[MH^+]$-PF_6 813.007.

8.6.13 Synthesis of (1-Ferrocenyl-3-(4-bromophenyl)propane-1,3-dione)bis(bipyridine)bis(bipyridine)Ru(II)PF_6 C'13

Prepared using 1-ferrocenyl-3-(4-bromophenyl)propane-1,3-dione (0.12 g, 0.3 mmol) and purified by column chromatography, eluting 1:9 v/v acetonitrile/dichloromethane to give dark red solid (0.05 g, 19 %).

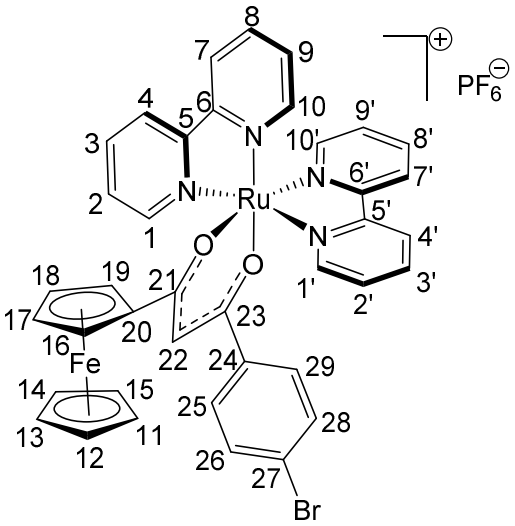

δ_H (500 MHz, $(CD_3)_2CO$); 8.87 (d, 1H, *J 5.5* Hz, bpyH, $H_{1'}$), 8.73 (d, 1H, *J 5.3* Hz, bpyH, H_1), 8.70 (d, 1H, *J 8.3* Hz, bpyH, $H_{4'}$), 8.60 (d, 2H, *J 8.3* Hz, bpyH, $H_{7',7}$), 8.52 (d, 1H, *J 7.8* Hz, bpyH, H_4), 8.06 (dt, 2H, *J 12.8, 7.8* Hz, bpyH, $H_{3',3}$), 8.01 (d, 1H, *J 5.7* Hz, bpyH, $H_{10'}$), 7.95 (d, 1H, *J 5.3* Hz, bpyH, H_{10}), 7.85 (dt, 2H, *J 12.8, 7.8* Hz, bpyH, $H_{8',8}$), 7.68 (t, 1H, *J 6.4* Hz, bpyH, $H_{2'}$), 7.61 (t, 1H, *J 6.4* Hz, bpyH, H_2), 7.55 (d, 2H, *J 8.3* Hz, ArH, $H_{25,29}$), 7.34 (d, 2H, *J 8.4* Hz, ArH, $H_{26,28}$), 7.22 (t, 2H, *J 6.4* Hz, bpyH, $H_{9',9}$), 6.37 (s, 1H, CH, H_{22}), 4.68 (borad s, 1H, Cp CH, $H_{16/19}$), 4.39 (broad s, 1H, Cp CH, $H_{16/19}$), 4.21 (broad s, 2H, Cp CH, $H_{17,18}$), 3.67 (s, 5H, Cp ring, $H_{11\text{-}15}$); **δ_C**{^{1}H} (125 MHz, $(CD_3)_2CO$); 186.9 (quaternary CO, C_{21}), 177.1 (quaternary CO, C_{23}), 160.3 (quaternary bpyC, $C_{5'}$), 160.3 (quaternary bpyC, C_5), 159.1 (quaternary bpyC, $C_{6'}$), 159.0 (quaternary bpyC, C_6), 154.4 (bpyC, $C_{1'}$), 154.4 (bpyC, C_1), 151.3 (bpyC, $C_{10'}$), 151.0 (bpyC, C_{10}), 139.8 (quaternary ArC, C_{24}), 137.6 (bpyC, $C_{3'}$), 137.5 (bpyC, C_3), 135.9 (bpyC, $C_{8',8}$), 132.1 (ArC, $C_{25,29}$), 129.2 (ArC, $C_{26,28}$), 127.5 (bpyC, $C_{2'}$), 127.2 (bpyC, C_2), 126.4 (bpyC, $C_{9'}$), 126.3 (bpyC, C_9), 124.8 (quaternary ArCBr, C_{27}), 124.2 (bpyC, $C_{4'}$), 124.1 (bpyC, C_4), 124.1 (bpyC, $C_{7'}$), 124.0 (bpyC, C_7), 94.7 (CH, C_{22}), 83.4 (quaternary Cp, C_{20}), 71.7 (Cp CH, $C_{16/19}$), 71.6 (Cp CH, $C_{16/19}$), 70.6 (Cp ring, $C_{11\text{-}15}$), 69.8 (Cp CH, $C_{17/18}$), 68.3 (Cp CH, $C_{17/18}$); **Analysis**: Calculated C 48.37, H 3.12, N 5.79 %, Found C 48.27, H 3.06, N 5.71 %; **H.R.M.S. [ES+]** found $[MH^+]$-PF_6 822.994.

8.6.14 Synthesis of (1-Ferrocenyl-3-(4-iodophenyl)propane-1,3-dione)bis(bipyridine)bis(bipyridine)Ru(II)PF_6 C'14

Prepared using 1-ferrocenyl-3-(4-iodophenyl)propane-1,3-dione (0.14 g, 0.3 mmol) and purified by column chromatography, eluting 1:9 v/v acetonitrile/dichloromethane to give dark red solid (0.09 g, 28 %).

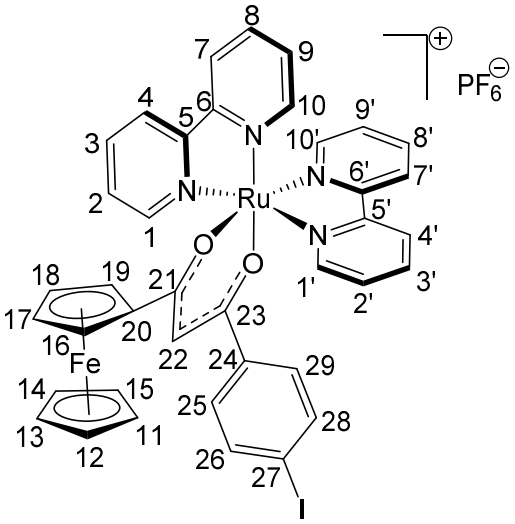

δ_H (500 MHz, $(CD_3)_2CO$); 8.87 (d, 1H, *J 5.0* Hz, bpyH, $H_{1'}$), 8.71 (m, 2H, bpyH, $H_{1,4'}$), 8.60 (d, 2H, *J 8.0* Hz, bpyH, $H_{7',7}$), 8.52 (d, 1H, *J 7.8* Hz, bpyH, H_4), 8.06 (dt, 2H, *J 13.3, 7.8* Hz, bpyH, $H_{3',3}$), 8.00 (d, 1H, *J 5.5* Hz, bpyH, H_{10}), 7.95 (d, 1H, *J 5.7* Hz, bpyH, H_{10}), 7.85 (dt, 2H, *J 13.3, 7.8* Hz, bpyH, $H_{8',8}$), 7.69 (t, 1H, *J 6.4* Hz, bpyH, $H_{2'}$), 7.61 (t, 1H, *J 6.4* Hz, bpyH, H_2), 7.55 (d, 2H, *J 8.3* Hz, ArH, $H_{25,29}$), 7.39 (d, 2H, *J 8.3* Hz, ArH, $H_{26,28}$), 7.21 (t, 2H, *J 5.5* Hz, bpyH, $H_{9',9}$), 6.36 (s, 1H, CH, H_{22}), 4.67 (broad s, 1H, Cp CH, $H_{16/19}$), 4.38 (broad s, 1H, Cp CH, $H_{16/19}$), 4.21 (broad s, 2H, Cp CH, $H_{17,18}$), 3.67 (s, 5H, Cp ring, $H_{11\text{-}15}$); **δ_C**{^{1}H} (125 MHz, $(CD_3)_2CO$); 186.8 (quaternary CO, C_{21}), 179.4 (quaternary CO, C_{23}), 160.3 (quaternary bpyC, $C_{5'}$), 160.2 (quaternary bpyC, C_5), 159.1 (quaternary bpyC, $C_{6'}$), 159.0 (quaternary bpyC, C_6), 154.4 (bpyC, $C_{1'}$), 154.4 (bpyC, C_1), 151.3 (bpyC, $C_{10'}$), 151.0 (bpyC, C_{10}), 148.9 (quaternary ArC, C_{24}), 138.3 (ArC, $C_{25,29}$), 137.6 (bpyC, $C_{3'}$), 137.5 (bpyC, C_3), 135.9 (bpyC, $C_{8',8}$), 129.2 (ArC, $C_{26,28}$), 127.4 (bpyC, $C_{2'}$), 127.1 (bpyC, C_2), 126.4 (bpyC, $C_{9'}$), 126.3 (bpyC, C_9), 124.2 (bpyC, $C_{4'}$), 124.1 (bpyC, C_4), 124.1 (bpyC, $C_{7'}$), 124.0 (bpyC, C_7), 118.9 (quaternary ArCl, C_{27}), 94.6 (CH, C_{22}), 83.6 (quaternary Cp, C_{20}), 71.7 (Cp CH, $C_{16/19}$), 71.6 (Cp CH, $C_{16/19}$), 70.6 (Cp ring, $C_{11\text{-}15}$), 69.8 (Cp CH, $C_{17/18}$), 68.3 (Cp CH, $C_{17/18}$); **Analysis**: Calculated C 46.13, H 2.98, N 5.52 %, Found C 45.27, H 2.58, N 5.00 %; **H.R.M.S. [ES+]** found $[MH^+]$-PF_6 870.983.

8.6.15 Synthesis of (1-Ferrocenyl-3-(4-methoxyphenyl)propane-1,3-dione)bis(bipyridine)bis(bipyridine)Ru(II)PF_6 C'15

Prepared using 1-ferrocenyl-3-(4-methoxyphenyl)propane-1,3-dione (0.11 g, 0.3 mmol) and purified by column chromatography, eluting 1:9 v/v acetonitrile/dichloromethane to give dark red solid (0.08 g, 30 %).

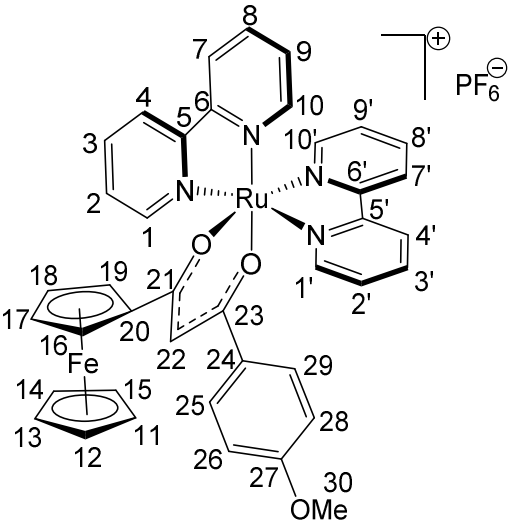

δ_H (500 MHz, $(CD_3)_2CO$); 8.84 (d, 1H, *J 4.8* Hz, bpyH, $H_{1'}$), 8.74 (d, 1H, *J 5.5* Hz, bpyH, H_1), 8.69 (d, 1H, *J 8.0* Hz, bpyH, $H_{4'}$), 8.60 (d, 2H, *J 8.0* Hz, bpyH, $H_{7',7}$), 8.52 (d, 1H, *J 7.6* Hz, bpyH, H_4), 8.04 (m, 3H, bpyH, $H_{3',3,10'}$), 7.94 (d, 1H, *J 6.2* Hz, bpyH, H_{10}), 7.84 (m, 2H, bpyH, $H_{8',8}$), 7.67 (t, 1H, *J 6.2* Hz, bpyH, $H_{2'}$), 7.60 (m, 3H, bpyH and ArH, $H_{2,\ 25,29}$), 7.21 (t, 2H, *J 6.9* Hz, bpyH, $H_{9',9}$), 6.70 (d, 2H, *J 8.2* Hz, ArH, $H_{26,28}$), 6.33 (s, 1H, CH, H_{22}), 4.65 (broad s, 1H, Cp CH, $H_{16/19}$), 4.38 (broad s, 1H, Cp CH, $H_{16/19}$), 4.19 (borad s, 2H, Cp CH, $H_{17,18}$), 3.67 (s, 8H, Cp ring and OMe, $H_{11\text{-}15,30}$); **δ_C**{^{1}H} (125 MHz, CD_3CN); 184.5 (quaternary CO, C_{21}), 179.0 (quaternary CO, C_{23}), 159.1 (quaternary bpyC, $C_{5'}$), 158.9 (quaternary bpyC, C_5), 157.7 (quaternary bpyC, $C_{6'}$), 157.6 (quaternary bpyC, C_6), 153.1 (bpyC, $C_{1',1}$), 150.0 (bpyC, $C_{10'}$), 149.7 (bpyC, C_{10}), 136.9 (quaternary ArC, C_{24}), 136.1 (bpyC, $C_{3'}$), 136.0 (bpyC, C_3), 134.4 (bpyC, $C_{8',8}$), 127.8 (ArC, $C_{25,29}$), 126.0 (bpyC, $C_{2'}$), 125.7 (bpyC, C_2), 124.9 (bpyC, $C_{9'}$), 124.8 (bpyC, C_9), 122.8 (bpyC, $C_{4'}$), 122.7 (bpyC, C_4), 122.7 (bpyC, $C_{7'}$), 122.7 (quaternary ArCOMe), 122.6 (bpyC, C_7), 113.1 (ArC, $C_{26,28}$), 92.8 (CH, C_{22}), 79.6 (quaternary Cp, C_{20}), 70.2 (Cp CH, $C_{16/19}$), 70.1 (Cp CH, $C_{16/19}$), 69.4 (Cp ring, $C_{11\text{-}15}$), 68.4 (Cp CH, $C_{17/18}$), 66.8 (Cp CH, $C_{17/18}$), 54.7 (OCH_3, C_{30}); **Analysis**: Calculated C 52.24, H 3.62, N 6.09 %, Found C 52.18, H 3.55, N 6.02 %; **H.R.M.S. [ES+]** found [MH^+]-PF_6 775.096.

8.7 Cytotoxic Evaluation

Cytotxic studies were carried out by Pablo Caramés-Méndez at the University of Huddersfield. Sterile techniques were used throughout this work. Chemicals were purchased from Sigma-Aldrich Chemical Co. MIA PaCa-2 (human pancreatic carcinoma), HCT116+/+ (human colorectal carcinoma) and ARPE-19 (human retinal pigment epithelial cells) cells were obtained from Prof. Roger Phillips (University of Huddersfield). Stock cell cultures were grown in T-25 or T-75 flasks containing RPMI-1640 complete cell medium (20 mL) and incubated at 37 °C in an atmosphere of 5 % carbon dioxide. The complete medium was prepared from RPMI-1640 incomplete medium (500 mL), sodium pyruvate (5 mL, 0.5 mmol), L-glutamine (5 mL, 1.0 mmol) and foetal bovine serum (FBS) (50 mL). Hank's balanced salt solution (HBSS) was used to wash cells before use and 0.25 % trypsin-EDTA solution was used to detach cells from the flask. MTT stock solutions (5 mg mL-1) were prepared by dissolving MTT (250 µg) in distilled water (50 mL) followed by passage through a 0.2 µm sterile filter. RPMI-1640 incomplete medium, RPMI-1640 complete medium, sodium pyruvate, MTT and MTT stock solutions were all stored at 4 °C. L-glutamine, FBS and 0.25 % trypsin-EDTA solution were all stored at -20 °C. All chemicals except the MTT stock solution were incubated at 37 °C prior to use.

Cells were washed with HBSS (3 × 10 mL) and HBSS carefully removed. 0.25 % trypsinEDTA solution (5 mL) was added and the flasks incubated at 37 °C for 5 minutes. Following cellular detachment from the flask wall, cell media (10 mL) was added. Cells were split into new flasks, diluted with cell media, the lids loosened and the flasks transferred into the incubator at 37 °C. Each cell suspension (10 µL) was transferred to each side of the glass haemocytometer and cells were counted using an optical microscope and an average taken with units of 10^4 cells mL^{-1}.

8.7.1 Five-day MTT Assay (Normoxia)

The cell suspension was diluted with RPMI-1640 complete media to give a concentration of 2 × 104 cells mL^{-1}. 100 µL of cell media was added to the first lane of the 96-well plate to act as a blank. 100 µL of diluted cell suspension were added

to the other wells and the plate incubated at 37 °C overnight with 5 % CO_2. Complexes were prepared in DMSO and then further diluted with RPMI-1640 media to give a final concentration of 250 μM (with a final DMSO concentration at 0.1 %). Further dilutions were carried out to give eight different drug concentrations. All experiments were carried out in triplicate. Drug solutions were added to the cells and the plate incubated for five days at 37 °C with 5 % CO_2. After four days, 20 μL of a MTT stock solution (5 mg mL-1) was added to each well and incubated for a further 3 hours at 37 °C with 5 % CO_2. The media and MTT wasremoved and 150 μL of DMSO added to each well to dissolve any formazan crystals. The absorbance at 540 nm was determined with a Thermo Scientific Multiskan EX microplate photometer. Cell survival was determined at the absorbance of treated cells compared to the absorbance of non-treated cells (negative control). IC_{50} values were determined from plots of percentage survival against drug concentration.

8.7.2 Five-day MTT Assay (hypoxia)

The assay was conducted according to the protocol stated previously for normoxic conditions. However, all the incubations periods, the addition of the drug and the addition of the MTT solution were carried out inside a Don Whitley Scientific H35 Hypoxystation with the oxygen level set at 0.1 %. Cell culture media was conditioned for 24 hours at 0.1 % O_2 prior to the start of the experiment.

8.8 Antimicrobial Studies

Antimicrobial screening was performed by CO-ADD (The Community for Antimicrobial Drug Discovery), funded by the Wellcome Trust (UK) and The University of Queensland (Australia).

8.8.1 Antibacterial Evaluation

Complexes were prepared in DMSO and water to a give a final concentration of 32 μg mL^{-1} in 384-well non-binding surface (NBS) plate. The final DMSO concentration was at a maximum of 1.0 %. All bacteria were cultured in Cationadjusted Mueller Hinton broth (CAMHB) at 37 °C overnight. A sample of each culture was diluted 40-fold in fresh broth and incubated at 37 °C for 1.5 - 3 hours. The resultant mid-log phase cultures were diluted (CFU mL^{-1} measured by OD_{600}), then added to each well of the compound containing plates, giving a cell density of 5×10^5 CFU mL^{-1} and a total volume of 50 μL. Colistin and vancomycin were used as positive bacterial inhibitor standards for Gram-negative and Gram-positive bacteria, respectively. Each standard was provided in 4 concentrations, with 2 above and 2 below its MIC or CC_{50} value, and plated into the first 8 wells of column 23 of the 384-well NBS plates. All the plates were covered and incubated at 37 °C for 18 hours without shaking. All experiments were carried out in duplicate. Inhibition of bacterial growth was determined measuring absorbance at 600 nm (OD_{600}), using a Tecan M1000 Pro monochromator plate reader. The percentage of growth inhibition was calculated for each well, using the negative control (media only) and positive control (bacteria without inhibitors) on the same plate as references. The significance of the inhibition values was determined by modified Z-scores, calculated using the median and MAD of the samples (no controls) on the same plate. Samples with inhibition value above 80 % and Z-Score above 2.5 for either replicate were classed as actives. Samples with inhibition values in the range 50 to 80 % and Z-Score above 2.5 for either replicate were classed as partial actives.

8.8.2 Antibacterial Hit Confirmation

Complexes were prepared in DMSO and water to a give a final concentration of 32 μg mL^{-1} and serially diluted two fold for eight times. Each sample concentration was prepared in 384-well non-binding surface (NBS) plate for each bacterial strain or tissue-culture treated plates for mammalian cell types. The final DMSO concentration was at a maximum of 0.5 % DMSO. All bacteria were cultured in

Cation-adjusted Mueller Hinton broth (CAMHB) at 37 °C overnight. A sample of each culture was then diluted 40-fold in fresh broth and incubated at 37 °C for 1.5-3 h. The resultant mid-log phase cultures were diluted (CFU mL^{-1} measured by OD_{600}), then added to each well of the compound containing plates, giving a cell density of 5×10^5 CFU mL^{-1} and a total volume of 50 µL. Colistin and vancomycin were used as positive bacterial inhibitor standards for Gram-negative and Gram-positive bacteria, respectively. Each standard was provided in 4 concentrations, with 2 above and 2 below its MIC or CC_{50} value, and plated into the first 8 wells of column 23 of the 384-well NBS plates. All the plates were covered and incubated at 37 °C for 18 h without shaking. All experiments were performed in duplicate. Inhibition of bacterial growth was determined measuring absorbance at 600 nm (OD_{600}), using a Tecan M1000 Pro monochromator plate reader. The percentage of growth inhibition was calculated for each well, using the negative control (media only) and positive control (bacteria without inhibitors) on the same plate as references. The percentage of growth inhibition was calculated for each well, using the negative control (media only) and positive control (bacteria without inhibitors) on the same plate. The MIC was determined as the lowest concentration at which the growth was fully inhibited, defined by an inhibition ≥ 80%. In addition, the maximal percentage of growth inhibition is reported as D_{Max}, indicating any compounds with partial activity. Hits were classified by MIC ≤ 16 µg mL^{-1} or MIC ≤ 10 µM in either replicate.

8.8.3 Antifungal Evaluation

Complexes were prepared in DMSO and water to a give a final concentration of 32 µg mL^{-1} in 384-well non-binding surface (NBS) plate. The final DMSO concentration was at a maximum of 1.0 %. Fungal strains were cultured for three days on yeast extract-peptone dextrose (YPD) agar at 30 °C. A yeast suspension of 1 x 10^6 to 5 x 10^6 CFU mL^{-1} (as determined by OD_{530}) was prepared from five colonies. The suspension was diluted and added to each well of the compound-containing plates giving a final cell density of fungi suspension of 2.5 × 10^3 CFU mL^{-1} and a total volume of 50 µL. Fluconazole was used as a positive fungal inhibitor standard and provided in 4 concentrations, with 2 above and 2 below its MIC or CC_{50} value, and plated into the

first 8 wells of column 23 of the 384-well NBS plates. All the plates were covered and incubated at 35 °C for 36 hours without shaking. All experiments were carried out in duplicate. Growth inhibition of *C. albicans* was determined measuring absorbance at 630 nm (OD_{630}) and the growth inhibition of *C. neoformans* was determined measuring the difference in absorbance between 600 and 570 nm ($OD_{600-570}$), after the addition of 0.001 % resazurin and incubation at 35 °C for an additional 2 hours. The absorbance was measured using a Biotek Synergy HTX plate reader. The percentage of growth inhibition was calculated for each well, using the negative control (media only) and positive control (fungi without inhibitors) on the same plate. The significance of the inhibition values was determined by modified Z-scores, calculated using the median and MAD of the samples (no controls) on the same plate. Samples with inhibition value above 80 % and Z-Score above 2.5 for either replicate were classed as actives. Samples with inhibition values in the range 50 to 80 % and Z-Score above 2.5 for either replicate were classed as partial actives.

8.8.4 Antifungal Hit Confirmation

Complexes were prepared in DMSO and water to a give a final concentration of 32 µg mL^{-1} and serially diluted two fold for eight times. Each sample concentration was prepared in 384-well non-binding surface plate for each fungal strain or tissue-culture treated plates for mammalian cell types. The final DMSO concentration was at a maximum of 0.5 % DMSO. Fungal strains were cultured for three days on YPD agar at 30 °C. A yeast suspension of 1 x 10^6 to 5 x 10^6 CFU mL^{-1} (as determined by OD_{530}) was prepared from five colonies. The suspension was subsequently diluted and added to each well of the compound-containing plates giving a final cell density of fungi suspension of 2.5 × 10^3 CFU mL-1 and a total volume of 50 µL. Fluconazole was used as a positive fungal inhibitor standard and provided in 4 concentrations, with 2 above and 2 below its MIC or CC_{50} value, and plated into the first 8 wells of column 23 of the 384-well NBS plates. All plates were covered and incubated at 35 °C for 36 hours without shaking. All experiments were performed in duplicate. Growth inhibition of *C. albicans* was determined measuring absorbance at 630 nm (OD_{630}) and the growth inhibition of *C. neoformans* was determined measuring the

difference in absorbance between 600 and 570 nm ($OD_{600-570}$) after the addition of 0.001 % resazurin and incubation at 35 °C for 2 hours. The absorbance was measured using a Biotek Multiflo Synergy HTX plate reader. The percentage of growth inhibition was calculated for each well, using the negative control (media only) and positive control (fungi without inhibitors) on the same plate. The MIC was determined as the lowest concentration at which the growth was fully inhibited, defined by an inhibition ≥ 80% for *C. albicans* and an inhibition ≥ 70% for C. neoformans. Due to a higher variance in growth and inhibition, a lower threshold was applied to the data for *C. neoformans*. In addition, the maximal percentage of growth inhibition is reported as DMax, indicating any compounds with marginal activity. Hits were classified by MIC ≤ 16 μg mL^{-1} or MIC ≤ 10 μM in either replicate.

8.8.5 Cytotoxicity Assay

To assess the cytotoxicity, HEK293 cells were counted manually in a Neubauer haemocytometer and then plated in the 384-well plates containing the compounds to give a density of 5000 cells $well^{-1}$ in a final volume of 50 μL. Dulbecco's modified eagle medium (DMEM) supplemented with 10 % FBS was used as growth media and the cells were incubated together with the compounds for 20 hours at 37 °C in 5 % CO_2. Tamoxifen was used as a positive cytotoxicity standard in 8 concentrations in 2 fold serial dilutions with 50 μg mL^{-1} highest concentration. All experiments were performed in duplicate. Cytotoxicity was measured by fluorescence with excitation at 560 nm and emission at 590 nm ($F_{560/590}$), after addition of 5 μL of resazurin (25 μg mL^{-1}) and incubation for a further 3 hours at 37 °C in 5% CO_2. The fluorescence intensity was measured using a Tecan M1000 Pro monochromator plate reader, using automatic gain calculation. CC_{50} were calculated by curve fitting the inhibition values against log(concentration) using sigmoidal dose-response function, with variable fitting values for bottom, top and slope. The maximal percentage of cytotoxicity is reported as D_{Max}, indicating any compounds with partial cytotoxicity. The curve fitting was implemented using Pipeline Pilot's dose-response component. Any value with > indicates a sample with no activity (low D_{Max} value) or samples with CC_{50} values above the maximum tested concentration (higher D_{Max} value). Cytotoxic

samples were classified by CC_{50} ≤ 32 µg mL^{-1} or CC_{50} ≤ 10 µM in either replicate. In addition, samples were flagged as partial cytotoxic if D_{Max} ≥ 50%, even with CC_{50} > the maximum tested concentration.

8.8.6 Haemolysis Assay

To assess blood toxicity, Human whole blood was washed three times with 3 volumes of 0.9% NaCl and then resuspended in same to a concentration of 0.5 x 10_8 cells mL^{-1}, as determined by manual cell count in a Neubauer haemocytometer. The washed cells were then added to the 384-well compound-containing plates for a final volume of 50 µL. After a 10 min shake on a plate shaker the plates were then incubated for 1 h at 37 °C. Melittin was used as a positive heamolytic standard in 8 concentrations in 2 fold serial dilutions with 50 µg mL^{-1} highest concentration. After incubation, the plates were centrifuged at 1000g for 10 min to pellet cells and debris, 25 µL of the supernatant was then transferred to a polystyrene 384-well assay plate. Haemolysis was determined by measuring the supernatant absorbance at 405 mm (OD_{405}). The absorbance was measured using a Tecan M1000 Pro monochromator plate reader. HC_{10} and HC_{50} (concentration at 10% and 50% haemolysis, respectively) were calculated by curve fitting the inhibition values vs. log(concentration) using a sigmoidal dose-response function with variable fitting values for top, bottom and slope. In addition, the maximal percentage of haemolysis is reported as D_{Max}, indicating any compounds with partial haemolysis. The curve fitting was implemented using Pipeline Pilot's dose-response component. Any value with > indicate sample with no activity (low D_{Max} value) or samples with HC_{10} values above the maximum tested concentration (higher D_{Max} value). Haemolysis samples were classified by HC10 ≤ 32 µg mL^{-1} or HC_{10} ≤ 10 µM in either replicate. In addition, samples were flagged as partial haemolytic if D_{Max} ≥ 50%, even with HC_{10} > the maximum tested concentration.

8.9 Hydrolysis

Hydrolysis samples of complexes for investigation by NMR spectroscopy were prepared from a 9:1 mixture of d3-acetonitrile/deuterium oxide to give a final concentration of 8 mg mL^{-1}. The NMR spectra of these samples were acquired every 24 hours over a four day period. Hydrolysis samples of complexes for investigation by UV/vis spectroscopy were prepared from a 9:1 mixture of acetonitrile/water to give a final concentration of 50 μM. The UV/vis spectra of these samples were acquired every 24 hours over a four day period. After the four day investigation period, the mass spectra of the hydrolysis samples were acquired.

8.10 Hydrophobicity

Equal volumes of 1-octanol and sodium chloride saturated distilled water were stirred for 16 hours and separated to give water-saturated octanol and octanol-saturated water. Standard solutions of each complex (5, 10, 20, 40 and 60 μM) were prepared in water-saturated octanol. The calibration curve of absorbance against concentration was determined from the maximum absorbance (λ_{max}) of the standard solutions. Stock solutions of each complex (50 μM) in water-saturated octanol (25 mL) were prepared. Six independent samples were prepared by the addition of the stock solution (3 mL) to a 15 mL Falcon tube followed by layered addition of octanol-saturated water (3 mL). Samples were shaken at 1000 g min^{-1} for 2 hours using an IKA Vibrax VXC basic shaker. The layers were separated and the water-saturated octanol layer retained. The concentration of each sample in the water-saturated octanol layer was determined by UV/vis spectroscopy with reference to the individual calibration curves to give an average concentration for shaken samples ($[C]_{final}$). The concentration of an unshaken sample of stock solution was determined to give $[C]_{initial}$. The partition coefficient (logP) was determined with:

$$\mathbf{Log}\boldsymbol{P} = \mathbf{Log}_{\mathbf{10}}\left(\frac{[\boldsymbol{C}]_{\boldsymbol{final}}}{[\boldsymbol{C}]_{\boldsymbol{initial}} - [\boldsymbol{C}]_{\boldsymbol{final}}}\right)$$

8.11 Biomembrane Studies

The biomembrane studies were performed by Miss. Danielle Marriott and Dr. Shahrzad Mohamadi at the University of Leeds. The micro fabricated electrode coated with DOPC lipid was contained in a closed flow cell. A constant flow of phosphate-buffered saline (PBS) (pH 7.4) was passed over the electrode using a peristaltic pump at a flow rate of 5 - 10 mL min^{-1}. A constant flow of DOPC dispersion in PBS was deposited on the electrode with the Experimental Chapter 8 265 application of a potential excursion from -0.4 to -3.0 V at a scan rate of 100 Vs^{-1}. The electrode in the flow cell was connected to the PGSTATI2 potentiostat interfaced to a Powerlab signal generator and controlled by Scope software. A flow of argon gas is maintained over the electrolytes and the DOPC layer throughout. RCVs were obtained by applying a saw-tooth waveform from -0.4 to -1.2 V (vs Ag/AgCl) with ramp rate 40 V s^{-1} applied to the electrode surface. In the absence of faradaic reactions, the current on the RCV plot was directly proportional to the capacitance of the surface and is displayed as a function of voltage. All assays were carried out with 15.6 µM solutions of each complex in acetone with a constant flow of 0.1 M PBS. The complexes are sampled for 400 seconds followed by PBS for 400 seconds to allow in situ cleaning of the electrode.[12, 13]

8.12 References

1. J. Cosier and A. M. Glazer, *Journal of Applied Crystallography*, 1986, **19**, 105-107.
2. Z. Otwinowski and W. Minor, *in 'DENZO and SCALEPACK programs'*, 1995.
3. J. Glusker, *Acta Crystallographica Section B: Structural Science*, 1986, **42**, 522-524.
4. G. M. Sheldrick, *Acta Crystallographica. Section C, Structural Chemistry*, 2015, **71**, 3-8.
5. G. M. Sheldrick, *Acta Crystallographica Section A: Foundations and Advances*, 2015, **71**, 3-8.
6. G. Sheldrick, *in 'SHELXS86, Program for Crystal Structure Solution'*, 1986.
7. O. V. Dolomanov, L. J. Bourhis, R. J. Gildea, J. A. Howard and H. Puschmann, *Journal of Applied Crystallography*, 2009, **42**, 339-341.
8. A. Spek, *Journal of Applied Crystallography*, 2003, **36**, 7-13.
9. J. C. Swarts, T. G. Vosloo, S. J. Cronje, W. C. Du Plessis, C. E. J. Van Rensburg, E. Kreft and J. E. Van Lier, *Anticancer Research*, 2008, **28**, 2781-2784.
10. Y.-C. Shi, H.-M. Yang, W.-B. Shen, C.-G. Yan and X.-Y. Hu, *Polyhedron*, 2004, **23**, 15-21.
11. Y. Y. Lee, D. B. Walker, J. J. Gooding and B. A. Messerle, *Dalton Transactions*, 2014, **43**, 12734-12742.
12. Z. Coldrick, P. Steenson, P. Millner, M. Davies and A. Nelson, *Electrochimica Acta*, 2009, **54**, 4954-4962.
13. S. Mohamadi, D. J. Tate, A. Vakurov and A. Nelson, *Analytica chimica acta*, 2014, **813**, 83-89.

Appendix

Crystallographic Data

Name	L1	L2	L3
Empirical formula	$C_{14}H_{14}O_2Fe$	$C_{14}H_{11}O_2F_3Fe$	$C_{14}H_{12}O_2F_2Fe$
Formula weight	270.10	324.08	306.09
Temperature/K	119.99(10)	119.99(10)	119.97(10)
Crystal system	orthorhombic	monoclinic	monoclinic
Space group	$P2_12_12_1$	$P2_1/n$	$P2_1/n$
a/Å	5.7213(6)	5.8522(4)	5.7964(13)
b/Å	12.3631(16)	10.2689(7)	9.8412(17)
c/Å	16.259(2)	20.7234(14)	21.224(3)
α/°	90	90	90
β/°	90	91.540(6)	90.662(16)
γ/°	90	90	90
Volume/Å^3	1150.1(2)	1244.94(15)	1210.6(4)
Z	4	4	4
ρ_{calc}g/cm^3	1.560	1.729	1.679
μ/mm^{-1}	1.295	1.246	1.264
F(000)	560.0	656.0	624.0
Crystal size/mm^3	0.40 × 0.08 × 0.08	0.39 × 0.16 × 0.12	0.33 × 0.13 × 0.11
Radiation	MoKα (λ = 0.71073)	MoKα (λ = 0.71073)	MoKα (λ = 0.71073)
2Θ range for data collection/°	6.592 to 59.276	7.112 to 59.08	7.094 to 59.482
Index ranges	-7 ≤ h ≤ 7, -11 ≤ k ≤ 17, -17 ≤ l ≤ 21	-7 ≤ h ≤ 8, -13 ≤ k ≤ 14, -27 ≤ l ≤ 20	-7 ≤ h ≤ 7, -13 ≤ k ≤ 13, -28 ≤ l ≤ 19
Reflections collected	4902	6502	2490
Independent reflections	2555 [R_{int} = 0.0654, R_{sigma} = 0.1169]	2940 [R_{int} = 0.0486, R_{sigma} = 0.0781]	2490 [R_{int} = ?, R_{sigma} = 0.1895]
Data/restraints/parameters	2555/213/156	2940/18/182	2490/18/183
Goodness-of-fit on F^2	1.065	1.060	0.916
Final R indexes [I>=2σ (I)]	R_1 = 0.0580, wR_2 = 0.0798	R_1 = 0.0823, wR_2 = 0.1937	R_1 = 0.0715, wR_2 = 0.1566
Final R indexes [all data]	R_1 = 0.0867, wR_2 = 0.0965	R_1 = 0.1229, wR_2 = 0.2222	R_1 = 0.1284, wR_2 = 0.1731
Largest diff. peak/hole / e Å^{-3}	0.68/-0.52	1.59/-0.86	0.90/-1.02

Name	L4	L5	L6
Empirical formula	$C_{17}H_{14}FeO_3$	$C_{17}H_{14}O_3Fe$	$C_{19}H_{16}FeO_2$
Formula weight	322.13	322.13	332.17
Temperature/K	119.99(14)	120.02(17)	120.1(3)
Crystal system	tetragonal	orthorhombic	monoclinic
Space group	I-4	$P2_12_12_1$	$P2_1/c$
a/Å	21.5997(7)	10.0711(4)	10.6800(8)
b/Å	21.5997(7)	10.1028(5)	12.4980(8)
c/Å	5.9013(4)	13.3273(5)	11.3058(8)
α/°	90.00	90.00	90.00
β/°	90.00	90.00	105.695(7)
γ/°	90.00	90.00	90.00
Volume/Å^3	2753.2(2)	1356.00(10)	1452.82(17)
Z	8	4	4
ρ_{calc}g/cm^3	1.554	1.578	1.519
μ/mm^{-1}	1.102	1.119	1.042
F(000)	1328.0	664.0	688.0
Crystal size/mm^3	0.12 × 0.09 × 0.08	0.09 × 0.06 × 0.04	0.25 × 0.14 × 0.07
Radiation	MoKα (λ = 0.71073)	MoKα (λ = 0.71073)	MoKα (λ = 0.71073)
2Θ range for data collection/°	7.16 to 59.64	6.48 to 59.26	6.52 to 52.74
Index ranges	-28 ≤ h ≤ 24, -29 ≤ k ≤ 19, -5 ≤ l ≤ 8	-9 ≤ h ≤ 13, -10 ≤ k ≤ 11, -11 ≤ l ≤ 17	-13 ≤ h ≤ 11, -15 ≤ k ≤ 13, -14 ≤ l ≤ 13
Reflections collected	4289	4095	7863
Independent reflections	2775 [R_{int} = 0.0328, R_{sigma} = 0.0662]	2518 [R_{int} = 0.0306, R_{sigma} = 0.0535]	2970 [R_{int} = 0.0648, R_{sigma} = 0.0735]
Data/restraints/parameters	2775/0/191	2518/0/191	2970/0/200
Goodness-of-fit on F^2	1.028	1.056	1.093
Final R indexes [I>=2σ (I)]	R_1 = 0.0379, wR_2 = 0.0687	R_1 = 0.0376, wR_2 = 0.0682	R_1 = 0.0451, wR_2 = 0.0914
Final R indexes [all data]	R_1 = 0.0432, wR_2 = 0.0706	R_1 = 0.0515, wR_2 = 0.0740	R_1 = 0.0571, wR_2 = 0.0970
Largest diff. peak/hole / e Å^{-3}	0.30/-0.25	0.28/-0.47	0.46/-0.41

Name	L7	L8	L9
Empirical formula	$C_{23}H_{18}O_2Fe$	$C_{20}H_{18}FeO_2$	$C_{20}H_{18}O_2Fe$
Formula weight	382.22	346.19	346.19
Temperature/K	120.03(11)	120.02(10)	120.01(16)
Crystal system	monoclinic	monoclinic	monoclinic
Space group	$P2_1/n$	$P2_1/n$	$P2_1/n$
a/Å	8.1103(2)	6.0823(5)	5.8242(3)
b/Å	23.0948(7)	34.008(2)	20.8201(11)
c/Å	37.1744(13)	7.5433(7)	12.8959(6)
α/°	90	90.00	90.00
β/°	89.946(3)	99.547(8)	96.123(5)
γ/°	90	90.00	90.00
Volume/Å^3	6963.0(4)	1538.7(2)	1554.84(14)
Z	15	4	4
ρ_{calc}g/cm^3	1.367	1.494	1.479
μ/mm^{-1}	0.825	0.987	0.977
F(000)	2970.0	720.0	720.0
Crystal size/mm^3	0.23 × 0.16 × 0.12	0.31 × 0.17 × 0.11	0.54 × 0.25 × 0.19
Radiation	MoKα (λ = 0.71073)	MoKα (λ = 0.71073)	MoKα (λ = 0.71073)
2Θ range for data collection/°	5.756 to 59.622	5.6 to 59.5	6.36 to 59.66
Index ranges	-10 ≤ h ≤ 11, -31 ≤ k ≤ 31, -51 ≤ l ≤ 46	-7 ≤ h ≤ 7, -37 ≤ k ≤ 43, -10 ≤ l ≤ 7	-7 ≤ h ≤ 7, -28 ≤ k ≤ 24, -17 ≤ l ≤ 14
Reflections collected	48495	9385	9449
Independent reflections	16628 [R_{int} = 0.0677, R_{sigma} = 0.0915]	3759 [R_{int} = 0.0873, R_{sigma} = 0.1059]	3804 [R_{int} = 0.0522, R_{sigma} = 0.0723]
Data/restraints/parameters	16628/0/942	3759/44/246	3804/0/210
Goodness-of-fit on F^2	0.963	1.208	1.026
Final R indexes [I>=2σ (I)]	R_1 = 0.0605, wR_2 = 0.1478	R_1 = 0.0782, wR_2 = 0.1741	R_1 = 0.0445, wR_2 = 0.0847
Final R indexes [all data]	R_1 = 0.0994, wR_2 = 0.1824	R_1 = 0.1007, wR_2 = 0.1883	R_1 = 0.0642, wR_2 = 0.0959
Largest diff. peak/hole / e Å^{-3}	0.80/-0.62	0.57/-0.51	0.43/-0.45

Name	L10	L11	L12
Empirical formula	$C_{21}H_{20}O_2Fe$	$C_{19}H_{15}FFeO_2$	$C_{19}H_{15}O_2FFe$
Formula weight	360.22	350.16	350.16
Temperature/K	120.00(10)	120.00(16)	120.01(11)
Crystal system	monoclinic	monoclinic	monoclinic
Space group	$P2_1/c$	$P2_1/c$	$P2_1/n$
a/Å	16.6707(7)	14.9206(5)	7.5254(3)
b/Å	9.2042(4)	9.6135(3)	12.5232(6)
c/Å	10.7241(5)	10.6994(4)	15.8320(8)
α/°	90.00	90.00	90.00
β/°	90.123(4)	104.132(3)	90.632(4)
γ/°	90.00	90.00	90.00
Volume/Å^3	1645.49(12)	1488.26(8)	1491.95(12)
Z	4	4	4
ρ_{calc}g/cm^3	1.454	1.563	1.559
μ/mm^{-1}	0.926	1.031	1.028
F(000)	752.0	720.0	720.0
Crystal size/mm^3	0.35 × 0.23 × 0.16	0.14 × 0.06 × 0.06	0.31 × 0.20 × 0.09
Radiation	MoKα (λ = 0.71073)	MoKα (λ = 0.71073)	MoKα (λ = 0.71073)
2Θ range for data collection/°	5.84 to 59.38	6.84 to 52.74	6.32 to 59.44
Index ranges	-21 ≤ h ≤ 22, -12 ≤ k ≤ 8, -14 ≤ l ≤ 13	-18 ≤ h ≤ 16, -11 ≤ k ≤ 12, -13 ≤ l ≤ 13	-9 ≤ h ≤ 10, -15 ≤ k ≤ 17, -21 ≤ l ≤ 20
Reflections collected	11240	8051	11936
Independent reflections	4025 [R_{int} = 0.0441, R_{sigma} = 0.0533]	3031 [R_{int} = 0.0297, R_{sigma} = 0.0327]	3704 [R_{int} = 0.0502, R_{sigma} = 0.0545]
Data/restraints/parameters	4025/0/220	3031/2/213	3704/0/209
Goodness-of-fit on F^2	1.069	1.068	1.050
Final R indexes [I>=2σ (I)]	R_1 = 0.0397, wR_2 = 0.0838	R_1 = 0.0296, wR_2 = 0.0703	R_1 = 0.0450, wR_2 = 0.0894
Final R indexes [all data]	R_1 = 0.0511, wR_2 = 0.0914	R_1 = 0.0363, wR_2 = 0.0738	R_1 = 0.0634, wR_2 = 0.0965
Largest diff. peak/hole / e Å^{-3}	0.40/-0.51	0.31/-0.21	0.54/-0.78

Name	L13	L14	L15
Empirical formula	$C_{19}H_{15}O_2FFe$	$C_{19}H_{14}O_2F_2Fe$	$C_{19}H_{15}ClFeO_2$
Formula weight	350.16	368.15	366.61
Temperature/K	120.00(10)	120.00(11)	120.01(10)
Crystal system	monoclinic	triclinic	monoclinic
Space group	$P2_1/c$	P-1	$P2_1/n$
a/Å	6.6106(2)	6.1461(5)	6.0395(4)
b/Å	11.4523(4)	7.2741(6)	33.719(2)
c/Å	20.1433(6)	17.3881(14)	7.6325(5)
α/°	90.00	88.372(6)	90
β/°	99.109(3)	85.025(7)	99.641(7)
γ/°	90.00	74.844(7)	90
Volume/Å^3	1505.76(8)	747.50(10)	1532.40(17)
Z	4	2	4
ρ_{calc}g/cm^3	1.545	1.636	1.589
μ/mm^{-1}	1.019	1.040	1.164
F(000)	720.0	376.0	752.0
Crystal size/mm^3	0.40 × 0.29 × 0.17	0.42 × 0.09 × 0.04	0.14 × 0.06 × 0.04
Radiation	MoKα (λ = 0.71073)	MoKα (λ = 0.71073)	Mo Kα (λ = 0.71073)
2Θ range for data collection/°	6.9 to 59.58	6.24 to 62.54	5.928 to 59.312
Index ranges	-8 ≤ h ≤ 8, -15 ≤ k ≤ 14, -28 ≤ l ≤ 25	-8 ≤ h ≤ 8, -10 ≤ k ≤ 9, -25 ≤ l ≤ 22	-6 ≤ h ≤ 8, -44 ≤ k ≤ 46, -10 ≤ l ≤ 7
Reflections collected	9632	8548	9008
Independent reflections	3687 [R_{int} = 0.0240, R_{sigma} = 0.0293]	4185 [R_{int} = 0.0506, R_{sigma} = 0.0826]	3704 [R_{int} = 0.0546, R_{sigma} = 0.0807]
Data/restraints/parameters	3687/0/209	4185/0/218	3704/28/245
Goodness-of-fit on F^2	1.065	1.071	1.045
Final R indexes [I>=2σ (I)]	R_1 = 0.0317, wR_2 = 0.0794	R_1 = 0.0520, wR_2 = 0.1011	R_1 = 0.0836, wR_2 = 0.1709
Final R indexes [all data]	R_1 = 0.0373, wR_2 = 0.0837	R_1 = 0.0716, wR_2 = 0.1146	R_1 = 0.1052, wR_2 = 0.1814
Largest diff. peak/hole / e Å^{-3}	0.32/-0.30	0.49/-0.55	0.47/-0.72

Name	L16	L18	L19
Empirical formula	$C_{19}H_{15}ClFeO_2$	$C_{19}H_{15}O_2FeBr$	$C_{19}H_{15}BrFeO_2$
Formula weight	366.61	411.07	411.07
Temperature/K	120.0(2)	119.99(10)	119.99(18)
Crystal system	monoclinic	monoclinic	monoclinic
Space group	C2/c	$P2_1/n$	C2/c
a/Å	18.5701(10)	6.0794(4)	18.5887(10)
b/Å	8.4583(5)	33.9257(14)	8.4492(4)
c/Å	20.0424(11)	7.6388(4)	20.5237(10)
α/°	90.00	90	90.00
β/°	103.602(6)	99.609(5)	103.869(5)
γ/°	90.00	90	90.00
Volume/Å^3	3059.8(3)	1553.38(15)	3129.5(3)
Z	8	4	8
ρ_{calc}g/cm^3	1.592	1.758	1.745
μ/mm^{-1}	1.166	3.549	3.523
F(000)	1504.0	824.0	1648.0
Crystal size/mm^3	0.16 × 0.14 × 0.04	0.45 × 0.40 × 0.19	0.18 × 0.10 × 0.05
Radiation	MoKα (λ = 0.71073)	MoKα (λ = 0.71073)	MoKα (λ = 0.71073)
2Θ range for data collection/°	6.44 to 59.84	5.918 to 59.396	7.04 to 59.62
Index ranges	-25 ≤ h ≤ 25, -11 ≤ k ≤ 11, -27 ≤ l ≤ 24	-6 ≤ h ≤ 8, -46 ≤ k ≤ 45, -8 ≤ l ≤ 10	-24 ≤ h ≤ 25, -11 ≤ k ≤ 11, -28 ≤ l ≤ 26
Reflections collected	9189	8492	10058
Independent reflections	3697 [R_{int} = 0.0234, R_{sigma} = 0.0310]	3754 [R_{int} = 0.0488, R_{sigma} = 0.0746]	3793 [R_{int} = 0.0300, R_{sigma} = 0.0378]
Data/restraints/parameters	3697/0/209	3754/144/245	3793/0/209
Goodness-of-fit on F^2	1.068	1.266	1.058
Final R indexes [I>=2σ (I)]	R_1 = 0.0334, wR_2 = 0.0787	R_1 = 0.0815, wR_2 = 0.1726	R_1 = 0.0270, wR_2 = 0.0577
Final R indexes [all data]	R_1 = 0.0424, wR_2 = 0.0833	R_1 = 0.1044, wR_2 = 0.1820	R_1 = 0.0366, wR_2 = 0.0617
Largest diff. peak/hole / e Å^{-3}	0.41/-0.24	0.83/-1.13	0.43/-0.48

Name	L20	L21	L22
Empirical formula	$C_{19}H_{15}O_2FeI$	$C_{19}H_{15}FeIO_2$	$C_{20}H_{17}FeO_3$
Formula weight	458.06	253.18	361.19
Temperature/K	120.00(11)	120.03(10)	120.4(8)
Crystal system	monoclinic	tetragonal	monoclinic
Space group	$P2_1/c$	$P4_2/n$	$P2_1/c$
a/Å	6.7169(4)	23.3147(6)	18.5141(12)
b/Å	23.1415(12)	23.3147(6)	7.8814(6)
c/Å	10.5163(5)	6.0679(2)	10.7330(9)
α/°	90.00	90	90.00
β/°	95.487(5)	90	93.702(7)
γ/°	90.00	90	90.00
Volume/Å^3	1627.16(15)	3298.38(19)	1562.9(2)
Z	4	8	4
ρ_{calc}g/cm^3	1.870	1.784	1.535
μ/mm^{-1}	2.830	2.790	0.980
F(000)	896.0	1673.0	748.0
Crystal size/mm^3	0.22 × 0.07 × 0.05	0.34 × 0.14 × 0.06	0.26 × 0.06 × 0.04
Radiation	MoKα (λ = 0.71073)	MoKα (λ = 0.71073)	MoKα (λ = 0.71073)
2Θ range for data collection/°	6.1 to 59.4	6.938 to 59.438	6.42 to 59.54
Index ranges	-8 ≤ h ≤ 8, -28 ≤ k ≤ 32, -14 ≤ l ≤ 14	-30 ≤ h ≤ 31, -28 ≤ k ≤ 32, -6 ≤ l ≤ 8	-23 ≤ h ≤ 24, -10 ≤ k ≤ 10, -14 ≤ l ≤ 9
Reflections collected	10586	13311	4203
Independent reflections	3957 [R_{int} = 0.0384, R_{sigma} = 0.0502]	4123 [R_{int} = 0.0614, R_{sigma} = 0.0730]	4203 [R_{int} = 0.0000, R_{sigma} = 0.0566]
Data/restraints/parameters	3957/0/209	4123/0/209	4203/0/219
Goodness-of-fit on F^2	1.044	1.063	1.043
Final R indexes [I>=2σ (I)]	R_1 = 0.0334, wR_2 = 0.0590	R_1 = 0.0454, wR_2 = 0.0833	R_1 = 0.0468, wR_2 = 0.1074
Final R indexes [all data]	R_1 = 0.0465, wR_2 = 0.0647	R_1 = 0.0909, wR_2 = 0.1038	R_1 = 0.0610, wR_2 = 0.1109
Largest diff. peak/hole / e Å^{-3}	0.49/-0.62	0.92/-1.11	1.06/-0.46

Name	L23	L24	L26
Empirical formula	$C_{20}H_{18}FeO_3$	$C_{21}H_{20}O_3Fe$	$C_{18}H_{15}NO_2Fe$
Formula weight	362.19	376.22	333.16
Temperature/K	120.0(2)	120.01(10)	120.00(17)
Crystal system	orthorhombic	monoclinic	monoclinic
Space group	Pbca	$P2_1/c$	$P2_1/c$
a/Å	7.8804(5)	7.3774(3)	10.4632(10)
b/Å	12.2936(9)	19.9872(9)	12.5638(12)
c/Å	32.965(2)	11.5735(5)	11.1284(11)
α/°	90	90.00	90.00
β/°	90	94.357(4)	104.247(10)
γ/°	90	90.00	90.00
Volume/Å^3	3193.7(4)	1701.62(13)	1417.9(2)
Z	8	4	4
ρ_{calc}g/cm^3	1.507	1.469	1.561
μ/mm^{-1}	0.959	0.903	1.069
F(000)	1504.0	784.0	688.0
Crystal size/mm^3	0.28 × 0.16 × 0.05	0.36 × 0.18 × 0.13	0.14 × 0.11 × 0.06
Radiation	MoKα (λ = 0.71073)	MoKα (λ = 0.71073)	MoKα (λ = 0.71073)
2Θ range for data collection/°	6.264 to 59.59	6.66 to 59.38	6.48 to 59.54
Index ranges	-10 ≤ h ≤ 10, -17 ≤ k ≤ 16, -37 ≤ l ≤ 41	-8 ≤ h ≤ 10, -27 ≤ k ≤ 26, -15 ≤ l ≤ 15	-13 ≤ h ≤ 14, -16 ≤ k ≤ 17, -14 ≤ l ≤ 15
Reflections collected	14752	12219	8466
Independent reflections	4044 [R_{int} = 0.0593, R_{sigma} = 0.0659]	4130 [R_{int} = 0.0443, R_{sigma} = 0.0515]	3462 [R_{int} = 0.0523, R_{sigma} = 0.0709]
Data/restraints/parameters	4044/0/219	4130/0/228	3462/2/207
Goodness-of-fit on F^2	1.108	1.074	1.092
Final R indexes [I>=2σ (I)]	R_1 = 0.0581, wR_2 = 0.0775	R_1 = 0.0477, wR_2 = 0.1007	R_1 = 0.0489, wR_2 = 0.0883
Final R indexes [all data]	R_1 = 0.0837, wR_2 = 0.0847	R_1 = 0.0611, wR_2 = 0.1086	R_1 = 0.0725, wR_2 = 0.0999
Largest diff. peak/hole / e Å^{-3}	0.36/-0.40	0.62/-0.47	0.43/-0.34

Name	C1	C3	C4
Empirical formula	$C_{24}H_{27}ClFeO_2Ru$	$C_{24}H_{25}O_2F_2ClFeRu$	$C_{29}H_{30}ClFeNO_3Ru$
Formula weight	539.83	575.81	632.91
Temperature/K	120.0(2)	119.97(16)	120.00(10)
Crystal system	monoclinic	orthorhombic	monoclinic
Space group	$P2_1/c$	Pbca	$P2_1/c$
a/Å	7.4917(3)	19.5151(5)	12.5821(3)
b/Å	16.7786(7)	7.64427(16)	11.0033(2)
c/Å	34.6443(13)	29.7943(7)	18.9377(5)
α/°	90.00	90.00	90.00
β/°	93.844(3)	90.00	100.613(3)
γ/°	90.00	90.00	90.00
Volume/Å^3	4345.0(3)	4444.67(18)	2576.98(11)
Z	8	8	4
ρ_{calc}g/cm^3	1.650	1.721	1.631
μ/mm^{-1}	1.503	12.153	1.285
F(000)	2192.0	2320.0	1288.0
Crystal size/mm^3	0.05 × 0.04 × 0.02	0.15 × 0.12 × 0.06	0.17 × 0.12 × 0.09
Radiation	MoKα (λ = 0.71073)	CuKα (λ = 1.54184)	MoKα (λ = 0.71073)
2Θ range for data collection/°	5.96 to 52.74	5.94 to 148.4	6.2 to 59.66
Index ranges	-9 ≤ h ≤ 9, -20 ≤ k ≤ 20, -42 ≤ l ≤ 43	-24 ≤ h ≤ 22, -9 ≤ k ≤ 7, -34 ≤ l ≤ 37	-17 ≤ h ≤ 16, -15 ≤ k ≤ 15, -21 ≤ l ≤ 25
Reflections collected	34705	21602	20080
Independent reflections	8869 [R_{int} = 0.0777, R_{sigma} = 0.0811]	4521 [R_{int} = 0.0918, R_{sigma} = 0.0585]	6317 [R_{int} = 0.0443, R_{sigma} = 0.0537]
Data/restraints/parameters	8869/0/531	4521/3/292	6317/0/329
Goodness-of-fit on F^2	1.097	1.044	1.094
Final R indexes [I>=2σ (I)]	R_1 = 0.0564, wR_2 = 0.0805	R_1 = 0.0586, wR_2 = 0.1295	R_1 = 0.0358, wR_2 = 0.0663
Final R indexes [all data]	R_1 = 0.0853, wR_2 = 0.0872	R_1 = 0.0837, wR_2 = 0.1448	R_1 = 0.0533, wR_2 = 0.0758
Largest diff. peak/hole / e Å^{-3}	0.69/-0.70	1.38/-1.09	1.24/-0.63

Name	C5	C6	C8
Empirical formula	$C_{27}H_{27}ClFeO_3Ru$	$C_{29}H_{29}ClFeO_2Ru$	$C_{30}H_{31}ClFeO_2Ru$
Formula weight	591.86	601.89	615.92
Temperature/K	120.00(17)	120.03(14)	120.02(10)
Crystal system	monoclinic	monoclinic	monoclinic
Space group	$P2_1/n$	$P2_1/n$	$P2_1/n$
a/Å	10.3157(10)	17.1925(10)	13.6289(4)
b/Å	7.7100(5)	7.8494(3)	11.1315(3)
c/Å	29.976(3)	19.8402(11)	17.4025(5)
α/°	90.00	90.00	90.00
β/°	98.403(8)	114.807(7)	104.404(3)
γ/°	90.00	90.00	90.00
Volume/Å^3	2358.5(4)	2430.4(2)	2557.14(13)
Z	4	4	4
ρ_{calc}g/cm^3	1.667	1.645	1.600
μ/mm^{-1}	1.396	1.354	1.289
F(000)	1200.0	1224.0	1256.0
Crystal size/mm^3	0.09 × 0.07 × 0.01	0.17 × 0.14 × 0.04	0.23 × 0.17 × 0.08
Radiation	MoKα (λ = 0.71073)	MoKα (λ = 0.71073)	MoKα (λ = 0.71073)
2Θ range for data collection/°	5.96 to 59.46	5.28 to 52.74	6.24 to 52.74
Index ranges	-8 ≤ h ≤ 13, -10 ≤ k ≤ 8, -39 ≤ l ≤ 39	-21 ≤ h ≤ 21, -8 ≤ k ≤ 9, -22 ≤ l ≤ 24	-17 ≤ h ≤ 13, -12 ≤ k ≤ 13, -21 ≤ l ≤ 21
Reflections collected	17457	19425	17005
Independent reflections	5933 [R_{int} = 0.0472, R_{sigma} = 0.0607]	4963 [R_{int} = 0.0759, R_{sigma} = 0.0667]	5211 [R_{int} = 0.0721, R_{sigma} = 0.0737]
Data/restraints/parameters	5933/0/301	4963/0/310	5211/0/320
Goodness-of-fit on F^2	1.183	1.103	1.095
Final R indexes [I>=2σ (I)]	R_1 = 0.0565, wR_2 = 0.0824	R_1 = 0.0383, wR_2 = 0.0812	R_1 = 0.0402, wR_2 = 0.0844
Final R indexes [all data]	R_1 = 0.0799, wR_2 = 0.0884	R_1 = 0.0521, wR_2 = 0.0917	R_1 = 0.0529, wR_2 = 0.0955
Largest diff. peak/hole / e Å^{-3}	0.65/-0.76	0.71/-0.59	0.58/-0.66

Name	C10	C11	C12
Empirical formula	$C_{31}H_{33}O_2ClFeRu$	$C_{30.25}H_{31.5}ClFFeO_2Ru$	$C_{29}H_{28.5}ClFFeO_{2.25}Ru$
Formula weight	629.94	638.42	624.39
Temperature/K	119.97(13)	120.02(18)	119.98(18)
Crystal system	monoclinic	monoclinic	monoclinic
Space group	$P2_1/c$	I2/a	$P2_1/c$
a/Å	26.3687(8)	27.2044(9)	12.5415(9)
b/Å	10.8733(3)	10.8246(3)	10.8998(6)
c/Å	19.1980(6)	19.3956(6)	19.2961(11)
α/°	90.00	90.00	90.00
β/°	97.429(3)	102.313(3)	97.400(6)
γ/°	90.00	90.00	90.00
Volume/$Å^3$	5458.1(3)	5580.2(3)	2615.8(3)
Z	8	8	4
$\rho_{calc}g/cm^3$	1.533	1.520	1.585
μ/mm^{-1}	1.209	1.189	1.267
F(000)	2576.0	2600.0	1266.0
Crystal size/mm^3	0.14 × 0.06 × 0.04	0.41 × 0.09 × 0.06	0.16 × 0.13 × 0.05
Radiation	MoKα (λ = 0.71073)	MoKα (λ = 0.71073)	MoKα (λ = 0.71073)
2Θ range for data collection/°	6.16 to 59.54	5.56 to 52.74	6.26 to 59.5
Index ranges	-35 ≤ h ≤ 36, -15 ≤ k ≤ 14, -26 ≤ l ≤ 23	-33 ≤ h ≤ 33, -13 ≤ k ≤ 12, -23 ≤ l ≤ 24	-16 ≤ h ≤ 13, -14 ≤ k ≤ 14, -26 ≤ l ≤ 24
Reflections collected	52077	29606	20406
Independent reflections	13791 [R_{int} = 0.0479, R_{sigma} = 0.0529]	5706 [R_{int} = 0.0439, R_{sigma} = 0.0338]	6443 [R_{int} = 0.0671, R_{sigma} = 0.0884]
Data/restraints/parameters	13791/0/659	5706/0/319	6443/0/332
Goodness-of-fit on F^2	1.085	1.029	1.153
Final R indexes [I>=2σ (I)]	R_1 = 0.0445, wR_2 = 0.0782	R_1 = 0.0284, wR_2 = 0.0572	R_1 = 0.0758, wR_2 = 0.1357
Final R indexes [all data]	R_1 = 0.0627, wR_2 = 0.0841	R_1 = 0.0382, wR_2 = 0.0599	R_1 = 0.1101, wR_2 = 0.1470
Largest diff. peak/hole / e $Å^{-3}$	0.86/-0.55	0.40/-0.29	1.95/-0.89

Name	C13	C14	C15
Empirical formula	$C_{29}H_{28}ClFFeO_2Ru$	$C_{29}H_{27}O_2F_2ClFeRu$	$C_{29}H_{28}Cl_2FeO_2Ru$
Formula weight	619.88	637.88	636.33
Temperature/K	119.99(13)	120.00(10)	120.00(10)
Crystal system	monoclinic	triclinic	monoclinic
Space group	$P2_1/c$	P-1	$P2_1/n$
a/Å	9.8233(2)	7.6330(3)	13.6335(7)
b/Å	24.0372(5)	12.2543(7)	11.1308(5)
c/Å	10.9711(3)	14.0013(8)	17.3417(9)
α/°	90	73.783(5)	90.00
β/°	101.171(3)	82.163(4)	104.646(5)
γ/°	90	89.834(4)	90.00
Volume/Å^3	2541.46(10)	1244.94(11)	2546.1(2)
Z	4	2	4
ρ_{calc}g/cm^3	1.620	1.702	1.660
μ/mm^{-1}	10.619	1.338	1.399
F(000)	1256.0	644.0	1288.0
Crystal size/mm^3	0.09 × 0.07 × 0.05	0.14 × 0.11 × 0.06	0.34 × 0.31 × 0.25
Radiation	CuKα (λ = 1.54184)	MoKα (λ = 0.71073)	MoKα (λ = 0.71073)
2Θ range for data collection/°	7.356 to 148.096	6.12 to 59.52	6.82 to 59.68
Index ranges	-12 ≤ h ≤ 12, -26 ≤ k ≤ 29, -13 ≤ l ≤ 12	-10 ≤ h ≤ 8, -16 ≤ k ≤ 16, -19 ≤ l ≤ 17	-15 ≤ h ≤ 19, -14 ≤ k ≤ 15, -24 ≤ l ≤ 23
Reflections collected	18908	14927	17793
Independent reflections	5063 [R_{int} = 0.0790, R_{sigma} = 0.0635]	6055 [R_{int} = 0.0477, R_{sigma} = 0.0691]	6285 [R_{int} = 0.0762, R_{sigma} = 0.0775]
Data/restraints/parameters	5063/0/319	6055/0/328	6285/0/319
Goodness-of-fit on F^2	1.042	1.042	1.093
Final R indexes [I>=2σ (I)]	R_1 = 0.0428, wR_2 = 0.0963	R_1 = 0.0427, wR_2 = 0.0775	R_1 = 0.0459, wR_2 = 0.1014
Final R indexes [all data]	R_1 = 0.0620, wR_2 = 0.1070	R_1 = 0.0571, wR_2 = 0.0862	R_1 = 0.0570, wR_2 = 0.1135
Largest diff. peak/hole / e Å^{-3}	1.10/-0.78	0.68/-0.75	0.84/-0.74

Name	C16	C17	C18
Empirical formula	$C_{31}H_{32}Cl_2FeO_3Ru$	$C_{29}H_{27}O_2Cl_3FeRu$	$C_{29}H_{28}O_2ClFeBrRu$
Formula weight	680.38	670.77	680.79
Temperature/K	290.42(10)	290.42(10)	120.00(10)
Crystal system	monoclinic	monoclinic	monoclinic
Space group	C2/c	$P2_1/c$	$P2_1/n$
a/Å	27.5025(7)	26.1643(4)	13.7350(7)
b/Å	11.1189(2)	10.8621(2)	11.0892(5)
c/Å	19.0656(4)	19.1456(3)	17.3899(10)
α/°	90	90	90.00
β/°	102.835(2)	96.426(2)	105.003(5)
γ/°	90	90	90.00
Volume/Å^3	5684.5(2)	5406.98(16)	2558.4(2)
Z	8	8	4
ρ_{calc}g/cm^3	1.590	1.648	1.768
μ/mm^{-1}	1.261	1.417	2.849
F(000)	2768.0	2704.0	1360.0
Crystal size/mm^3	0.20 × 0.18 × 0.09	0.14 × 0.11 × 0.04	0.20 × 0.15 × 0.03
Radiation	MoKα (λ = 0.71073)	MoKα (λ = 0.71073)	MoKα (λ = 0.71073)
2Θ range for data collection/°	5.656 to 59.614	5.582 to 59.636	5.72 to 62.52
Index ranges	-38 ≤ h ≤ 30, -14 ≤ k ≤ 15, -25 ≤ l ≤ 26	-32 ≤ h ≤ 36, -14 ≤ k ≤ 13, -26 ≤ l ≤ 26	-19 ≤ h ≤ 19, -13 ≤ k ≤ 15, -24 ≤ l ≤ 20
Reflections collected	24289	47874	20795
Independent reflections	7106 [R_{int} = 0.0352, R_{sigma} = 0.0405]	13518 [R_{int} = 0.0434, R_{sigma} = 0.0494]	7335 [R_{int} = 0.0604, R_{sigma} = 0.0817]
Data/restraints/parameters	7106/35/375	13518/0/655	7335/0/319
Goodness-of-fit on F^2	1.183	1.064	1.028
Final R indexes [I>=2σ (I)]	R_1 = 0.0431, wR_2 = 0.0804	R_1 = 0.0352, wR_2 = 0.0616	R_1 = 0.0471, wR_2 = 0.0758
Final R indexes [all data]	R_1 = 0.0580, wR_2 = 0.0856	R_1 = 0.0621, wR_2 = 0.0723	R_1 = 0.0739, wR_2 = 0.0860
Largest diff. peak/hole / e Å^{-3}	0.84/-0.71	0.61/-0.58	0.66/-0.88

Name	C19	C20	C21
Empirical formula	$C_{31}H_{32}BrClFeO_3Ru$	$C_{29}H_{28}O_2ClFeRuI$	$C_{29}H_{28}O_2ClFeRuI$
Formula weight	724.84	727.78	727.78
Temperature/K	120.1(3)	119.99(18)	120.1(4)
Crystal system	monoclinic	monoclinic	monoclinic
Space group	C2/c	$P2_1/n$	I2/a
a/Å	27.7319(5)	13.9912(7)	20.2251(4)
b/Å	11.1421(3)	11.0716(5)	7.77335(16)
c/Å	19.0333(4)	17.4043(8)	33.7938(11)
α/°	90	90.00	90
β/°	102.770(2)	105.450(5)	91.661(2)
γ/°	90	90.00	90
Volume/Å^3	5735.6(2)	2598.6(2)	5310.7(2)
Z	8	4	8
ρ_{calc}g/cm^3	1.679	1.860	1.820
μ/mm^{-1}	2.550	2.456	19.233
F(000)	2912.0	1432.0	2864.0
Crystal size/mm^3	0.14 × 0.10 × 0.04	0.16 × 0.11 × 0.03	0.14 × 0.05 × 0.05
Radiation	MoKα (λ = 0.71073)	MoKα (λ = 0.71073)	CuKα (λ = 1.54184)
2Θ range for data collection/°	5.656 to 59.572	6.2 to 59.48	8.748 to 147.572
Index ranges	-38 ≤ h ≤ 37, -14 ≤ k ≤ 10, -24 ≤ l ≤ 26	-19 ≤ h ≤ 18, -13 ≤ k ≤ 14, -24 ≤ l ≤ 24	-24 ≤ h ≤ 25, -9 ≤ k ≤ 7, -38 ≤ l ≤ 39
Reflections collected	26100	17635	10588
Independent reflections	7254 [R_{int} = 0.0394, R_{sigma} = 0.0418]	6258 [R_{int} = 0.0538, R_{sigma} = 0.0735]	4952 [R_{int} = 0.0393, R_{sigma} = 0.0486]
Data/restraints/parameters	7254/35/376	6258/0/319	4952/0/319
Goodness-of-fit on F^2	1.200	1.065	1.074
Final R indexes [I>=2σ (I)]	R_1 = 0.0570, wR_2 = 0.1174	R_1 = 0.0472, wR_2 = 0.0753	R_1 = 0.0426, wR_2 = 0.1040
Final R indexes [all data]	R_1 = 0.0707, wR_2 = 0.1226	R_1 = 0.0713, wR_2 = 0.0826	R_1 = 0.0545, wR_2 = 0.1112
Largest diff. peak/hole / e Å^{-3}	1.28/-1.77	1.50/-0.89	1.09/-0.74

Name	C22	C23	C24
Empirical formula	$C_{30}H_{31}O_3ClFeRu$	$C_{30}H_{31}O_3ClFeRu$	$C_{31}H_{33}O_3ClFeRu$
Formula weight	631.92	631.94	645.94
Temperature/K	120.02(10)	120.01(10)	119.99(11)
Crystal system	monoclinic	monoclinic	monoclinic
Space group	$P2_1/n$	$P2_1/c$	$P2_1/n$
a/Å	14.1001(4)	8.0188(2)	8.1226(3)
b/Å	11.0079(2)	10.5765(3)	7.4214(3)
c/Å	17.4370(4)	29.8235(9)	44.6460(13)
α/°	90.00	90	90.00
β/°	105.602(3)	92.186(3)	91.909(3)
γ/°	90.00	90	90.00
Volume/Å^3	2606.73(11)	2527.52(12)	2689.81(16)
Z	4	4	4
ρ_{calc}g/cm^3	1.610	1.6606	1.595
μ/mm^{-1}	1.269	1.309	1.232
F(000)	1288.0	1285.5	1320.0
Crystal size/mm^3	0.25 × 0.16 × 0.15	0.56 × 0.35 × 0.14	0.52 × 0.15 × 0.11
Radiation	MoKα (λ = 0.71073)	Mo Kα (λ = 0.71073)	MoKα (λ = 0.71073)
2Θ range for data collection/°	6.2 to 52.74	5.62 to 59.46	5.8 to 59.52
Index ranges	-15 ≤ h ≤ 17, -13 ≤ k ≤ 11, -19 ≤ l ≤ 21	-10 ≤ h ≤ 11, -14 ≤ k ≤ 11, -31 ≤ l ≤ 39	-10 ≤ h ≤ 11, -7 ≤ k ≤ 10, -57 ≤ l ≤ 60
Reflections collected	17274	15946	19235
Independent reflections	5324 [R_{int} = 0.0742, R_{sigma} = 0.0702]	6124 [R_{int} = 0.0629, R_{sigma} = 0.0856]	6455 [R_{int} = 0.0494, R_{sigma} = 0.0600]
Data/restraints/parameters	5324/0/329	6124/0/328	6455/0/338
Goodness-of-fit on F^2	1.094	1.084	1.080
Final R indexes [I>=2σ (I)]	R_1 = 0.0416, wR_2 = 0.0946	R_1 = 0.0496, wR_2 = 0.0819	R_1 = 0.0400, wR_2 = 0.0733
Final R indexes [all data]	R_1 = 0.0501, wR_2 = 0.1040	R_1 = 0.0817, wR_2 = 0.0978	R_1 = 0.0520, wR_2 = 0.0794
Largest diff. peak/hole / e Å^{-3}	0.69/-0.68	1.24/-1.12	0.46/-0.70

Name	C'1	C'2	C'4
Empirical formula	$C_{34}H_{29}F_6FeN_4O_2PRu$	$C_{34}H_{26}N_4O_2F_9PFeRuCl_{0.5}$	$C_{39}H_{31}F_6FeN_4O_2PRu$
Formula weight	827.50	899.20	889.58
Temperature/K	119.99(16)	119.97(13)	119.96(17)
Crystal system	monoclinic	triclinic	triclinic
Space group	I2/a	P-1	P-1
a/Å	22.6760(8)	11.6698(7)	12.5718(10)
b/Å	10.6551(3)	11.7149(7)	12.8149(11)
c/Å	26.2259(10)	15.0528(6)	14.8974(9)
α/°	90	111.259(4)	91.133(6)
β/°	92.863(3)	92.925(4)	114.006(7)
γ/°	90	107.395(5)	116.548(8)
Volume/Å^3	6328.7(4)	1800.48(18)	1900.7(3)
Z	8	2	2
ρ_{calc}g/cm^3	1.737	1.659	1.5543
μ/mm^{-1}	1.062	0.988	7.281
F(000)	3328.0	897.0	897.3
Crystal size/mm^3	0.29 × 0.22 × 0.15	0.32 × 0.25 × 0.12	0.16 × 0.04 × 0.03
Radiation	MoKα (λ = 0.71073)	MoKα (λ = 0.71073)	Cu Kα (λ = 1.54184)
2Θ range for data collection/°	6.222 to 59.616	5.796 to 59.696	6.7 to 147.64
Index ranges	-27 ≤ h ≤ 30, -14 ≤ k ≤ 14, -34 ≤ l ≤ 34	-14 ≤ h ≤ 14, -15 ≤ k ≤ 16, -16 ≤ l ≤ 21	-15 ≤ h ≤ 15, -15 ≤ k ≤ 9, -18 ≤ l ≤ 18
Reflections collected	12388	19543	14361
Independent reflections	12388 [R_{int} = ?, R_{sigma} = 0.0487]	8661 [R_{int} = 0.0566, R_{sigma} = 0.0896]	7188 [R_{int} = 0.0576, R_{sigma} = 0.0755]
Data/restraints/parameters	12388/0/447	8661/0/469	7188/0/486
Goodness-of-fit on F^2	1.003	1.283	0.951
Final R indexes [I>=2σ (I)]	R_1 = 0.0498, wR_2 = 0.1250	R_1 = 0.0837, wR_2 = 0.2279	R_1 = 0.0709, wR_2 = 0.2195
Final R indexes [all data]	R_1 = 0.0650, wR_2 = 0.1300	R_1 = 0.1118, wR_2 = 0.2550	R_1 = 0.0917, wR_2 = 0.2446
Largest diff. peak/hole / e Å^{-3}	1.13/-2.00	3.56/-1.70	2.99/-1.30

Name	C'7	C'8	C'10
Empirical formula	$C_{41}H_{35}F_6FeN_4O_2PRu$	$C_{39}H_{30}F_7FeN_4O_2PRu$	$C_{40.65}H_{32.3}F_8FeN_4O_{2.55}PRu$
Formula weight	917.62	907.56	957.49
Temperature/K	120.3(7)	120.0(2)	120.01(12)
Crystal system	monoclinic	monoclinic	triclinic
Space group	$P2_1/n$	$P2_1/c$	P-1
a/Å	13.7236(13)	12.3359(2)	11.5358(5)
b/Å	12.5273(12)	20.1065(4)	11.8110(5)
c/Å	22.629(2)	14.6967(3)	15.7319(7)
α/°	90	90	102.635(4)
β/°	95.299(8)	97.1081(16)	95.616(4)
γ/°	90	90	104.201(4)
Volume/Å^3	3873.8(6)	3617.25(12)	2001.46(16)
Z	4	4	2
ρ_{calc}g/cm^3	1.573	1.667	1.589
μ/mm^{-1}	0.876	7.707	0.859
F(000)	1856.0	1824.0	963.0
Crystal size/mm^3	0.15 × 0.10 × 0.04	0.16 × 0.09 × 0.06	0.34 × 0.14 × 0.05
Radiation	MoKα (λ = 0.71073)	CuKα (λ = 1.54184)	MoKα (λ = 0.71073)
2Θ range for data collection/°	6.324 to 59.354	7.222 to 147.822	5.358 to 59.272
Index ranges	-19 ≤ h ≤ 18, -17 ≤ k ≤ 17, -30 ≤ l ≤ 30	-15 ≤ h ≤ 15, -23 ≤ k ≤ 24, -18 ≤ l ≤ 18	-15 ≤ h ≤ 14, -15 ≤ k ≤ 14, -18 ≤ l ≤ 20
Reflections collected	35647	29073	21623
Independent reflections	9722 [R_{int} = 0.0779, R_{sigma} = 0.0980]	7333 [R_{int} = 0.0449, R_{sigma} = 0.0389]	9487 [R_{int} = 0.0641, R_{sigma} = 0.1051]
Data/restraints/parameters	9722/0/507	7333/0/496	9487/18/546
Goodness-of-fit on F^2	1.042	1.047	1.038
Final R indexes [I>=2σ (I)]	R_1 = 0.0562, wR_2 = 0.0790	R_1 = 0.0348, wR_2 = 0.0866	R_1 = 0.0727, wR_2 = 0.1579
Final R indexes [all data]	R_1 = 0.0965, wR_2 = 0.0891	R_1 = 0.0417, wR_2 = 0.0905	R_1 = 0.1198, wR_2 = 0.1889
Largest diff. peak/hole / e Å^{-3}	0.52/-0.67	0.96/-0.76	2.54/-1.07

Name	C'11	C'12	C'13
Empirical formula	$C_{39}H_{31}ClF_6FeN_4O_{2.5}PRu$	$C_{39}H_{31}Cl_2F_6FeN_4O_3PRu$	$C_{39}H_{30}BrF_6FeN_4O_2PRu$
Formula weight	933.02	976.47	968.47
Temperature/K	120.4(9)	120.1(3)	293(2)
Crystal system	triclinic	monoclinic	triclinic
Space group	P-1	$P2_1/c$	P-1
a/Å	12.5053(5)	13.1656(4)	12.6098(19)
b/Å	16.5786(9)	20.9269(6)	16.989(4)
c/Å	19.9096(11)	14.0300(4)	19.373(5)
α/°	99.243(4)	90	98.47(2)
β/°	106.818(4)	98.331(3)	106.116(18)
γ/°	102.522(4)	90	103.128(18)
Volume/$Å^3$	3745.3(3)	3824.67(18)	3783.7(16)
Z	4	4	4
$\rho_{calc}g/cm^3$	1.655	1.696	1.700
μ/mm^{-1}	8.073	8.574	1.860
F(000)	1876.0	1960.0	1928.0
Crystal size/mm^3	0.17 × 0.04 × 0.04	0.14 × 0.08 × 0.04	0.01 × 0.02 × 0.03
Radiation	CuKα (λ = 1.54184)	CuKα (λ = 1.54184)	Synchrotron (λ = 0.6889)
2Θ range for data collection/°	6.45 to 149.42	7.642 to 147.99	2.448 to 51.004
Index ranges	-15 ≤ h ≤ 15, -20 ≤ k ≤ 20, -17 ≤ l ≤ 24	-15 ≤ h ≤ 16, -25 ≤ k ≤ 23, -17 ≤ l ≤ 17	-15 ≤ h ≤ 15, -21 ≤ k ≤ 21, -24 ≤ l ≤ 22
Reflections collected	32402	30029	36914
Independent reflections	14201 [R_{int} = 0.0635, R_{sigma} = 0.0791]	7718 [R_{int} = 0.0827, R_{sigma} = 0.0715]	14682 [R_{int} = 0.1712, R_{sigma} = 0.1885]
Data/restraints/parameters	14201/126/995	7718/0/517	14682/0/991
Goodness-of-fit on F^2	1.021	1.142	0.919
Final R indexes [I>=2σ (I)]	R_1 = 0.0642, wR_2 = 0.1464	R_1 = 0.0814, wR_2 = 0.2145	R_1 = 0.1087, wR_2 = 0.2605
Final R indexes [all data]	R_1 = 0.1037, wR_2 = 0.1675	R_1 = 0.1003, wR_2 = 0.2316	R_1 = 0.1915, wR_2 = 0.2979
Largest diff. peak/hole / e $Å^{-3}$	1.28/-1.36	2.81/-1.74	2.25/-0.58

Name	C'14
Empirical formula	$C_{39}F_6FeIN_4O_2PRu$
Formula weight	985.22
Temperature/K	100(2)
Crystal system	triclinic
Space group	P-1
a/Å	12.6452(2)
b/Å	17.0679(3)
c/Å	18.9907(4)
α/°	98.076(2)
β/°	105.417(2)
γ/°	103.430(2)
Volume/Å^3	3752.72(13)
Z	4
ρ_{calc}g/cm^3	1.744
μ/mm^{-1}	1.595
F(000)	1880.0
Crystal size/mm^3	0.06 × 0.04 × 0.02
Radiation	synchrotron (λ = 0.6889)
2Θ range for data collection/°	3.376 to 54.68
Index ranges	-16 ≤ h ≤ 16, -22 ≤ k ≤ 22, -25 ≤ l ≤ 25
Reflections collected	45950
Independent reflections	17988 [R_{int} = 0.0629, R_{sigma} = 0.0517]
Data/restraints/parameters	17988/0/991
Goodness-of-fit on F^2	1.083
Final R indexes [I>=2σ (I)]	R_1 = 0.0918, wR_2 = 0.2537
Final R indexes [all data]	R_1 = 0.1036, wR_2 = 0.2635
Largest diff. peak/hole / e Å^{-3}	3.43/-2.12